

Haematopoiesis During Native Conditions and Immune Thrombocytopenia Progression

Oliver Herd

Doctor of Philosophy

**University of York
Biology**

March 2021

Abstract

The maintenance of haematopoietic stem cell (HSC) self-renewal and differentiation throughout life is essential for ongoing haematopoiesis and is highly dependent upon cytokine-cytokine receptor interactions and direct cell-cell contact between the HSC and components of the perivascular bone marrow (BM) microenvironment.

Thrombopoietin (TPO) is one of two such cytokines essential for HSC self-renewal. Although the majority of TPO is produced distally by the liver, lower amounts of TPO are thought to be produced locally in the BM, directly at the site of utilisation. However, the exact cellular sources of BM derived TPO are unclear and remains an active area of research. Contrary to previous studies, the results in this thesis indicate that megakaryocytes do not express *Thpo*, and instead $\text{LepR}^+/\text{Cxcl12-DsRed}^{\text{high}}$ BM stromal cells (BMSCs) are major sources of *Thpo* in mice.

Immune thrombocytopenia (ITP) is an acquired autoimmune condition characterised by reduced platelet production and increased platelet destruction by sustained immune attack. In this thesis, a novel mouse model of sustained ITP was generated and the effect on the immune and haematopoietic system was assessed. Platelet destruction was antibody dependent and appeared to be primarily driven by splenic macrophages. Additionally, ITP progression was associated with considerable progenitor expansion and BM remodelling. Single cell assays using $\text{Lin}^- \text{Sca1}^+ \text{c-Kit}^+ \text{CD48}^- \text{CD150}^+$ long-term HSCs (LT-HSCs) revealed elevated LT-HSC activation and proliferation *in vitro*. However, LT-HSC functionality was maintained as measured by *in vivo* serial transplantations. ITP progression was associated with considerable BM vasodilation and angiogenesis, as well as a 2-fold increase in local production of CXCL12; a cytokine essential for LT-HSC function and BM homing expressed at high levels by LepR^+ BMSCs. This was associated with a 1.5-fold increase in LepR^+ BMSCs and a 5.5-fold improvement in progenitor homing to the BM. Whereas the increase in BMSCs was transient and reverted back to baseline after platelet count returned to normal, vasculature changes in the BM persisted. Together, these studies demonstrate that LT-HSCs expand in response to ITP, and that LT-HSC functionality during sustained haematopoietic stress is maintained through an adapting BM microenvironment.

Table of Contents

1	Introduction.....	1
1.1	Overview of haematopoiesis.....	1
1.2	HSC identification.....	1
1.3	Steady state haematopoiesis.....	2
1.4	Cytokines in haematopoiesis.....	4
1.5	The bone marrow niche.....	5
1.5.1	Niche components.....	6
1.6	Extramedullary niches.....	9
1.7	Pathological haematopoiesis.....	9
1.7.1	Haematopoietic stem cell niche in ageing and disease.....	10
1.8	Thrombopoietin.....	11
1.8.1	Thrombopoietin biology: haematopoietic stem cell self-renewal and megakaryopoiesis.....	11
1.8.2	Bone marrow sources of thrombopoietin.....	14
1.9	Overview of the immune system.....	15
1.9.1	Innate immune system.....	15
1.10	T cell overview.....	17
1.11	T cell activation.....	18
1.12	B cell overview.....	19
1.13	ITP.....	19
1.13.1	Definition and epidemiology.....	19
1.13.2	Etiology.....	20
1.13.3	Immune thrombocytopenia treatment.....	22
1.14	Research aims.....	22
2	General materials and methods.....	23
2.1	Cell culture.....	23
2.1.1	Cell culture plasticware and reagents.....	23
2.1.2	Cell line culture conditions.....	23

2.2	RNA isolation.....	23
2.2.1	Cells: RNeasy mini kit.....	23
2.2.2	Whole organs: Trizol plus miRNAeasy mini kit.....	24
2.2.3	Sorted cells: Manual QIAzol method.....	24
2.3	Reverse transcription polymerase chain reaction.....	25
2.3.1	High input (cells/whole organs): High Capacity Reverse Transcription Kit	25
2.3.2	Low input (sorted cells): Superscript IV.....	25
2.4	Mouse models	25
2.4.1	Genotyping.....	27
2.5	Tissue Processing	28
2.5.1	Bleeds	28
2.5.2	Primary cell isolation.....	29
2.6	Cell preparation for flow cytometry analysis.....	29
2.7	Tissue processing for imaging	31
2.7.1	Pre-freezing steps	31
2.7.2	Sectioning.....	31
2.8	H&E staining.....	31
3	The sources and roles of thrombopoietin in haematopoietic stem cell niche self- renewal.....	32
3.1	Introduction.....	32
3.2	Materials and methods	33
3.2.1	Immunofluorescence microscopy	33
3.2.2	Fluorescence-activated cell sorting.....	33
3.2.3	Cultured megakaryocyte isolation by magnetic-activated cell sorting....	34
3.2.4	Real-time polymerase chain reaction.....	34
3.2.5	Acute immune thrombocytopenia mouse model	35
3.3	Results	35
3.3.1	Published thrombopoietin antibody is non-specific.....	35
3.3.2	Megakaryocytes do not express <i>Thpo</i>	39

3.3.3	<i>Cxcl12</i> -DsRed/LepR ⁺ bone marrow stromal cells express <i>Thpo</i>	44
3.3.4	Bone marrow stromal cells do not upregulate <i>Thpo</i> expression after acute thrombocytopenia.....	46
3.3.5	Analysis of bone marrow stromal cell clonal lines suggest that <i>THPO</i> expressing bone marrow stromal cells are rare <i>in vivo</i>	48
3.4	Discussion	50
4	Generation of a model of sustained immune thrombocytopenia.....	57
4.1	Introduction.....	57
4.2	Materials and methods	58
4.2.1	Immune thrombocytopenia model.....	58
4.2.2	Thrombopoietin enzyme-linked immunosorbent assay	58
4.2.3	Quantification of bone marrow megakaryocyte number	58
4.2.4	Determination of whether injected anti-CD41 binds to megakaryocytes: flow cytometry.....	58
4.2.5	Determination of whether injected anti-CD41 binds to megakaryocytes: microscopy	59
4.3	Results	59
4.3.1	Repeated anti-CD41 intraperitoneal injection as a model of sustained immune thrombocytopenia.....	59
4.3.2	Dose escalation is required to maintain severe thrombocytopenia in WT mice, but not <i>Rag2</i> ^{-/-} mice	62
4.3.3	Sustained immune thrombocytopenia model exhibits clinical features of immune thrombocytopenia.....	64
4.3.4	Injected anti-CD41 binds BM Mks.....	69
4.3.5	Platelet recovery is similar between mice with sustained immune thrombocytopenia and acute immune thrombocytopenia	71
4.4	Discussion	73
5	Characterisation of the immune system using the sustained ITP mouse model ..	81
5.1	Introduction.....	81
5.2	Materials and methods	82
5.2.1	Flow cytometry	82

5.3	Results	86
5.3.1	Induction of immune thrombocytopenia model is dependent on expression of FcyRIII	86
5.3.2	Sustained ITP is achieved in <i>Rag2</i> ^{-/-} , but not NSG-SGM3 mice	88
5.3.3	Characterisation of the innate immune system in immune thrombocytopenia	91
5.3.4	Characterisation of T cell subsets in chronic ITP	99
5.4	Discussion	109
6	Haematopoiesis in immune thrombocytopenia.....	115
6.1	Introduction.....	115
6.2	Methods and materials	115
6.2.2	Flow cytometry	116
6.2.3	Competitive transplantation	117
6.2.4	Cell sorting and transplantation experiments	117
6.2.5	<i>In vitro</i> long term haematopoietic stem cell assays	118
6.2.6	Immunostaining	118
6.2.7	Imaging and image analysis	119
6.2.8	Real-time polymerase chain reaction.....	119
6.3	Results	120
6.3.1	Immune thrombocytopenia progression drives haematopoietic stem cell and progenitor expansion	120
6.3.2	Sustained immune thrombocytopenia increases the number of functional haematopoietic stem cells.....	129
6.3.3	ITP progression drives physical and biochemical changes within the BM HSC microenvironment.....	132
6.4	Discussion	142
7	General discussion	148
7.1	The sustained model of immune thrombocytopenia.....	152
7.2	Future research	153
7.3	Concluding remarks.....	155
8	Abbreviations.....	156

9	References	158
---	------------------	-----

Figures

Figure 1.1 The BM niche.	8
Figure 3.1. bs-10407R is non-specific.	37
Figure 3.2. Staining pattern of WT BM with bs-10407R is consistent with images generated by Nakamura-Ishizu et al.	38
Figure 3.3. Cultured Mks were isolated to a high degree of purity.	41
Figure 3.4. Cultured Mks stain positive with bs-10407R.	42
Figure 3.5. Neither cultured Mks nor sorted Mks express Thpo.	43
Figure 3.6. BMSC subsets express Thpo at different levels.	45
Figure 3.7. Acute ITP does not influence BMSC Thpo expression.	47
Figure 3.8. THPO expressing human BMSC subsets may be extremely rare.	49
Figure 3.9. Hepatic TPO is required for BM HSC maintenance.	52
Figure 4.1. Repeated intraperitoneal injection of mice is a model for sustained ITP. ...	61
Figure 4.2. <i>Rag2^{-/-}</i> mice maintain severe thrombocytopenia at low doses of anti-CD41.	63
Figure 4.3. Sustained ITP model appears to induce occasional spontaneous bleeding.	65
Figure 4.4. Mild splenomegaly during ITP progression occurs in the absence of a functional adaptive immune system.	66
Figure 4.5. Plasma TPO levels are normal during ITP progression.	67
Figure 4.6. BM Mk numbers increased with ITP progression.	68
Figure 4.7. Injected anti-CD41 binds BM Mks.	70
Figure 4.8. Platelet recovery is similar between mice with sustained ITP and acute ITP.	72
Figure 4.9. A model for sustained ITP.	80
Figure 5.1. Summary of platelet labelling experiment.	84
Figure 5.2. FcγRIII expression is required for ITP induction.	87
Figure 5.3. NSG-SGM3 mice cannot maintain thrombocytopenia using the ITP model.	89
Figure 5.4. <i>Rag2^{-/-}</i> mice maintain severe thrombocytopenia using the ITP model.	90
Figure 5.5. Labelled platelets bind to a minority of peripheral monocytes during sustained ITP.	94
Figure 5.6. Labelled platelets bind to a minority of BM monocytes during sustained ITP.	96
Figure 5.7. Labelled anti-CD41/IgG binds non-specifically to peritoneal macrophages.	97

Figure 5.8. Labelled platelets bind to the majority of splenic F4/80 ⁺ macrophages during sustained ITP.....	99
Figure 5.9. Splenic T cell phenotype in the sustained ITP mouse model.....	102
Figure 5.10. BM T cell phenotype in the sustained ITP mouse model.....	104
Figure 5.11. No alteration in proportion of T follicular helper cells in the sustained ITP mouse model.....	105
Figure 5.12. No alteration in proportion of Tregs in the sustained ITP mouse model.....	106
Figure 5.13. CD4 ⁺ and CD8 ⁺ T cells in the spleen have no change in activation status in the sustained ITP mouse model.....	107
Figure 5.14. CD4 ⁺ and CD8 ⁺ T cells in the BM have no change in intracellular cytokine production in the sustained ITP mouse model.....	108
Figure 5.15. ITP is initiated and maintained by splenic macrophages and associated with an increase in naïve T cells.....	114
Figure 6.1. Cytokine signature in plasma and BM supernatant is altered in sustained ITP.....	122
Figure 6.2. Mice with sustained ITP develop a pro-inflammatory cytokine signature in plasma and BM supernatant in mice with ITP.....	123
Figure 6.3. Sustained ITP drives BM primitive progenitor expansion.....	124
Figure 6.4. Sustained ITP drives extramedullary haematopoiesis.....	125
Figure 6.5. Sustained ITP drives BM committed progenitor expansion.....	126
Figure 6.6. ITP progression is associated with progenitor expansion.....	127
Figure 6.7. Sustained ITP drives progenitor proliferation.....	128
Figure 6.8. Sustained ITP increases the frequency of functional LT-HSCs <i>in vivo</i> ..	130
Figure 6.9. Fewer functional LT-HSCs exist in the phenotypic LT-HSC pool in ITP..	131
Figure 6.10. Sustained ITP remodels the BM niche.....	134
Figure 6.11. 2 Week ITP causes an increase in average vessel area but no changes in vessel number or LepR ⁺ stromal cell number.....	135
Figure 6.12. Platelet counts return to baseline after cessation of anti-CD41 administration in the sustained ITP model.....	136
Figure 6.13. ITP progression increases BM <i>Cxcl12</i> expression.....	137
Figure 6.14. Strong co-localisation between perivascular LepR ⁺ stromal cells and <i>Cxcl12</i> expression.....	138
Figure 6.15. Expansion of <i>Cxcl12</i> expressing perivascular cells in ITP.....	139
Figure 6.16. ITP progression increases BM CXCL12 expression.....	140
Figure 6.17. ITP progression is associated with increased BM homing.....	141
Figure 6.18. Sustained ITP causes expansion of HSCs in the BM and spleen.....	147

Figure 7.1. A summary of data using the murine model of sustained ITP..... 151

Acknowledgements

First and foremost I would like to thank my supervisors Ian Hitchcock and Paul Genever for their guidance, support and advice especially at times of challenging circumstance. I would also like to thank David Kent and James Hewitson, whose time and expertise in the haematopoietic stem cell and immunology fields have been invaluable. I thank my TAP panel Nathalie Signoret and Will Brackenbury for their advice and the BBSRC for funding this research.

I wish to thank the Technology Facility and Biological Services Facility, especially Karen Hogg and Graeme Park from the Imaging and Cytometry Team for their time in training me and helping troubleshoot experiments.

Thank you to Nichola Cooper at Imperial College London for the ITP patient bone marrow aspirate samples and for welcoming me to the lab and to Michelle Tan for experimental assistance.

Finally, thank you to members of the Hitchcock and Genever labs both past and present, especially to Andy Stone for his friendship inside and outside the lab.

Author's Declaration

I declare that this thesis is a presentation of original work and I am the sole author. All of the work presented in this thesis was performed by myself with the following exceptions: 1) intravenous injections during bone marrow transplantation experiments which were performed by David Kent and James Hewitson, 2) the vessel analysis protocol was designed by TissueGnostics specialists and Karen Hogg, analysis was performed by myself. This work has not previously been presented for an award at this, or any other, University. All sources are acknowledged as References.

Some of this work has been presented at the *Disorders of Platelet Number or Function: Insights into the Pathophysiology of Platelet Disorders* oral session at the 61st Annual ASH meeting in Orlando in 2019, and some of this work has been accepted for publication in the journal *Blood Advances*.

1 Introduction

1.1 Overview of haematopoiesis

Haematopoiesis is the ongoing process of blood cell production that occurs throughout life. Mature blood cells have relatively short life spans (1), therefore must be constantly replenished from progenitors. Without haematopoiesis, pancytopenia and death would occur within weeks as a result of anaemia (due to erythrocyte depletion), bleeding (due to platelet depletion) and infection (due to the depletion of immune effector cells) (2). At the top of the differentiation hierarchy is the haematopoietic stem cell (HSC); a rare cell with the highest potential in the blood. HSCs are defined by two essential characteristics: 1) the ability to differentiate into mature blood cells (largely through restricted progenitor intermediates allowing for cell amplification), and 2) the ability to self-renew to maintain the HSC pool. In contrast, intermediates and committed progenitors have reduced self-renewal ability and display restricted lineage differentiation potential before exhaustion after several weeks after transplant (3, 4). The balance between the differentiation and self-renewal of HSCs is tightly regulated through cell intrinsic and cell extrinsic factors: excessive differentiation or insufficient self-renewal can cause depletion of the HSC pool, whilst differentiation defects or excessive self-renewal can lead to the development of myeloproliferative diseases or leukaemia (5).

1.2 HSC identification

The existence of HSCs was first functionally demonstrated during early transplantation experiments. Multi-lineage differentiation occurred in the spleen of irradiated recipient mice (spleen colony-forming cells, CFU-S) when murine BM cells were injected intravenously (6), and this was derived from single clones (7) capable of self-renewal (8). Early attempts to identify HSCs relied on their functional characteristics: isolation of HSCs was enriched when selecting for BM cells that were resistant to 5-fluorouracil (5-FU) (9) treatment or gamma (Gy) irradiation (10).

The advent of fluorescence-activated cell sorting (FACS) using cell surface markers allowed for the enrichment (and later near purity), of HSCs. As HSCs do not express mature lineage markers such as those expressed by lymphocytes, granulocytes and leukocytes (11), HSCs are enriched by gating on cells that are negative for such markers, termed Lineage⁻ (Lin⁻) cells. The combination of lineage cocktails with additional antibodies enriched for HSCs further such as Lin⁻ Sca-1⁺c-kit⁺ (LSK) Thy-1^{lo} cells (12) or CD34⁻LSK (13) which allowed for the prospective isolation of HSCs with up to 20% efficiency. The combination of these markers with the use of fluorescent dyes

such as Hoechst 33342 (14) or Rhodamine 123 (15) increased the efficiency further to up to absolute purity (16, 17), however this demanded the use of highly complex FACS panels that most likely only identified a subset of HSCs (18). The identification that haematopoietic progenitors differentially expressed signalling lymphocyte activation molecule (SLAM) markers in a way that correlated with primitiveness and predicted developmental potential allowed for the separation of HSCs from restricted progenitors using only two markers (18). Using CD150 and CD48 alone isolated HSCs to a purity of 20% whilst combination with earlier markers isolated HSCs with a purity up to 50% with a combined phenotype of LSK CD48⁻CD150⁺ (18). However, the LSK CD48⁻CD150⁺ phenotype still required the use of many markers for identification and isolation. Further refinement of HSC markers identified that expression of Endothelial protein C receptor (EPCR) explicitly identifies murine progenitors (19) and that the combined phenotype of CD45⁺EPCR⁺CD48⁻CD150⁺ can isolate HSCs to a purity of 43% (20).

1.3 Steady state haematopoiesis

HSCs reside primarily in the bone marrow (BM), which is the main site of haematopoiesis. The classical model of haematopoiesis suggests that differentiation occurs in a stepwise fashion, with the HSC differentiating into the common myeloid progenitor (CMP) and common lymphoid progenitor (CLP), followed by further sub-branching and lineage commitment (21, 22). However, recent evidence indicates that both HSCs and downstream progenitors are highly heterogeneous with respect to cellular output and that differentiation during early haematopoiesis occurs through a continuum of transitory states rather than discrete progenitor cell types (23-26). HSCs are transcriptionally primed towards certain lineages, followed by activation of lineage specific transcriptional programs in downstream progenitors and definitive lineage commitment (27). As such, the majority of intermediate cell types (e.g. CMP, MEP; common erythroid/Mk progenitor) are already functionally committed; only very few cells are primed towards mixed lineages (25-29). The tendency of phenotypic HSCs to produce certain lineages above others during transcriptional priming resulted in the term 'lineage bias' being used. The direction and extent of transcriptional priming is functionally linked to lineage bias of the HSC, with the amount of lineage specific priming linked to functional lineage commitment (27). Even the most primitive HSC subset, despite remaining multipotent, exhibits considerable lineage bias (30-32).

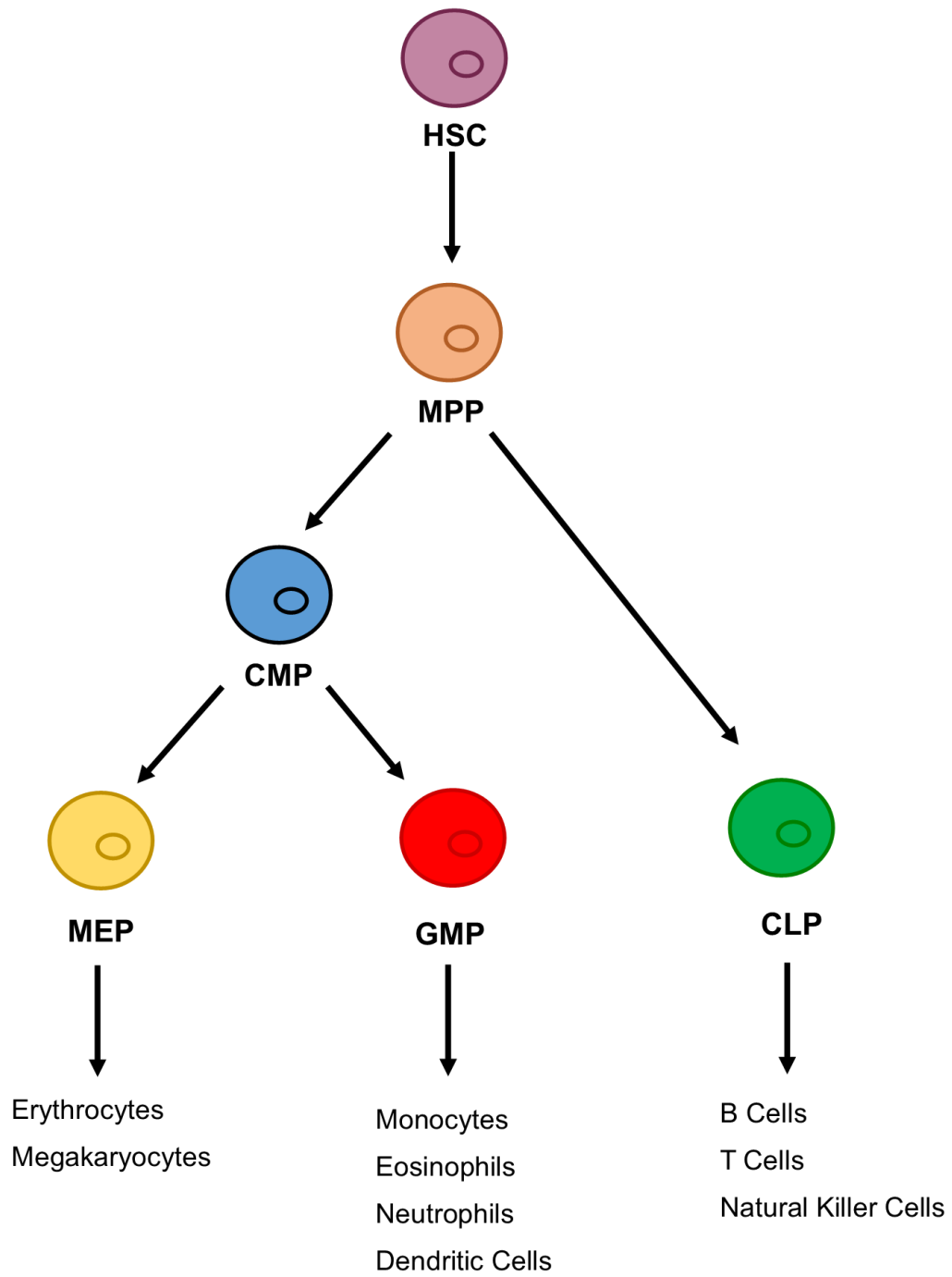


Figure 1.1 The classical model of haematopoiesis. Haematopoiesis originates from an HSC, downstream of which the first lineage bifurcation separates the myeloid and lymphoid branches via the CMP and the CLP

1.4 Cytokines in haematopoiesis

Haematopoiesis during steady state, or in response to physiological stresses such as bleeding or infection, is a tightly regulated process that is largely governed by cytokines and their cognate receptors. Whilst some cytokines support the development of specific lineages such as the role of erythropoietin (EPO) in the production of erythrocytes (33), colony-stimulating factors (CSFs) in the production of granulocyte-macrophage lineages (34) and thrombopoietin (TPO) in megakaryopoiesis and platelet production (35, 36), other cytokines such as IL-3 stimulate the growth of many haematopoietic lineages (37). The instructive model of haematopoiesis suggests that stimulation of progenitors with specific cytokines direct lineage commitment and differentiation, whilst the permissive model suggests that the role of cytokines is to permit the growth and survival of progenitors in which lineage commitment and differentiation is intrinsically predetermined (37). Evidence of the permissive model of haematopoiesis arose during experiments where ectopic expression of receptors or the use of chimeric receptors indicated that cytokine receptors provide nonspecific survival and proliferation signals. For example the expression of the non-haematopoietic prolactin receptor in primary erythroid progenitors results in the generation of erythroid colonies when stimulated with prolactin (38). Similarly, progenitors that had the endogenous *Mpl* gene replaced with a chimeric construct encoding the extracellular domain of Mpl and the cytoplasmic domain of granulocyte CSF receptor (G-CSFR) exhibited normal levels of megakaryopoiesis and platelet production (39). Conversely, when a chimeric receptor composed of the extracellular domain of human interleukin (IL)-3 receptor and the cytoplasmic domain of granulocyte-macrophage CSF receptor (GM-CSFR) was expressed in murine IL-3 dependent Factor-dependent cell Paterson mixed potential (FSCPmix) cells, differentiation towards the granulocyte and monocyte/macrophage lineage was observed after stimulation with IL-3 (40), suggesting that the cytoplasmic domain delivered an instructive signal influencing lineage commitment. Together, the data suggests that haematopoiesis can exhibit plasticity, however some cytokines can also 'instruct' differentiation.

The concentration of local cytokine levels or strength of cytokine-receptor signalling can also highly influence cell fate. During steady state, low levels of multiple cytokines are sufficient to sustain the normal ratios of blood cells. The increase in local cytokine levels, such as during infection or blood loss, may influence the lineage output of progenitors by instructing lineage fate. For example, increased FMS-like tyrosine kinase 3 ligand (FLT3L) signalling drives myeloid-lymphoid development at the expense of megakaryocyte and erythroid development (41). In addition to the stimulation of megakaryopoiesis from progenitors, TPO has an essential role in HSC self-renewal (42),

which may be linked to the strength of TPO/MPL signalling (43). Studies using TPO agonists and partial agonistic diabodies revealed that the strength of signalling determined cell fate, with stronger signalling associated with megakaryopoiesis whilst weaker signalling was associated with increased HSC self-renewal (43). Clinical application of TPO diabodies have the potential to offer greater control of MPL signalling outputs, resulting in the fine-tuning of cell fate decisions in thrombocytopenic or malignant conditions.

Whilst cytokines are critical for regulated differentiation from HSCs, they are also critical in regulating HSC function itself: including maintenance, quiescence, retention, proliferation as well as indirect effects that exert their effects on HSC activity by influencing the expression of other niche factors (5). Of these, the best characterised are stem cell factor (SCF), TPO and C-X-C motif chemokine ligand 12 (CXCL12). SCF and TPO are essential cytokines that maintain HSCs *in vitro* and *in vivo* (44), whilst CXCL12 is required for HSC maintenance *in vivo* as well as retention in the BM (45-49). SCF binds to c-Kit (44, 50-53), whilst TPO binds to MPL (54-58) and CXCL12 binds to CXCR4 (59), all of which are transmembrane receptors expressed by HSCs. SCF is expressed in both membrane bound and soluble forms, both of which stimulates downstream c-Kit signalling (44, 53, 60). Together, SCF and TPO can maintain HSCs in culture for 28 days with complete media changes (and fibronectin to prevent HSC detachment during media changes) (42).

1.5 The bone marrow niche

Early studies showed that HSCs in culture are dependent upon support from non-haematopoietic BM derived cells (61), and that HSPCs are spatially organised within the BM, with more primitive progenitors residing away from bone surfaces (62). In 1978, Schofield provided the first formal conceptualisation of the BM niche (63). Based upon experimental evidence that CFU-S displayed decreased proliferative potential compared to BM derived HSCs, he proposed that HSCs were functionally dependent on the BM local environment, the so called 'niche' (63). In 2003 the first experimental evidence for the BM niche was obtained, where genetically engineered mice were used to demonstrate that by driving an increase in osteoblastic cells, the number of functional HSCs were increased (64, 65). Further to simply demonstrating the existence of the BM niche, these studies demonstrated that the niche was experimentally tractable, and suggested that osteoblastic cells were important components of the BM niche (later termed the 'endosteal niche').

More recent studies support the existence of a vasculature niche, rather than an endosteal niche. Multiple studies have shown that HSCs are in direct contact or in close

proximity to sinusoidal blood vessels (18, 66-70), where vascular or perivascular cells maintain HSCs through a variety cytokine-cytokine receptor interactions and direct cell-cell contact (45, 60, 71-73). Although HSCs preferentially home to endosteal regions in irradiated mice after transplantation (74), this is thought to be due to the irradiation induced disruption of the sinusoidal network, rather than the endosteum being a preferable site for haematopoiesis (75, 76). Indeed, few HSCs were observed to be in direct contact with osteoblastic cells in non-irradiated mice (67, 74). Finally, mature osteoblasts are not recognised to be major sources of factors needed for HSC maintenance (45, 71, 72), whilst their ablation did not lead to an acute loss in HSCs (77) which is in keeping with the observation that low levels of HSCs are maintained in extramedullary sites such as the spleen throughout life, which does not contain osteoblasts. However, some early lymphoid progenitors do appear to depend on an endosteal niche created by osteoblasts, based upon observations that *Cxcl12* depletion from mature osteoblasts gave significantly lower levels of T and B cell reconstitution in irradiation mice relative to controls, and that ablation of osteoblasts acutely depletes lymphoid progenitors (45, 77).

1.5.1 Niche components

Recent evidence suggests that heterogeneity may exist within the HSC vascular niche, which may be subdivided into the sinusoidal and arteriolar niches, and these different sites may offer differential HSC support. It has been proposed that the degree of niche heterogeneity could match the heterogeneity within the HSC pool and that functional pairings may exist between niche cells and the HSCs which they regulate (78). For example, quiescent stem-like *Nes-GFP^{bright}* BMSCs are found exclusively along arterioles (Figure 1.2), and their ablation causes a migration of dormant HSCs from arterioles to sinusoids and a reduction in their number and long-term repopulating ability (79). However, this is disputed by studies concluding that dividing and non-dividing HSCs do not reside in spatially distinct niches (68-70).

Endothelial cells (ECs) in both sinusoidal and arteriolar niches (Figure 1.2) express key niche factors CXCL12 and SCF (45, 71, 72). Historically, sinusoidal ECs were considered to be the more important EC for HSC maintenance. This was based upon their association with *Cxcl12^{high}* BMSCs which were initially thought to be exclusively peri-sinusoidal (45), and the lack of markers to separate sub-populations of ECs (72). However, recent evidence suggests that arteriolar ECs may produce higher levels of *Cxcl12* and *Kitl* (the gene encoding SCF), and that arteriolar, not sinusoidal ECs regulate HSC maintenance through SCF production (80).

The highest production of CXCL12 in the BM is from perivascular BMSCs (81), with lower amounts expressed by ECs (including arteriolar ECs) and osteoblasts (45, 82). Consistent with the chemotactic role of CXCL12 (46, 83), localisation studies revealed that HSCs are adjacent or close proximity to *Cxcl12*^{high} BMSCs (69, 70), positioning HSCs well for maintenance from other BMSC-derived factors. Indeed, perivascular BMSCs are also major sources of SCF (72), indicating that these cell types are molecularly primed for HSC maintenance. HSCs are depleted in *Sl/S^l* mice (60), which express soluble SCF but not membrane bound SCF (84), providing a functional role for cell-cell contact. Broad deletion of *Cxcl12* from BMSCs and osteoblasts using *Prx1-cre* resulted in HSC depletion and loss of HSC function and BM retention, highlighting the essential role of BMSCs in CXCL12 production (85). However, like the expression of other key niche factors, *Cxcl12* expression in BMSCs is heterogeneous. A recent study using single-cell and spatial transcriptomic approaches identified two distinct *Cxcl12*^{high}*Kitl*^{high} BMSC subsets which expressed adipocyte and osteo-lineage genes differentially, and were found in peri-sinusoidal or arteriolar niches respectively (81). Besides the expression of stem cell maintenance factors, these subsets devoted the largest proportion of their transcriptional activity to cytokine synthesis among all BM cell types, including the main cytokines mediating myeloid and lymphoid differentiation (73, 81, 86). In acknowledgement of their now established broad role in haematopoiesis, perivascular *Cxcl12*^{high}*Kitl*^{high} BMSCs have been referred to as 'professional cytokine-secreting cells' (81, 87).

The adipocyte lineage expressing *Cxcl12*^{high} (Adipo-CAR) BMSCs overlapped considerably with previously described LepR⁺ BMSCs, which when *Cxcl12* was deleted from this population resulted in HSC mobilisation, but not depletion (45, 88). LepR⁺ BMSCs comprise 70% of CD45/Ter119-PDGFR α ⁺ BMSCs (45), therefore are considered a major source of BMSCs. In contrast, osteo-lineage expressing *Cxcl12*^{high} (Osteo-CAR) BMSCs may overlap with previously described *Nes*-GFP^{bright} peri-arteriolar BMSCs. *Cxcl12* deletion from this population causes HSC mobilisation and depletion, indicating that CXCL12 production from *Nes*-GFP^{bright} BMSCs may have a more important role than LepR⁺ BMSCs in HSC maintenance (88). In contrast, *Kitl* deletion from LepR⁺ BMSCs, but not *Nes*-GFP^{bright} BMSCs causes HSC depletion (88). *Nes*-GFP^{bright} BMSCs are innervated by the sympathetic nervous system and are thought to regulate HSC traffic during homeostasis by the downregulation of *Cxcl12* expression during circadian oscillations (89, 90).

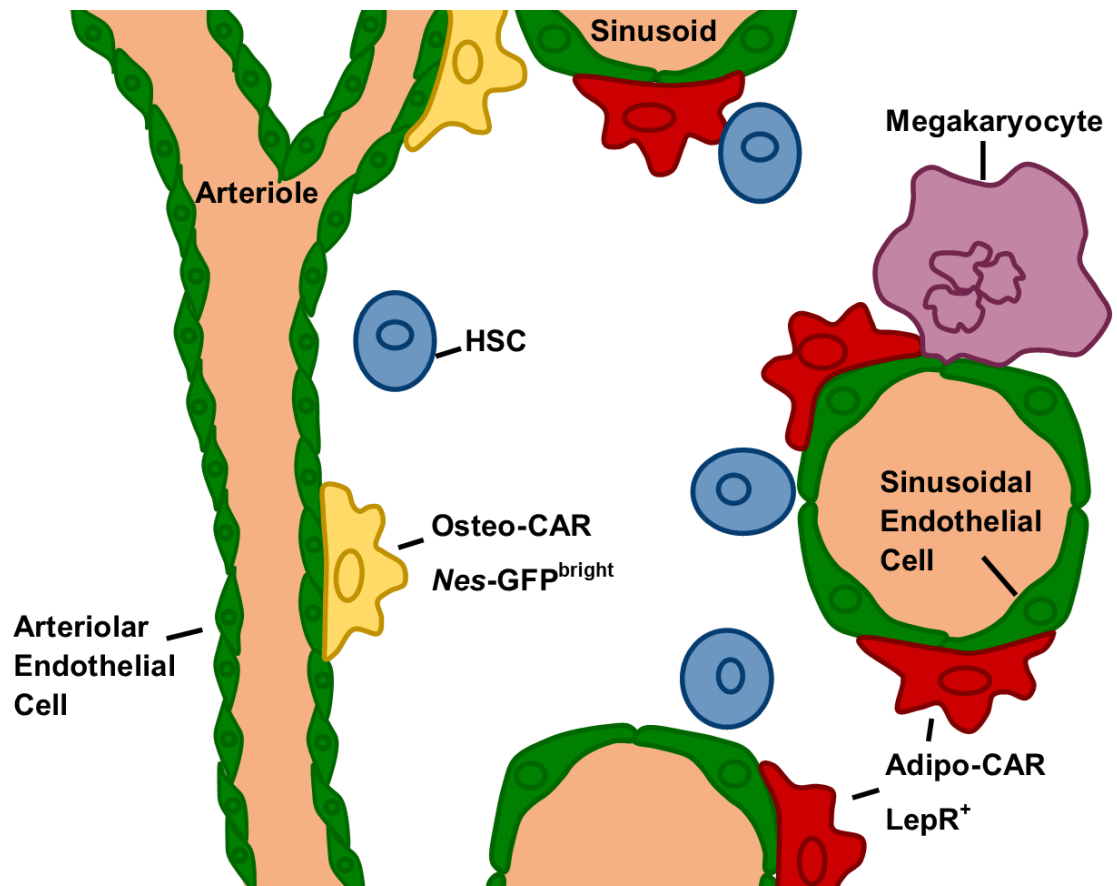


Figure 1.2. The BM niche. HSCs reside in a perivascular niche maintained by a diverse group of cells. Adapted from Crane et al (2)

1.6 Extramedullary niches

Whilst the BM is the primary and preferential site for steady state haematopoiesis in healthy adults, haematopoiesis can occur in almost any tissue (although the most common sites are the liver and spleen) (91). This is termed extramedullary haematopoiesis (EMH) and can occur when HSCs are mobilised and colonise niches in extramedullary tissues. EMH is associated with mobilisation of BM derived progenitors that become entrapped at peripheral sites and proliferate, damage to the BM microenvironment (e.g. during malignancy), or the production of haematopoietic growth factor by a tumour or at sites of tissue damage (91). During steady-state haematopoiesis, the spleen contains approximately 15-fold fewer HSCs than the BM (92). Similar to the BM, perivascular cells in the spleen maintain HSCs through the production of CXCL12 and SCF (93). In parabiosis experiments (an experimental approach where pairs of two CD45.1⁺ and CD45.2⁺ mice were surgically joined together to develop a single, shared haematopoietic system), phenotypic HSCs within the spleen were not replaced by circulating HSCs after 14 weeks (92). This suggests that the perivascular niche cells in the spleen can maintain HSCs long term, and the presence of HSPCs are not simply BM derived circulating cells transiently occupying an extramedullary niche (92). During infection or malignancy, EMH can be driven by loss of BM CXCL12 signalling (94-98), where HSCs leave the BM and populate extramedullary tissues such as the spleen.

1.7 Pathological haematopoiesis

HSCs are highly resistant to stress, which is essential to the preservation of haematopoiesis and homeostasis throughout life. They are highly quiescent (99), which protects them against DNA damage and functional decline associated with metabolic stress and DNA replication errors (100, 101). Additionally, HSCs are autophagy dependent which protects HSCs from metabolic stress, permitting survival and functionality during growth factor fluctuations and nutrient deprivations (102, 103) and are glycolytic which allows for prolonged survival in hypoxic conditions (104). Finally, HSCs synthesise less protein than most haematopoietic progenitors, even when undergoing self-renewing divisions (105), which together with their predisposition to apoptosis after accumulation of misfolded protein (106), may protect the HSC pool against damage accumulation and reduce malignancy risk.

Under steady state conditions, HSCs divide only once every few months (107), however, during stress conditions where demand on haematopoiesis is elevated (such as during blood loss, transplantation or infection), HSCs transiently proliferate and differentiate (activate). Haematopoiesis during infection and inflammation is necessary to drive

expansion of immune effector cells and may be triggered directly such as through stimulation of toll-like receptors (TLRs) expressed by HSCs (108) or indirectly through inflammatory cytokine signalling such as type-I interferon (IFN)- α/β and type-II IFN (IFN- γ) (109-111), IL-1 (112) or G-CSF (113). Whilst these cytokine signals are produced by mature immune cells and components of the BM niche, haematopoietic stem and progenitor cells (HSPCs) can also generate their own cytokine signals such as IL-6 production after TLR activation which acts as an amplification signal both in a paracrine and autocrine fashion (114). In fact, HSPCs are capable of producing far more cytokines in both quantity and breadth than mature myeloid and lymphoid cells which may be important during situations when mature immune cells are depleted such as during transplantation (114).

Stimulatory factors appear to have differential effects on the HSC response, most likely because they selectively target a specific HSC biased subset. For example, during emergency myelopoiesis, G-CSF stimulates multipotent progenitor cell (MPP) 2/3 to contribute granulocyte expansion (115), whilst during emergency megakaryopoiesis type-1 IFN cytokines stimulate rapid maturation of CD41⁺ HSCs in order to replenish the platelet pool (116). Whilst this is essential to control the infection, prolonged signalling impairs self-renewal and may lead to HSC exhaustion (108, 112, 116-118). It is therefore critical that the inflammatory response resolves after the inflammatory insult is cleared. An impaired haematopoietic system, is therefore common in chronic autoimmune or inflammatory diseases and may be characterised by cytopenia, myeloid skewing at the expense of lymphoid production, anaemia or BM failure (119, 120).

1.7.1 Haematopoietic stem cell niche in ageing and disease

Physiological ageing is associated with an increase in phenotypic HSCs (121, 122). However, they are functionally impaired: they exhibit decreased homing efficiency and reconstitution ability, which is driven by an expansion of a myeloid biased subset that outcompetes lineage balanced HSCs by virtue of a superior self-renewal capacity (123-127). Both HSC-intrinsic and extrinsic effects drive HSC impairment, as aged HSCs maintain a lymphoid developmental defect when transplanted into young recipients (124), however aged HSCs have a reduction in myeloid output and engraftment efficiency when transplanted into young recipients (126, 128). Interestingly, myeloid restricted aged HSCs maintain their myeloid restriction when transplanted into young primary recipients, however return to multipotency when transplanted into secondary recipients (127), both confirming the role of an aged BM microenvironment in driving myeloid skewing, and that rejuvenation can occur after exposure to a young BM microenvironment.

Dissection of the aged BM niche revealed significant remodelling such as increased vasodilation, leakiness and imbalances in β_2/β_3 -adrenergic (AR) innervation, changes in niche cellularity and increased local inflammation (128-131). The number of BM ECs decrease with age which is associated with the downregulation of *Kitl* and *Cxcl12* production (129). Infusion of aged ECs into mice promoted a myeloid bias and inhibited HSC engraftment, whilst the infusion of young ECs promoted rejuvenation of HSCs by increasing their lymphocyte output and engraftment ability (129). Aging could also be partially reversed by treating mice with β_3 -AR which reduced HSC number and myeloid skewing, whilst improving repopulating after transplantation (130, 131). Finally, aging is associated with BMSC expansion; however they have reduced expression of key maintenance factors and are primed towards adipogenesis which is known to be detrimental to HSC function (129, 131-134).

Similarities between the processes of normal ageing and chronic inflammation (e.g. myeloid skewing, pro-inflammatory microenvironment) has led to the hypothesis that the two may be mechanistically linked (135). Levels of circulating pro-inflammatory cytokines are upregulated in elderly populations (136), leading to the hypothesis that subclinical inflammation may contribute to the initiation and/or acceleration of haematopoietic aging (135).

Malignancy and infection may also contribute to a reduction in healthy haematopoiesis in the BM niche. Oncogenic mutations in niche cells (such as loss-of-function mutations in the *SBDS* gene) can stimulate the secretion of pro-inflammatory factors (137, 138), whilst malignant haematopoietic cells can drive transformation of niche cells which reduces their capacity to support healthy haematopoiesis (95, 139). Aside from the development of inflammation during infection, infection can decrease the number of niche cells which compromises haematopoietic support (96, 97). Together, evidence suggests that the BM niche has a reduced capacity to support healthy haematopoiesis during normal physiological aging, and during the progression of malignancy and infection.

1.8 Thrombopoietin

1.8.1 Thrombopoietin biology: haematopoietic stem cell self-renewal and megakaryopoiesis

As described earlier, TPO is one of two essential cytokines that can maintain HSCs *in vitro* for up to 28 days, with the other being SCF (42). Patients with congenital amegakaryotic thrombocytopenia have loss-of-function mutations in *MPL* or *THPO* which cause an age progressive loss of HSCs, leading to BM failure (140, 141).

Similarly, *Thpo*^{-/-} and *Mpl*^{-/-} mice progressively lose HSC numbers with age, translating to a 150-fold reduction in 1-year old *Thpo*^{-/-} mice (142).

The role of TPO as a humeral factor with a major role in platelet production was first identified in the 1950s based upon the observation that plasma from patients with essential thrombocythemia raises the platelet count of recipients when infused into normal individuals (143), however it was not until 1994 that TPO was cloned and purified, and was directly shown to drive megakaryopoiesis *in vivo* and *in vitro* (54, 56-58). TPO is indispensable for megakaryopoiesis, although other factors such as SCF, IL-3 and IL-11 can augment Mk production in the presence of TPO (35, 36). Although MPL is expressed on both haematopoietic progenitors and Mks (35), TPO acts on progenitors upstream of Mks and MPL expression on Mks is dispensable for thrombopoiesis (144). More recent evidence indicates that TPO does not play an instructive role in the fate of uncommitted progenitor differentiation; rather, it enhances the proliferation, survival and differentiation of already committed Mk progenitors (145, 146).

1.8.1.1 *Thrombopoietin regulation.*

TPO is produced by the liver, and to a lesser extent the kidney (55, 57, 147, 148), representing the only known distal maintenance factor in the mammalian haematopoietic system (147). Results from early studies indicated that TPO may be produced locally at trace amounts in the BM and this expression may be inducible in response to thrombocytopenia (discussed in greater detail below) (148-150). TPO levels are thought to be partially regulated by platelet mass, based upon the capacity of platelets to bind, internalise and destroy TPO and the observation that platelet levels are inversely proportional to circulating TPO levels (151, 152). Mks may also control TPO levels through a similar mechanism, and may partially explain why patients with immune thrombocytopenia (associated with an increase in BM Mks) have normal TPO levels, which is in contrast to conditions of hypoproduction of Mks (such as aplastic anaemia and BM hypoplasia) where patients have increased levels of circulating TPO (153). The removal of aged, desialylated platelets by the hepatic Ashwell-Morell receptor (AMR) induces hepatic expression of TPO and therefore represents an additional mechanism of TPO production (154). This discovery demonstrated that TPO production is regulated and challenged the notion that TPO expression in hepatocytes is constitutive. The AMR signalling cascade shares similarities with IL-6R signalling on hepatocytes (154, 155), which is known to increase TPO during inflammation (156-158).

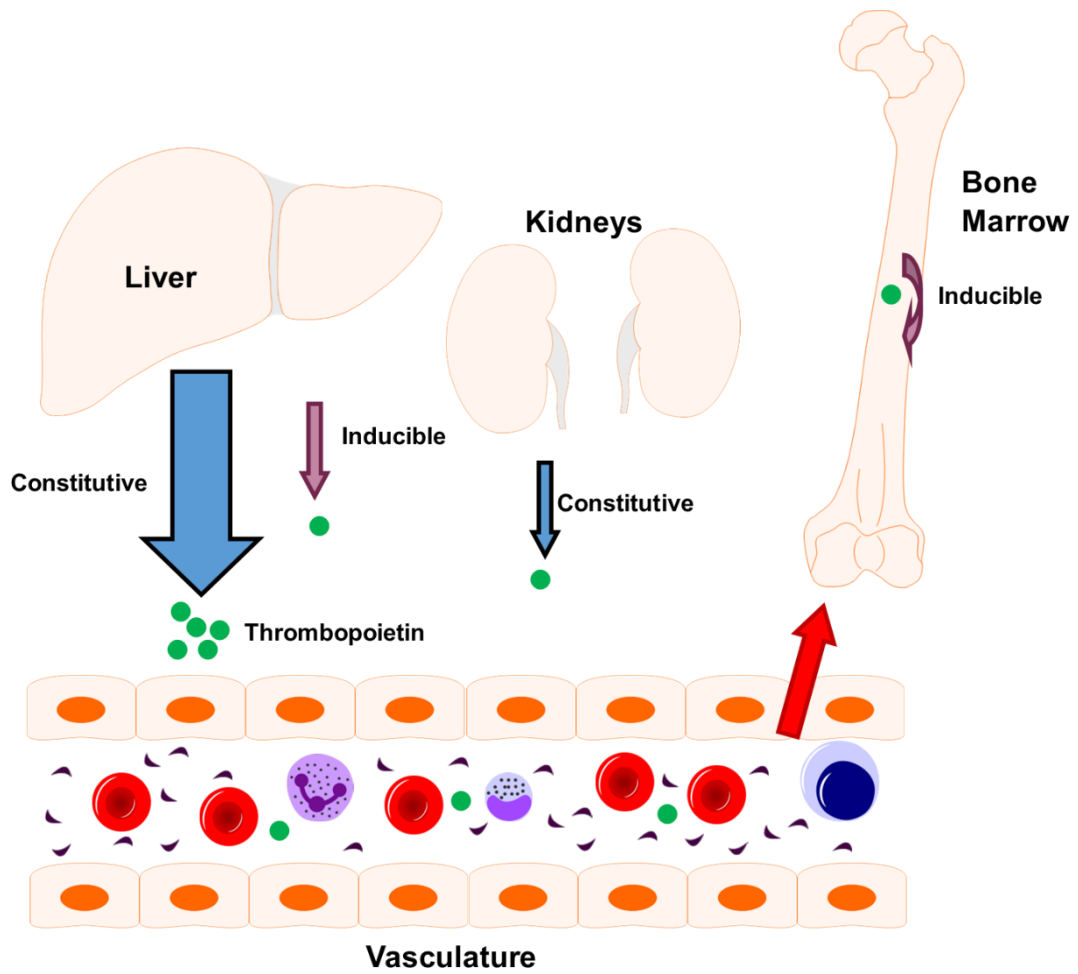


Figure 1.3 Regulation of TPO. TPO is primarily produced by the liver and to a lesser extent the kidneys, where it travels through the circulation to act on Mpl expressing cells in the BM. TPO production is both constitutive (blue arrows) and inducible (red arrows). The binding of desialylated platelets by the hepatic AMR induces TPO production from the liver, whilst thrombocytopenia or irradiation causes local TPO upregulation by BMSCs. The level of circulating TPO is regulated by binding to Mpl expressing platelets and Mks

1.8.2 Bone marrow sources of thrombopoietin

The earliest report that the BM may produce TPO locally was in 1996, two years after the discovery of TPO. Nagahisa and colleagues showed by qPCR analysis that as well as liver and kidney, mouse whole BM was a local source of *Thpo* expression (159). This was confirmed at the protein level by a cell reporter assay, where they transfected IL-3-dependent mouse proB cells (BaF3 cells) to express human or mouse MPL (BaF3-MPL). They found that the mouse stromal PA6 cells or primary mouse BMSCs support the growth of BaF3-MPL but not BaF3 parental cells in the absence of IL-3. Later, cultures of human BMSCs were shown to produce low levels of TPO at the gene and protein level (150).

In 1997, the first attempt to map BM *THPO* expression was through in situ hybridisation (148). Using BM trephines from: 1) subjects with a normal platelet count, 2) patients with thrombocytosis, 3) patients with marrow aplasia (severe aplastic anaemia or postchemotherapy aplasia), or 4) patients with thrombocytopenia (immune thrombocytopenia [ITP] or secondary ITP), Guerriero and colleagues reported expression by BMSCs. Intriguingly, whilst very weak hybridisation signal was detected in BMSCs from the subjects with normal platelet counts and reactive thrombocytosis, this increased in patients with marrow aplasia and patients with thrombocytopenia. The strongest staining observed was in the BMSCs of a patient with Hodgkin's disease and secondary thrombocytopenia. However, whilst an important discovery, the results were somewhat limiting as the identification of the BMSCs appeared to be based on their morphology as no further probes to confirm their stromal identity was performed.

Despite this limitation, the discovery that the BM was able to respond to conditions of haematopoietic stress by *THPO* upregulation was important as it supported the idea that the paracrine production of TPO serves to fine tune HSC homeostasis and platelet production. Furthermore, this phenomenon appeared to be BM specific, as no upregulation was observed in the liver or kidney. This confirmed a finding by McCarty and colleagues showing that acute antibody mediated thrombocytopenia or BM suppression by irradiation or carboplatin causes *Thpo* upregulation in the whole BM of mice whilst *Thpo* levels in liver or kidney remained constant (149). Subsequent experiments suggested that this was in response to low platelet counts rather than high TPO levels following the discovery that platelet granule proteins suppress the production of *Thpo* production in OP9 cells (160) (a murine BMSC line).

Yoshihara and colleagues used a TPO specific antibody to identify osteoblasts as the TPO producing cells in murine BM sections (161). This supported the idea of an endosteal niche at the time, where osteoblasts are thought to maintain HSC quiescence

over the long term (162). The same laboratory later used a different anti-TPO antibody to confirm that osteoblasts produce TPO, but in addition showed that Mks produce TPO at the protein level (163). Surprisingly, they showed by qPCR analysis that Mks express significantly higher amounts of *Thpo* than non-haematopoietic niche cells (BMSCs, osteoblasts and ECs) and that *Thpo* transcript levels increased with Mk ploidy. They noted that more than half of all LT-HSCs reside < 3 cell diameters apart from Mks, suggesting that Mks may have important paracrine influences on progenitor function. Mk depletion resulted in a decrease in BM, but not serum TPO levels and a decrease in LT-HSC number. *In vitro* culture of Mks and HSCs show that Mks support HSC number through TPO secretion; TPO neutralisation using soluble Mpl or *Thpo* knockdown in Mks supported fewer HSCs. In a follow up paper, they showed that Mk derived TPO production was dependent on CLEC-2 signalling, and that mice deficient in CLEC-2 specifically in the Mk lineage (*PF4-Cre:Clec2^{flox/flox}*) had a bias towards immature Mks of lower ploidy and HSCs that were less quiescent and had reduced stem cell potential (164).

In 2016, it was known that BMSCs as a whole produce TPO (148, 159, 160, 165, 166), however the exact subsets necessary to maintain HSCs remained elusive. The first 18 months of my PhD were dedicated to the identification of TPO expressing BMSCs using a combination of murine BM and human BMSC clonal cell lines. Thereafter, I researched haematological and immunological changes during ITP progression using a murine mouse model. Introduction to ITP and important cell players in ITP will be covered in the remainder of this section.

1.9 Overview of the immune system

1.9.1 Innate immune system

The innate immune system is an evolutionary conserved host defence system dependent on the activity of cell dependent mechanisms such as phagocytosis and cytotoxicity, or secreted factors such as complement and antimicrobial peptides (167). Innate immune responses recognise conserved features of pathogens and are able to respond quickly to insults, therefore are important during the initial containment of the infection. Mature cells of the innate immune system include granulocytes comprising neutrophils, eosinophils, basophils and mast cells and monocytes/macrophages and dendritic cells. Monocytes, macrophages and dendritic cells will be briefly introduced here due to their relevance in subsequent chapters.

Monocytes are phagocytic myeloid cells present in several organs including the BM, blood and spleen. Classical monocytes are Ly6C⁺ and are recruited to sites of infection and inflammation where they terminally differentiate into macrophages (168). They are

best known for their replenishment of monocyte-derived tissue macrophages in the gut, skin, heart and lung (169). However, they can also be considered as having effector function themselves, as under homeostatic conditions classical monocytes have been described to adopt a surveillance role where they enter non-lymphoid organs and upregulate MHC class II molecules (MHC II), before recirculating to secondary lymphoid organs to present antigen to T cells (170). They are also steady state precursors of Ly6C⁻ patrolling monocytes (171), which as the name suggests, patrol the vascular endothelium and monitor its integrity (172). Patrolling monocytes are intravascular housekeepers which sense the perturbation of homeostasis (e.g. viral infection or local cell death), and contribute to its resolution by the removal of cellular debris and the recruitment of neutrophils to mediate necrosis of ECs (173).

Macrophages are specialised non-migratory phagocytic cells that remove cellular debris and hazardous material (including pathogens) by phagocytosis, followed by degradation and neutralisation of the ingested material by the formation of the phagolysosome (174). This is achieved by the direct recognition of apoptotic cells and pathogens through pathogen-associated molecular patterns or danger-associated molecular patterns as well as the indirect recognition of targets through their coating in antibodies and complement components (opsonisation), which are in turn recognised by receptors on the macrophage surface. For example, autoreactive antibodies contribute to the destruction of platelets by macrophages through opsonisation mediated phagocytosis in ITP. In addition, macrophages direct the inflammatory response by the production of chemokines and cytokines that recruit and activate other immune cells as well as contributing to tissue repair after resolution of inflammation (175). Under steady states, the majority of macrophages that reside in healthy tissue are established prenatally and self-maintain through their self-renewal ability and longevity. Here, they monitor their local environment through the expression of a range of receptors and adhesion molecules. In contrast, classical monocytes act as a reservoir for rapid macrophage recruitment. Under inflammatory conditions, classical monocytes infiltrate into tissues and differentiate into macrophages where they perform their effector functions associated with the initiation and subsequent resolution of the inflammatory reaction. However, in tissues such as the intestine, skin and heart, monocyte infiltrates represent major sources of macrophages under steady state conditions (176).

Dendritic cells (DCs) are specialised antigen-presenting cells with essential roles in controlling immunity and tolerance (177), which originate from a DC restricted progenitor downstream of the monocyte-dendritic cell progenitor (178, 179). DCs are a

heterogeneous group of cells that upon activation and capturing of antigen, migrate to T cell zones in the spleen or lymph nodes to present antigen to naïve T cells.

1.10 T cell overview

T cells originate from BM progenitors that migrate to the thymus where they mature and undergo selection processes to select for clones that recognise self-antigen (positive selection), but remove clones that are strongly self-reactive (negative selection), before emigrating to the periphery (180). Peripheral naïve T cells express a diverse repertoire of different T cell receptors that are generated during maturation in the thymus, allowing for recognition of a wide variety of antigen (181). Recognition of antigen and co-stimulatory ligands leading to subsequent activation and clonal expansion occurs via interactions with antigen presenting cells (APCs) presenting antigenic peptides bound to a MHC I or II molecule (182). T cells are subdivided into CD4⁺ or CD8⁺ cells based on expression of CD4 or CD8 glycoproteins. CD4⁺ cells broadly have a 'helper' function: they activate naïve B cells which in turn leads to the production of antibodies, activate and recruit phagocytes to the site of infection, and activate CD8⁺ cells (183, 184). CD8⁺ cells on the other hand broadly have a cytotoxic function: they eliminate infected and cancerous cells through the release of cytotoxic granules such as perforin and granzymes (185). Naïve CD4⁺ cells differentiate into different subsets including Th (T helper cells) 1, Th2, Th9, Th17, Th22 and Treg (regulatory T cells) and Tfh (T follicular helper cells) based upon the local inflammatory environment created by the innate immune system (186). Therefore the T cell response is tailored to the specific immunological challenge. For example, Th1 differentiation is induced by IL-12 and IFN γ , whilst Th2 differentiation is induced by IL-4. Each Th subset in turn secretes specific cytokines to fine tune the immune response e.g. with pro- or anti-inflammatory or survival or protective functions (186). These cytokines can feed back into the local immune environment, for example activating neighbouring cells like macrophages to increase their phagocytic and antigen presenting properties (182).

Tregs regulate or suppress persistent or excessive immune responses which may otherwise cause immunopathology (187). Tregs can suppress different immune cells directly or indirectly: direct mechanisms include the secretion of suppressive cytokines such as IL-10 and TGF β or the production of granzyme and perforin to kill autoreactive cells, whilst indirect mechanisms include starving the local microenvironment of proliferative factors (188, 189). Tregs are identified by the expression of FOXP3 and can be produced during thymic selection as well as being induced by suppressive cytokines such as TGF- β (190). Tregs are heterogeneous and can be divided into resting and activated (rTreg and aTreg) cells based on the expression of homing (CD62L) and

activation (CD44) molecules (191). aTregs are more suppressive, shorter lived and are enriched in peripheral tissues whilst rTregs are quiescent and enriched in secondary lymphoid organs (191).

Differentiation of naïve T cells into Tfh cells is induced by IL-21 and IL-27 which stimulates the migration to B cell follicles in secondary lymph nodes where they assist in the germinal centre reaction of B cells. Tfh cells are characterised by the expression of CXCR5 and PD-1 which are involved in follicular recruitment (192, 193).

After pathogen clearance, the majority of antigen specific T cells die leaving behind a pool of long-lived memory cells. Central memory T cells (T_{CM}) and effector memory T cells (T_{EM}) are $CD62L^{high}CD44^{high}$ and $CD62L^{low}CD44^{high}$, respectively and exist within each of the $CD4^+$ or $CD8^+$ subsets (194). The high expression of CD62L on T_{CM} cells allow for preferential homing to secondary lymphoid organs where they proliferate in response to antigen and produce high numbers of new effector cells. Similarly, naïve T cells express high levels of CD62L, allowing for homing to the secondary lymphoid organ and increasing the likelihood of encounter with their specific antigen presented by APCs. On the other hand, low expression CD62L on T_{EM} cells results in trafficking through nonlymphoid tissues at sites where reinfection could occur, therefore acting as 'first responders' where they display rapid effector function (e.g. granzyme B and IFN γ production) (182).

1.11 T cell activation

T cell activation is tightly regulated in order to prevent reactivity and damage to self-tissue. As such, two or three signals are required for T cell activation, otherwise the T cell becomes unresponsive (anergic) and cannot develop an effector response (195). The first of these signals is TCR recognition of antigen presented by MHC molecules. $CD8^+$ T cells recognise MHC I which are expressed on the surface of all cells except erythrocytes and present endogenously generated peptides, whilst $CD4^+$ T cells recognise MHC II which are expressed by antigen presenting cells and present peptides derived from extracellular proteins. The second is the receipt of co-stimulatory signals generated by the engagement of CD28 on the surface of naïve T cells with its ligands B7-1 and B7-2 on APCs. B7-1 and B7-2 are constitutively expressed at low levels, however expression is upregulated during APC activation (196, 197). CD28 signalling induces a transcriptional program resulting in IL-2 production (a T cell proliferative factor) and expression of members of the TNF receptor superfamily, which promote the survival of proliferating T cells through the differentiation process when interacting with their specific con-stimulatory ligand on APCs (182, 198). Many costimulatory ligands required for T cell activation require activation of the APC before expression on its

surface. In the absence of this activation, T cell interactions with its specific antigen on resting APCs result in anergy and immune tolerance which is necessary to remove self-reactive T cells and protect against autoimmunity (182). Therefore innate inflammatory signals are necessary to bridge the innate immune system with the adaptive.

1.12 B cell overview

B cells are responsible for the production of antigen-specific immunoglobulin (antibodies) directed against foreign antigens, which are secreted by terminally differentiated B cells known as plasma cells. B cell development begins in the BM with subsequent functional maturation occurring in the secondary lymphoid tissue. Additionally, as APCs, B cells are responsible for the initiation of T cell immune responses (199).

1.13 ITP

1.13.1 Definition and epidemiology

Primary ITP is an acquired autoimmune disorder characterised by isolated thrombocytopenia (platelet count $< 100 \times 10^9/L$ compared to the normal range of $150-450 \times 10^9/L$ in humans) due to the destruction of functionally normal platelets and impaired platelet production (200). Primary ITP can present as a bleeding phenotype, which is typically mild such as bleeding in skin and mucosal regions, however bleeding may also occur as a more life-threatening form such as in gastrointestinal or intracranial areas (200). ITP patients with platelet counts above $50 \times 10^9/L$ rarely bleed (201), however a platelet count below this threshold is not necessarily a good prediction of bleeding tendency (202-204). Indeed, the majority of children with newly diagnosed ITP lack significant bleeding despite having a platelet count of $< 50 \times 10^9/L$ and therefore a 'watch and wait' policy is preferred by clinicians, where intervention to raise platelet count is based on symptoms rather than counts (205). Incidence of primary ITP is 2-5 per 100,000 (206-208), and primary ITP patients can be classified as 'newly diagnosed' (< 3 months) or 'persistent' (< 12 months) which is more common in children, as well as 'chronic' (> 12 months) which is more common in adults (200, 209). The initiating events of primary ITP remain unclear, however the involvement of autoantibodies and autoreactive $CD8^+$ T cells are strongly implicated in platelet destruction and impaired platelet production.

In adults, primary ITP accounts for approximately 80% of ITP (210) and is the focus of this research. The remainder of ITP patients develop ITP secondary to another condition (termed 'secondary ITP') such as: other autoimmune disorders including systemic lupus erythematosus, antiphospholipid syndrome and thyroid disease; lymphoproliferative

disorders; chronic infection by infectious agents such as human immunodeficiency virus and *Helicobacter pylori*; and drug induced thrombocytopenia (211). Therapy for secondary ITP is different from primary ITP as it requires treatment of the underlying condition.

However, there are suggestions that this distinction between primary and secondary ITP is somewhat outdated. Even in patients with primary ITP (hereafter referred to as 'ITP'), there must be a triggering event that initiates the autoimmune response against platelet antigens (201). In other autoimmune diseases, infection is recognised as this trigger (212), however in ITP this is considered a secondary form. Furthermore, patients with a pre-existing autoimmune disease are more likely to develop ITP, suggesting that a dysregulated immune system may contribute to ITP disease progression. In light of this, Swinkels and colleagues (201) proposed a simplified model of ITP in which both loss of immune tolerance and exposure of platelet antigens (such as during infection) are required to induce ITP. Transient forms of ITP may develop if CD4⁺ T cell help is insufficient, which is required for the generation of a strong anti-platelet antibody response.

1.13.2 Aetiology

1.13.2.1 Autoantibodies

In 1951, Harrington and colleagues transfused 5 L of whole blood or plasma from ITP patients into non-thrombocytopenic recipients (213). The majority of recipients developed transient (often dramatic) thrombocytopenia, demonstrating the presence of a 'thrombocytopenic factor' in the blood or plasma from ITP patients. It is now known that this 'thrombocytopenic factor' was a cocktail of autoantibodies specific for platelet glycoproteins or glycoprotein complexes. Approximately 60% of patients have detectable circulating autoantibodies (201). These are predominantly against platelet glycoprotein (GP) IIb/IIIa (~70%) and/ or the GP Ib-IX-V complex (~25%), whilst a minority are against GPIa-IIa or GPVI (214-216). The autoantibodies are generally of the IgG class, but IgA and IgM autoantibodies have also been reported (217). Plasma cells are found in the peripheral blood and BM, where they secrete platelet-reactive autoantibodies that bind to platelets and Mks (218).

1.13.2.2 CD8⁺ T cells

Autoantibodies cannot be detected in up to 40% of ITP patients (201), suggesting that alternative mechanisms of platelet destruction exist, independent of autoantibody mediated autoimmunity. This was demonstrated in the experiments performed by Harrington and colleagues, as not all blood or plasma from ITP patients caused transient thrombocytopenia in recipients (213). In these patients, platelet destruction is thought to

be driven by autoreactive CD8⁺ T cells (219), which are preferentially found in the spleen of ITP patients that do not respond to the B cell depleting antibody rituximab (220). CD8⁺ T cells are capable of directly lysing platelets (221, 222), triggering platelet apoptosis (222) and inhibiting Mk apoptosis (223). Similar to anti-GPIb α antibody binding (discussed in 1.13.2.4), CD8⁺ T cells are thought to trigger desialylation through sialidase translocation (224). However, the exact mechanism behind this remain elusive.

1.13.2.3 Role of the spleen in ITP

The spleen is the primary site of platelet destruction, and autoantibody production (225, 226). Approximately 80% of ITP patients receiving a splenectomy have a raised platelet count to $> 200 \times 10^9$ for at least one year (227). Splenic macrophages and dendritic cells bind opsonised platelets through their Fc γ -receptors (Fc γ Rs), resulting in phagocytosis and destruction of the antibody-platelet complex (228). Following this, platelet antigens are presented to Th cells. ITP patients have an increased Th1/Th2 ratio, indicating a Th1 polarised immune response (229, 230). This is increased in patients with low platelet counts (231) and corrected following splenectomy or rituximab treatment (232, 233). Splenic Tfh cell frequency is also increased in ITP, which drives B cell differentiation and autoantibody production (234).

ITP patients also display decreased numbers and function of Tregs (235), which act to suppress T cell activation and proliferation, as well autoreactive B cells and T cells (189, 236, 237). Treatment with corticosteroids and/or rituximab in responding patients helped to revert this phenotype (232, 238, 239).

1.13.2.4 Platelet desialylation

15-20% of ITP patients are refractory to first-line therapies such as immunosuppressive and immunomodulatory agents and even splenectomy (240, 241). Within this cohort, levels of platelet desialylation are increased (242), and platelet clearance is thought to occur independently of Fc mediated clearance via hepatocyte Ashwell-Morrell receptors (243). Platelet desialylation is triggered by anti-GPIb α , but not anti-GPIIb/IIIa through platelet activation causing surface expression of sialidase (243, 244). Anti-GPIb α antibodies bind to the GPIb α subunit of GPIb-IX, crosslinking platelets and unfolding its mechanosensory domain (MSD) under shear flow (245). In turn, the unfolding of the MSD leads to intracellular signalling events, including desialylation and platelet clearance.

1.13.2.5 Impaired platelet production

Platelet turnover studies have demonstrated that as well as increased platelet destruction, impaired platelet production contributes to the low platelet counts in ITP (246, 247). Mks express the common ITP autoantigens (GPIIb-IIIa and GPIb-IX) (248),

therefore Mks are similarly susceptible to humeral and cellular autoimmune responses. Additionally, autoantibodies have been visualised binding to Mks in BM of ITP patients (249).

1.13.3 Immune thrombocytopenia treatment

Newly diagnosed adults with a platelet count $< 30 \times 10^9/L$ who are asymptomatic or have minor mucocutaneous bleeding are typically managed with a low dose of corticosteroids such as prednisone or dexamethasone, which may be combined with IVIG (200). In contrast, a 'watch and wait' policy is preferred patients with a higher platelet count. Patients with persistent ITP who are corticosteroid dependent or unresponsive to treatment are typically treated with a TPO receptor agonist (TPO-RA) such as eltrombopag or romiplostim, however rituximab may be preferred if the patient wishes to avoid long term medication (200). For patients with chronic ITP, a combination of TPO-RA, splenectomy and rituximab is preferred according to the patient's values and preferences (200, 250).

1.14 Research aims

This thesis aimed to explore how haematopoiesis is maintained under normal conditions and during ITP progression and had two overarching aims:

- 1) To characterise the sources and roles of BM derived TPO in HSC self-renewal.

This was achieved using murine BM and aided by using a panel of human BMSC clonal cell lines (Chapter 3).

- 2) To characterise the immune and haematopoietic system using a murine model of sustained ITP.

This was achieved by:

- a. Developing and characterising a murine model of sustained ITP (Chapter 4).
- b. Studying the effect of ITP progression on the immune system using the model of sustained ITP (Chapter 5).
- c. Studying the effect of ITP progression on the haematopoietic system using the model of sustained ITP and human ITP patient BM aspirates (Chapter 6).

2 General materials and methods

2.1 Cell culture

2.1.1 Cell culture plasticware and reagents

Tissue culture plates and pipettes were purchased from Sarstedt. Dulbecco's Modified Eagle Medium (DMEM), and Opti-MEM Reduced Serum Medium were supplemented with 10,000 U/mL penicillin-streptomycin (PS), 200 mM L-glutamine (G) and trypsin-EDTA (0.05%), all purchased from Life Technologies. Additionally, DMEM was supplemented with Fetal Bovine Serum (FBS) purchased from Hyclone.

2.1.2 Cell line culture conditions

Immortalised human BMSC clonal lines (Y101, Y102, Y201, Y202, Y204, Y205, Y301, Y302) were generated by James et al (251). This was achieved by using a lentiviral expression system to overexpress human telomerase reverse transcriptase (hTERT) in primary BMSCs which were derived from one donor to protect against inter-donor variation. Clonal lines were derived from single-cell-derived colonies and were selected for their strong clonal and stable growth characteristics. Clonal lines were used between passage 50-100.

BHK-IL3 and BHK-TPO are baby hamster kidney fibroblasts transfected to overexpress IL-3 and TPO respectively (55), which is used as a recombinant source of IL-3 and TPO protein in cell culture assays. HepG2 cells are a hepatocellular carcinoma cell line and were purchased from ATCC.

All cell lines were incubated at 37 °C in a humidified atmosphere of 5% CO₂ in DMEM supplemented with 10% FBS, 1% PSG. All cells were plated at 70% confluency and were passaged at ~90% confluency. Media change was twice a week.

2.2 RNA isolation

2.2.1 Cells: RNeasy mini kit

Total RNA was isolated using the RNeasy Mini Kit (QIAGEN) as instructed by the manufacturer. Cells were lysed in buffer RLT + 10 µL/ml β- mercaptoethanol and stored at -80 °C until use.

Thawed samples were vortexed thoroughly and mixed with 1 volume of 70% ethanol. This was then loaded onto an RNeasy spin column and centrifuged for 15 sec at 8,000 g. Contaminating gDNA was digested with DNase I in Buffer RDD (QIAGEN) for 20 min at room temperature. Samples were washed with Buffer RW1, followed by centrifugation for 15 sec at 8,000 g. Samples were then washed twice with Buffer RPE, followed by a final centrifugation for 2 min at 8,000 g to dry the membrane and ensure that no ethanol

was carried over during RNA elution. RNA was eluted from the membrane by the addition of RNase-free water and collected by centrifugation at 8,000 g for 1 min. RNA concentration was quantified using a Nanodrop 2000 Spectrophotometer (ThermoScientific) and purity indicated by the A260/A280 ratio. An absorbance of ~2.0 was accepted as “pure” for RNA.

2.2.2 Whole organs: Trizol plus miRNAeasy mini kit

Total RNA was isolated using the miRNeasy Mini Kit (QIAGEN). Tissue was lysed in 700 μ L QIAzol Lysis Reagent with thorough vortexing and pipetting for disruption and homogenisation. Samples were stored at -80 °C until required.

Thawed samples were incubated at room temperature for 5 min before proceeding with RNA isolation. 200 μ L chloroform was added and the tube vigorously shaken for 15 sec, followed by incubation at room temperature for 3 min. Samples were centrifuged for 15 min at 12,000 g (4 °C) for phase separation. The aqueous phase RNA containing phase was transferred to a separate collection tube and mixed with 1.5 volumes of 100% ethanol, which was then loaded onto an RNeasy spin column and centrifuged for 15 sec at 8,000 g. Contaminating gDNA was digested with DNase I in Buffer RDD (QIAGEN) for 20 min at room temperature, which were then washed with Buffer RW1, followed by centrifugation for 15 sec at 8,000 g. Samples were then washed twice with buffer RPE, followed by a final centrifugation for 2 min at 8,000 g to dry the membrane and ensure no ethanol is carried over during RNA elution. RNA was eluted from the membrane by the addition RNase-free water and collected by centrifugation at 8,000 g for 1 min. As an alternative to quantification using the Nanodrop, the Qubit RNA HS Assay Kit (Molecular Probes) was used to determine the RNA concentration of samples as per the manufacturer’s instructions. This is because components of the QIAzol Lysis Reagent such as phenol strongly absorbs near 280 nm, and so can give inaccurate readings. The Qubit RNA HS Assay Kit relies on ability of fluorescent binding dyes rather than absorbance to quantify RNA concentration, and is therefore tolerant of contaminants.

2.2.3 Sorted cells: Manual QIAzol method

Cells were sorted directly into 700 μ L QIAzol Lysis Reagent and immediately placed on ice until the sample could be stored at -80 °C. Thawed samples were incubated at room temperature for 5 min before proceeding with RNA isolation. 200 μ L chloroform was added and the tube vigorously shaken for 15 sec, followed by incubation at room temperature for 3 min. Samples were centrifuged for 15 min at 12,000 g (4 °C) for phase separation. The aqueous phase RNA containing phase was transferred to a separate collection tube, with 10 μ g of glycogen (Invitrogen) added as a carrier. 1.5 volumes of 100% isopropanol was mixed with the sample and incubated for 10 min at 4 °C, followed

by centrifugation at 12,000 g (4 °C) for another 10 min. The supernatant was removed with a micropipettor and washed with 1 ml of 75% ethanol, followed by centrifugation at 7500 g (4 °C) for 5 min. The supernatant was aspirated with a micropipettor and then air dried for 10 min. RNase-free water was added to solubilise the RNA pellet, followed by incubation at 60 °C for 10 min. The Qubit RNA HS Assay Kit (Molecular Probes) was used to determine the RNA concentration as described previously.

2.3 Reverse transcription polymerase chain reaction

2.3.1 High input (cells/whole organs): High Capacity Reverse Transcription Kit

cDNA was derived from total RNA of cell lines using High Capacity cDNA Reverse Transcription Kit (Applied Biosystems). RNA, 10X RT Buffer, 10X RT Random Primers, 25X dNTP Mix (100 mM) and Multiscribe Reverse Transcriptase (50 U/μL) were combined in a sterile 0.2 mL polymerase chain reaction (PCR) tube and incubated at 25 °C for 10 min, 37 °C for 120 min and terminated by heating to 85 °C for 5 min. Samples were then cooled to 4 °C.

2.3.2 Low input (sorted cells): Superscript IV

cDNA was derived from total RNA of sorted cells and whole tissue using SuperScript IV First-Strand Synthesis System (ThermoFisher Scientific). RNA, 10 mM dNTP mix and 50 μM random hexamers were heated together in a sterile 0.2 mL PCR tube at 65 °C for 5 min, and then incubated at 4 °C for 2 min. A 2X reaction mastermix was prepared by combining 5x SSIV Buffer, 100 mM DTT, RNaseOUT Recombinant RNase Inhibitor and Superscript IV Reverse Transcriptase (200 U/μL), and combined with the annealed RNA. The samples were heated to 23 °C for 10 min, 53 °C for 10 min and terminated by heating to 80 °C for 10 min. Samples were then cooled to 4 °C.

2.4 Mouse models

All mouse strains were developed on the C57/Bl6 background apart from the NSGSGM3 mouse strain which was developed on a NOD background. Male and female mice were used between 8-12 weeks of age.

Table 1. Mouse models

Mouse Strain	Method of Generation	Phenotype
<i>Cxcl12^{DsRed/+}</i>	A <i>DsRed Express 2-polyA-Frt-Neo-Frt</i> cassette was inserted into exon 2 of <i>Cxcl12</i> to identify <i>Cxcl12</i> expressing cells in the BM (45).	<i>Cxcl12^{DsRed/+}</i> mice have no known effects on the haematopoietic system (45). <i>Cxcl12^{DsRed/DsRed}</i> mice were not born alive, as CXCL12 is required for perinatal survival (252).
<i>Thpo^{-/-}</i>	The insertion of a <i>neo^r</i> cassette removed 23 amino acids of the third coding exon of <i>Thpo</i> (253).	<i>Thpo^{-/-}</i> mice have a > 80% decrease in Mk and platelet number, as well as an age progressive loss of HSCs (142, 253).
<i>FcRγ^{-/-}</i>	The insertion of the poly(A) trap vector pMC1- <i>neo</i> into exon 2 of the γ subunit gene which generated a premature stop codon (254).	<i>FcRγ^{-/-}</i> mice do not express FcγRI, FcγRIII and FcγRIV as the γ subunit is required for their surface expression and consequently cannot phagocytose opsonised antigens (254).
<i>Rag2^{-/-}</i>	The replacement of a 0.85 kb segment of the <i>Rag-2</i> gene with the poly(A) trap vector pMC1- <i>neo</i> gene generated a premature stop codon and preventing V(D)J recombination (255).	<i>Rag2^{-/-}</i> have an absence of mature B and T cells.
NSG-SGM3	NOD. <i>scid.II2Ryc^{null}</i> (NSG) mice were created by crossing a NOD/LtSz- <i>scid</i> mouse with a B6- <i>II2Rγ^{null}</i> mouse. NSG mice were bred with	NSG mice have multiple defects in adaptive and innate immunity. NOD/Lt mice are deficient in NK cells and have an absence of circulating complement and defects in the differentiation and function of antigen presenting cells such as macrophages (257). Mice homozygous for

	NOD/LtSz- <i>scid</i> mice engineered to express human <i>Kitl</i> , <i>CSF2</i> and <i>IL3</i> to generate the NSG-SGM3 strain (256).	the severe combined immunodeficiency (<i>scid</i>) mutation lack functional B and T cells (258). Therefore NOD/LtSz- <i>scid</i> mice have multiple defects in adaptive as well as innate immunity. However, NOD/LtSz- <i>scid</i> mice have some residual NK activity (259), therefore hindering engraftment efficiency. The IL-2 receptor γ chain is indispensable for IL-2, IL-4, IL-7, IL-9 and IL-15 signalling, therefore the B6- <i>Il2Rγ^{null}</i> mouse has no NK cells and a decreased number of B and T cells (260, 261). The expression of the human transgenes by NSG-SGM3 aids the stable engraftment of human CD34 ⁺ cells.
B6- <i>W⁴¹/W⁴¹</i> -CD45.1	The <i>W⁴¹</i> mutation was generated by the V to M (position 831) point mutation in the kinase domain of <i>c-Kit</i> , affecting c-Kit activity (262).	B6- <i>W⁴¹/W⁴¹</i> -CD45.1 mice support the engraftment of murine HSCs with reduced (sub-lethal) or no host irradiation (263-265). c-kit is required for normal haematopoiesis; B6- <i>W⁴¹/W⁴¹</i> -CD45.1 mice have mild anaemia arising from the mutated <i>c-Kit</i> expressed in haematopoietic populations (262).

2.4.1 Genotyping

Genomic DNA (gDNA) was isolated from ear notches using the Gentra Puregene Mouse Tail Kit (QIAGEN) as described by the manufacturers and the DNA dissolved in 50 μ L DNA Hydration Solution at 65 °C for 1 h.

Polymerase chain reaction (PCR) was performed using the HotStarTaq DNA polymerase Kit (QIAGEN). A final concentration of 1X Q Solution, 1X PCR Buffer, 2.5 mM MgCl₂, 0.25 μ M of forward and reverse primer, 0.200 μ M of each dNTP and 0.625 U HotStarTaq DNA polymerase was made up with PCR grade water in a sterile 0.2 mL PCR tube. The PCR reaction was initiated at 95 °C for 15 min, followed by 30 cycles of denaturation (94 °C for 1 min), annealing (variable temperature; see Table 2 for 1 min) and extension (72° C for 1 min) followed by a final extension (72 °C for 10 min). Amplified product was run on an agarose gel for 40 min at 100 V.

Table 2. Genotyping primer sequences and annealing temperatures

Gene	Sequence	Size (bp)	Annealing Temperature (°C)
<i>DsRed</i> <i>Express-2</i>	F-5'-AAGAAGCCCGTGAAGCTGC-3' R-3'-TCCTCGTTGTGGGAGGTGAT-3'	~90	60
<i>Thpo (WT)</i>	F-5'- GTCGACCCTTTGTCTATCCCT-3' R-5'- GGTGAATGTAACCTGGGATAA-3'	~300	60
<i>Thpo (Neo')</i>	F-5'- TAGCCAACGCTATGTCCTGATA-3' R-5'- AAGTATCCATCATGGCTGATG-3'	~350	58

2.5 Tissue Processing

2.5.1 Bleeds

2.5.1.1 Blood sampling

Mice were placed in an induction chamber and exposed to 5% isoflurane for induction, followed by 1-2% for maintenance thereafter. Anesthetised mice were restrained in a 50 mL falcon tube head first and their hind leg shaved with clippers to expose their saphenous vein. A thin layer of Vaseline (Unilever) was applied to prevent blood from seeping into the fur and allow for blood drop formation. A 25 g needle was used to puncture the saphenous vein at a 90 ° angle, and the blood collected into EDTA-coated tubes (BD Biosciences). An appropriate amount of blood was removed (approximately 20 µL complete blood counts (CBCs) analysis, approximately 50 µL for flow cytometry analysis). Afterwards, blood flow was stemmed by applying pressure to the wound site with blue roll.

2.5.1.2 Cardiac puncture

Cardiac puncture was the preferred method of whole blood isolation when required for plasma isolation, as this avoids the rupture of major vessels and is considered to result in minimal platelet and endothelial activation, thereby protecting against the release of clotting factors into the plasma (266). A 1 mL syringe with a 25G ⁵/₈ needle attached was preloaded with 100 µl ACD buffer (SLS). Mice were administered an overdose of anaesthesia by intraperitoneal injection. After confirmation of insentience, the mice were placed in dorsal recumbency and cut through the rib cage to expose the heart, with care taken not to sever any major blood vessels. The needle was inserted into the heart and plunger retracted until 500 µL blood was aspirated. Cervical dislocation was performed as a tertiary method of euthanasia. Isolated blood was centrifuged at 8,000 g for 10 min and the supernatant (platelet poor plasma) collected and stored at -80 °C.

2.5.1.3 *Brachial bleed*

Brachial bleed was the preferred method of whole blood collection for FACS analysis when combined with a peritoneal wash, as it is quick to perform and avoids the use of the peritoneal cavity to deliver anaesthesia. Mice were administered with an overdose of anaesthesia (1:1 ratio of medetomidine and ketamine) by subcutaneous injection. After confirmation of insentience, the brachial artery was severed and blood collected into 3 ml ACD buffer. Cervical dislocation was performed as a secondary method of euthanasia.

2.5.2 **Primary cell isolation**

Cells from femurs, tibia, pelves and humeri were isolated and pooled for downstream analysis to 1) protect against intra-BM cellular composition variation, 2) increase the yield of starting material. To isolate haematopoietic cells, BM was flushed with ~7 mL 2%FBS/PBS for femurs and pelves and ~3 mL for tibia and humeri using a 25 G ⁵/₈ needle attached to a 10 mL syringe, flushing into a 50 mL falcon tube.

To isolate BMSCs, BM was also flushed as previously described. Additionally, leftover bones were cut into small pieces and digested with DMEN supplemented with 200 U/ml collagenase IV and 200 U/ml DNase I for 30 min at 37 °C with gentle agitation. Flushed haematopoietic cells were added to the bone digestion mix. All BM cells (haematopoietic and BMSCs) were passed through a 19 G needle to mechanically dissociate cells from BM plugs, with the resultant single cell suspension passed through a 70 µM cell strainer (Greiner bio-one). The cell strainer was washed with 2%FBS/PBS and the flow-through collected for downstream analysis.

The spleen was homogenised by crushing with a plunger flange of a syringe into a 70 µM cell strainer. The cell strainer was washed with 2%FBS/PBS and the flow-through collected for downstream analysis.

Red blood cells were lysed in ACK lysing buffer (Gibco), followed by a PBS wash.

2.6 **Cell preparation for flow cytometry analysis**

For FACS analysis, cells were stained with one of the following viability dyes for 10mins at 4 °C according to the manufacturer's instructions: Zombie Aqua Fixable Viability Kit/Zombie Violet Fixable Viability Kit (Biolegend) or Fixable Viability Dye eFluor 780 (eBioscience). Cells were washed in 1xPBS supplemented with 0.5% BSA and 2mM EDTA (FACS buffer) and then stained Mouse TruStain FcX (101320, Biolegend)/ Human TruStain FcX (422302, Biolegend) for 20 min at 4 °C. Mouse committed progenitors were not stained with Mouse TruStain FcX, as the panel relies on the detection of CD16/32, which are the same receptors the Mouse TruStain FcX blocks.

Table 3. FACS antibody information

Company	Antibody	Catalogue Number	Clone	Dilution
Biolegend	Anti-mouse CD115-PE	135506	AFS98	1:200
Biolegend	Anti-mouse CD115-PE/Dazzle 594	135528	CSF-1R	1:200
Biolegend	Anti-mouse CD117-BV421	105828	2B8	1:200
Biolegend	Anti-mouse CD150-BV605	115927	TC15-12F12.2	1:200
Biolegend	Anti-mouse CD11b-APC	101212	M1/70	1:500
Biolegend	Anti-mouse CD16/32-PE/Cy7	101318	93	1:200
Biolegend	Anti-mouse CD19-PE	115507	605	1:200
Biolegend	Anti-mouse CD25-PE	101903	RMPI-30	1:200
eBioscience	Anti-mouse CD31-FITC	11-0311-82	390	1:100
eBioscience	Anti-mouse CD34-FITC	11-0341-82	RAM34	1:250
Biolegend	Anti-mouse CD4-APC/Cy7	100526	RM4-5	1:200
Biolegend	Anti-mouse CD41-PE	133906	MReg30	1:100
Biolegend	Anti-mouse CD44-FITC	103006	1M7	1:200
Biolegend	Anti-mouse CD45-APC/Cy7	103116	30-F11	1:50
Biolegend	Anti-mouse CD45.1-BV650	110735	A20	1:200
Biolegend	Anti-mouse CD45.1-PE/Cy7	110730	A20	1:200
Biolegend	Anti-mouse CD45.1-PE	110708	A20	1:200
Biolegend	Anti-mouse CD45.2-Alexa Fluor 488	109816	104	1:200
Biolegend	Anti-mouse CD45.2-Alexa Fluor 700	56-0454-82	104	1:200
Biolegend	Anti-mouse CD48-PE/Cy7	103423	HM48-1	1:400
Biolegend	Anti-mouse CD62L-PE/Cy7	104417	MEL-14	1:200
Biolegend	Anti-mouse CD8a-APC	100711	53-6.7	1:200
Biolegend	Anti-mouse CXCR5-APC	145505	L13857	1:200
Biolegend	Anti-mouse F4/80-PE	123110	BM8	1:500
Biolegend	Anti-mouse FOXP3-Alexa Fluor 647	126407	MF-14	1:200
Biolegend	Anti-mouse GranzymeB-PE/Cy7	372213	QA16A02	1:200
Biolegend	Anti-mouse IL17 α -PE/Cy7	506921	TC11-18H10.1	1:200
Biolegend	Anti-mouse IL2-PE	503807	JES6-5H4	1:200
Biolegend	Anti-mouse IL4-PE/Dazzle594	504131	11B11	1:200
Biolegend	Anti-mouse IFN γ -FITC	505806	XMG1.2	1:200
BD Pharmingen	Anti-mouse Lineage Cocktail-PerCP-Cy5.5	51-9006964	145-2C11, M1/70, RA3-6B2, TER-119, RB6-8C5	1:25
Biolegend	Anti-mouse Ly6C-BV605	128036	HK1.4	1:500
Biolegend	Anti-mouse Ly6G-PE/Cy7	127618	1A8	1:500
Biolegend	Anti-mouse MHC II-Alexa Fluor 700	107622	M5/114.15.2	1:500
Biolegend	Anti-mouse Sca1-APC	105828	2B8	1:200
Biolegend	Anti-mouse TCR β -PerCP/Cy5.5	109227	H57-597	1:200
Biolegend	Anti-mouse TNF α -BV421	506327	MP6-XT22	1:200
Biolegend	Anti-human CD34-APC	343608	561	1:25
BD Biosciences	Anti-human CD38-BB515	564499	HIT2	1:25
Biolegend	Anti-human CD34-APC	343608	561	1:25
Biolegend	Anti-human CD45RA-PerCP/Cy5.5	304121	HI100	1:25
ThermoFisher	Goat anti-Rat Alexa Fluor 488	A-11006	[polyclonal]	1:500
ThermoFisher	Goat anti-Rat Alexa Fluor 647	A-21247	[polyclonal]	1:500
R&D Systems	LepR	AF497	[goat polyclonal]	1:100

2.7 Tissue processing for imaging

2.7.1 Pre-freezing steps

Femurs were collected and epiphyses removed using a scalpel. Bones were processed by the sequential incubation at 4 °C: 4% (v/v) PFA/PBS for 24 h, 10% (v/v) EDTA/PBS for 24 h, 20% (w/v) sucrose/PBS overnight. Livers were processed by the sequential incubation at 4 °C: 4% (v/v) PFA/PBS for 24 h, and 20% (w/v) sucrose/PBS overnight. After drying, tissue was embedded in OCT (VWR) and snap frozen in a dry ice/100% ethanol slurry and stored at -80 °C until sectioning.

2.7.2 Sectioning

A Bright OTF500 cryostat equipped with tungsten carbide blades was used for sectioning, with sections cut at 12 µm. Superfrost Plus slides (ThermoFisher Scientific) were numbered as they were used to capture the generated sections, allowing the identification and comparison of sections of a similar longitudinal plane from different samples. Sections were allowed to dry for approximately 30 min at room temperature, during which they were inspected under a light microscope. Sections that were folded or torn were discarded. Slides were stored at -80 °C until staining.

2.8 H&E staining

Slides were allowed warm to room temperature for approximately 30 min. Next, slides were submerged in distilled water for 3 min, then in filtered Harris haematoxylin for 5 min to stain the nuclei. Slides were then washed in running tap water for 10 min to blue the haematoxylin. They were then differentiated in 1% (v/v) hydrochloric acid/70% ethanol for 5 sec, washed in tap water briefly and then submerged in 0.1% eosin for 30 sec to stain proteins. After washing in tap water briefly, slides were dehydrated in increasing concentrations of ethanol for 30 sec each: 50%, 70%, 90% and 100%. Afterwards the slides were submerged in HistoClear for 1 min, before mounting in DPX (Sigma-Aldrich).

3 The sources and roles of thrombopoietin in haematopoietic stem cell niche self-renewal

3.1 Introduction

TPO is a critical cytokine in blood homeostasis. Acting through its receptor, MPL, TPO is both the primary regulator of megakaryopoiesis and a crucial factor required for the maintenance of HSCs. The majority of TPO is produced by the liver and travels to the BM as a soluble plasma protein. However, numerous groups have shown that low concentrations of TPO is also produced in the in the BM (150, 159, 161, 163, 164), where cells capable of responding to conditions of thrombocytopenia or HSC stress by upregulating TPO production in a paracrine fashion are likely to be significant regulators of platelet production and HSC maintenance (148, 149, 160, 165).

Since the cloning and isolation of TPO over 25 years ago, huge advances have been made in characterising the BM niche, and determining which cells are critical for HSC maintenance. Despite this work, the identification of TPO producing cells has remained a challenge due to the combination of low expression and the lack of reliable TPO specific antibodies. Illustrating this, TPO producing cells were not identified by immunofluorescence microscopy using an anti-TPO antibody until ten years after *THPO* expressing cells were identified in human bone marrow using in situ hybridisation. In 2007, Yoshihara and colleagues identified osteoblasts as key TPO-producing components of the endosteal HSC niche in mice (161). As osteoblasts are mature, terminally differentiated cells from multipotent mesenchymal stromal cells (267, 268), this discovery suggested that TPO producing cells may exist across the mesenchymal lineage, therefore supporting earlier research showing that BMSCs produce TPO.

In 2014, the first use of a commercially available anti-TPO antibody was used to show that paracrine production of TPO also occurs at the vascular HSC niche, with Mks being the key players (163). Strong TPO staining was observed in Mks, with weaker staining observed in bone lining cells (taken to be osteoblasts). Notably, despite the authors reporting that BMSCs produce comparatively more *Thpo* than osteoblasts, they did not show any BMSC TPO staining at the protein level.

As TPO-expressing BMSCs have not been previously identified *in situ*, we set out to bridge this missing gap using the commercially available antibody used by Nakamura-Ishizu and colleagues (163). As BMSCs are a heterogeneous population of cells with varying stemness (differentiation potential and self-renewal), HSC support and immunomodulatory capacity, it is likely that only subsets produce TPO. I found that, BMSCs exhibited heterogeneous *Thpo* expression, however, in contrast with findings

from some previous studies (163, 164), Mks did not express any *Thpo*. The results also indicate that long awaited commercially available anti-TPO antibody is non-specific, questioning some previous studies.

3.2 Materials and methods

3.2.1 Immunofluorescence microscopy

Samples were permeabilised in 0.1% (v/v) Triton X-100/PBS for 10 min, and then washed in PBS. The slides were blocked in 10% (v/v) goat serum in 0.1% (v/v) tween-20/PBS (PBST) for 1 h. All primary antibodies used at 1:100 dilution and were as follows: anti-TPO rabbit (bs-10407R; Bioss), anti-CD41 rat (553847; BD Pharmingen) with the following isotype controls: rabbit IgG (AI-1000, Vector) and rat IgG1 κ (400401; Biologend). Antibodies were used in 10% (v/v) goat serum/ PBST overnight at 4 °C. Samples were washed three times in PBST and incubated for 1 h at room temperature in the dark with secondary antibodies. All secondary antibodies were used at 1:500 dilution and were as follows: goat anti-rabbit IgG-Alexa Fluor 647 (A-21245; ThermoFisher) and goat anti-rat IgG-Alexa Fluor 568 (A11077, Molecular Probes). The slides were washed three times in PBST and stained with DAPI (0.5 μ g/ml, 40833; Cell Signalling) for 5 min. After rinsing in PBS, slides were mounted in Mowiol 4-88.

3.2.2 Fluorescence-activated cell sorting

3.2.2.1 Megakaryocytes

Haematopoietic BM cells were isolated as described previously (2.5.2), however a 100 μ M filter (Greiner bio-one) was used instead of a 70 μ M filter due to the larger size of Mks. Lineage positive cells were depleted using the Lineage Cell Depletion Kit (Miltenyi Biotec) and magnetic activated cell sorting (MACS) according to the manufacturer's instructions. MACS was carried out in PBS supplemented with 0.5% BSA and 2 mM EDTA (MACS buffer). Lineage negative cells were collected and stained with Mouse TruStain FcX in MACS buffer for 20 min at 4 °C, followed by staining with anti-CD41-PE for 20 min at 4 °C. Specific antibody information is found in Table 3. Stained cells were washed three times with MACS buffer and resuspended in MACS buffer. DAPI (Cell Signalling) was added at a final concentration of 1 μ g/ml immediately before sorting to exclude dead cells. Cells were sorted using a MoFlo Astrios sorter equipped with a 100 μ M nozzle (Beckman Coulter); Summit Version 6 was used for gating. Cells were sorted directly into 700 μ L QIAzol at 4 °C.

3.2.2.2 Bone marrow stromal cells

BMSCs were isolated as described previously (2.5.2). Cells were stained with Mouse TruStain FcX in FACS buffer for 20 min at 4 °C, followed by staining with primary

antibodies in FACS buffer for 20 min at 4 °C. To isolate *Cxcl12*^{DsRed/+} BMSCs, BM was stained with CD31-FITC and CD45-APC/Cy7; to isolate LepR⁺ BMSCs, BM was stained with CD45-APC/Cy7 and LepR (unconjugated). After washing three times in FACS buffer, LepR⁺ BMSCs were additionally stained with donkey anti-goat IgG-Alexa Fluor 647 for 20 min at 4 °C, followed by a further three washes. Specific antibody information is found in 2.6. DAPI was added at a final concentration of 1 µg/ml immediately before sorting to exclude dead cells and cells were sorted using a MoFlo Astrios sorter equipped with a 90 µM nozzle (Beckman Coulter); Summit Version 6 was used for gating. Cells were sorted directly into 700 µL QIAzol at 4 °C.

3.2.3 Cultured megakaryocyte isolation by magnetic-activated cell sorting

Haematopoietic BM cells were isolated as described previously (2.5.2). Cells were cultured in Opti-MEM Reduced Serum Medium (Gibco) containing 3% (v/v) TPO conditioned media and 3% (v/v) IL-3 conditioned media for 72 h. IL-3 and TPO supernatant was obtained by previously collecting the conditioned media generated by culturing BHK-IL3 and BHK-TPO cells respectively for 48 h and then stored at -20 °C until use. Mature Mks were harvested by low speed centrifugation (100 g for 5 min) and enriched for by passing the culture through a discontinuous bovine serum albumin (BSA) density gradient (0%/2%/4% w/v). Enriched Mks settled to the bottom within 30 min as determined by visual inspection using a light microscope. The Mk containing fraction was then incubated with Accutase (STEMCELL) for 10 min at 37 °C to detach contaminating cells from Mks. Cells were pelleted and re-suspended in MACS buffer followed by staining with CD41-PE antibody for 20 min at 4 °C (2.6). Stained cells were washed in MACS buffer, followed by staining with anti-PE microbeads (1:10 dilution, 130-048-801; Miltenyi Biotec) in MACS buffer for 20 min at 4 °C which were separated from unstained contaminating cells using an EasySep Magnet (18000; STEMCELL Technologies), where stained cells are selectively retained after inversion. The separation was performed four times with thorough washes to achieve maximal purity. For downstream mRNA analysis, Mks were lysed in 700 µL QIAzol and stored at -80 °C. The purification process was assessed by flow cytometry and microscopy analysis of cytopsin slides. To generate cytopsin slides, Mks were cytopspun at 18 g for 5 min followed by fixation in 4% paraformaldehyde for 5 min. Slides were stored at -80 °C until use.

3.2.4 Real-time polymerase chain reaction

All reagents and equipment used were purchased from Applied Biosystems. Singleplex qPCR was performed using cDNA generated from human cell lines. The following reagents were added to the combined mastermix in the ratio 10:1:7; TaqMan Fast

Advanced MasterMix, gene expression assay and RNase-free water. The gene expression assays used were *THPO* (Hs01061346_m1) or *HGPRT* (Hs99999909_m1). Duplex qPCR was performed using cDNA generated from sorted mouse cells and homogenised whole tissue. The following reagents were added to the combined mastermix in the ratio 10:1:6; TaqMan Fast Advanced MasterMix, gene expression assay and RNase-free water. The gene expression assays used were *Thpo* (Mm00437040_m1) or *Hprt* (Mm03024075_m1). 2 µl of cDNA and 18 µl of the combined master mix, gene expression assay and water were added to each well of a MicroAmp Fast 96-well reaction plate.

Each sample was prepared in triplicate. The plates were run using the StepOne Plus Realtime PCR System (Applied Biosystems). Data was exported into Microsoft Excel and fold change was calculated using the delta-delta method where $\text{ratio} = 2^{-\Delta\Delta\text{CT}}$ (269). *THPO* or *Thpo* gene expression was determined as fold induction over HepG2 cells or WT liver, respectively. The amplified product was run on a 3% (w/v) agarose/tris-acetate-EDTA (TAE) gel stained with 5 mg/mL ethidium bromide and GeneRuler 1kb DNA Ladder Plus (Fermentas) was used as a DNA ladder.

3.2.5 Acute immune thrombocytopenia mouse model

WT or *Cxcl12^{DsRed/+}* mice were bled (2.5.1.1) to obtain baseline platelet counts. Mice were administered unconjugated anti-CD41 antibody (2.6) to induce haematological stress by acute thrombocytopenia induction, or PBS to act as a control, via a single intraperitoneal injection. Mice were bled 24 and 48 h after injection. After the 48 h bleed, mice were sacrificed and BMSCs FACS sorted for downstream qPCR analysis.

3.3 Results

3.3.1 Published thrombopoietin antibody is non-specific

To determine whether murine BM is a site of local TPO production, and if so, to identify the TPO expressing cells, immunofluorescence microscopy was performed using the commercially available anti-TPO antibody (bs-10407R) which was used by Nakamura-Ishizu and colleagues to demonstrate that BM Mks produce TPO (163). As the liver is the major source of TPO (55, 57, 147, 148), WT and *Thpo*^{-/-} liver served as important controls for primary antibody specificity, whilst IgG controls were used to account for non-specific interactions from the secondary antibody. When comparing the pattern and intensity of TPO staining between sections generated from WT and *Thpo*^{-/-} liver (Figure 3.1), I found that the images were similar, suggesting that the primary antibody was non-specific. This was not due to non-specific staining from the secondary antibody due to a complete absence of staining when using isotype controls at the same concentration.

Despite the indication using liver that the primary antibody was non-specific, WT and *Thpo*^{-/-} BM was then also stained in order to determine whether a similar pattern of staining was achieved as Nakamura-Ishizu and colleagues (163, 164). Diffuse staining was observed throughout the BM with brighter staining observed with Mks (Figure 3.2A-B), which was similarly observed between both WT and *Thpo*^{-/-} BM, albeit fewer cells of bright TPO staining (Mks) in *Thpo*^{-/-} BM. This is to be expected given the essential role of TPO in megakaryopoiesis and the subsequent low numbers of mature Mks in *Thpo*^{-/-} BM (253). Again, no background staining was observed in BM staining with isotype controls.

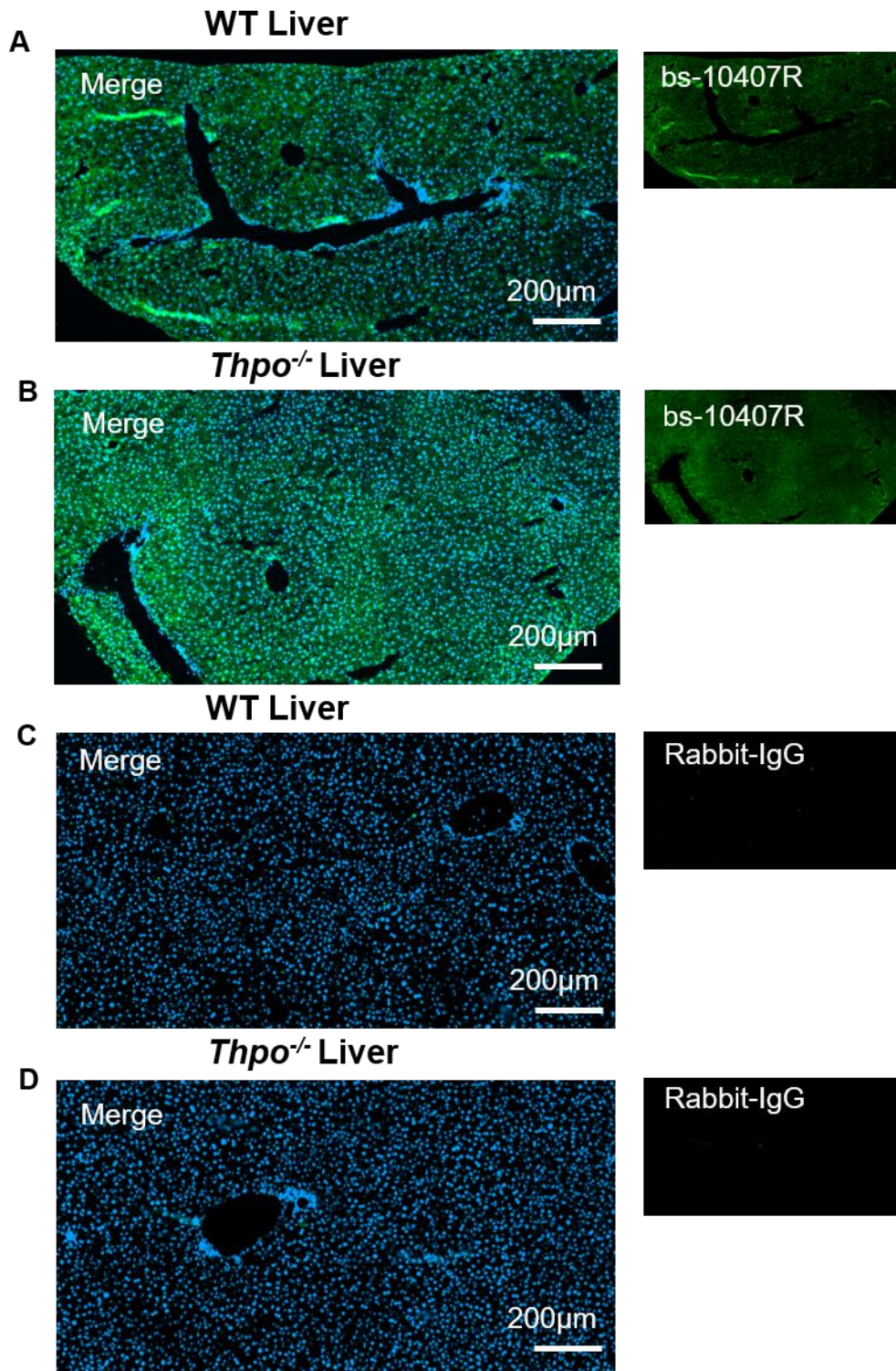


Figure 3.1. bs-10407R is non-specific. **A)** WT, and **B)** *Thpo*^{-/-} liver were stained with bs-10407R and AF647 secondary antibody. **C)** WT, and **D)** *Thpo*^{-/-} liver were stained with a rabbit isotype control and AF647 secondary antibody. All images are representative images from N = 3 mice, representative of 3 independent experiments.

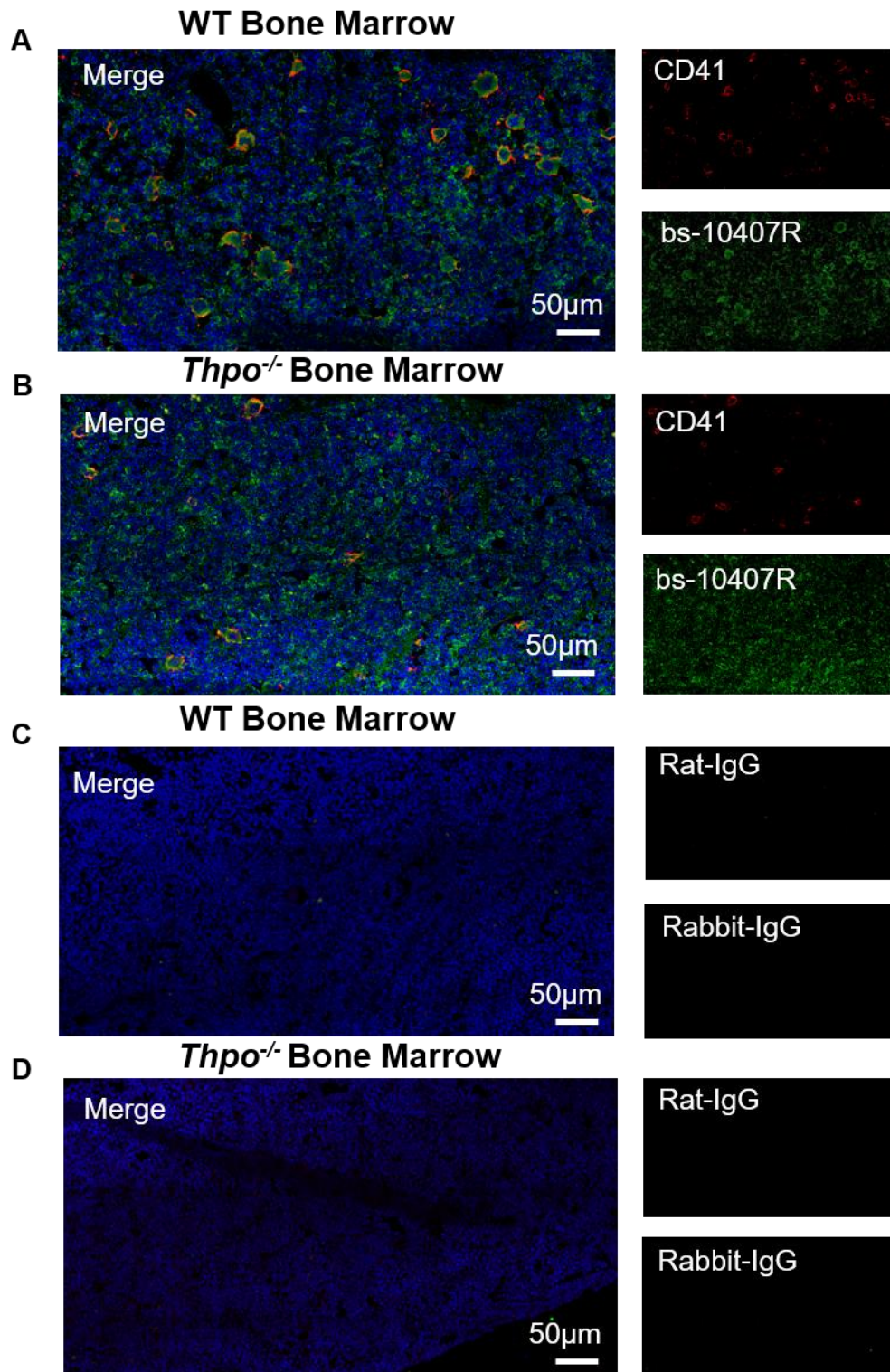


Figure 3.2. Staining pattern of WT BM with bs-10407R is consistent with images generated by Nakamura-Ishizu et al. A) WT, and **B)** *Thpo*^{-/-} femur BM were stained with bs-10407R and AF647 secondary antibody. Strong TPO staining is seen by Mks, identified by CD41 staining. **C)** WT, and **D)** *Thpo*^{-/-} femur BM were stained with a rabbit isotype control and AF647 secondary antibody. All images are representative images from N = 3 mice, representative of 3 independent experiments.

3.3.2 Megakaryocytes do not express *Thpo*

Next Mks were isolated to determine whether they transcribe *Thpo*, and therefore to clarify whether the bs-10407R primary antibody was non-specific. As mature Mks are large (mean diameter ~ 25 μm (270)), fragile cells, isolation by methods other than FACS sorting are often used as there is a tendency for Mks to become ruptured during the sorting process (271). Instead, researchers can purify them from other BM cells by exploiting their physical properties (as large, dense cells). Mks can be enriched using a density gradient (271) and optionally further enriched using their specific markers (272). As Mks represent less than 1% of BM cells, the proportion of mature Mks were expanded by culturing flushed BM with BHK-TPO for 72 h, therefore driving megakaryopoiesis. After 72 h the cultured BM was harvested and passed through a discontinuous BSA density gradient, with the enriched Mk containing fraction being further enriched for Mks via a MACS sort. The increasing purity of Mks isolated at each stage of the purification process is shown by Figure 3.3. Figure 3.3Ai-iii shows the FSC-H vs Log SSC-H plots of the events passing through the flow cytometer; with increasing purity, a lower percentage of total events were intact cells due to Mks breaking apart. Therefore, it is likely that the 82.6% purity shown in Figure 3.3Aiv is an underrepresentation of Mk purity that was used for downstream analysis as only the smaller Mks and non-Mk contaminants survived to analysis. The cells that stained positive for CD41 were the largest, most granular cells analysed (Figure 3.3Av), which is in keeping with the known phenotype of Mks and therefore giving further confidence that the cells isolated were highly purified, mature Mks.

To visually inspect the purified Mks, and to confirm co-localisation with the bs-10407R antibody and an anti-CD41 antibody the cells were cytopun onto a glass slide and stained. It was unclear at the time whether the CD41-PE antibody used in the purification process could be visualised long enough to capture an image by immunofluorescence microscopy, therefore the cells were re-stained with CD41-AF568. This is because PE is known to be sensitive to photobleaching and consequently is rarely used for immunofluorescence microscopy (273). Figure 3.4 shows co-localisation between CD41 expressing Mks and TPO staining.

To determine whether Mks express *Thpo*, they were analysed by qPCR. As shown by Figure 3.5B, the cultured Mks isolated by the combination of BSA density gradient and MACs depletion had no *Thpo* expression relative to WT liver. However, it remained possible that the 72 h stimulation in BHK-TPO during the expansion process may act to repress *Thpo* transcription through a negative feedback loop. Therefore CD41^{high} cells were directly isolated from lineage depleted BM by cell sorting. To minimise the rupture

of larger cells, a wide sorting nozzle was used at low pressure (274). However, as previously mentioned, the cells isolated were likely to be biased towards smaller Mks rather than larger, mature Mks. qPCR analysis of this population revealed that directly sorted Mks that had not been cultured also do not transcribe *Thpo*. Together, these results confirm that *Thpo* is not expressed by Mks and that the antibody used to report TPO production from Mks is non-specific.

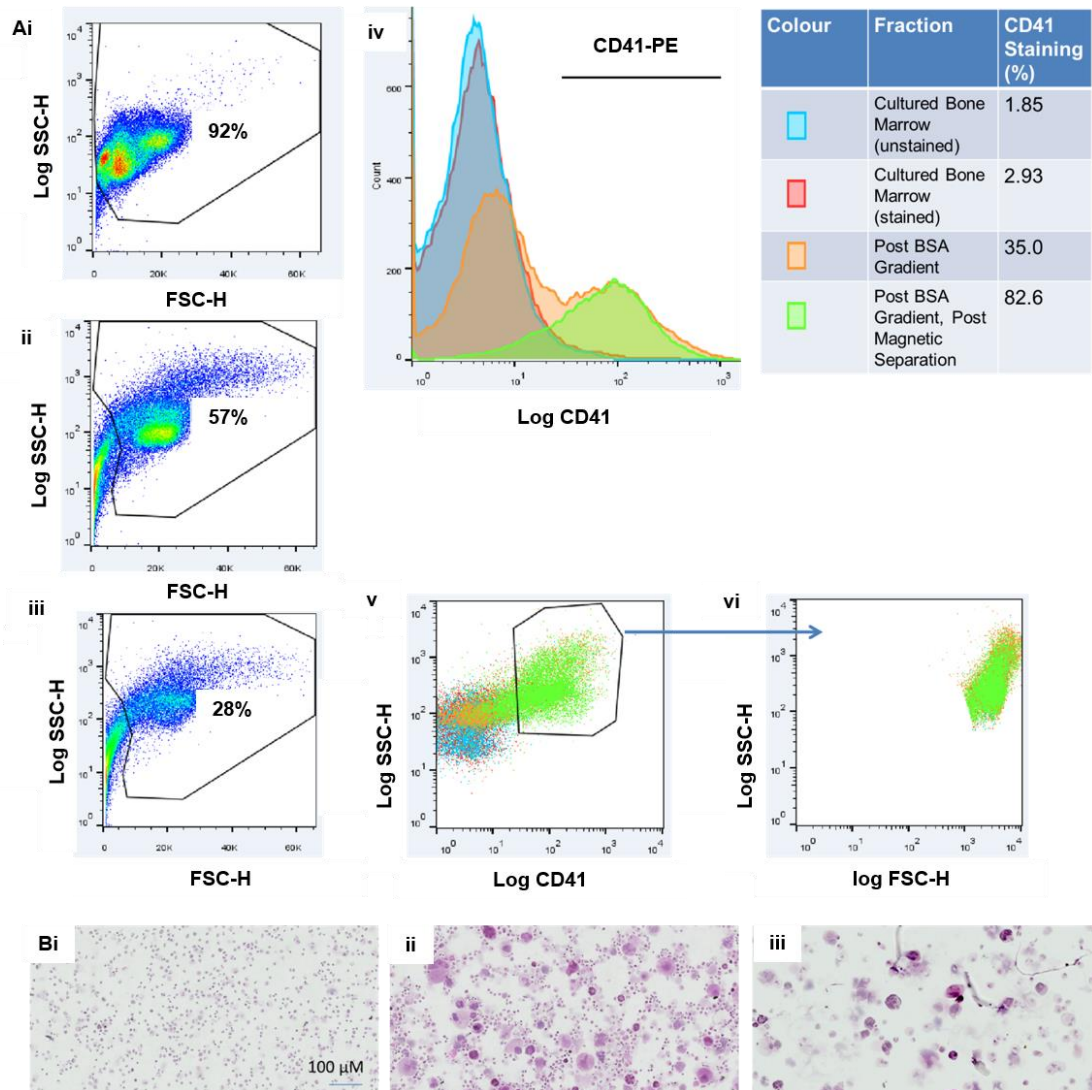


Figure 3.3. Cultured Mks were isolated to a high degree of purity. **Ai and Bi** are cultured BM fractions that have not been subject to Mk enrichment. **Aii and Bii** are partially enriched fractions that have been subject to enrichment by BSA density gradient, but not MACS sorting. **Aiii and Biii** are the most purified fractions that have been subject to enrichment by BSA density gradient and MACs sorting. **Ai-iii)** First gate showing FSC-H vs Log SSC-H plots. With increasing purity, a lower percentage of total events were intact cells due to Mks breaking apart as they passed through the flow cytometer. **iv)** Overlay showing CD41-PE staining. **v)** CD41^{high} cells are large, granular cells. **Bi-iii)** H&E stain of cytopsin slides showing an enrichment of larger cells with increasing purification steps. The data is representative of the purity achieved from 3 independent experiments.

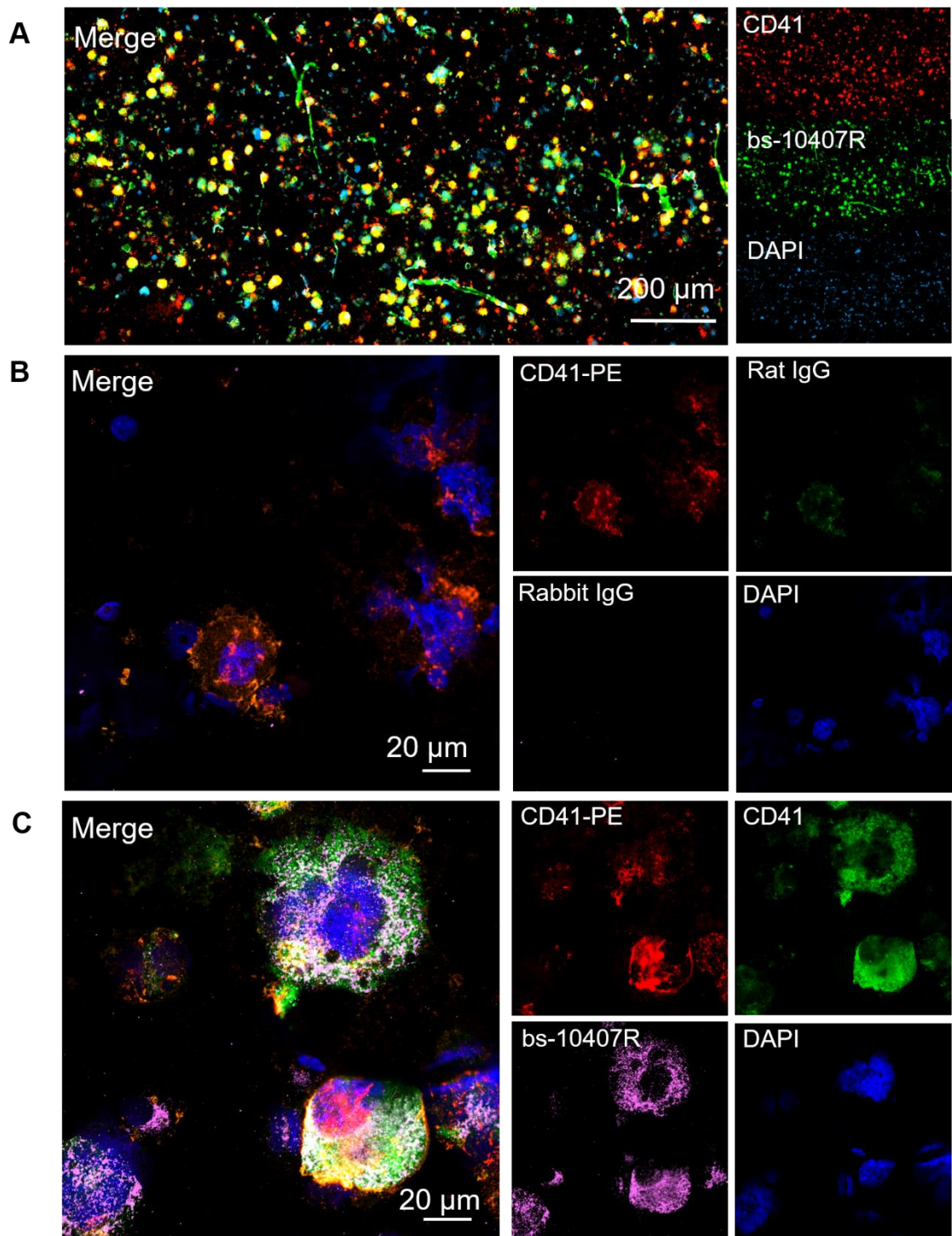


Figure 3.4. Cultured Mks stain positive with bs-10407R. Cultured Mks were the most purified fraction described in Figure 3.3; post BSA gradient, post MACS depletion. **A** Slide scanner image, **B and C** confocal microscopy image showing colocalisation between CD41 expressing Mks and TPO staining. Cultured Mks were additionally stained with CD41-AF568 as the PE (used in the MACS process) is suboptimal for visualisation by immunofluorescence microscopy. The slide scanner cannot distinguish between PE and AF568 emission, whilst this is possible using spectral unmixing techniques with confocal microscopy. N = 3, representative of 3 independent experiments.

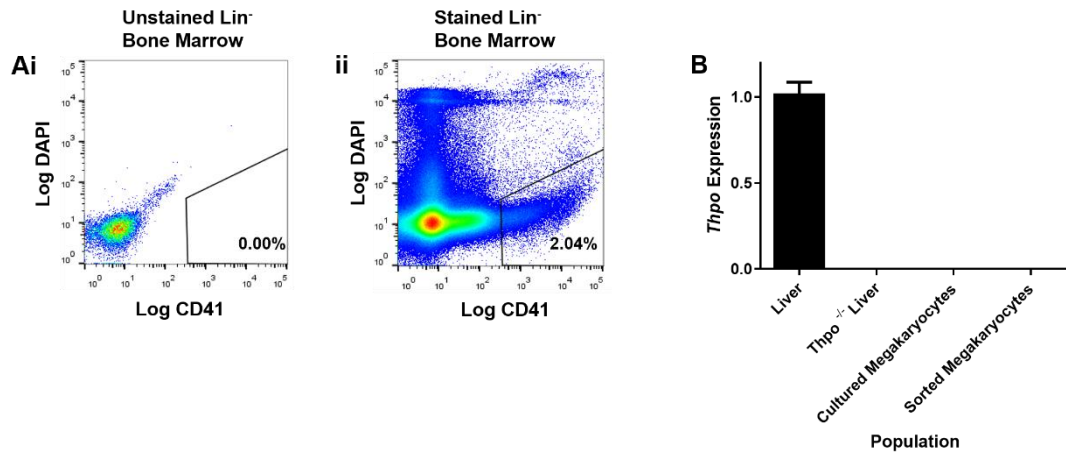


Figure 3.5. Neither cultured Mks nor sorted Mks express *Thpo*. **A)** WT BM was MACS depleted for lineage markers prior to being sorted for CD41^{high} expression. **B)** qPCR analysis on cultured Mks (most purified fraction described in Figure 3.3; post BSA gradient, post MACS depletion) and sorted Mks. N = 3 cultured Mks, N = 2 sorted Mks.

3.3.3 *Cxcl12*-DsRed/LepR⁺ bone marrow stromal cells express *Thpo*

The *Cxcl12*^{DsRed/+} reporter mouse generated by Ding and Morrison was used to phenotype perivascular stromal cells by immunofluorescence microscopy and flow cytometry (45). In their paper, they characterise sources of *Cxcl12* in the murine BM, reporting that the majority of *Cxcl12* was produced by LepR⁺ BMSCs, whilst lower amounts were expressed by ECs (~100-fold lower). As BM stromal cells characteristically do not express CD45 or CD31, when FACS sorting *Cxcl12*⁺ BMSCs, antibodies against these markers were used to distinguish the BMSCs from haematopoietic cells and ECs respectively (Figure 3.6B).

Cxcl12⁺ BMSCs are not uniform in their levels of *Cxcl12* expression, and therefore can be subdivided into *Cxcl12*-DsRed^{low} and *Cxcl12*-DsRed^{high} populations (88), as shown in Figure 3.6B. There is considerable overlap between *Cxcl12*-DsRed^{high} and LepR⁺ BMSCs; 98.8% of LepR⁺ BMSCs are *Cxcl12*-DsRed^{high} and 88.8% of *Cxcl12*-DsRed^{high} are LepR⁺ (268). *Cxcl12*-DsRed^{low}, *Cxcl12*-DsRed^{high} and LepR⁺ BMSCs express *Thpo* at ~0.06, 0.25 and 0.29 fold WT liver levels (Figure 3.6Di).

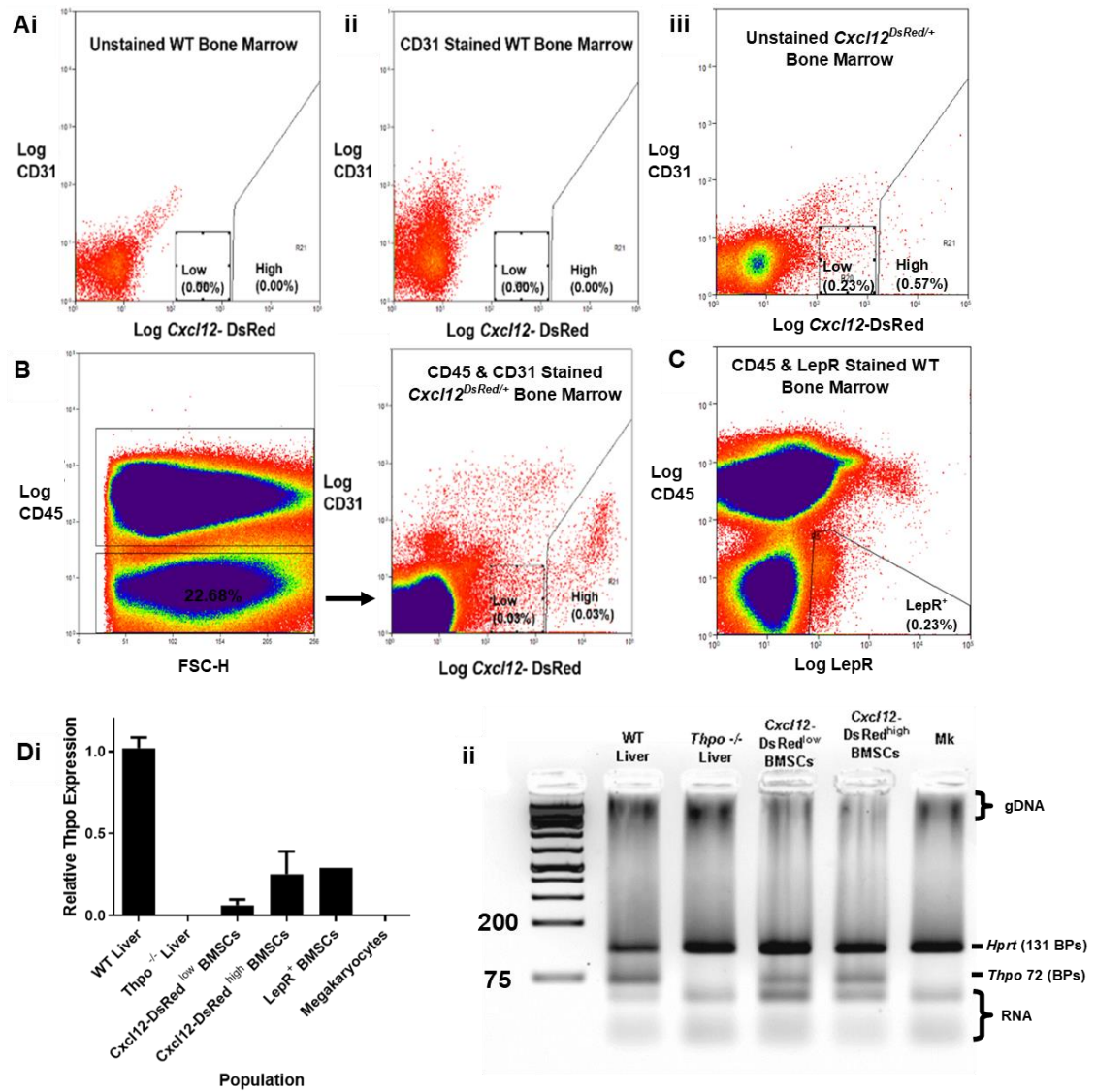


Figure 3.6. BMSC subsets express *Thpo* at different levels. **A)** Single stained BM cells from WT or *Cxcl12*^{DsRed/+} femurs were used to set the gates prior to *Cxcl12*-DsRed BMSC sorting. **B)** Gating strategy used to isolate *Cxcl12*-DsRed^{low} and *Cxcl12*-DsRed^{high} BMSCs. **C)** Gating strategy used to isolate LepR⁺ BMSCs. **Di)** qPCR analysis on isolated *Cxcl12*-DsRed^{low}, *Cxcl12*-DsRed^{high} and LepR⁺ BMSCs determined that they express *Thpo* at ~0.06, 0.25 and 0.29 fold WT liver levels. N = 5 livers and BMSCs from *Cxcl12*^{DsRed/+} mice, N = 1 LepR BMSCs from WT mice. **ii)** The amplicon from *Cxcl12*-DsRed^{low}, *Cxcl12*-DsRed^{high} BMSCs and cultured Mks were visualised on a 3% w/v agarose gel.

3.3.4 Bone marrow stromal cells do not upregulate *Thpo* expression after acute thrombocytopenia

As previously mentioned, it has been reported that cells in the BM (149), namely BMSCs are inducible (148, 160), and can be stimulated to upregulate *Thpo/THPO* under conditions of haematopoietic stress such as ITP, aplastic anaemia or irradiation. To determine whether *Cxcl12*-DsRed^{low}, *Cxcl12*-DsRed^{high} and LepR⁺ BMSCs upregulate *Thpo* expression after induction of haematological stress, a model of acute thrombocytopenia was established. *Cxcl12*^{DsRed/+} or WT mice were injected with anti-CD41 antibody to induce thrombocytopenia and were sacrificed at 48 h post-injection (Figure 3.7A). McCarty and colleagues demonstrated an increase in BM *Thpo* expression as early as 6 h after the induction of acute thrombocytopenia, and this peaked between 30 and 54 h (149). Therefore, 48 h post-injection seemed an appropriate time point to sacrifice the mice and analyse *Thpo* expression.

Contrary to past studies on BMSCs under conditions of haematopoietic stress, *Thpo* expression from *Cxcl12*-DsRed^{low}, *Cxcl12*-DsRed^{high} and LepR⁺ BMSCs remained constant after acute thrombocytopenia (Figure 3.7B). As expected, no change was observed in whole liver. The results therefore indicate that acute thrombocytopenia does not alter *Thpo* expression from *Cxcl12*-DsRed^{low}, *Cxcl12*-DsRed^{high} and LepR⁺ BMSCs.

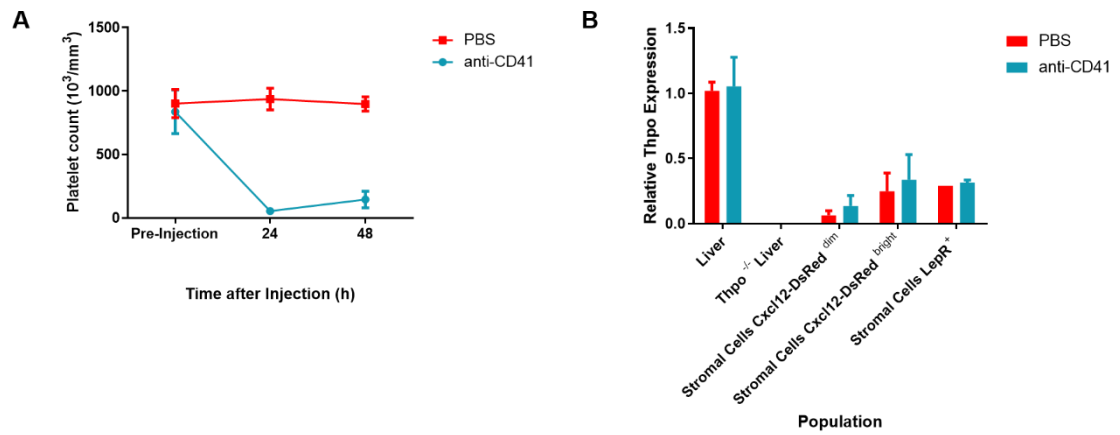


Figure 3.7. Acute ITP does not influence BMSC *Thpo* expression. *Cxcl12^{DsRed/+}* or WT mice were injected with anti-CD41 antibody to induce thrombocytopenia and were sacrificed at 48 h post-injection. **A)** Mice were bled pre-injection, and 24 h and 48 h post-injection to monitor platelet counts and confirm thrombocytopenia induction. **B)** BMSC subsets and whole liver were isolated and *Thpo* expression determined by qPCR. Thrombocytopenia did not alter *Thpo* expression by the liver ($P = 0.69$), *Cxcl12-DsRed^{low}* BMSCs ($P = 0.84$) or *Cxcl12-DsRed^{high}* BMSCs ($P = 0.42$). $N = 5$ livers and BMSCs from *Cxcl12^{DsRed/+}* mice, $N = 1-2$ LepR BMSCs from WT mice. *Hprt* was used to normalise *Thpo* expression between samples. P values were calculated by Mann-Whitney tests.

3.3.5 Analysis of bone marrow stromal cell clonal lines suggest that *THPO* expressing bone marrow stromal cells are rare *in vivo*

To better characterise *THPO*-expressing BMSC subsets, eight immortalised human BMSC clonal lines generated by James and colleagues were used (251), alongside total BMSCs from three independent donors. Each clonal line has differing characteristics in terms of differentiation capacity, gene expression, immunomodulation, and BM distribution of their *in vivo* counterparts. This variation likely represents differing functions *in vivo* and together; they represent a heterogeneous population of BMSCs. However their immortalisation allows for in-depth, reproducible analysis on functionality and gene/protein expression.

As shown in Figure 3.8, all eight BMSC clonal lines displayed extremely low *THPO* expression (normalised to *THPO* expression from HepG2 cells). The highest expresser was Y302; at 0.037% the amount level of *THPO* expressed by HepG2 cells, this is likely to be background noise rather than *THPO* expression. The total BMSCs from three independent donors had higher *THPO* expression; however, with the highest amount expressed by Donor 2 (0.66%), this is still low *THPO* expression relative to HepG2 cells. Together, the data suggests that *THPO* expressing BMSCs are extremely rare, and were not captured by the eight clonal lines. The low *THPO* expression observed from Donor 1-3 likely originates from very rare subpopulations of unidentified BMSCs existing within the total BMSC population, which express comparatively high *THPO* expression. On a population level this presents as low *THPO* expression due to dilution effects from the vast majority of BMSCs that express little or no *THPO*.

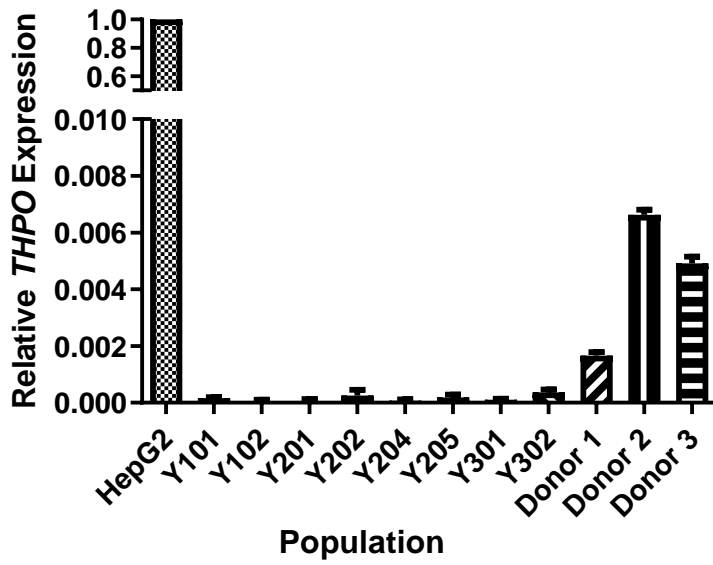


Figure 3.8. THPO expressing human BMSC subsets may be extremely rare. HepG2 cells, total BMSCs from three independent donors (donors 1-3) and a panel of clonal BMSC lines were analysed for THPO expression by qPCR. N = 3 independent experiments.

3.4 Discussion

Whilst it has long been appreciated that the liver is the major source of TPO (55, 57, 147, 148), whether cells in the BM are responsible for local TPO production remains unclear. Here I show that *Thpo* is expressed on a population level by *Cxcl12*-DsRed BMSCs and not, as described previously, by Mks (163, 164). Within this population, *Thpo* expressing BMSCs are predominantly LepR⁺ /*Cxcl12*-DsRed^{high} BMSCs and therefore are expected to reside in close proximity to HSCs. However, studies using human BMSCs of overlapping phenotype suggest that not all LepR⁺ /*Cxcl12*-DsRed^{high} BMSCs express *Thpo* and that further characterisation work is needed. Although previous studies suggest that BM *Thpo* expression increases during ITP (148, 149) *Thpo* expression by LepR⁺ /*Cxcl12*-DsRed^{high} BMSCs remains unchanged after platelet depletion.

Nakamura-Ishizu and colleagues reported that Mks transcribe *Thpo* and used a commercially available antibody to confirm this at the protein level (163). In contrast, my results suggest that Mks do not transcribe *Thpo* and the antibody used was non-specific, based upon the observation that staining was similar between the liver and BM of WT and *Thpo*^{-/-} mice. This was not due to non-specific staining from the secondary antibody due to a complete absence of staining when using isotype controls at the same concentration. This suggests that the non-specific binding of the TPO antibody is due to non-specific binding of the antigen-binding (Fab) fragment to epitopes other than TPO rather than the fragment crystallisable (Fc) region binding to Fc receptors throughout the BM. Nakamura-Ishizu and colleagues did not report the use of these additional controls in their papers, so it was not possible to compare results (163, 164).

Similar to results described by Nakamura-Ishizu and colleagues, the antibody bound the strongest to Mks. In contrast however, weaker, more diffuse staining was also observed in my images throughout the BM of WT and *Thpo*^{-/-} mice which was not reported by Nakamura-Ishizu and colleagues and was perhaps indicative of non-specific staining. There could be several reasons for the differences in antibody staining. Firstly, the authors did not report the concentration at which the antibody was used. If they used it at far lower concentration than I did, the weaker, diffuse staining may not have appeared. Secondly, the authors did not report the use of an isotype control. If one was not used, the diffuse staining may have been interpreted as background staining and therefore removed from the final image.

In April 2018, an important paper was published in *Science* showing that *Thpo* is transcribed, but not translated in murine BM, and that liver derived TPO is essential for HSC maintenance (147). In their study, Decker and colleagues analysed the *Thpo*

expression levels of Mks, LepR⁺ BMSCs and Col2.3-GFP osteoblasts by qPCR. In agreement with my results, no *Thpo* expression was observed in Mks, however LepR⁺ BMSCs expressed approximately 30% of *Thpo* expressed by whole liver. This was remarkably consistent with my results (29% and 25% observed by LepR⁺ BMSCs and *Cxcl12*-DsRed^{high} BMSCs respectively). Considering HSCs are adjacent to (94%) or within 5 μ M of (97%) *Cxcl12*-DsRed^{high} BMSCs, (and 93% within 5 μ M of LepR⁺ BMSCs) (69), it is perhaps both surprising how much *Thpo* they transcribe, and unsurprising that they do not translate TPO, given the established role of the liver in TPO production.

To assess the expression of TPO protein, Decker and colleagues generated *Thpo*^{DsRed-CreER} knock-in mice by replacing the stop codon of *Thpo* with a *P2A-DsRed-P2A-CreER* cassette (Figure 3.9). This allowed the translation of TPO, DsRed and CreER recombinase under the control of *Thpo* endogenous regulatory elements. *LoxpZsGreen* mice had a strong CAG promoter driven ZsGreen construct inserted into the ubiquitously expressed *Gt(ROSA)26Sor* locus (275). The ZsGreen is an enhanced green fluorescent protein engineered for brighter expression and higher expression. *Thpo*^{DsRed-CreER} mice were crossed with *LoxpZsGreen* mice to generate *Thpo*^{DsRed-CreER};*loxpZsGreen* mice (147). In cells that express TPO, and therefore Cre-mediated recombination, ZsGreen is expressed.

No DsRed fluorescence was observed in the *Thpo*^{DsRed-CreER};*loxpZsGreen* mouse (including liver, kidney and BM). Broad expression of ZsGreen was observed in hepatocytes and in rare cells in the kidney, however no fluorescence was observed in the BM. Firstly, the lack of DsRed fluorescence demonstrates that TPO is translated at very low levels *in vivo*, even in the liver which is considered to be the major site of TPO production (55, 57, 147, 148), and that amplification of signal by Cre-mediated recombination is required to visualise TPO expression. Secondly, the lack of ZsGreen in the BM demonstrates that *Thpo* is transcribed, but not translated in the BM.

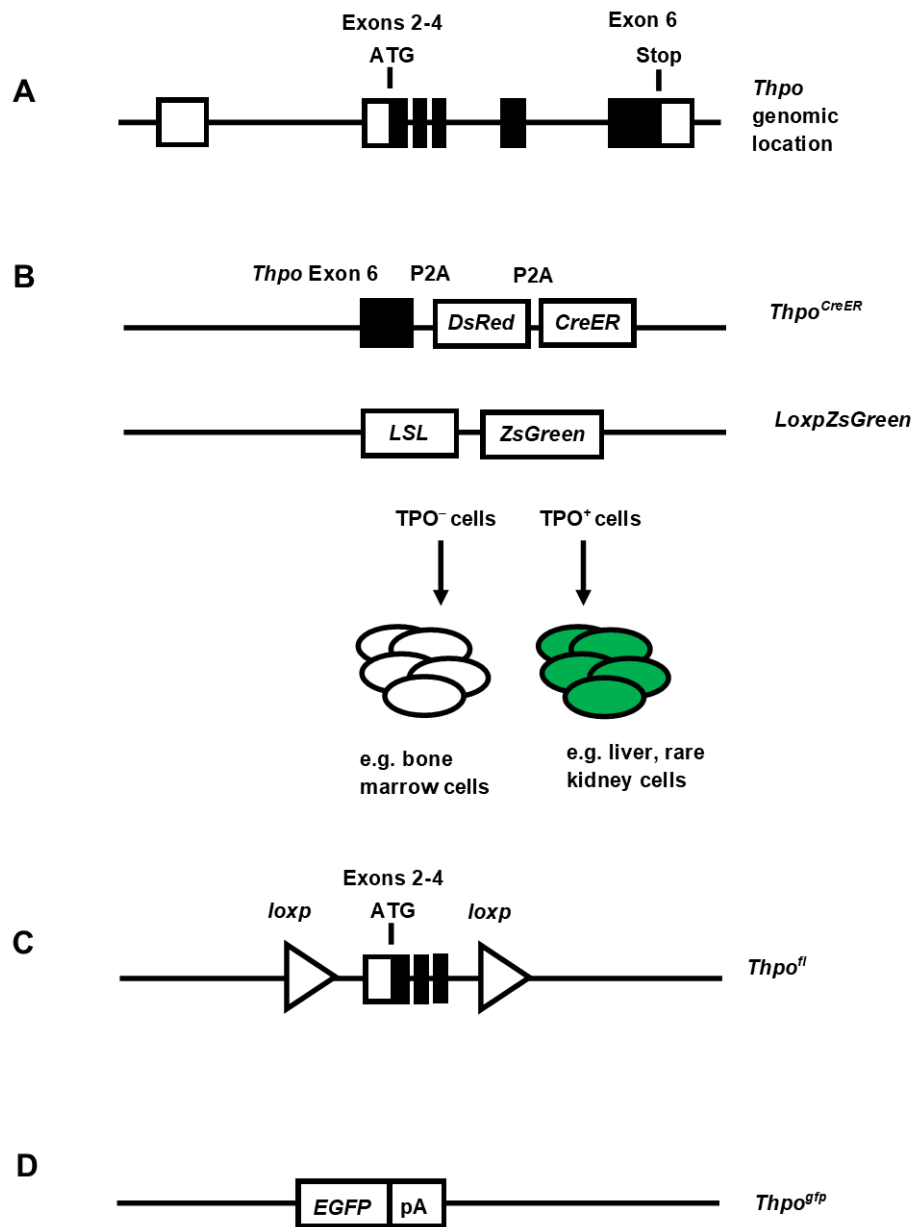


Figure 3.9. Hepatic TPO is required for BM HSC maintenance. **A)** *Thpo* genomic location. **B)** Generation of the *Thpo*^{DsRed-CreER};*loxpZsGreen* translational reporter mouse. **C)** Generation of the conditional *Thpo*^{fl} knock-out allele. **D)** Generation of the global *Thpo*^{gfp} knock-out allele.

To confirm that the liver and not the BM, produce TPO in sufficient amounts to support haematopoiesis, a conditional knockout mouse was generated (147). They generated a floxed allele of *Thpo* by inserting *loxP* sequences flanking *Thpo* exons 2-4, where recombination would result in the deletion of the start codon and the generation of a frameshift (Figure 3.9). To confirm that haematopoietic cells (including Mks), osteoblasts and LepR⁺ BMSCs are not sources of TPO for HSC maintenance, *Vav1-cre;Thpo^{fl/gfp}*, *Col2.3-cre;Thpo^{fl/gfp}* and *Lepr-cre;Thpo^{fl/gfp}* mice were phenotyped. All three mouse strains had normal cellularity and HSC frequency showing that TPO produced locally in the BM is not required for HSC maintenance. To confirm that TPO production by hepatocytes is essential for HSC maintenance, *Alb-cre;Thpo^{fl/fl}* mice were phenotyped. They had 5x reduction in platelet count and Mk count as well as a 25x reduction in HSC frequency. BM cells from *Alb-cre;Thpo^{fl/fl}* mice had severe defects in their ability to reconstitute irradiated recipients, demonstrating that HSC self-renewal was compromised.

To determine whether TPO is translated in the BM under conditions of haematopoietic stress, *Thpo^{DsRed-CreER};loxPZsGreen* were treated with a single dose of 5-fluorouracil (5-FU), and analysed 10 days later. No ZsGreen fluorescence was observed, suggesting that TPO was not translated under these conditions. 5-FU treatment is a fast acting, anti-cancer treatment that targets all dividing cells non-specifically (276). Although upregulation of *Thpo* transcripts have been previously observed in the BM after carboplatinum treatment (149) (another anti-cancer treatment), *THPO* upregulation has also been observed during ITP or aplastic anaemia (148). Whilst total *Thpo* mRNA expression was not altered during our model of acute thrombocytopenia, increased TPO production may still have occurred through other mechanisms such as preferential alternative splicing of *Thpo* isoforms that have a higher translational efficiency, or downregulation of RNA-binding proteins/miRNAs that usually act to repress TPO translation.

TPO production has previously been studied *in vitro* using total RNA from human liver and has been shown to be efficiently inhibited by a translational mechanism. Studies by Ghilardi and colleagues show that translation of *THPO* mRNA is almost completely inhibited by the presence of seven AUG codons upstream of the actual start site (uAUG) in the 5'-untranslated region (5'-UTR) (277). This can inhibit translation by causing premature ribosomal initiation, followed by translation of a short peptide and partial dissociation of the ribosome from the mRNA when a stop codon is encountered, thereby preventing the ribosome from initiating at the physiological start codon (278). Alternative promoter usage and differential splicing events can generate at least three *THPO* mRNA

isoforms that differ in the composition of their 5'-UTR. A rare alternatively spliced isoform (P1ΔE2; accounting for only 2% of *THPO* mRNA) that lacks exon 2 is the most efficiently translated, whilst the remainder of *THPO* mRNA is almost completely inhibited by the uAUGs. BMSCs and osteoblasts may preferentially exclude the use of P1ΔE2 in response to extracellular signals received from the BM microenvironment such as local cytokines or other tissue specific differences between the liver and BM, such as hypoxia. The BM is considered a tissue with limited oxygen supply; several lines of evidence suggest that HSCs prefer this hypoxic environment or 'hypoxic niche' to other more oxygen rich locations (279). Hypoxia may influence alternative splicing by changing the intracellular localisation of some splicing factors. For example, hypoxia causes the accumulation of the splicing factor tra2-beta1 in the cytosol rather than the nucleus, resulting in alterations in the splicing of its target genes (280).

Determining the sources of TPO production by cells in the human BM (both at the transcriptional and translational level) is an important area of research. Recent communication with collaborators has identified a monoclonal anti-human TPO antibody sold by Abcam (ab196026) to be highly specific on human sections, so tools to study BM TPO production exist. If, like in the mouse, *THPO* is transcribed but not translated, studying the mechanism of translational repression would have important therapeutic consequences. If *THPO* expressing BMSCs could be therapeutically targeted to overcome translational repression and start producing TPO protein, this would be hugely beneficial for the 64-84% of patients with liver cirrhosis or fibrosis that have thrombocytopenia (281). To identify *THPO* expressing BMSCs, we used a panel of immortalised human BMSC clonal lines alongside total BMSCs from three independent donors. None of the eight stromal lines expressed any *THPO*, whilst the total BMSCs from the three donors expressed very low levels of *THPO*. Similarly, on a population level, murine BMSCs express very low levels of *Thpo* (too low levels to be detected by qPCR (data not shown)). Total murine BMSCs were isolated by culturing flushed BM in 10%FCS/DMEM for 72 h, followed by washing away the suspension haematopoietic cells (similar to how primary human BMSCs are isolated). This shows that at a population level, *THPO/Thpo* expression from BMSCs is extremely low as the vast majority of BMSCs do not express *THPO/Thpo*. In mice, these *Thpo* expressing BMSCs are enriched in LepR⁺ BMSCs/*Cxcl12*-DsRed^{high} BMSCs.

There is considerable overlap in phenotype between human Y101/Y201 like cells and murine LepR⁺ BMSCs/*Cxcl12*-DsRed^{high} BMSCs *in vivo*. Y101/Y201 express high amounts of CXCL12 (unpublished data from the Genever lab) and are LepR⁺ (251). They are also CD146⁺; CD146⁺ BMSCs are perivascular and widely considered to be the

human equivalents of murine LepR⁺ BMSCs/*Cxcl12*-DsRed^{high} BMSCs (282). Despite their grouping based on similar expression of LepR and *Cxcl12*, LepR⁺ BMSCs/*Cxcl12*-DsRed^{high} BMSCs are a heterogeneous population of cells which may have different functions *in vivo*. For example, 9% of LepR⁺ BMSCs are tripotent, whilst 58% form osteoblastic cells in culture (268). Likewise, despite being 'LepR⁺ BMSC-like,' Y101 and Y201 each have distinctive expression profiles and different differentiation biases; although both Y101 and Y201 are tripotent, Y101 has osteogenic bias. On a population level, LepR⁺ BMSCs and *Cxcl12*-DsRed^{high} BMSCs express 29% and 25% respectively of *Thpo* expressed by whole liver. However, neither Y101 nor Y201 express any *THPO* transcripts. Assuming mouse to human translatability, this indicates that there are subpopulations of LepR⁺ BMSC-like cells distinct from Y101 and Y201-like cells that express high levels of *THPO*. Expression of *Thpo* by *Thpo*-expressing LepR⁺ BMSCs on a single cell level is likely to be even higher than the indicated 29%, as the population analysed will be diluted by non *Thpo*-expressing LepR⁺ BMSCs.

However, an argument could be made to caution against the therapeutic driving of TPO translation from *THPO* expressing BMSCs. Found in the low picomolar range in the plasma of healthy individuals (283), TPO is clearly a very potent cytokine. TPO overstimulation can be pathogenic; the abnormally low expression of MPL in platelets and Mks of human patients with myeloproliferative neoplasms (MPN) is associated with thrombocytosis (284, 285). Similarly, mice that express *Mpl* normally on HSPCs but lack expression on Mks and platelets (*Mpl*^{PF4cre/PF4cre}) develop a myeloproliferative neoplasm (MPN)-like phenotype due to the lack of TPO clearance by Mks and platelets (144). HSPCs from both *Mpl*^{PF4cre/PF4cre} and from patients with MPNs had a gene signature associated with TPO overstimulation (144). Considering that HSCs reside adjacent to or in very close proximity to LepR⁺/*Cxcl12*-DsRed^{high} BMSCs (69), the inhibition of TPO translation in sub-populations of BMSCs that express high levels of *Thpo*/*THPO* may therefore be a protective mechanism against TPO overstimulation. Any therapeutics designed to uninhibit TPO translation from *THPO* expressing BMSCs would have to be reversible and carefully monitored.

In conclusion, my data showing that Mks do not transcribe *Thpo* is in agreement with a recent study by Decker and colleagues (147), which contradicts previous studies by Nakamura-Ishizu and colleagues (163, 164). In further agreement with Decker and colleagues (147), I show that LepR⁺/*Cxcl12*-DsRed^{high} BMSCs transcribe approximately 1/3 of *Thpo* transcribed by murine liver. Further analysis indicates that *Thpo* transcription by BMSCs is heterogeneous and does not respond to thrombocytopenia. Importantly, Decker and colleagues show that murine BM does not translate TPO (147); if human

BM also does not translate TPO, characterising the mechanism of translational repression is an important area of future research as it may have therapeutic potential in conditions where liver TPO production is impaired.

4 Generation of a model of sustained immune thrombocytopenia

4.1 Introduction

ITP is an acquired autoimmune disorder characterised by both the destruction of functionally normal platelets and reduced platelet production, which manifests as a bleeding tendency (200). The majority of ITP patients develop serum platelet specific autoantibodies that target platelets for destruction and are primarily against platelet glycoprotein (GP) IIb/IIIa (CD41/CD61), GPIb/IX (CD42c/CD42a), GPV (CD42d) and GPIa/IIa (CD49b) (214, 286-288). Of these, autoantibodies against CD41/CD61 are the most common (287, 288). The spleen is the major site of platelet clearance which is primarily mediated through phagocytosis by splenic macrophages or dendritic cells (225, 228). Antigenic peptides derived from platelet glycoproteins are presented to CD4⁺ cells which causes activation and expansion of autoreactive B and T cells (289, 290). ITP patients can be classified as 'newly diagnosed' (< 3 months) or 'persistent' (< 12 months) which is more common in children, as well as 'chronic' (> 12 months) which is more common in adults (200, 209).

The majority of studies using animal models of ITP utilise the passive transfer model where anti-platelet antiserum or platelet specific monoclonal antibodies are injected into recipients, causing thrombocytopenia via antibody mediated platelet destruction (291-293). Passive transfer models are typically used to evaluate the efficacy of therapeutics (such as IVIg therapy or cell based therapies) or to understand ITP disease progression (294-297). However, these studies are typically short in duration, lasting up to one week (294, 297), or two weeks in the case of one isolated study (117).

To better model sustained ITP, I extended the passive transfer model to 4 weeks, where the mice shared a number of features associated with the clinical progression of chronic ITP such as increased megakaryopoiesis (whilst maintaining normal circulating TPO levels), mild splenomegaly and spontaneous bleeding. This mouse model will therefore be useful in investigating ITP progression, especially in investigating the mechanism behind the increased megakaryopoiesis in ITP, which is currently unknown. Recent evidence has shown that inflammation can drive emergency megakaryopoiesis (116, 298), which is of interest as autoimmune diseases are often associated with chronic inflammation. However, when inflammation is maintained over several weeks, HSC functionality is impaired suggesting that there may be broader implications for haematopoiesis during sustained ITP (112). This chapter defines and phenotypes the

sustained model of ITP, whilst subsequent chapters use the model to further explore the immune and haematopoietic systems.

4.2 Materials and methods

4.2.1 Immune thrombocytopenia model

Mice were administered rat unconjugated anti-CD41 antibody to selectively deplete platelets, or rat unconjugated IgG1 to act as a control (2.6), via intraperitoneal injection every 48 h. Concentration of anti-CD41/IgG1 began at 0.2 mg/kg and was increased by 0.1 mg/kg when the average platelet count of the anti-CD41 injected group rose above $200 \times 10^3/\text{mm}^3$ (typically a 0.1 mg/kg increase every 7 days). Mice were bled (2.5.1.1) before the first injection to obtain baseline complete blood counts, minimum once a week thereafter for monitoring. The time courses used were 48 h, 2 or 4 weeks.

4.2.2 Thrombopoietin enzyme-linked immunosorbent assay

Plasma samples were obtained by cardiac puncture as described previously (2.5.1.2). 50 μL of sample was analysed for TPO concentration using the Mouse Thrombopoietin Quantikine ELISA Kit (MTP00; R&D systems) according to the manufacturer's instructions. The optical density of each sample-containing well of the provided microplate strips was read at 450 nm with wavelength correction set to 595 nm (iMark Microplate Absorbance Reader, Bio-Rad).

4.2.3 Quantification of bone marrow megakaryocyte number

Mice were administered anti-CD41 antibody/IgG1 for 2 or 4 weeks (4.2.1), before culling. One femur per mouse was isolated, prepared and sectioned (2.7) and BM sections were H&E stained (2.8) and Mk numbers were manually counted using a light microscope (20x objective) by an independent researcher under blinded conditions. 5-8 random fields of view were obtained per section, and 4 sections were analysed per mouse.

4.2.4 Determination of whether injected anti-CD41 binds to megakaryocytes: flow cytometry

Mice were administered anti-CD41 antibody/IgG1 for 2 weeks (4.2.1), before culling. Haematopoietic BM cells were collected (2.5), followed by a wash in FACS buffer. As standard FcR blocking antibodies are raised in rat, the BM cells were not blocked beforehand as this would have resulted in non-specific binding of the goat anti-rat secondary antibody. To ensure that the majority of SSC^{high} events were of the Mk lineage, cells were stained with rat unconjugated anti-CD41 antibody for 20 min at 4 °C. Specific antibody information is found in 2.6. Cells were then washed 3x in FACS buffer, before being stained with goat anti-rat Alexa Fluor 488 for 20 min at 4 °C. To determine whether injected anti-CD41 binds to Mk, 4×10^6 BM cells were stained with goat anti-rat

Alexa Fluor 488 only (no primary). After staining, cells were washed three times in FACS buffer. After the final wash, cells were resuspended in FACS buffer and acquired on the Cytotflex LX or CytoFLEX S (Beckman Coulter). All cells were pre-gated on viable and single cells. All data was analysed with FCS Express (De Novo) software.

4.2.5 Determination of whether injected anti-CD41 binds to megakaryocytes: microscopy

To confirm the results of 4.2.4 by microscopy, one femur per mouse was prepared and sectioned (2.7). Sections were prepared for blocking by rehydration in PBS for 5 min, followed by permeabilisation in 0.1% (v/v) Triton X-100/PBS for 10 min, followed by a final PBS wash. The slides were blocked in 10% (v/v) goat serum in 0.1% (v/v) tween-20/PBS (PBST) for 1 h. To stain the vasculature, slides were stained with anti-laminin (L9393; Sigma) at 1:200 dilution in 10% goat serum/PBST overnight at 4 °C. The following secondary antibodies were purchased from ThermoFisher and were used at 1:500 dilution: goat anti rat IgG-AF568 (A-11077) and goat anti rabbit IgG-AF488 (A-11008). Sections were mounted with ProLong Gold with DAPI (ThermoFisher). All images were acquired using the LSM 880 confocal microscope (Zeiss) with a 40x objective in lambda mode and were spectrally unmixed.

4.3 Results

4.3.1 Repeated anti-CD41 intraperitoneal injection as a model of sustained immune thrombocytopenia

To study ITP progression, a model for sustained ITP was established by the repeated intraperitoneal injection of mice with a monoclonal rat anti-CD41 antibody, maintaining severe thrombocytopenia (defined as a mean platelet count below $200 \times 10^9/L$). At the same time points and at equal concentrations, mice in the control group were injected with rat IgG1 isotype control to monitor for non-specific immune responses. With time, mice become refractory to anti-CD41 injection (299), so after the first 14 days of the time course, an increase of 0.1 mg/kg every 7 days was necessary to maintain severe thrombocytopenia for a 4 week period. Hereafter, mice treated with anti-CD41 are referred to as the 'ITP' group; mice treated with IgG1 are referred to as the 'control' group.

A typical complete blood counts of a 4 week experiment is shown by Figure 4.1, however 2 week and 48 h time points were also used. Figure 4.1A shows a rapid induction of ITP from a resting platelet count of $865 \pm 57.2 \times 10^9/L$ (mean values \pm SD) to mean platelet count of $107 \pm 14.6 \times 10^9/L$, 24 h after antibody injection. Severe thrombocytopenia was maintained throughout the 4 week experiment, with a final mean platelet count of $128 \pm$

18.4x10⁹/L, 29 days after the first antibody injection. Figure 4.1B shows the mean platelet volume (MPV), which is an indicator of increased thrombopoiesis (300). 24 h after antibody injection the resting MPV (6.08 ± 0.068 μm) increases to 6.81 ± 0.118 μm. It continues to rise until it reaches a maximum value of 7.30 ± 0.131 μm, 15 days after first antibody injection.

The red blood cell count does not differ significantly from controls (Figure 4.1C), which is also reflected in the haematocrit (Figure 4.1D). Initially (24 h after the first injection), there are slightly higher levels of subpopulations of white blood cells of control mice relative to mice with ITP (Figure 4.1E-G). However, with the exception of the granulocyte count which remains at slightly higher levels throughout, the monocyte and lymphocyte counts revert back to similar levels as mice with ITP.

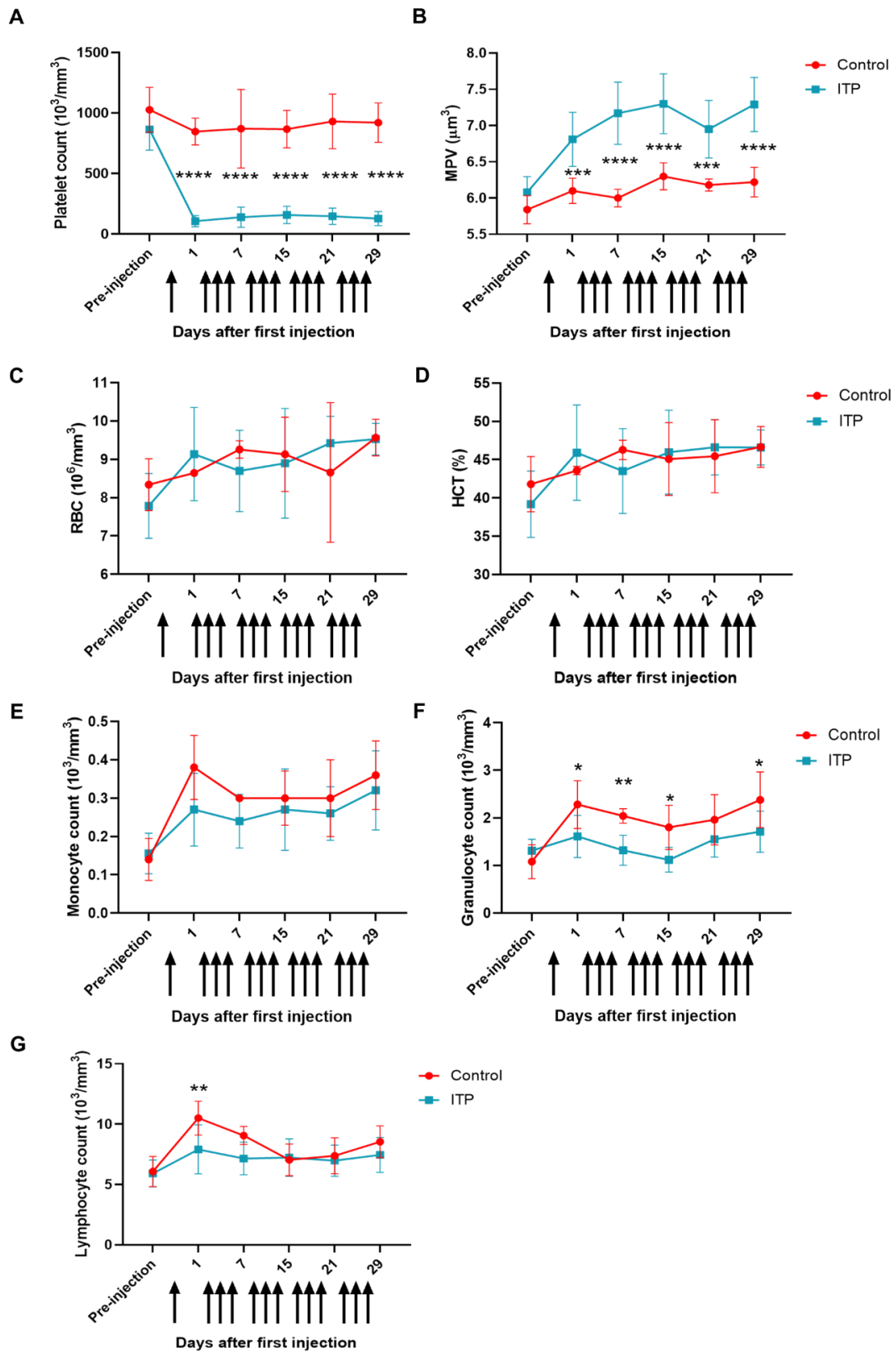


Figure 4.1. Repeated intraperitoneal injection of mice is a model for sustained ITP. A single intraperitoneal injection of anti-CD41 antibody (delineated by an arrow) every 48 h induces severe thrombocytopenia. For routine monitoring of ITP induction, mice were bled 24 h after injection and complete blood counts measured. For the first 14 days, anti-CD41 antibody was used at 0.2 mg/kg in sterile PBS. Hereafter, the concentration of anti-CD41 antibody was increased by 0.1 mg/kg every 7 days. **A** Platelet count, **B** mean platelet volume (MPV), **C** red blood cell (RBC) count, **D** haematocrit (HCT) percentage, **E** monocyte count, **F** granulocyte count, **G** lymphocyte count. $P^* < 0.05$, $P^{**} < 0.01$, $P^{****} < 0.0001$. P values were calculated by a Two-way ANOVA with Sidak's post hoc analysis. $N = 5$.

4.3.2 Dose escalation is required to maintain severe thrombocytopenia in WT mice, but not *Rag2*^{-/-} mice

To maintain severe thrombocytopenia in WT mice, a dose escalation model was needed. As it was not clear whether this was due to compensatory thrombopoiesis or to production of antibodies against the rat anti-CD41 antibody, *Rag2*^{-/-} (which lack mature B or T cells therefore lack the ability to produce antibody) were used alongside WT mice. WT or *Rag2*^{-/-} mice were administered low doses (0.2 mg/kg) of anti-CD41 or IgG every 48 h for a 4 week period. Figure 4.2 demonstrates that *Rag2*^{-/-} mice maintain severe thrombocytopenia throughout the 4 week experiment. In contrast, WT mice exhibit a partial platelet rebound by day 17.

Together, the results suggest that the production of antibodies by WT mice against the injected rat anti-CD41 antibody is, at least partially, responsible for platelet rebound by day 17. Therefore for subsequent experiments, a dose escalation model will be used to maintain severe thrombocytopenia for long periods of time.

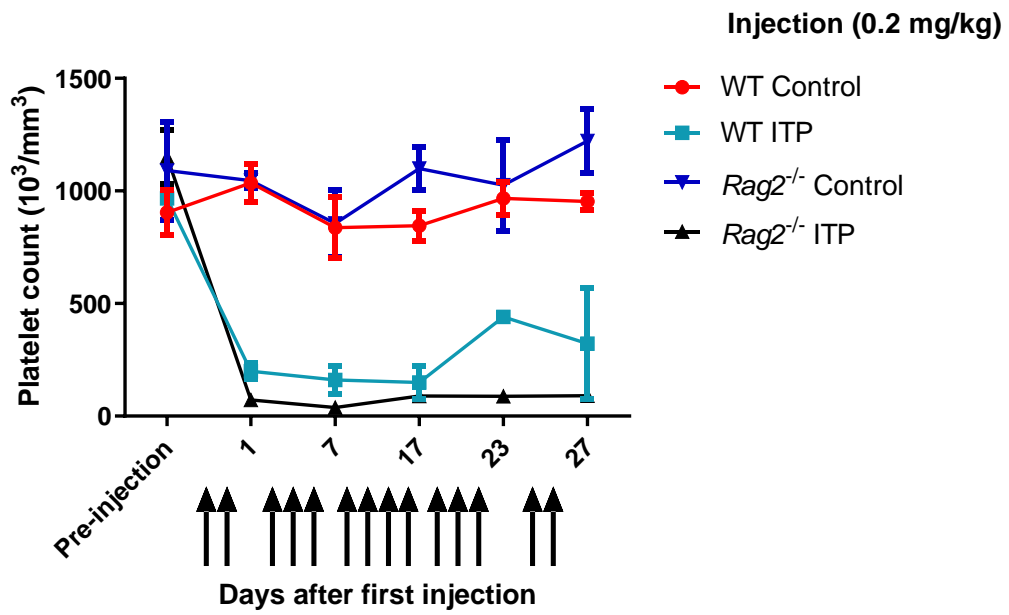


Figure 4.2. *Rag2*^{-/-} mice maintain severe thrombocytopenia at low doses of anti-CD41. WT or *Rag2*^{-/-} mice were administered low doses (0.2 mg/kg) of anti-CD41 or IgG via intraperitoneal injections (delineated by an arrow) every 48 h for a 4 week period. Mice were bled 24 h after injection and complete blood counts measured. WT and *Rag2*^{-/-} mice both maintained severe thrombocytopenia initially, but by day 17, WT mice exhibited a partial platelet rebound. *Rag2*^{-/-} mice maintained severe thrombocytopenia throughout the experiment. N = 3.

4.3.3 Sustained immune thrombocytopenia model exhibits clinical features of immune thrombocytopenia

Spontaneous bleeding is a common feature that can occur in ITP patients due to their low platelet count (201). Post-mortem analysis of mice with 4 week ITP revealed that 40% of mice appeared to have evidence of sub-cutaneous bleeding (an example of which is shown in Figure 4.3), which was not observed in control mice.

Moderate or massive splenomegaly (enlarged spleen between 4.1 and 10 cm, and greater than 10 cm below the left costal edge in human adults respectively (301)) is not typical of ITP and may suggest an alternative cause, however mild splenomegaly may be found in younger patients (205). In the model of sustained ITP, the spleen is not obviously palpable, therefore does not suggest moderate or massive splenomegaly. Figure 4.4A shows a freshly isolated spleen from a mouse with 4 week ITP alongside a spleen from a control mouse for comparison. Upon isolation, there does not appear to be any obvious differences in terms of morphology or size. However, in the absence of significant splenomegaly, one of the biggest influencers on splenic size is the overall size of the mouse. In order to more accurately determine whether ITP progression causes splenomegaly, the spleen length (Figure 4.4Aii) and weight (Figure 4.4B) were normalised to the total mouse weight (taken immediately before the mouse was sacrificed). Although the spleen length remains consistent between the two groups at 4 weeks (Figure 4.4Aii), a 45.1% increase was observed in spleen weight for mice with ITP at the same time point (Figure 4.4B). Furthermore, this increase in spleen weight is independent of the adaptive immune system, as *Rag2*^{-/-} mice exhibited a 74.0% increase in spleen weight at 4 weeks of anti-CD41 treatment (Figure 4.4C). Together, the results show that moderate or massive splenomegaly does not occur in the model of sustained ITP. However, mild splenomegaly does occur with ITP progression and this is mainly driven by an increase in spleen weight, rather than an increase in spleen length.

Despite the low observed platelet levels characteristic in ITP, plasma TPO levels are normal (153). This is reflected in Figure 4.5; plasma TPO levels from mice with 48 h, 2 week and 4 week ITP are unchanged from controls. Despite this, BM Mk numbers increase with ITP progression, suggesting the occurrence of TPO independent emergency megakaryopoiesis. Mk numbers were unchanged at 2 weeks, but by 4 weeks, the number of Mks had increased by 81.5% (Figure 4.6). Increased megakaryopoiesis is observed in ITP patients (302-304).

Control



ITP



Figure 4.3. Sustained ITP model appears to induce occasional spontaneous bleeding. Post-mortem analysis of mice with 4 week ITP or controls revealed that 40% of mice with 4 week ITP appeared to have evidence of subcutaneous bleeding (highlighted by black arrows). No such observations were found in control mice. N = 5.

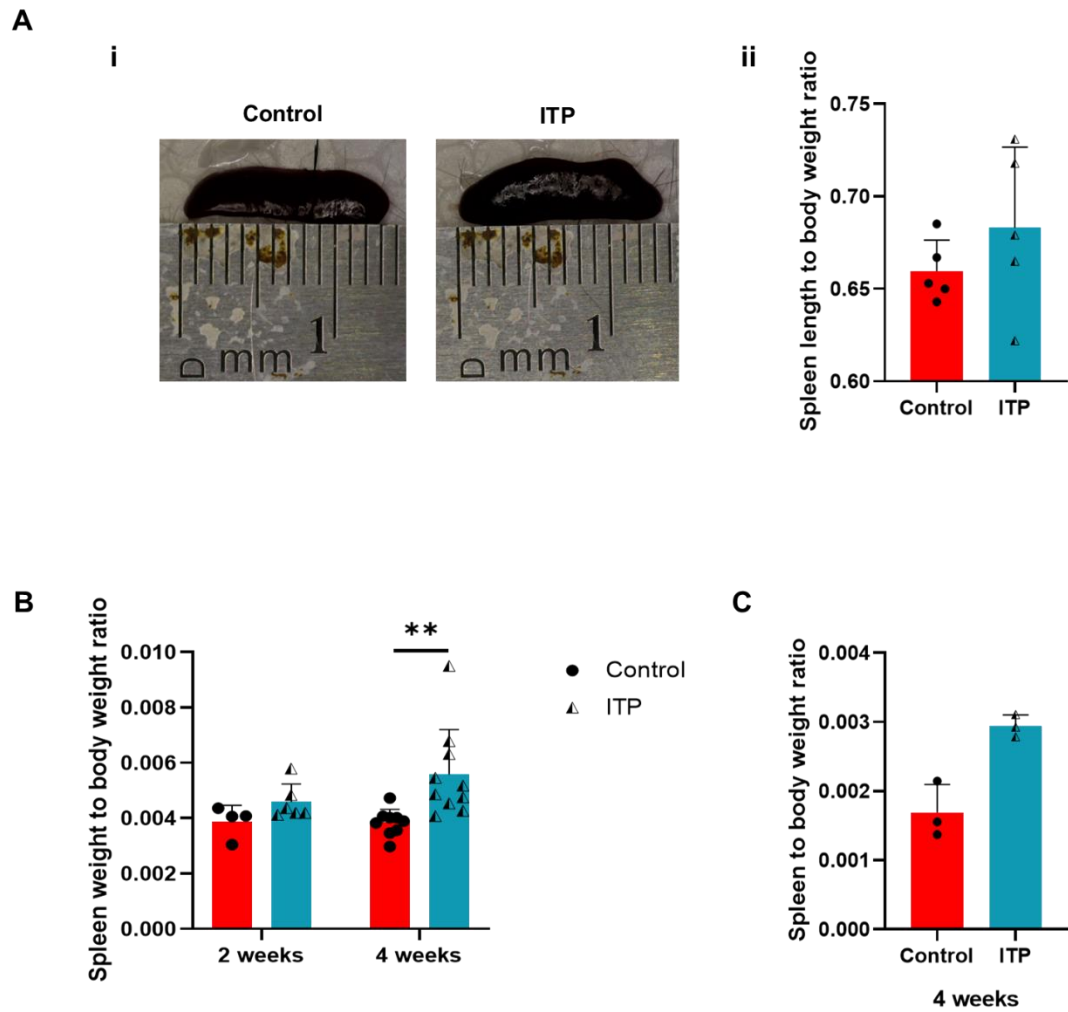


Figure 4.4. Mild splenomegaly during ITP progression occurs in the absence of a functional adaptive immune system. **Ai)** representative images of spleen from mice with 4 week ITP and controls. **ii)** spleen length to final body weight ratio in mice with 4 week ITP and controls. *P* values were calculated by a Mann-Whitney test (*P* = 0.42). *N* = 5. **B)** and **C)** show the spleen weight to body weight ratio of WT and *Rag2*^{-/-} mice, respectively. *P* values for B) were calculated by 2way ANOVA with Sidak's multiple comparisons test (***P* = 0.0034). *N* = 4-10. *P* value for C) was calculated by a Mann-Whitney test (*P* = 0.1). *N* = 3.

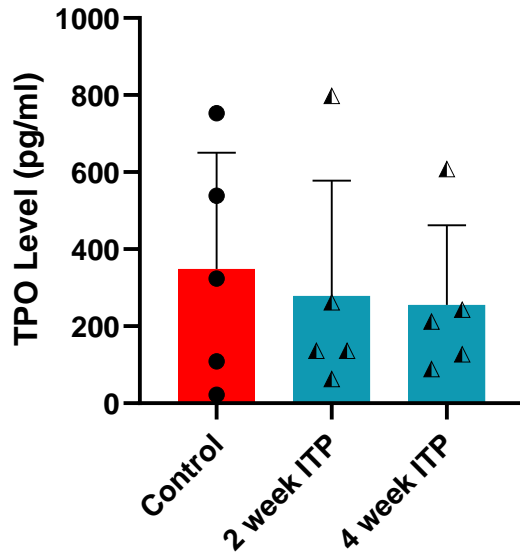


Figure 4.5. Plasma TPO levels are normal during ITP progression. Circulating thrombopoietin (TPO) levels during ITP progression (control vs 2 week ITP $P > 0.99$, control vs 4 week ITP $P > 0.99$, 2 week ITP vs 4 week ITP $P > 0.99$). $N = 4-5$ (2 independent experiments). P values calculated by a Kruskal-Wallis test with Dunn's multiple comparisons test.

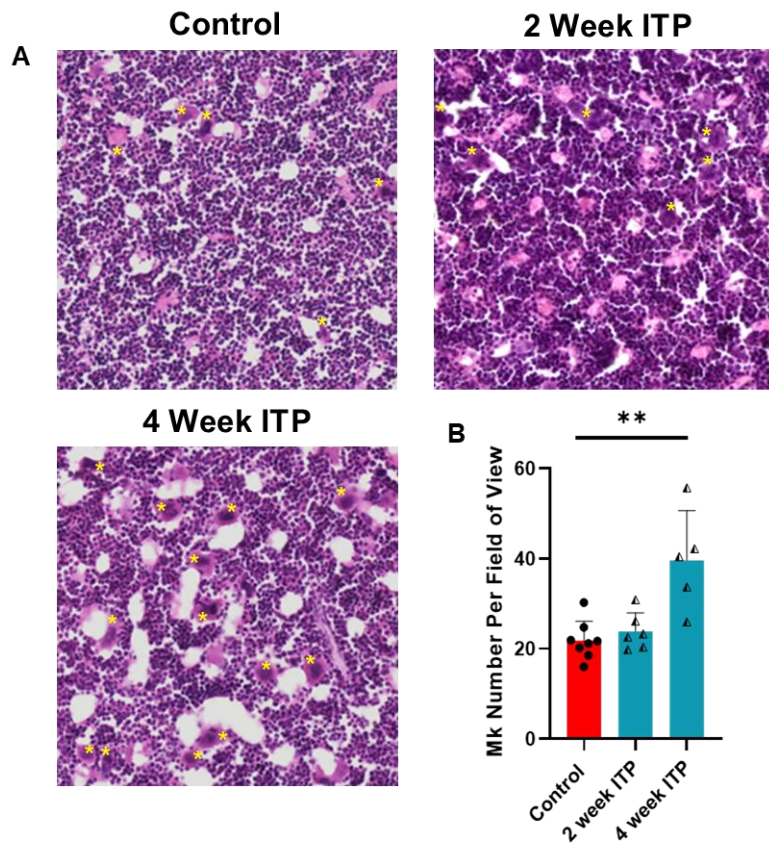


Figure 4.6. BM Mk numbers increased with ITP progression. A) Representative H&E stained BM sections from mice with 2 and 4 week ITP as well as control BM. Yellow stars indicate Mks. **B)** Mk numbers were manually counted using a light microscope (20x objective). Counts were obtained by an independent researcher under blinded conditions. Control vs 2 week ITP $P > 0.99$, control vs 4 week ITP $**P = 0.0069$, 2 week ITP vs 4 week ITP $P = 0.10$. $N = 5-8$. P values calculated by a Kruskal-Wallis test with Dunn's multiple comparisons test.

4.3.4 Injected anti-CD41 binds BM Mks

Defects in platelet production in ITP are thought to due to autoantibody binding to Mks and interactions of CD8⁺ T cells with Mks (218, 223). To determine whether the injected rat anti-CD41 antibody binds to Mks, flow cytometry and confocal approaches were used, exploiting the biophysical characteristics of Mks for their identification. Mature Mks are highly granular due to their α -granule content and appear as SSC^{high} cells by flow cytometry (305, 306). In agreement, the majority of SSC^{high} cells are CD41⁺ (Figure 4.7A). When this same gate was used on samples that were stained with anti-rat secondary antibody only, BM samples originating from mice treated with anti-CD41, but not IgG, had a shift in fluorescence. This indicated that the anti-CD41 antibody binds to SSC^{high} cells, most likely Mks.

As well as being highly granular, mature Mks are large, autofluorescent cells and have a polyploid nucleus. Using the three parameters of size, polyploidy and autofluorescence, mature Mks can therefore be identified with a high degree of certainty. When staining IgG and anti-CD41 treated mice with an anti-rat secondary antibody, the cell surface of Mks from anti-CD41 treated mice (but not IgG treated mice) stain positive for the secondary antibody (Figure 4.7B). This confirms that the injected anti-CD41 antibody binds to mature Mks in the model of sustained ITP.

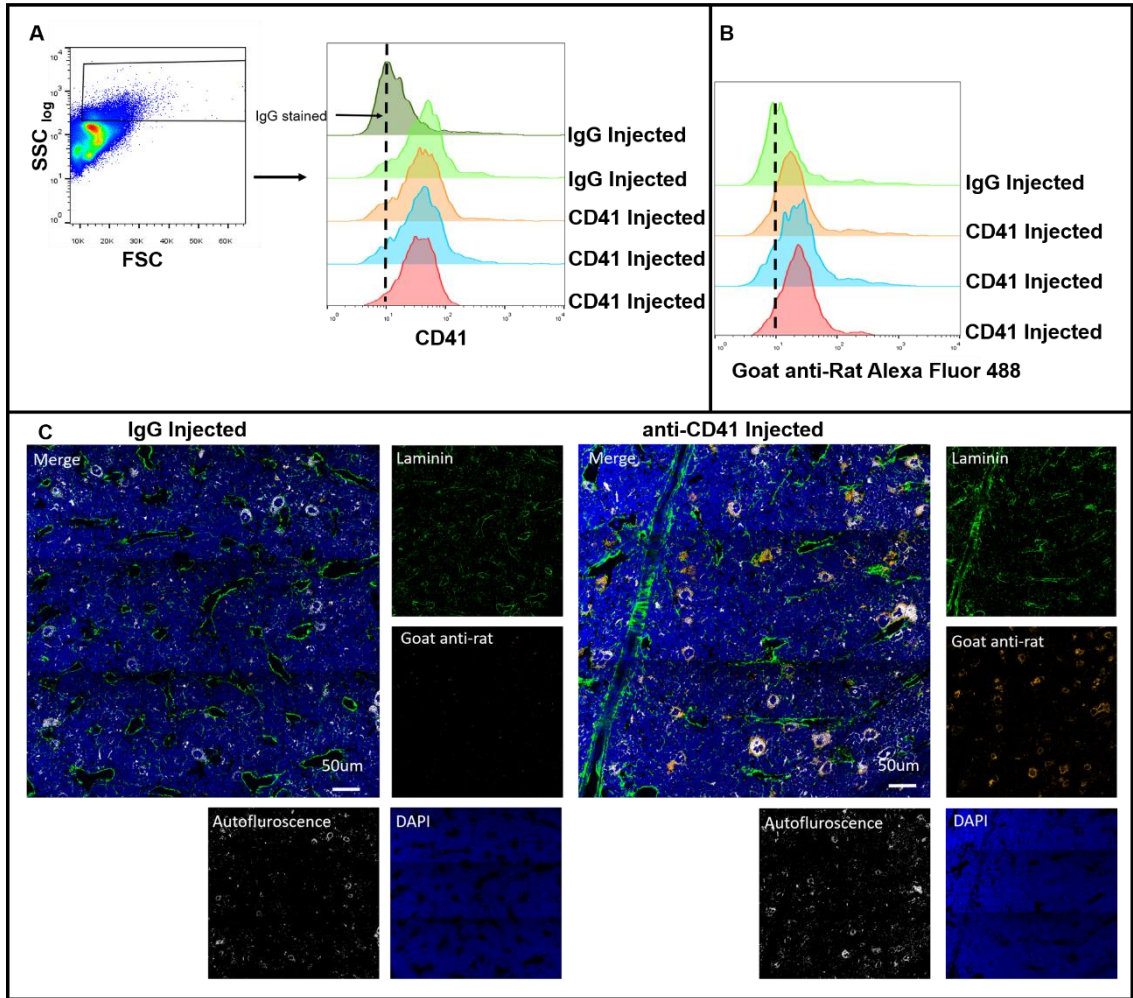


Figure 4.7. Injected anti-CD41 binds BM Mks. **A)** The majority of SSC^{high} cells in flushed BM are Mks (marked by CD41 expression). **B)** A fluorescently conjugated anti-rat secondary antibody binds SSC^{high} cells in mice injected with a rat anti-mouse CD41 antibody, but not rat IgG injected mice. **C)** Immunofluorescence microscopy analysis of stained BM sections confirms flow cytometry results. Mks are identified using a label free technique as autofluorescent^{high}, large cells with polyploidy nuclei.

4.3.5 Platelet recovery is similar between mice with sustained immune thrombocytopenia and acute immune thrombocytopenia

As well as peripheral platelet destruction, defects in platelet production are thought to occur in ITP (246, 247). To address whether mice with sustained ITP have defects in platelet production, mice were either administered anti-CD41 for 4 weeks (sustained ITP), or were administered a single dose of anti-CD41 (acute ITP) and platelet recovery monitored (Figure 4.8). Both groups had severe thrombocytopenia 1 day after the final injection; mice from the sustained ITP group had a platelet count of 107 ± 14.8 and mice from the acute ITP group had a platelet count of 46.4 ± 6.55 (Figure 4.8A). At this same time point, mice from the sustained ITP group had a significantly higher MPV value of $7.34 \pm 0.218 \mu\text{m}^3$ as opposed to $6.16 \pm 0.098 \mu\text{m}^3$ for the acute ITP group. By day 2, platelet counts in both groups had begun to rise, with steeper rise observed in the sustained ITP group, whilst MPV of the acute group rose to similar levels as the sustained ITP group.

By day 6, both groups had platelet counts more than double that of resting. This 'overshoot' effect where platelet counts climb to supranormal levels, then stabilise back to normal is a well-documented yet incompletely understood phenomenon (307). However, the platelet count was not statistically different between groups. Here, the MPV of both groups dropped to baseline, indicating that by day 6, platelet production was normal. By day 10, the platelet count of both groups return to baseline, however the return of the sustained ITP group was slower than the acute group. This trend continued and by day 18 the platelet counts were at similar levels between the two groups. Whilst still at higher levels than baseline at day 18, the platelet counts were considered to be within the normal range using our blood counter, therefore the experiment was terminated. Together, the results show that the trend of platelet recovery was similar between the two groups. However, the rise in platelet count was quicker (day 1-6) and the second drop in platelet count was slower (day 10-18) in the sustained ITP group (Figure 4.8A).

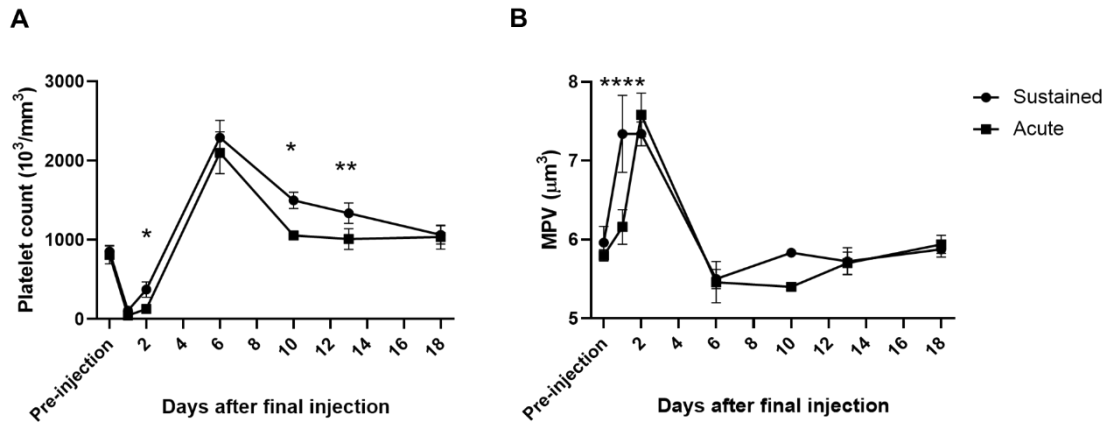


Figure 4.8. Platelet recovery is similar between mice with sustained ITP and acute ITP. Mice were administered anti-CD41 for 4 weeks (sustained) or administered a single dose of anti-CD41 (acute), and the **A**) platelet counts, and **B**) MPV determined at 1, 2, 6, 10, 13 and 18 days after the final anti-CD41 injection. $P^* < 0.05$, $P^{**} < 0.01$, $P^{****} < 0.0001$. P values were calculated by a Two-way ANOVA with Sidak's post hoc analysis. $N = 5$ with the exception of day 10 which was $N = 2$ due to a technical error.

4.4 Discussion

The passive and the adoptive transfer model are the two established murine models of ITP (291-293, 308). I found that the passive transfer model using anti-mouse CD41 antibody to induce thrombocytopenia was well tolerated by the mice used which allowed for its application over extended periods of time, and therefore study of ITP progression. This is in contrast with an adoptive transfer model where recipients have an 80% bleeding mortality within 21 days after transfer – therefore the ability to perform long term experiments is limited (308). ITP patients commonly develop anti-GPIIb/IIIa antibodies (214-216), may exhibit spontaneous bleeding and/or mild splenomegaly (201, 205, 309), have normal circulating levels of TPO and normal or increased megakaryopoiesis (153, 302-304). The sustained model of ITP exhibits all of these clinical manifestations, showing that it is clinically relevant. Furthermore, I demonstrated that anti-CD41 binds to BM Mks *in vivo*, the effect of which should be further investigated. The model of sustained ITP model can be applied to a variety of mouse strains (such as reporter mice and mice deficient in adaptive immunity), allowing for the dissection of mechanisms behind ITP progression.

ITP is characterised by isolated thrombocytopenia with an otherwise normal complete blood count (205). Our model of sustained ITP maintains severe thrombocytopenia throughout the 4 week period of anti-CD41 injections, whilst IgG treated controls had a normal platelet count. Platelets newly released from the BM are immature, larger and contain higher amounts of RNA (so called 'reticulated platelets') (300, 310), remaining in the circulation for 24-36 h, during which they progressively decrease their volume and RNA content (311). An increased MPV is therefore indicative of increased thrombopoiesis (300). ITP patients have an increase in MPV which can be useful to the clinician in determining whether thrombocytopenia is a result of hypo-production of platelets (such as aplastic anaemia) or hyper-destruction of platelets (312). Similarly, mice with sustained ITP have an elevated MPV showing the clinical relevance of the model.

The red blood cell count and haematocrit is normal during the model of sustained ITP, indicating that the thrombocytopenia is not due to BM failure. The white cell count follows the same trend between the ITP group and the control group, although there is a slight reduction of granulocytes in the peripheral blood of mice with ITP compared to controls. Although the causes of this are unclear, recent evidence has suggested that platelets can have a number of immunomodulatory roles (313). One hypothesis is that treatment of mice with rat IgG evokes an immune response, which is directly dampened down during ITP due to platelet depletion. Alternatively, ITP may indirectly modulate

granulocyte number, where phagocytosis of the antibody-platelet complex produces an anti-inflammatory factor that prevents the rat IgG mediated elevation in granulocyte numbers. This demonstrates the necessity of injecting control mice with IgG for the same duration and concentration as anti-CD41, thereby controlling against non-specific immune cell interactions caused by the injection of rat IgG.

Researchers who work with animal models of ITP historically refer to repeated injections of antibody as a model of 'chronic ITP,' despite the study typically not exceeding one week (294, 297), or two weeks in the case of one isolated study (117). It is appreciated that the term 'chronic' may be used to distinguish between 'acute ITP' which typically refers to a single injection, and repeated injections where the platelet nadir is maintained over several days. However, there is therefore a disconnect between basic research and the patients in which it serves as patients with chronic ITP have ITP for > 12 months (200). For this reason, I refer to the use of repeated injections of anti-CD41 as 'sustained ITP', or clearly state the duration of ITP e.g. mice with 4 week ITP.

The rat anti-CD41 antibody (MWReg30) was chosen for our model as the majority of ITP patients with detectable autoantibodies have autoantibodies against the CD41/CD61 complex (~70% of patients) (201). Hamster anti-mouse CD61 (2C9.G2) has previously been used to induce ITP in mice, however it requires approximately 5x higher dose than MWReg30 (314, 315). As well as being considerably more costly to perform long term experiments, the consequences of injecting 2C9.G2 at far higher doses than MWReg30 for a prolonged period is unclear. One might predict that the host immune response against 2C9.G2 would be greater than the response against MWReg30, requiring an exacerbated dose increase over time to maintain thrombocytopenia. Rat anti-CD42b is another alternative (297), however fewer ITP patients have autoantibodies against the CD42b-CD42c-CD42d complex (25%) than the CD41/CD61 complex (201). A mouse anti-platelet antibody such as the 6A6 antibody would have been advantageous in avoiding anti-rat/hamster immune responses (316, 317). However the specific antigen target of 6A6 is not clear, therefore may have off target effects which may be exasperated when used long term. For example, (NZW x BXSB) F1 mice (the strain from which the antibody was generated) have a high incidence of myocardial infarction for unknown reasons (318).

At low anti-CD41 doses, mice can become refractory to the antibody injection due to compensatory thrombopoiesis (299). However, this can be overcome by a dose escalation model. Compensatory thrombopoiesis is not observed in our model, possibly as we begin anti-CD41 injections at higher concentrations than a previous study where compensatory thrombopoiesis was reported (68 µg/kg vs 200 µg/kg) (299). Although

dose escalation is eventually needed, this is not until day 17 (as opposed to day 4), and appears to be due to the development of antibodies against rat anti-CD41 rather than compensatory thrombopoiesis. It usually takes at least two weeks for high affinity antibodies to be generated after first exposure to an antigen (319), therefore day 17 is within the expected timeframe. Furthermore, unlike WT mice, *Rag2*^{-/-} mice did not require an escalating dose to maintain severe ITP.

Another advantage of beginning the experiment at a higher concentration of antibody is that injections are only required once every 48 h, rather than once every 24 h. 48 h injections at higher doses are desirable from an NC3Rs standpoint as it reduces the number of injections each animal receives by 50%. From a researcher's perspective, it is also preferable as the generation of the model is less labour intensive.

As described in detail in the introduction, bleeding events in ITP patients are typically mild, such as bleeding in skin and mucosal regions, yet are unpredictable as not all ITP patients with severe thrombocytopenia exhibit spontaneous bleeding (201, 204). It is therefore unsurprising that only a minority of mice with sustained ITP appeared to have evidence of spontaneous bleeding at post-mortem analysis. However, the lack of spontaneous bleeding at the endpoint does not preclude the possibility of spontaneous bleeding at earlier time points. Fur was only shaven from the rear legs to aid the routine sampling of blood over the 4 week time period, so spontaneous bleeding would not have been observed had it occurred elsewhere. A previous one week long study using the dose escalation passive transfer model reported that 100% of mice with ITP developed multiple petechiae that were distributed over the skin (294). However it was not reported how this was assessed so direct comparisons cannot be made.

Moderate or massive splenomegaly is not typical of ITP and may suggest an alternative cause, however mild splenomegaly may occur, especially in younger patients (205, 309). The 'gold standard' definition of splenomegaly is splenic weight, however this can only be determined at splenectomy or post-mortem analysis (320). A palpable spleen is indicative of splenomegaly, however a mildly enlarged spleen could easily be missed on routine clinical examination (320, 321). Although mild splenomegaly may be detected by radiological assessment, this is usually performed to confirm clinical findings rather than a first port of call (322). Mice with sustained ITP did not have an obviously palpable spleen and did not have an increased spleen length to body weight ratio upon isolation. However, whilst assessment of splenic length is a useful index in determining splenomegaly, it is more informative in the context of the width and depth, which allows the clinician to calculate the 'splenic index' (323, 324). As an alternative to measuring three different parameters per spleen, I measured the spleen weight to calculate the

spleen weight to body weight ratio. Mice administered with 2 week ITP had a normal spleen weight to body weight ratio, however by 4 weeks it was increased. This suggests that ITP progression can cause mild splenomegaly. Furthermore, *Rag2*^{-/-} mice also had an increased spleen weight to body weight ratio by 4 weeks, suggesting that splenomegaly was driven by an expansion of some component of the innate immune system. It is hypothesised that this is due to increased numbers of macrophages (which are normal in both WT and *Rag2*^{-/-} mice), as this has been reported in histological analysis of the spleen in ITP patients (309).

The incubation of autoantibodies derived from ITP patients with healthy BM cells have two distinct effects: suppression of megakaryopoiesis (218, 325, 326) and inhibition of pro-platelet formation (327, 328) which is thought to occur via antibody binding to mature Mks and Mk progenitors. Direct evidence of autoantibody binding to mature Mks in ITP has been reported through the detection of Mks bound with IgG in BM trephines obtained from ITP patients (249), however there have been no past studies showing direct evidence of autoantibody binding to progenitors. Confocal microscopy on the BM of mice with ITP revealed that although antibody binding clearly occurred with Mks, there was also anti-CD41 binding to smaller nucleated cells. This was likely to be antibody binding to CD41-expressing progenitor populations (as opposed to non-specific binding as no staining was present in the BM of IgG treated mice). However, this would need to be confirmed by flow cytometry using specific markers of progenitor populations. The effect of anti-CD41 binding to mature Mks *in vivo* was not directly assessed, however, platelet recovery experiments suggested that sustained anti-CD41 treatment compromised thrombopoiesis to some degree. It has recently been shown that the injection of anti-GP1b α into mice also binds Mks (297), causing antibody-receptor internalisation. This led to a downregulation of GP1b α in newly formed platelets, which was postulated by the authors could partially explain the low sensitivity of diagnostic assays aimed at detecting autoantibodies bound to the surface of platelets in ITP patients (329). My data indicates that this may be a GP1b α specific mechanism as anti-CD41 binds the surface of Mks, but is not internalised even 24 h after the final injection.

The suppression of megakaryopoiesis in ITP appears at odds with clinical findings that ITP patients have normal or increased numbers of BM Mks (302-304), which is in agreement with our model. In our model of sustained ITP, Mk numbers were unchanged at 2 weeks. Although past studies have not addressed megakaryopoiesis using a 2 week passive transfer model of ITP, this is in agreement with studies using earlier (1 week) time point where they showed that ITP does not influence BM Mk numbers (297, 330). In contrast, by 4 weeks, the number of Mks had increased by 81.5% in our mouse model.

This is of interest, as increased megakaryopoiesis is associated with chronic ITP patients in particular (304). Morphologically, the majority of Mks in ITP are immature; they are smaller, display a reduction in granularity and platelet formation and have a higher nuclear/cytoplasmic ratio (303, 331, 332). The increase in Mk numbers but decrease in maturity and platelet production suggests compensatory megakaryopoiesis from progenitors.

Previous experiments addressing megakaryopoiesis in ITP have been performed *in vitro* assessing the effect of ITP plasma or purified antibodies on healthy progenitors, therefore independently of any effects that compensatory factors may have on megakaryopoiesis or progenitor activation or expansion (218, 325, 326). As discussed in detail previously, TPO is the master regulator of megakaryopoiesis; circulating levels of which are controlled by platelets and Mks (151, 152). However, TPO levels are normal in ITP patients (153), and is thought to be because platelets are produced in sufficient quantities to bind and internalise TPO before they are degraded by autoreactive B or T cells (201, 333). An alternate hypothesis is that the increased Mks in the BM of ITP patients acts as a TPO sink, which is in contrast to conditions where Mk production is reduced (such as aplastic anaemia and BM hypoplasia) which are associated with a significant increase in circulating TPO (153). Consistent with TPO levels in the plasma of ITP patients, TPO levels are normal in the plasma of mice with sustained ITP.

If TPO levels are normal during ITP, what is driving megakaryopoiesis? Other long range cytokines such as EPO have been shown to drive megakaryopoiesis independently of TPO (334). Alternatively, local signals through an altered BM niche in ITP may be of importance. The CXCL12-CXCR4 gradient guides progenitors to the BM perivascular niche which can stimulate megakaryopoiesis and thrombopoiesis in the absence of TPO signalling (335). Perivascular niche cells such as BMSCs can be induced to express factors such as angiopoietin-like 4, SCF, IL-3 or IL-6 (both singularly and in combination), which can increase both Mks and platelet counts *in vivo* (336, 337). Interestingly, IL-6 is upregulated in the BM and spleen following the induction of acute ITP in mice (292). Furthermore, IFN γ , which is usually upregulated in serum of ITP patients, has been shown to enhance the of megakaryopoietic activity of IL-3 (338, 339). IL-6 and IFN γ are both proinflammatory cytokines, indicating that inflammation may have a role in megakaryopoiesis. The involvement of inflammation in driving emergency megakaryopoiesis was recently confirmed *in vivo* (116, 298). Type-1 IFN signalling activates both Mk-biased HSCs and Mk progenitors (MkPs) to rapidly produce mature Mks (116), whilst a tyrosyl-tRNA synthetase variant has an ex-translational role in directing HSCs to differentiate into Mks as well as upregulating megakaryopoiesis

stimulating factors such as IL-6, VEGF-A and IL-1 α from monocytes within the BM microenvironment (298). Activated CD8⁺ T cells (223), or their secretory factors (325), can increase numbers of BM Mks through inhibition of Mk apoptosis, which is required during the final stages of platelet release (340). Whether activated CD8⁺ T cells are present in our ITP model will be addressed further in Chapter 5.

To determine whether sustained anti-CD41 binding to Mks affects the recovery in platelet counts, platelet recovery was compared between mice with acute ITP and mice with sustained ITP. The differences in platelet counts appear to be in the kinetics of platelet recovery (quicker rebound after nadir and slower decrease after overshoot peak) rather than peak number. This was surprising, as a faster platelet recovery and a slower return to baseline should also present as a higher peak platelet count. The reasons for this are unclear, however it is plausible that the blood counter is inaccurate at counting platelets outside the normal physiological range, and the true platelet count in the sustained ITP group was higher than recorded. An alternate method to determine platelet count could be a flow cytometry method (341). As platelet destruction occurs to a similar extent between groups, the differences in platelet recovery between the sustained and acute group are likely due to differences in thrombopoiesis and/or differences in megakaryopoiesis. In first few days of platelet recovery, increased thrombopoiesis from the sustained group was likely to have contributed to the earlier rise in platelet count based upon the significantly higher MPV. However, as platelet lifespan is 3-4 days in mice (342), and the MPV in both groups had returned to baseline, difference in the peak platelet count and subsequent return to baseline would be heavily influenced by differences in megakaryopoiesis. However, given that the sustained group had almost double the number of BM Mks than the acute group, one might expect that the differences in platelet counts would be greater than that observed. However, this is assuming that the increased Mks are all platelet producing. As previously stated, Mks in ITP are reported to be more immature (303, 331, 332) and may not all be capable of platelet production (303). Although the Mks in mice with 4 week ITP do not appear noticeably immature (e.g. smaller, less polyploid), this has not been formally quantified and therefore cannot be ruled out. Additionally, anti-CD41 binding to mature Mks may be detrimental to platelet production, potentially by inhibiting pro-platelet formation (327, 328). However, the necessary experiments to address this question (e.g. *in vitro* platelet production assays) were considered out of the scope of this PhD. Interestingly, rebound thrombopoiesis after 5-FU treatment is inhibited in *Mpl*^{-/-} mice injected with antibodies to CXCR4, highlighting the importance of the BM niche in reactive thrombopoiesis as well as steady state homeostasis (335).

The Mk lineage is the predominant fate of HSCs in the native, unperturbed setting and differentiation predominantly occurs directly, as opposed to through intermediates in the MPP compartment (32). This raises the question of whether sustained thrombocytopenia could be more detrimental to HSC function long term than other cytopenias. Another important question is whether HSCs are under direct autoimmune attack in ITP, in addition to Mks and platelets. In mice, CD41 is additionally expressed in subpopulations of HSCs (343, 344). Whilst CD41 expression on HSCs is not absolutely required for platelet bias (31, 32), CD41 expressing HSCs consist of a subpopulation of functional HSCs: they are quiescent, myeloid and platelet biased (yet with multi-lineage potential) and have serial repopulation ability (343, 344). Furthermore, CD41 expression is inducible. HSC CD41 expression increases with age (343, 345) and during inflammation (116). Other platelet autoantigens commonly targeted in ITP are also upregulated during inflammation such as CD61 and components of the GPIb-IX-V complex (116).

The clinical relevance of anti-CD41 binding to mouse progenitors is unclear, as Mk priming of HSCs has yet to be convincingly demonstrated in human haematopoiesis. Mk markers appear to be more highly expressed in murine HSCs than human HSCs, however this may also be due to less well developed purification strategies for human HSCs (346). However, this warrants further investigation, especially in adults where the majority of ITP patients have chronic ITP, therefore potential prolonged autoimmune attack on progenitors at a time where upregulation of platelet associated markers may occur on the most primitive of populations.

Together, the data indicates that the novel model of sustained ITP is useful in studying ITP progression (summarised in Figure 4.9). It is clinically relevant: mice are thrombocytopenic by the injection of anti-CD41 which is the most common autoantibody found in patients that display autoantibodies. However, further analysis of the immune system is needed to clarify which cell types are responsible for platelet depletion, and whether cell-mediated autoimmunity exists in this model. This is of importance, as minority of patients do not display autoantibodies, and in these patients ITP is thought to be driven through T cell involvement (201). Mice with ITP display mild splenomegaly and spontaneous bleeding and display increased megakaryopoiesis despite having normal levels of circulating TPO. The latter may indicate emergency megakaryopoiesis in ITP and may have broader implications for haematopoiesis (116), neither of which has previously been assessed. Direct HSC effects may also exist; anti-CD41 binds to BM Mks, and possibly also to CD41 expressing progenitors which may directly influence haematopoiesis.

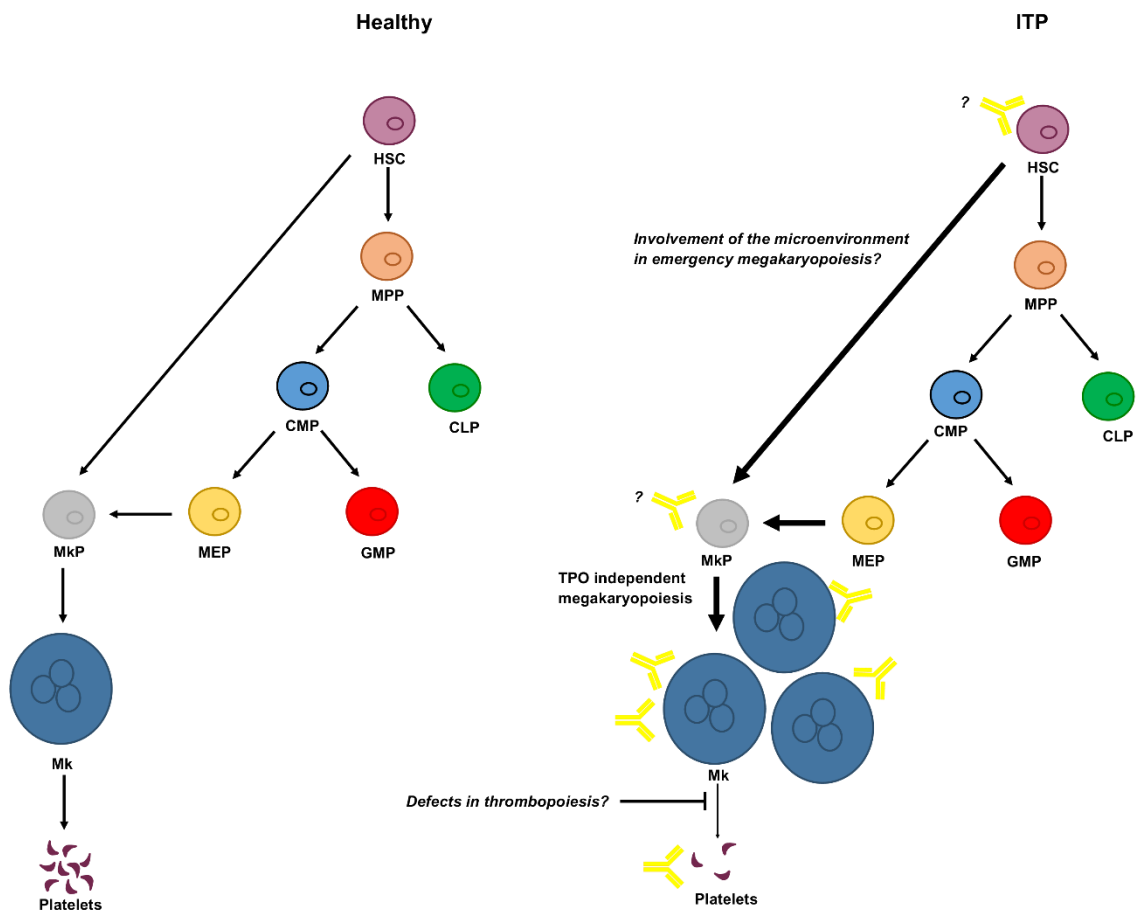


Figure 4.9. A model for sustained ITP. Autoantibody binding to the surface of platelets targets them for destruction. TPO independent emergency megakaryopoiesis occurs to increase thrombopoiesis, and this may be driven by changes in the BM niche. Autoantibody binding to the surface of Mks occurs, and is likely to compromise thrombopoiesis. Autoantibody binding to progenitors (including phenotypic HSCs) may have wider long term consequences for haematopoiesis.

5 Characterisation of the immune system using the sustained ITP mouse model

5.1 Introduction

Splenic macrophages and dendritic cells are major sources of platelet clearance in ITP, binding opsonised platelets through Fc γ -receptors (Fc γ Rs), resulting in phagocytosis and destruction of the antibody-platelet complex (228, 289). Despite their well-established role in platelet clearance, there may also be other, previously unrecognised cell types that also contribute to platelet clearance. For example, monocytes are phagocytic and express Fc γ RIII, the activating Fc receptor responsible for IgG1 binding (254). Characterisation of the immune cells responsible for platelet clearance is important for the identification of new pharmacological targets and may have major consequences for patient therapy.

The current treatment of ITP is based around the suppression of autoreactive platelet destruction (e.g. IVIG, corticosteroids, rituximab) and the stimulation of platelet production (e.g. TPO-RA) (200). However the two approaches are not mutually exclusive; TPO-RAs have been linked to disease remission through immune system modulation leading to a normalisation of the Treg/effector CD8⁺ cell ratio (347). A clinically relevant *in vivo* mouse model allowing for the in-depth analysis of immune populations during ITP progression would be useful in exploring the mechanisms behind ITP progression and response to novel therapies, as well as possible side effects associated with their use long term. Currently, most studies rely on peripheral blood from ITP patients (221, 229, 348, 349), and the use of samples from other clinically relevant sites such as BM or spleen is rare. Therefore, as well as allowing tractability within experiments, the use of a clinically relevant *in vivo* mouse model would allow for the harvest and analysis of important samples ordinarily out of reach.

Using the model of sustained ITP, I determined which immune populations bound labelled antibody-platelet complexes from multiple sites including the bone marrow, blood, spleen and peritoneal cavity, and determined the requirements for the initiation and maintenance of ITP using both immunocompetent WT mice and immunodeficient strains such as *Rag2*^{-/-} and NSG-SGM3 mice. Although NSG-SGM3 mice are typically used for humanisation studies (256), they were available to use and considered a useful model due to their NOD/LtSz-*scid* background and IL-2R γ chain deficiency (350, 351). Additionally, I analysed T cell subsets to determine whether the model mimicked clinical findings and therefore whether the model could be useful in increasing understanding

of cell mediated autoimmunity in ITP as well as in preclinical drug studies aimed at suppressing the T cell response.

5.2 Materials and methods

5.2.1 Flow cytometry

5.2.1.1 *FcRγ* genotyping

FcRγ^{+/-} mice were bred together genotyped by James Hewitson (University of York, results not shown). To confirm genotyping results, I performed FACS analysis of peripheral blood using the anti-mouse CD16/32 antibody as follows:

Mice were bled (2.5.1.1) and red blood cells were lysed in ACK lysing buffer, followed by a PBS wash. Cells were stained with anti-mouse CD16/32-PE/Cy7 diluted in FACS buffer for 20 min at 4 °C (2.6). Stained cells were then washed three times in FACS buffer. After the final wash, cells were resuspended in FACS buffer and analysed on the Cytoflex LX (Beckman Coulter). After the final wash, all cells were resuspended in FACS buffer and analysed on the Cytoflex LX (Beckman Coulter).

5.2.1.2 *Characterisation of the innate immune system at 2 weeks*

WT, *Rag2*^{-/-} or NSG-SGM3 mice were administered anti-CD41 antibody/IgG1 for 2 weeks (4.2.1). If platelets required labelling prior to analysis, mice were given an intraperitoneal injection with anti CD41-FITC or IgG1-FITC 1 h before euthanasia (summarised in Figure 5.1), which was achieved by an overdose of anaesthetic and exsanguinated by brachial bleed (2.5.1.3). After cervical dislocation, peritoneal macrophages were collected by a peritoneal wash.

To perform a peritoneal wash, a small incision was made along the midline of the euthanised mouse and the abdominal skin retracted to expose the intact peritoneal wall. 5 mL of ice-cold RPMI (Gibco) media was injected slowly into the peritoneum using a 25 G ⁵/₈ needle, with care taken not to puncture any organs. To suspend the cells in RPMI, the mouse was gently agitated for up to a minute. The needle was reinserted into the peritoneum and the fluid collected and placed on ice until the cells were needed.

Haematopoietic BM cells were collected as described previously (2.5.2). Splenic cell suspensions were prepared by dicing spleens with a razor blade and digested with DMEN supplemented with 0.25 mg/mL collagenase IV and 0.1 mg/mL DNase I (both Roche) for 20 min at 37 °C with gentle agitation. Digested tissue was then passed through a 70 μM cell strainer which was washed with 2%FBS/PBS and the flow-through collected for downstream analysis. All cells (blood, peritoneal, BM and spleen) were prepared for FACS analysis (2.6), with blood and BM cells were stained with the following antibodies at 4 °C for 20 min: CD115-PE, CD11b-APC, CD45-APC/Cy7, Ly6C-

BV605, Ly6G-PE/Cy7 and MHC II-AF700. Spleen cells were stained with the following antibodies at 4 °C for 20 min: F4/80-PE, CD11b-APC, CD45-APC/Cy7, Ly6C-BV605, Ly6G-PE/Cy7 and MHC II-Alexa Fluor 700. Peritoneal cells were stained with the following antibodies at 4 °C for 20 min: F4/80-PE, CD11b-APC and MHC II-AF700. Specific antibody information is found in Table 3. After staining, cells were washed three times in FACS buffer. After the final wash, cells were resuspended in FACS buffer and analysed on the Cytoflex S (Beckman Coulter).

All cells were pre-gated on viable and single cells. All data was analysed with FCS Express (De Novo) software.

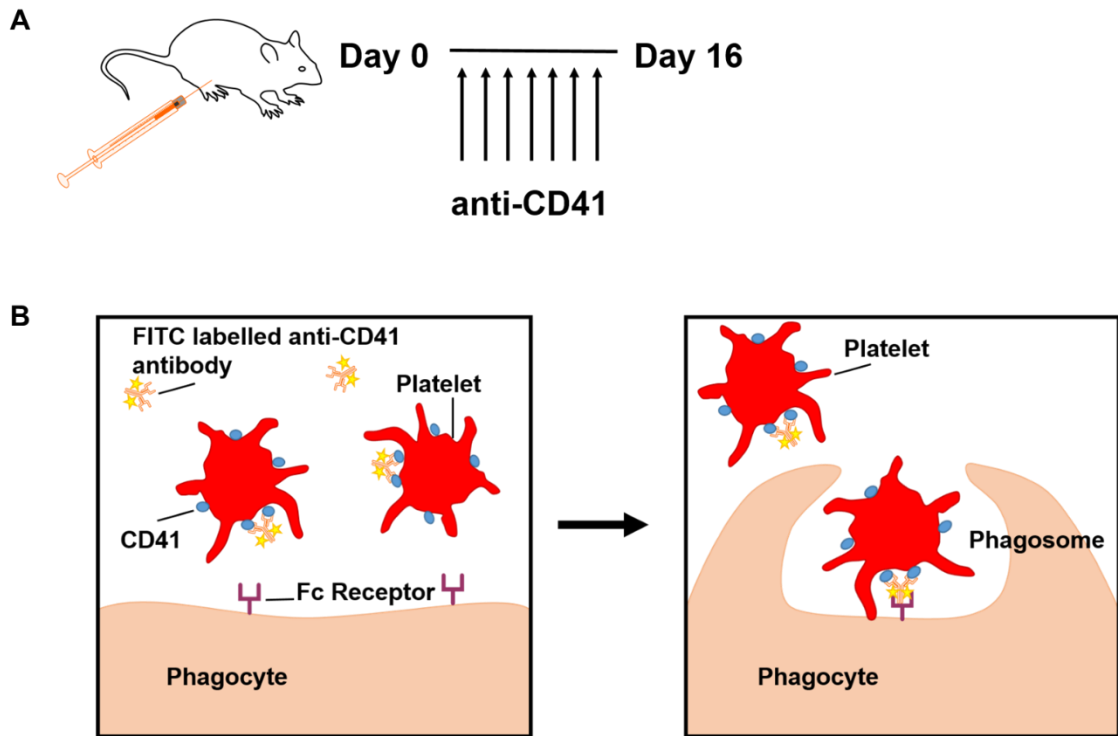


Figure 5.1. Summary of platelet labelling experiment. A) Mice were injected with unlabelled anti-CD41 every 48 h for 2 weeks. **B)** On day 16, mice were injected with anti-CD41-FITC, followed by culling 1 hr later and analysis to determine which cells bound to FITC labelled platelets.

5.2.1.3 Characterisation of T cell subsets at 4 weeks

WT mice were administered anti-CD41 antibody/IgG1 for 4 weeks (4.2.1), then euthanised prior to BM and splenic harvest (2.5.2). For T cell stimulation, cells were stimulated in RPMI supplemented with 0.5 µg/mL PMA, 1 µg/mL ionomycin and 10 µg/mL brefeldin (all Sigma) for 4 h in cell culture conditions. Cells were then prepared for FACS analysis (2.6).

Cell surface markers were stained with the following antibodies in FACS buffer for 20 min at 4 °C. General phenotype panel (to identify B cells, CD4 and CD8 subtypes): CD8a-APC, TCR-β-PerCP/Cy5.5, CD62L-PE/Cy7, CD44-FITC, CD19-PE and CD4-APC/Cy7. Tfh cell panel: TCR-β-PerCP/Cy5.5, CD4-APC/Cy7, CD44-FITC, CD62L-PE/Cy7, CXCR5-APC, PD-1-PE. Treg panel: TCR-β-PerCP/Cy5.5, CD4-APC/Cy7, CD44-FITC, CD62L-PE/Cy7 and CD25-PE. Intracellular cytokine panel: CD8a-APC and CD4-APC/Cy7. Specific antibody information is found in Table 2. Stained cells were then washed twice in FACS buffer.

Cells stained with the general phenotype or T Follicular Helper Cell panel were additionally fixed for 15 min at 4°C in 2%PFA/PBS, followed by a further two washes in FACS buffer.

Cells stained with the Treg panel were fixed/permeabilised with the eBioscience Foxp3 / Transcription Factor Fixation/Permeabilization Concentrate and Diluent kit at 1X concentration for 1 h in the dark at 4 °C. Cells were washed twice in 1X permabilisation buffer, followed by staining with Foxp3-AF647 in permabilisation buffer for 20 min at 4 °C (Table 3). Cells were washed twice more in permabilisation buffer, followed by once in FACS buffer.

Cells stained with the intracellular cytokine panel were fixed with the eBioscience IC Fixation Buffer for 20 min at 4 °C, followed by washing twice in 1X permabilisation buffer. All cell surface markers were stained with the following antibodies in permabilisation buffer for 20 min at 4 °C. Panel 1: IFN-γ-FITC, granzymeB-PE/Cy7, IL4-PE/Dazzle594, IL-2-PE and TNF-α-BV421. Panel 2: IL17-A-PE/Cy7, IFN-γ-FITC, granzymeB-PE/Cy7, IL-4-PE/Dazzle594, IL-10-PE and TNF-α-BV421. Cells were washed twice more in permabilisation buffer, followed by once in FACS buffer. After the final wash, all cells were resuspended in FACS buffer and analysed on the Cytoflex LX (Beckman Coulter).

All cells were pre-gated on viable and single cells. All data was analysed with FCS Express (De Novo) software.

5.3 Results

5.3.1 Induction of immune thrombocytopenia model is dependent on expression of FcγRIII

Activating IgG receptors require the association of the Fcγ subunit to be expressed and functional at the cell surface (352). Consequently, Fcγ^{-/-} mice do not express FcγRI, FcγRIII and FcγRIV and cannot phagocytose opsonised antigens (254). The anti-CD41 antibody used to deplete platelets is of the IgG1 isotype which is recognised by the low affinity receptors FcγRIII and FcγRIIB which are expressed on all myeloid populations (353). FcγRIII is an activating FcγR, whilst FcγRIIB is an inhibitory FcγR; therefore FcγRIII is the only activating FcγR capable of binding IgG1 (354).

Fcγ^{+/-} and Fcγ^{-/-} mice were a kind gift from James Hewitson, (University of York). As FcγRII but not FcγRIII is expressed by Fcγ^{-/-} mice (254), Fcγ^{+/-} and Fcγ^{-/-} mice can be distinguished from one another by the intensity of stain of mononuclear cells in peripheral blood using an antibody that recognises both FcγRIII and FcγRII (Figure 5.2A). An antibody with dual specificity for FcγRIII and FcγRII was used as antibodies uniquely specific for FcγRIII have not yet been generated. Although specific markers were not used to confirm the identity of the cells, granulocytes, monocytes and lymphocytes in peripheral blood can be distinguished based on their side scatter (SSC) profile. Fcγ^{+/-} and Fcγ^{-/-} mice can clearly be distinguished apart from one another based on the FcγRIII/II staining of the monocyte and granulocyte populations. Peripheral monocytes exhibited a near total reduction in FcγRIII/II staining in Fcγ^{-/-} mice, whilst granulocytes exhibited a less dramatic reduction in FcγRIII/II staining. A subpopulation of WT lymphocytes stained positive for FcγRIII/II and this was not altered in Fcγ^{+/-} or Fcγ^{-/-} mice.

To determine whether platelet depletion using the passive transfer model is solely dependent on FcγRIII expression, WT, Fcγ^{+/-} and Fcγ^{-/-} mice were injected with anti-CD41 antibody (Figure 5.2B). 24 h later, WT mice and Fcγ^{+/-} exhibited an 89.5% and 49.7% decrease in platelet count, respectively whilst Fcγ^{-/-} mice had no statistical change in platelet count.

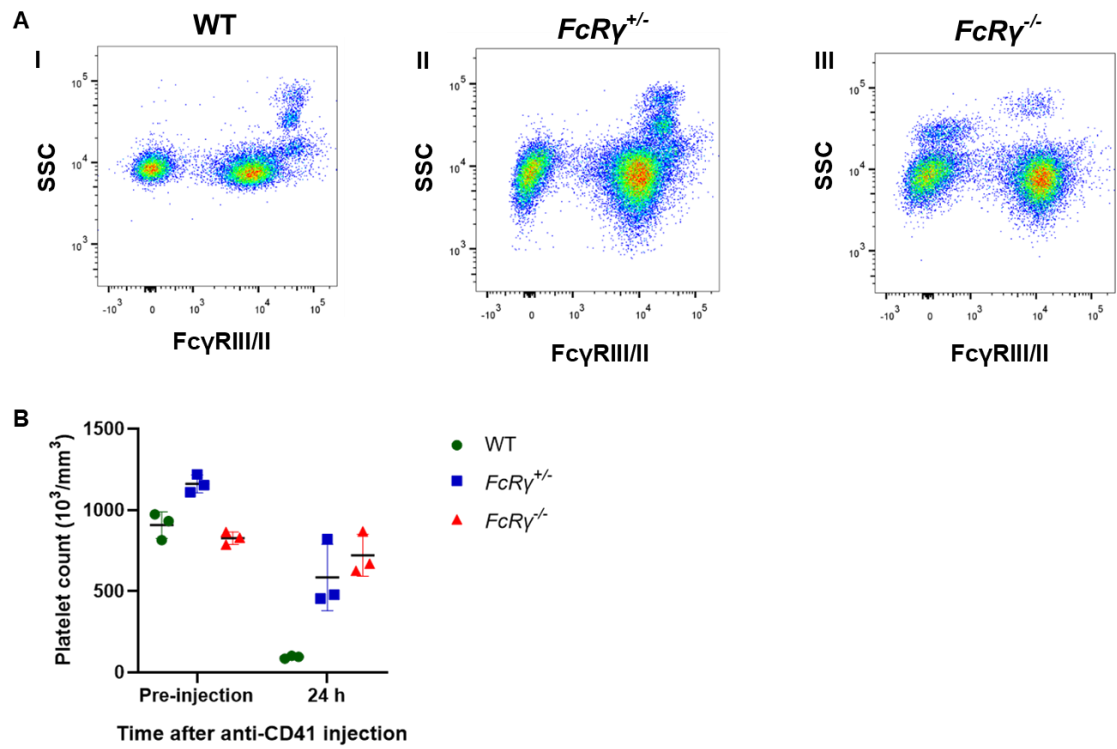


Figure 5.2. FcγRIII expression is required for ITP induction. A) Flow cytometry analysis of peripheral blood to confirm genotype of $Fc\gamma R^{+/-}$ and $Fc\gamma R^{-/-}$ mice. WT peripheral blood was also analysed as a comparison. **B)** Platelet counts from WT, $Fc\gamma R^{+/-}$ and $Fc\gamma R^{-/-}$ mice 24 h after anti-CD41 injection. N = 3.

5.3.2 Sustained ITP is achieved in *Rag2*^{-/-}, but not NSG-SGM3 mice

To dissect which immune cell populations were responsible for sustained platelet clearance in our model of sustained ITP, the immunocompromised NSG-SGM3 and *Rag2*^{-/-} mouse strains were injected with anti-CD41 or IgG for 2 weeks (Figure 5.3B and Figure 5.4B respectively). Severe thrombocytopenia was only transient at day 1 and day 9 in NSG-SGM3 mice, while *Rag2*^{-/-} mice had sustained severe thrombocytopenia. To explore the mechanism behind the observed differences, peripheral blood was analysed by flow cytometry on day 15.

As expected, the SSC vs FSC plot of red blood cell lysed peripheral blood from NSG-SGM3 mice (Figure 5.3A) was totally absent in lymphocytes (258, 260). Whilst lymphocytes were present in peripheral blood from *Rag2*^{-/-} mice (Figure 5.4A), they were reduced in number as compared to WT peripheral blood (Figure 5.5A) and were expected to be immature (255). Confirmation of specific staining and correct gating was achieved by backgating onto the SSC vs FSC plot; as expected, neutrophils appeared as granulocytes and monocytes appeared as leukocytes. In addition, differences in monocyte populations were observed between NSG-SGM3 and *Rag2*^{-/-} mice. CD115 expression by monocytes of NSG-SGM3 mice (Figure 5.3A) was lower than that observed in *Rag2*^{-/-} and WT mice (Figure 5.4A and Figure 5.5A, respectively). Additionally, no expression of MHC II was observed in NSG-SGM3 mice (Figure 5.2A), whilst *Rag2*^{-/-} mice expressed MHC II (Figure 5.3A). Despite MHC II expression by *Rag2*^{-/-} mice, expression levels were not altered by ITP.

Anti-CD41 treated NSG-SGM3 mice had a mean 55.7% decrease in classical monocytes ($P = 0.10$) and a mean 39.5% decrease in patrolling monocytes ($P = 0.20$) whilst neutrophil numbers remained constant. However, there did not appear to be any major differences in monocyte or neutrophil numbers in *Rag2*^{-/-} mice, although peripheral blood from more mice would need to be analysed before drawing any definitive conclusions.

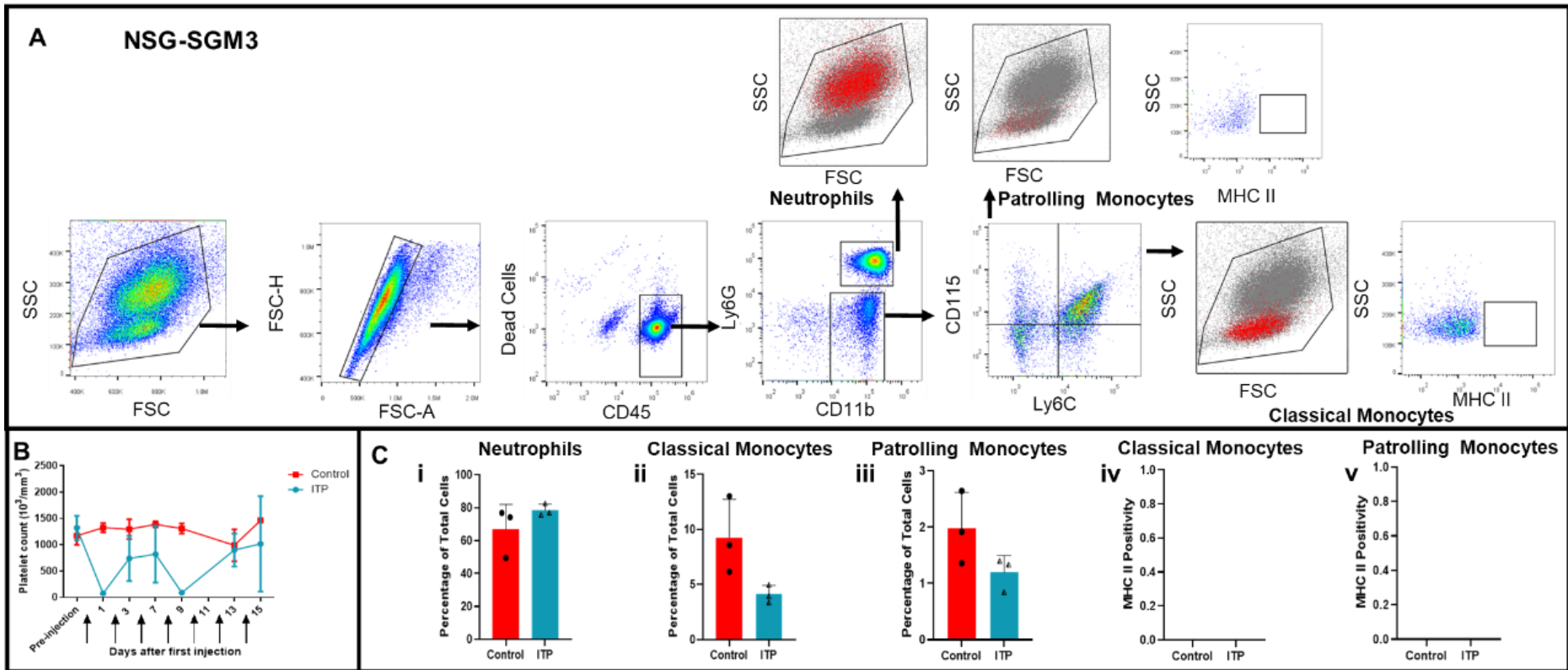


Figure 5.3. NSG-SGM3 mice cannot maintain thrombocytopenia using the ITP model. Flow cytometry analysis of NSG-SGM3 peripheral blood. **A)** Gating strategy showing example plots from IgG treated mice. Gated populations appear as red events when backgated onto the initial SSC vs FSC plot. **B)** Platelet counts during the 2 week ITP time course. **C)** Frequency of **i)** neutrophils ($P = 0.26$), **ii)** classical monocytes ($P = 0.067$) and **iii)** patrolling monocytes ($P = 0.13$). No expression of MHC II by **iv)** classical monocytes or **v)** patrolling monocytes was detected. P values were calculated by Mann-Whitney tests. $N = 3$.

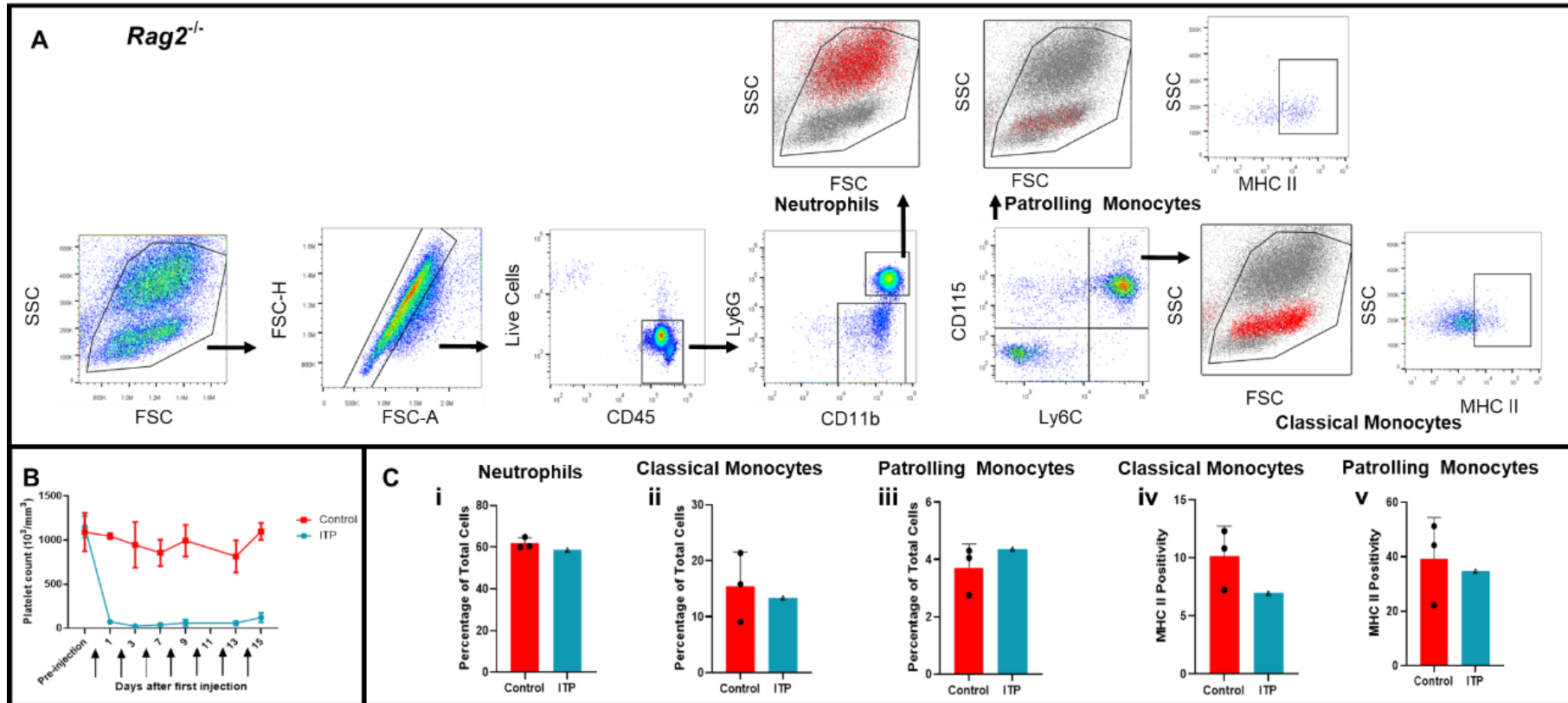


Figure 5.4. *Rag2*^{-/-} mice maintain severe thrombocytopenia using the ITP model. Flow cytometry analysis of *Rag2*^{-/-} peripheral blood. **A)** Gating strategy showing example plots from IgG treated mice. Gated populations appear as red events when backgated onto the initial SSC vs FSC plot. **B)** Platelet counts during the 2 week ITP time course. N=3. **C)** Frequency of **i)** neutrophils, **ii)** classical monocytes and **iii)** patrolling monocytes. MHC II expression by **iv)** classical monocytes or **v)** patrolling monocytes. N = 1-3.

5.3.3 Characterisation of the innate immune system in immune thrombocytopenia

Splenic macrophages and dendritic cells are thought to be the major cell types responsible for platelet clearance in ITP (228, 289). However, it remains possible that other cell types may also have a role in the phagocytosis of antibody bound platelets. To address this, immune cells of interest from WT mice with 2 week ITP were analysed for their ability to bind labelled platelets *in vivo*. On day 16, mice were injected with FITC labelled anti-CD41 1 h prior to euthanasia to label platelets or FITC labelled IgG to control for non-specific interactions (Figure 5.1). Flow cytometry was used to determine which immune cells were binding labelled platelets in ITP. Cell percentage and activation status (indicated by MHC II expression) were also recorded.

Analysis of peripheral blood, flushed BM, peritoneal wash and digested spleen is shown by Figures 5.5-8. Subfigure A of Figures 5.5-8 shows the gating strategy used to identify innate immune cells of interest; backgating onto the initial SSC vs FSC plot gave confidence to the staining and gating strategy as the gated cells appeared as expected based on their known biophysical properties. Classical and patrolling monocytes appeared to be increased in peripheral blood (both $P = 0.1$), whilst neutrophils are unaltered ($P > 0.99$) (Figure 5.5B). In contrast, in the BM there appeared to be an increase in neutrophils and patrolling monocytes (both $P = 0.1$), but not classical monocytes ($P = 0.4$) (Figure 5.6B). In the peritoneal wash and spleen, there were no differences in F4/80⁺ macrophages ($P = 0.8$; Figure 5.7B and $P = 0.4$; Figure 5.8B respectively). There were no differences in the MHC II expression of any monocyte or macrophage populations analysed, indicating that their activation status was unaltered.

Platelets are defined as FSC^{low}SSC^{low}CD41⁺ cells (355). Unlike injected anti-CD41-FITC, injected IgG-FITC does not bind to platelets (Figure 5.5Ci). Furthermore, injected IgG-FITC does not non-specifically bind larger mononucleated cells (Figure 5.5Cii). As platelets are the only circulating cell that expresses CD41 (356), I had confidence that FITC⁺ events corresponded to platelets or platelets bound to other cells. When applying the gates defined in Figure 5.5A, a minority of both classical and patrolling monocytes are shown to bind labelled platelets. However, when backgating onto the initial SSC vs FSC plot, FITC⁺ events appear mainly as FSC^{low}SSC^{low} events which are characteristic of lymphocytes (357). This indicates that in peripheral blood, classical monocytes and possibly lymphocytes bind platelets in ITP.

Similarly, FITC⁺ events are not observed in the BM of IgG-FITC treated mice, unlike anti-CD41-FITC treated mice (Figure 5.6Ci). However, the FITC⁺ events appeared diffuse

and did not exclusively fall within any of the monocyte or neutrophil gates characterised in Figure 5.6A.

FITC⁺ events appear in cells isolated from the peritoneal cavity in both IgG-FITC and anti-CD41-FITC treated mice, implying that anti-CD41 binding is nonspecific (Figure 5.7C). FITC⁺ events from both IgG-FITC and anti-CD41-FITC treated mice appear predominantly as F4/80⁺ macrophages, implying that nonspecific interactions occur predominantly with this population.

The majority of splenic F4/80⁺ macrophages were FITC⁺ in anti-CD41-FITC but not IgG-FITC treated mice implying that these cells are major contributors to antibody bound platelet destruction in ITP (Figure 5.8Cii). To predict which cells bind labelled platelets in an unbiased setting, FITC⁺ events were backgated onto the initial SSC vs FSC plot. FITC⁺ events were predominantly in the macrophage rich area defined in Figure 5.8A, confirming that splenic macrophages are the major contributors to antibody bound platelet destruction within the spleen.

Together, the results indicate that splenic macrophages are major contributors to antibody bound platelet destruction in ITP. Circulating and BM monocytes respond to sustained anti-CD41 treatment by expanding in number, however are likely to only be minor direct contributors to platelet phagocytosis.

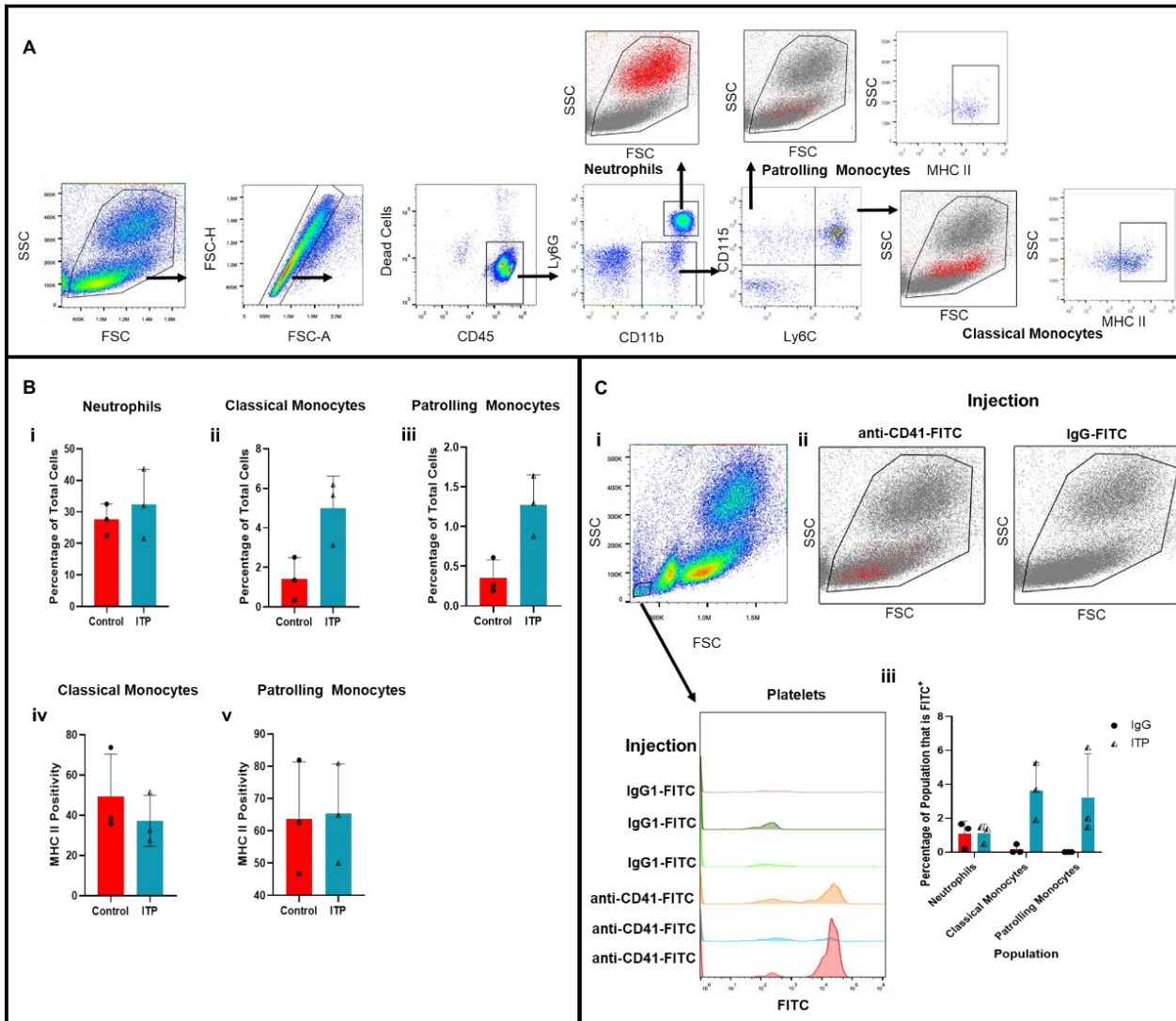


Figure 5.5. Labelled platelets bind to a minority of peripheral monocytes during sustained ITP. Flow cytometry analysis of peripheral blood from platelet labelling experiment (Figure 5.1). **A** Gating strategy showing example plots. Gated populations appear as red events when backgated onto the initial SSC vs FSC plot. **B** Frequency of **i**) neutrophils ($P > 0.99$), **ii**) classical monocytes ($P = 0.10$) and **iii**) patrolling monocytes ($P = 0.10$). MHC II expression by **iv**) classical monocytes ($P = 0.40$), or **v**) patrolling monocytes ($P > 0.99$). **Ci**) anti-CD41-FITC is specific for platelets. **ii**) FITC⁺ events mainly appear as lymphocytes when backgated onto the SSC vs FSC plot. **iii**) Populations defined in A) that were FITC⁺: neutrophils ($P > 0.99$), classical monocytes ($P = 0.10$) and patrolling monocytes ($P = 0.10$). P values were calculated by Mann-Whitney tests. N=3.

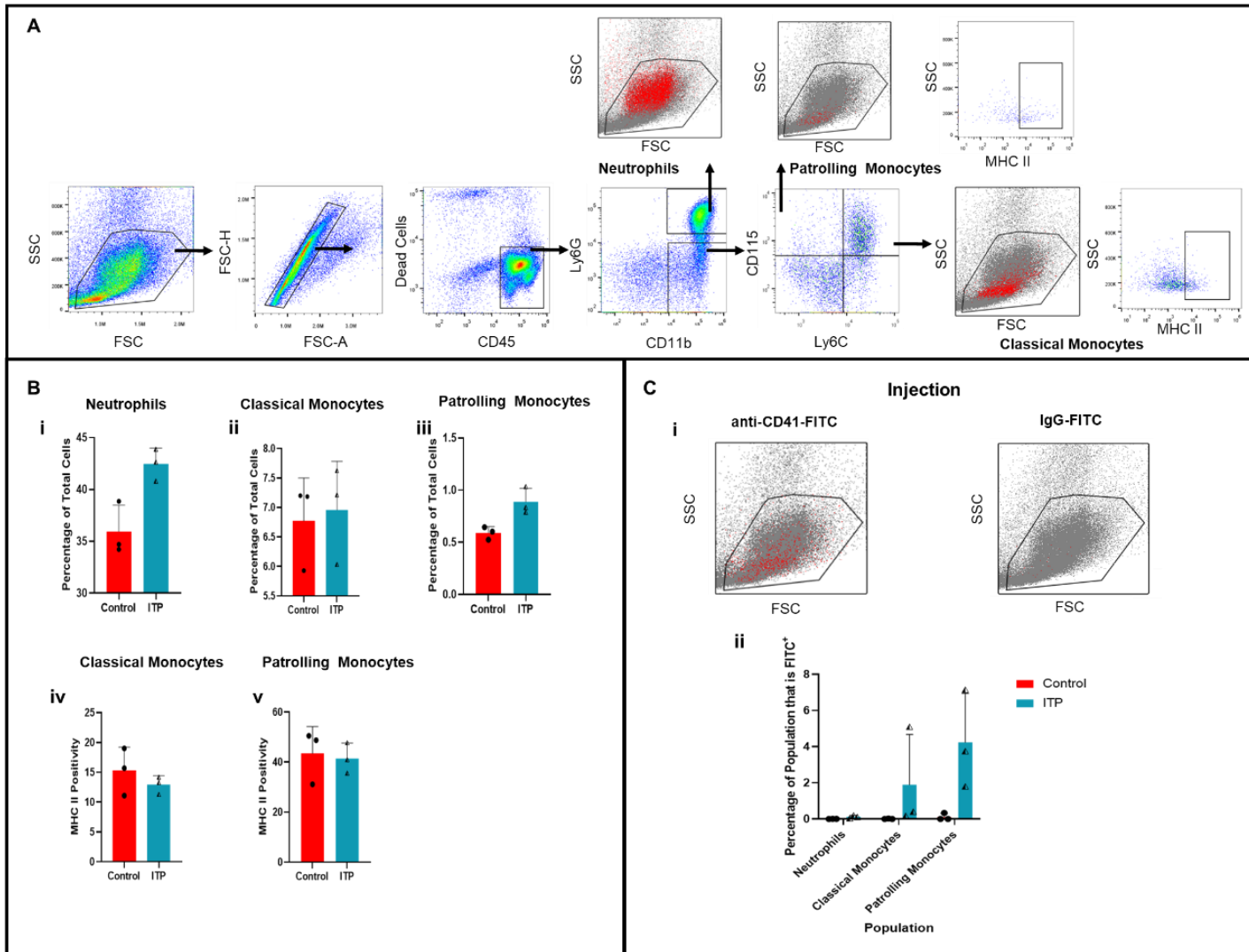


Figure 5.6. Labelled platelets bind to a minority of BM monocytes during sustained ITP. Flow cytometry analysis of BM from platelet labelling experiment (Figure 5.1). **A)** Gating strategy showing example plots from IgG treated mice. Gated populations appear as red events when backgated onto the initial SSC vs FSC plot. **B)** Frequency of **i)** neutrophils ($P = 0.10$), **ii)** classical monocytes ($P = 0.40$) and **iii)** patrolling monocytes ($P = 0.10$). MHC II expression by **iv)** classical monocytes ($P = 0.70$), or **v)** patrolling monocytes ($P = 0.70$). **i)** FITC⁺ events backgated onto the SSC vs FSC plot. **ii)** Populations defined in A) that were FITC⁺: neutrophils ($P = 0.10$), classical monocytes ($P = 0.10$) and patrolling monocytes ($P = 0.10$). P values were calculated by Mann-Whitney tests. N=3.

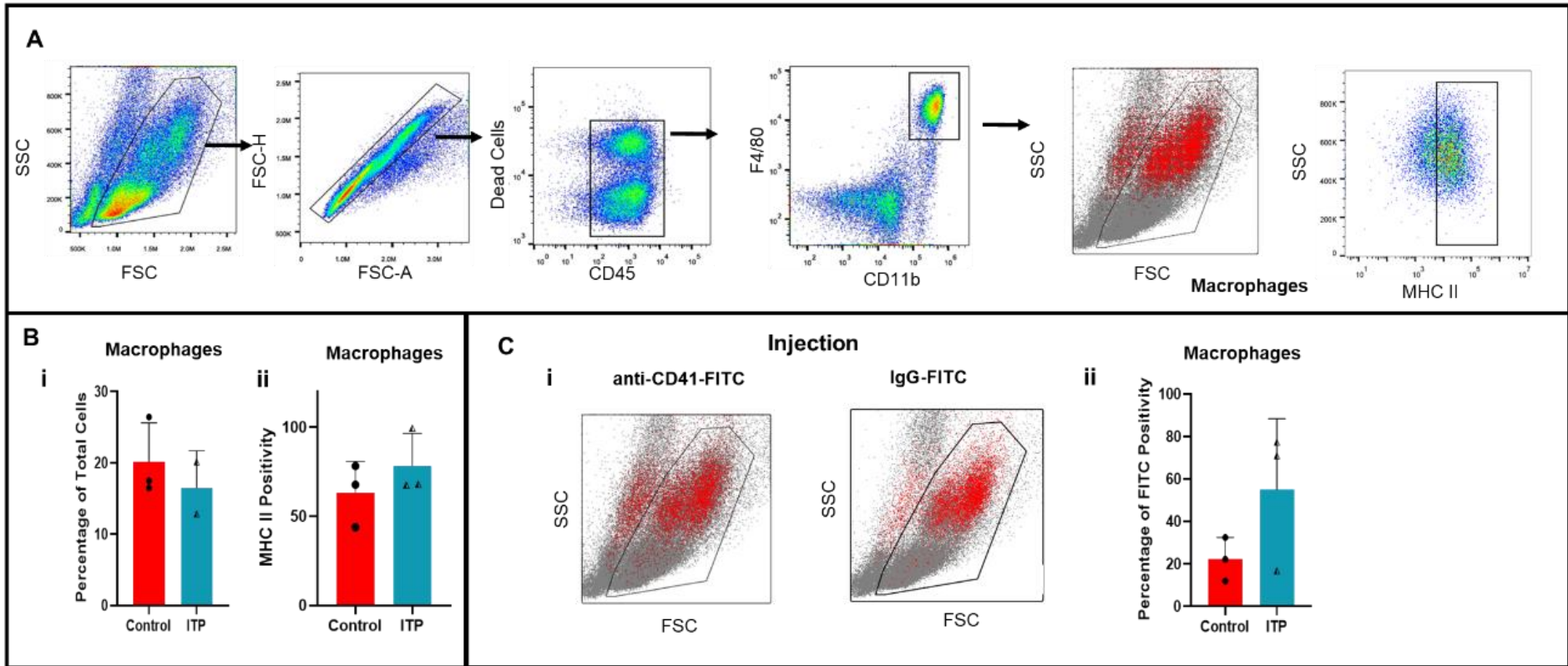


Figure 5.7. Labelled anti-CD41/IgG binds non-specifically to peritoneal macrophages. Flow cytometry analysis of cells from the peritoneal cavity of mice from platelet labelling experiment (Figure 5.1). **A**) Gating strategy showing example plots from IgG treated mice. Gated populations appear as red events when backgated onto the initial SSC vs FSC plot. **Bi**) Frequency of macrophages ($P = 0.80$). **ii**) MHC II expression by macrophages ($P = 0.70$). **i**) FITC⁺ events mainly appear as macrophages when backgated onto the SSC vs FSC plot. **ii**) FITC⁺ events within the macrophage gate ($P = 0.40$). P values were calculated by Mann-Whitney tests. $N=3$

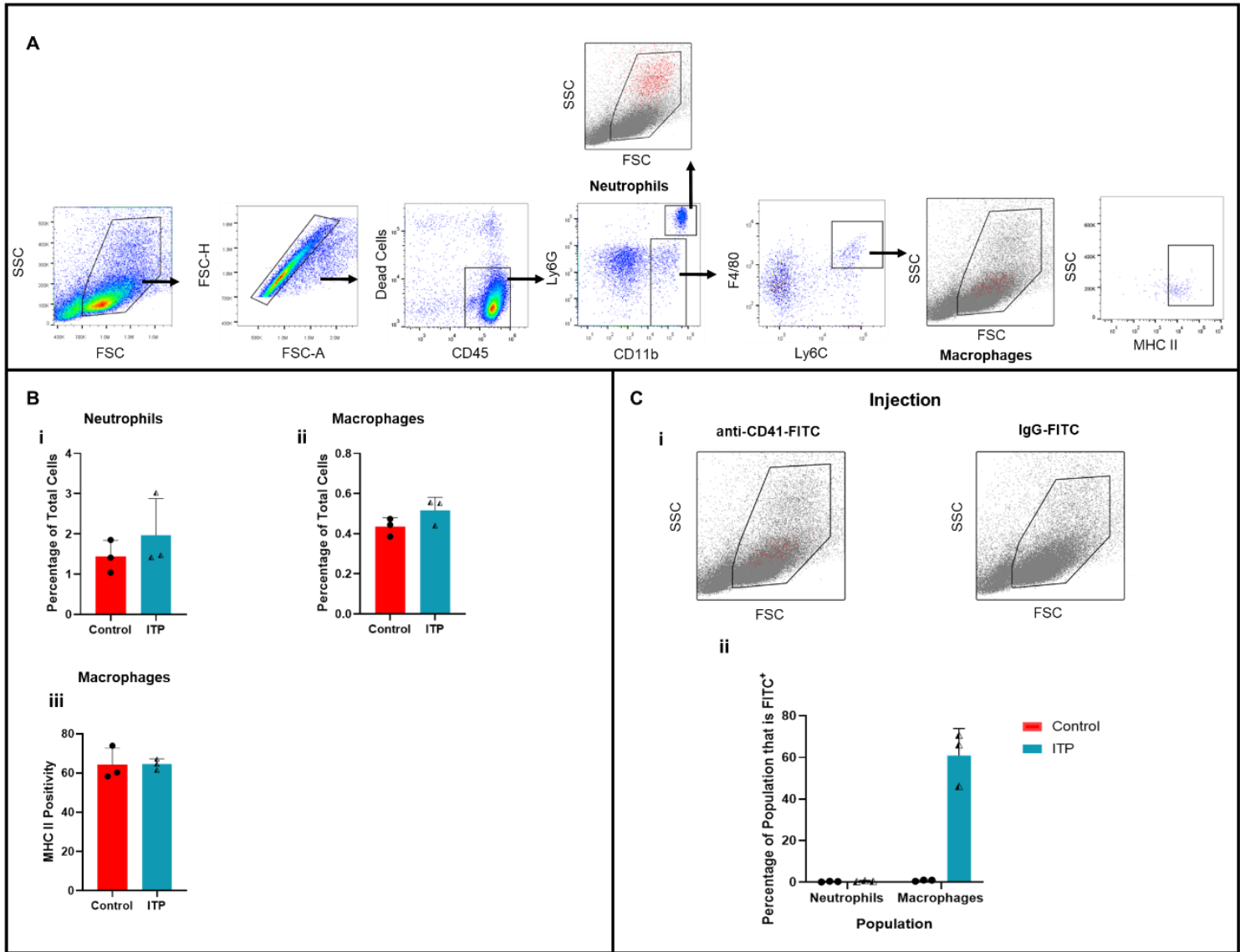


Figure 5.8. Labelled platelets bind to the majority of splenic F4/80⁺ macrophages during sustained ITP. Flow cytometry analysis of the spleen of mice from platelet labelling experiment (Figure 5.1). **A)** Gating strategy showing example plots from IgG treated mice. Gated populations appear as red events when backgated onto the initial SSC vs FSC plot. **B)** Frequency of **i)** neutrophils ($P = 0.40$), **ii)** F4/80⁺ macrophages ($P = 0.40$). **iii)** MHC II expression by F4/80⁺ macrophages ($P = 0.70$). **i)** FITC⁺ events backgated onto the SSC vs FSC plot. **ii)** Populations defined in A) that were FITC⁺: neutrophils ($P = 0.40$), F4/80⁺ macrophages ($P = 0.10$). P values were calculated by Mann-Whitney tests. $N = 3$.

5.3.4 Characterisation of T cell subsets in chronic ITP

Approximately 40% of ITP patients display no detectable anti-platelet antibodies and cellular immunity is thought to drive pathogenesis (201). The results so far indicated that the ITP model is initiated and sustained by a functional innate immune system, however it is possible that with longer anti-CD41 treatment, T cell involvement may occur. As it can take at least 2 weeks from the first exposure to an antigen to surmount an adaptive immune response (319), 4 weeks was chosen as an appropriate time point to study T cell subpopulations in the ITP model. Alongside IgG and anti-CD41 treated groups, a naïve group was used where possible to assist data interpretation.

Figure 5.9 and Figure 5.10 show the relative proportions of lymphocyte populations in the spleen and BM of mice with ITP vs IgG controls. Analysis of lymphocytes revealed that whilst the T cell proportion remained unchanged, there was a general decrease in B cells (12.2% and 37.8% decrease) in the spleen and BM respectively. In contrast, there was an increase in non-lymphocytes in the spleen and BM (58.4% and 10.3% increase respectively). The non-lymphocyte population comprised a wide variety of cell types that do not express CD19 or TCR- β , used to identify B cells and T cells respectively. There were no differences in the CD4/CD8 ratio in the spleen or BM. Within the spleen, naïve CD4⁺ and CD8⁺ T cells appeared to expand at the expense of activated effector cells, however this was not significant (naïve and activated effector CD4⁺ T cells $P = 0.058$ and $P = 0.39$ respectively, naïve and activated effector CD8⁺ T cells $P = 0.070$ and $P = 0.10$ respectively). In contrast, in the BM the naïve and activated effector CD4⁺ and CD8⁺ T cells appeared to decrease at the expense of an expansion in effector memory cells, however this was also mostly not significant.

Further analysis of CD4⁺ cell subsets within the spleen did not reveal differences between mice with ITP and IgG treated controls; there were no differences in the proportion of Tfh cells or Tregs (Figure 5.11 and Figure 5.12, respectively). Subsets of Tfh cells or Tregs based upon expression of CD62L and CD44 were also unchanged. Additionally, analysis of CD4⁺ and CD8⁺ cells in the spleen and BM did not reveal any differences in intracellular cytokine production (Figure 5.13 and Figure 5.14). Together

the data suggested that sustained ITP did not activate T cells, however there appeared to be an increase in naïve T cells within the spleen of mice with ITP, although this was not significant.

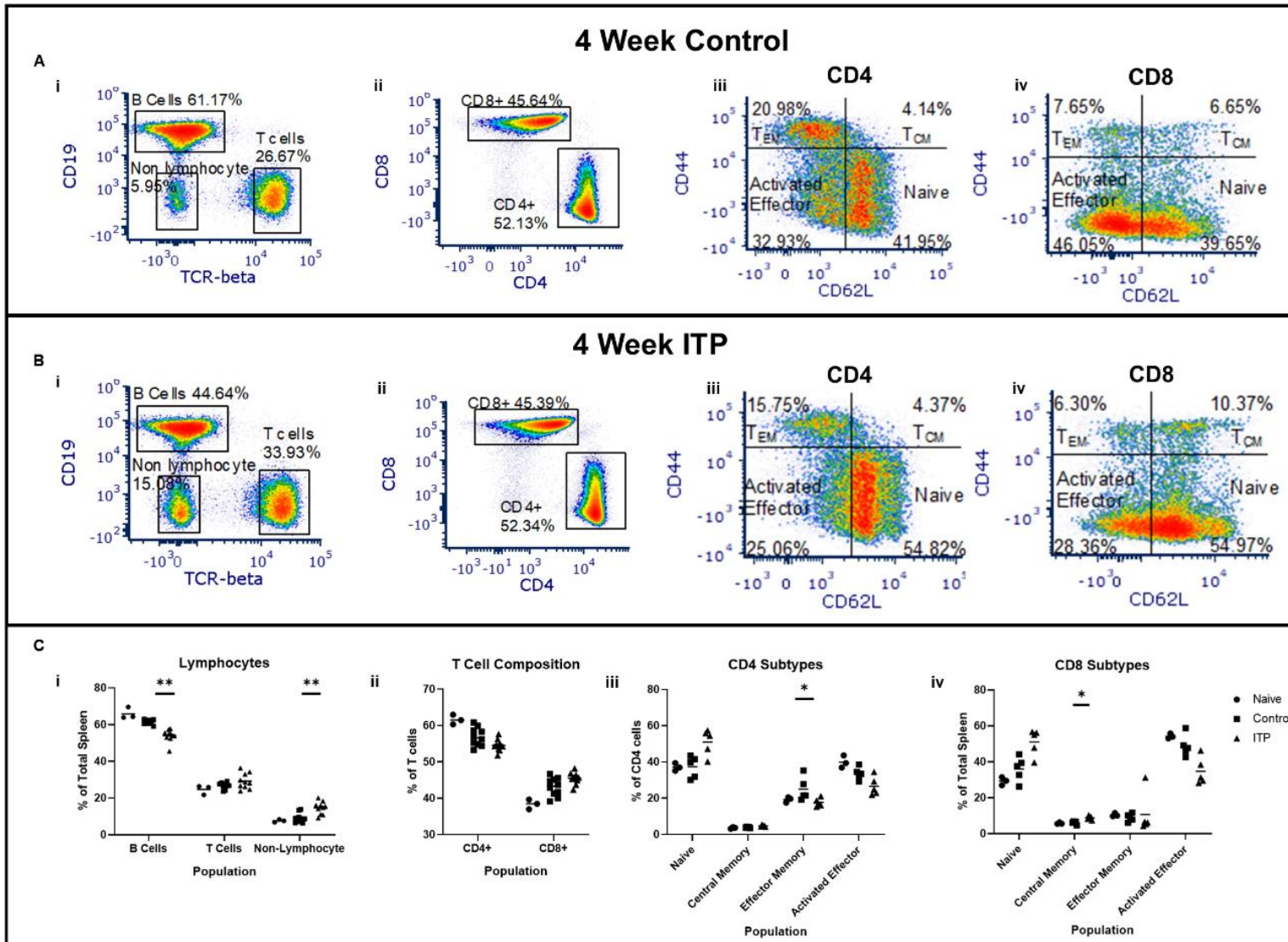


Figure 5.9. Splenic T cell phenotype in the sustained ITP mouse model. Flow cytometry analysis of the spleen from WT mice with 4 week ITP vs controls. **A)** Gating strategy showing example plots from controls. **B)** Gating strategy showing example plots from mice with 4 week ITP. **C)** Summary data of **i)** splenic cell populations: B cells (naïve vs control, $P = 0.44$; control vs 4 week ITP, $**P = 0.0029$), T cells (naïve vs control, $P = 0.52$; control vs 4 week ITP, $P = 0.89$) and non-lymphocyte (naïve vs control, $P > 0.99$; control vs 4 week ITP, $**P = 0.0073$), **ii)** CD4/CD8 ratio: CD4⁺ cells (naïve vs control, $P = 0.20$; control vs 4 week ITP, $P = 0.16$), and CD8⁺ cells (naïve vs control, $P = 0.20$; control vs 4 week ITP, $P = 0.16$), **iii)** CD4⁺ cells; naïve (naïve vs control, $P > 0.99$; control vs 4 week ITP, $P = 0.058$), central memory (naïve vs control, $P = 0.93$ control vs 4 week ITP, $P = 0.057$), effector memory (naïve vs control, $P = 0.30$, control vs 4 week ITP, $*P = 0.019$) and activated effector (naïve vs control, $P = 0.23$, control vs 4 week ITP, $P = 0.39$) **iv)** CD8⁺ cells: naïve (naïve vs control, $P = 0.72$; control vs 4 week ITP, $P = 0.070$), central memory (naïve vs control, $P > 0.99$, control vs 4 week ITP, $*P = 0.030$), effector memory (naïve vs control, $P > 0.99$, control vs 4 week ITP, $P = 0.58$) and activated effector (naïve vs control, $P = 0.65$, control vs 4 week ITP, $P = 0.10$). P values were calculated by Kruskal-Wallis test with Dunn's multiple comparisons test. Ci and ii N = 3-10, Ciii and iv N = 3-5.

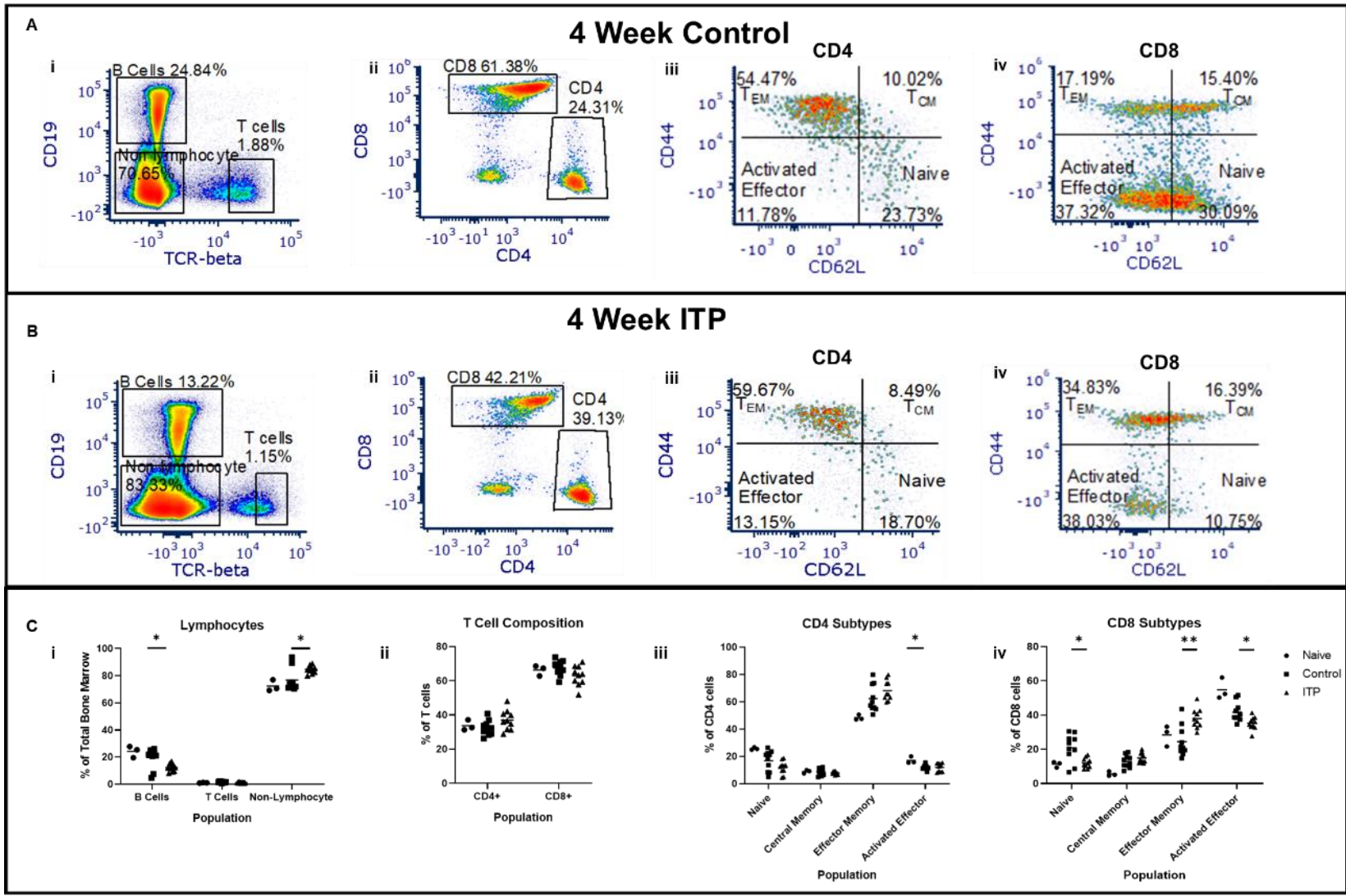


Figure 5.10. BM T cell phenotype in the sustained ITP mouse model. Flow cytometry analysis of the BM from WT mice with 4 week ITP vs controls. **A)** Gating strategy showing example plots from controls. **B)** Gating strategy showing example plots from mice with 4 week ITP. **C)** Alterations in **i)** BM cell populations: B cells (naïve vs control, $P = 0.61$; control vs 4 week ITP, $P = 0.046$), T cells (naïve vs control, $P = 0.050$; control vs 4 week ITP, $P = 0.042$) and non-lymphocyte (naïve vs control, $P = 0.56$ vs 4 week ITP, $P = 0.078$), **ii)** CD4/CD8 ratio: CD4⁺ cells (naïve vs control, $P > 0.99$; control vs 4 week ITP, $P = 0.14$), and CD8⁺ cells (naïve vs control, $P > 0.99$; control vs 4 week ITP, $P = 0.14$), **iii)** CD4⁺ cells: naïve (naïve vs control, $P = 0.12$; control vs 4 week ITP, $P = 0.23$), central memory (naïve vs control, $P > 0.99$; control vs 4 week ITP, $P = 0.44$), effector memory (naïve vs control, $P = 0.079$; control vs 4 week ITP, $P = 0.26$) and activated effector (naïve vs control, $P = 0.029$; control vs 4 week ITP, $P > 0.99$) **iv)** CD8⁺ cells: naïve (naïve vs control, $P = 0.16$; control vs 4 week ITP, $*P = 0.039$), central memory (naïve vs control, $P = 0.056$; control vs 4 week ITP, $P = 0.52$), effector memory (naïve vs control, $P > 0.99$; control vs 4 week ITP, $**P = 0.0060$) and activated effector (naïve vs control, $P = 0.24$, control vs 4 week ITP, $*P = 0.024$). P values were calculated by Kruskal-Wallis test with Dunn's multiple comparisons test. N = 3-10.

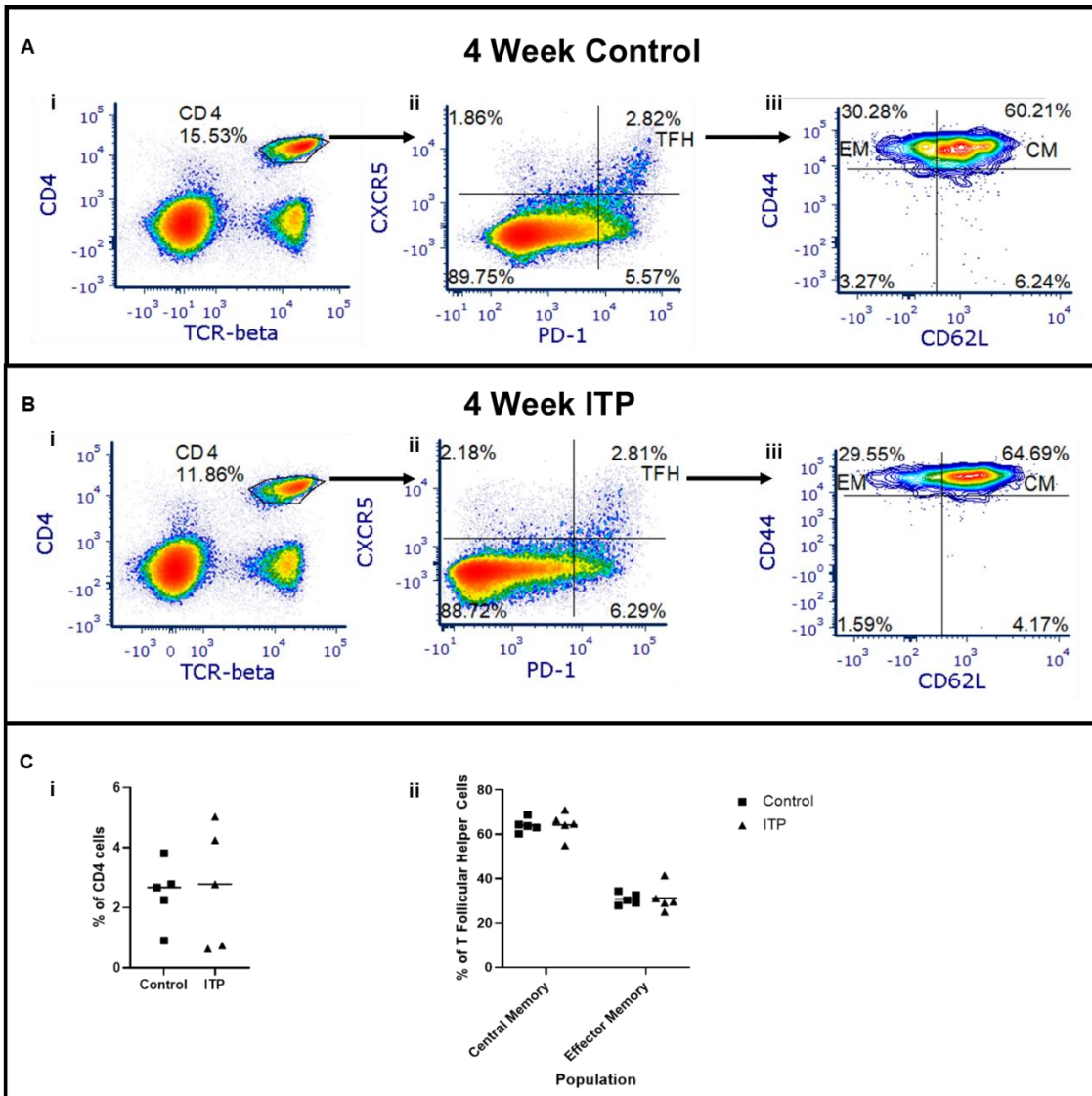


Figure 5.11. No alteration in proportion of T follicular helper cells in the sustained ITP mouse model. Flow cytometry analysis of the spleen from WT mice with 4 week ITP vs controls. **A)** Gating strategy showing example plots from controls. **B)** Gating strategy showing example plots from mice with 4 week ITP. **C)** The proportion of **i)** T follicular helper cells ($P = 0.88$) and **ii)** memory subsets of T follicular helper cells (central memory, $P = 0.55$; effector memory, $P = 0.84$) were not altered between groups. P values were calculated by Mann Whitney tests. $N = 5$.

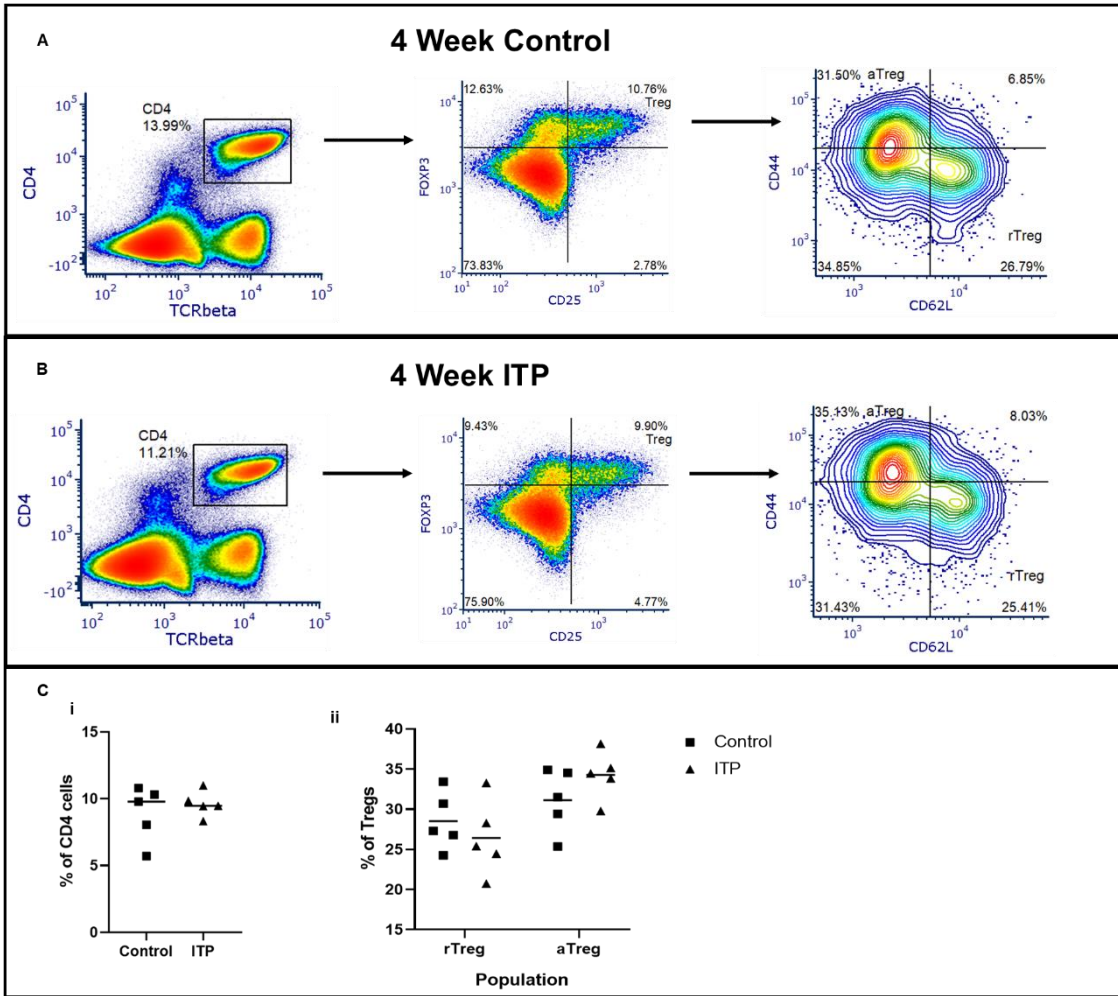


Figure 5.12. No alteration in proportion of Tregs in the sustained ITP mouse model. Flow cytometry analysis of the spleen from WT mice with 4 week ITP vs controls. **A)** Gating strategy showing example plots from controls. **B)** Gating strategy showing example plots from mice with 4 week ITP. **C)** The proportion of Tregs ($P = 0.84$, Mann-Whitney test) were not altered between groups. $N = 5$.

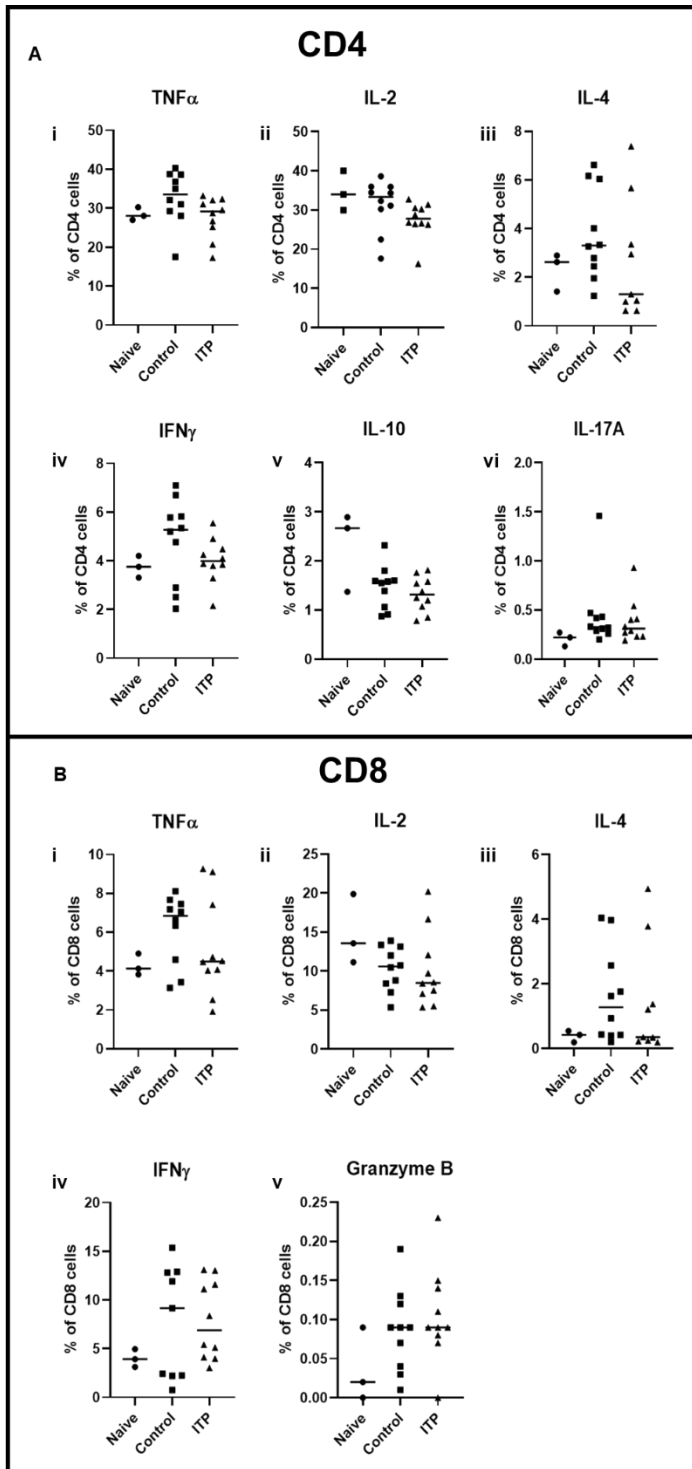


Figure 5.13. CD4⁺ and CD8⁺ T cells in the spleen have no change in activation status in the sustained ITP mouse model. A) CD4⁺ T cells: i) TNF α (naïve vs control, $P = 0.27$; control vs 4 week ITP, $P = 0.13$), ii) IL-2 (naïve vs control, $P > 0.99$; control vs 4 week ITP, $P = 0.089$), iii) IL-4 (naïve vs control, $P = 0.64$; control vs 4 week ITP, $P = 0.27$), iv) IFN γ (naïve vs control, $P = 0.35$; control vs 4 week ITP, $P = 0.45$), v) IL-10 (naïve vs control, $P = 0.41$; control vs 4 week ITP, $P = 0.82$), vi) IL-17A (naïve vs control, $P = 0.067$; control vs 4 week ITP, $P > 0.99$). B) CD8⁺ T cells: i) TNF α (naïve vs control, $P = 0.46$; control vs 4 week ITP, $P = 0.65$), ii) IL-2 (naïve vs 4 week ITP, $P = 0.31$; control vs 4 week ITP, $P > 0.99$), iii) IL-4 (naïve vs control, $P = 0.32$; control vs 4 week ITP, $P = 0.55$), iv) IFN γ (naïve vs control, $P = 0.85$; control vs 4 week ITP, $P > 0.99$), v) Granzyme B (naïve vs control, $P = 0.38$; control vs 4 week ITP, $P > 0.99$). P values were calculated by Kruskal-Wallis tests with Dunn's multiple comparisons test. $N = 3-10$.

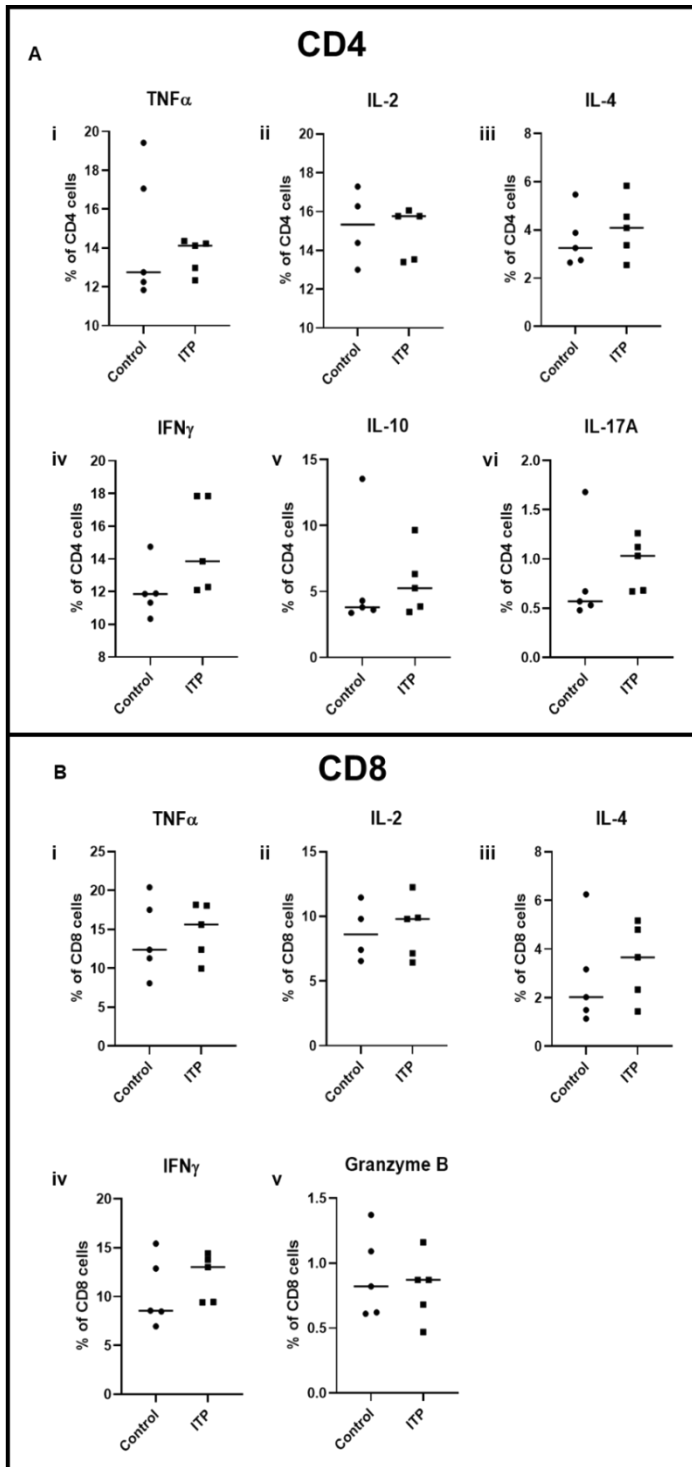


Figure 5.14. CD4⁺ and CD8⁺ T cells in the BM have no change in intracellular cytokine production in the sustained ITP mouse model. A) CD4⁺ T cells: i) TNF α ($P = 0.84$), ii) IL-2 ($P = 0.68$), iii) IL-4 ($P = 0.55$), iv) IFN γ ($P = 0.056$), v) IL-10 ($P = 0.55$), vi) IL-17A ($P = 0.17$). B) CD8⁺ T cells: i) TNF α ($P = 0.69$), ii) IL-2 ($P = 0.90$), iii) IL-4 ($P = 0.55$), iv) IFN γ ($P = 0.31$), v) Granzyme B ($P = 0.97$). P values were calculated by Kruskal-Wallis tests with Dunn's multiple comparisons test. $N = 4-5$.

5.4 Discussion

The versatility of the passive transfer model both in terms of the variability of the ITP time course and applicability to a wide variety of mouse strains allowed for the dissection of the requirements for the initiation and maintenance of ITP. Initiation of ITP was dependent on the expression of FcγRIII, whilst maintenance of ITP required a fully functional innate immune system. Immunocompetent WT mice were used to characterise components of the innate and adaptive immune response during sustained ITP. Progression of ITP was associated with monocyte and naïve T cell expansion, however analysed cells did not appear to be activated. Labelled platelets bound to the majority of splenic macrophages in ITP, with minimal binding observed from other innate immune cells from a variety of sites suggesting that splenic macrophages are the major cell type responsible for the phagocytosis and clearance of antibody bound platelets.

To validate genotyping results from FcRγ^{+/-} and FcRγ^{-/-} mice, peripheral blood was stained with an antibody specific for both FcγRIII and FcγRII and analysed by flow cytometry. Takai and colleagues found that splenic macrophages in FcRγ^{-/-} mice exhibited an 80% reduction in FcγRIII/II staining, whilst neutrophils exhibited a 50% reduction in staining (254). My results using peripheral blood of FcRγ^{-/-} mice are comparable. Similar to splenic macrophages, peripheral monocytes exhibited a near total reduction in FcγRIII/II staining in FcRγ^{-/-} mice, whilst granulocytes (of which neutrophils are the dominant population), exhibited a less dramatic reduction in FcγRIII/II staining (perhaps indicating that granulocytes express FcγRII at higher levels than monocytes). Interestingly, monocytes from the FcRγ^{+/-} mice had almost the levels of WT FcγRIII/II staining, rather than closer to 50% FcγRIII/II staining that might be expected if FcγRIII/II expression was driven by a gene dosage effect. However, after injection of anti-CD41, FcRγ^{+/-} mice have approximately a 50% reduction in platelet counts as expected. Possibly this discrepancy is due to an increase in FcγRII expression in FcRγ^{+/-} mice, therefore total staining is similar to WT mice when using an antibody with dual FcγRIII/II specificity. B cells express FcγRII but not FcγRIII, NK cells express FcγRIII but not FcγRII whilst T cells express neither (354). Therefore, it was expected that FcγRIII/II staining from NK cells, but not from B and T cells, would be reduced in FcRγ^{-/-} mice (254). However, NK cells contribute to approximately 3% of circulating lymphocytes in mice (358), therefore loss of staining from the total lymphocyte population would be expected to be minimal. As expected, lymphocyte staining in WT, FcRγ^{+/-} and FcRγ^{-/-} mice is comparable. The resistance of FcRγ^{-/-} mice to ITP, confirms that initiation of the model is mostly (or exclusively) dependent on the expression of FcγRIII and is therefore driven by components of the innate immune system. Macrophages and DCs both have high expression of FcγRIII (354), which is in keeping

with their reported role in the phagocytosis of antibody bound platelets in ITP (228, 289). However, 2/3 FcR γ ^{-/-} mice exhibited a mild drop in platelet count 24 h after anti-CD41 injection. Although this drop in platelet count was not significant, it would be interesting to repeat the experiment as a mild drop in platelet count in FcR γ ^{-/-} mice suggests there may be other mechanisms of platelet depletion present. As platelet desialylation is thought to be triggered by anti-GPIb α , but not anti-GPIIb/IIIa (243, 244), this would be an interesting avenue of research.

To address whether a functional innate immune system is required for the maintenance of sustained ITP, two immunocompromised mouse strains (NSG-SGM3 and *Rag2*^{-/-}) were injected with anti-CD41 or IgG for 2 weeks. NSG-SGM3 mice have multiple defects in adaptive and innate immunity, whilst *Rag2*^{-/-} mice have defects in adaptive immunity but a normal innate immune system (255, 257, 258, 260).

Rag2^{-/-} mice had severe thrombocytopenia throughout the 2 week experiment, however the NSG-SGM3 strain could induce but not sustain ITP. Whilst macrophages are present in NOD mice or mice bred on a NOD background (such as NSG-SGM3 mice), they are considered functionally immature (350, 351). Macrophages were not studied in the described experiment, however circulating monocytes appeared defective. CD115 expression was lower in NSG-SGM3 mice as compared to the similar levels expressed by WT and *Rag2*^{-/-} mice. The ligand for CD115 (colony-stimulatory factor-1; CSF-1) is required for monocyte survival and macrophage differentiation (359). Reduced signalling through this axis (which may occur due to the reduced expression of CD115 by NSG-SGM3 mice) may reduce survival of monocytes, especially under stress such as ITP. In support of this, there appeared to be lower percentages of classical and patrolling monocytes in NSG-SGM3 mice with ITP than controls (although this was not significant). Alternatively, monocytes could be subject to defective replenishment after ITP driven differentiation into inflammatory macrophages; NOD mice are known to have defects in monocyte differentiation from progenitors (350, 360).

MHC II expression by APCs is required to present antigen to CD4⁺ T cells. Although constitutively expressed by APCs, the presence of inflammatory cytokines such as IFN- γ derived from immune cells such as activated NK cells, Th1 or Tc1 cells upregulates MHC II expression on APCs and their ability to process antigens to CD4⁺ T cells is improved (361-363). MHC II expression on APCs can therefore be used as a surrogate for activation status. MHC II by tissue macrophages can create a positive feedback loop with IFN- γ producing lymphocytes where MHC II dependent antigen presentation and cytokines produced by activated macrophages stimulate T cells to produce IFN- γ which in turn upregulates MHC II expression in the macrophage (364). IFN- γ expression (or

any other cytokine expression analysed) by CD4⁺ and CD8⁺ T cells is not upregulated in mice with 4 week ITP. Although monocyte and macrophage populations were analysed at 2 weeks, not 4 weeks, MHC II expression in WT or *Rag2*^{-/-} monocyte or macrophage populations was not upregulated, suggesting that ITP does not result in activation of monocyte and macrophage populations.

Monocytes from NSG-SGM3 mice did not stain positive for MHC II. Although NOD mice have multiple defects in the function of macrophages (257), the lack of staining is due to NOD mice having a haplotype not recognised by the antibody clone used (M5/114.15.2) as opposed to a complete lack of MHC II expression (365). *Rag2*^{-/-} mice, on the other hand, are of the C57BL/6 background which have the H-2^b MHC haplotype (366). This is one of several polymorphic determinants recognised by the M5/114.15.2 clone used in my experiments. In contrast, mice of the NOD background (such as NSG-SGM3 mice) are of the H-2^{g7} haplotype (365). To determine whether MHC II expression of NSG-SGM3 mice alters after anti-CD41 treatment, an antibody recognising the H-2^{g7} haplotype such as clone AMS-32.1 should be used in future experiments (367). Additionally, it would be of interest to study both the numbers and intracellular cytokine production of splenic macrophage and dendritic cells from *Rag2*^{-/-} and NSG-SGM3 mice. Whilst MHC II expression is a useful surrogate for activation status, it is more informative to study their intracellular cytokine profile as this provides polarisation information (368, 369).

The pilot experiment assessing the innate immune response to ITP used a low number of mice in each group (N=3), therefore the results are indicative but definitive conclusions would require further experiments. Flow cytometry experiments indicated that the majority of splenic macrophages specifically bound labelled platelets in ITP, suggesting, in line with previous studies, that splenic macrophages are the main drivers of platelet clearance in ITP patients with autoantibody production (228). However, unaltered MHC II expression in macrophages isolated from mice with ITP suggested that phagocytosis of opsonised platelets did not stimulate their activation (although as previously described, in-depth intracellular cytokine analysis would have been more informative). Finally, the percentage of splenic macrophages appeared to slightly increase in ITP. In hindsight, it would have been informative to calculate absolute cell numbers, as macrophage numbers increase in ITP (309), however total cell counts were not retained.

Past studies using peripheral blood from ITP patients observed that the CD16⁺ monocyte population (patrolling monocytes) is expanded relative to healthy controls, and this appears to modulate the T cell response (348, 349). Similarly, both classical and

patrolling monocytes from the peripheral blood of WT mice appeared to be expanded in ITP when compared to controls. Whilst monocyte/T cell interactions were not directly assessed in my experiments (e.g. through co-culture experiments), no evidence of T cell activation was observed *in vivo* (discussed further in the subsequent paragraph). Indeed, ITP had no effect on MHC II expression and only a minority of classical and patrolling monocytes appeared to bind opsonised platelets. However, there may be other consequences of peripheral blood monocyte expansion, perhaps to replenish resident macrophage populations. Conversely, patrolling, but not classical monocytes appeared to be expanded in the BM of mice with ITP. However, it is possible that there may be some macrophage contamination in the BM populations – to rule this out, a F4/80 stain should be included in future experiments (370). ITP had no effect on the numbers or activation status of peritoneal macrophages, and although anti-CD41-FITC was observed to bind to the majority of peritoneal macrophages, some of this binding may be non-specific. There was a higher amount of non-specific IgG binding to peritoneal macrophages relative to monocytes/macrophages isolated from other sites which was likely to be a consequence of the anti-CD41/IgG injection being at the same site as sample isolation.

Autoantibodies cannot be detected in up to 40% of ITP patients (201), suggesting that cell mediated autoimmunity may have a significant role in ITP progression. To determine whether the passive transfer model is a clinically relevant model in studying T cell subsets in ITP, T cells from the spleen and BM of mice with 4 week ITP were characterised in-depth. Analysis of the intracellular cytokine profile of splenic and BM derived CD4⁺ and CD8⁺ T cells indicated that ITP did not cause T cell activation. ITP did not increase IL-2 production, suggesting that the cells were not expanding in response to activation, and there was no Th1 or Tc1 skewing. This is in agreement with a recent study where the authors concluded that the passive transfer model does not mimic the Th or Th17 profile of human ITP (371). Similarly, there were no differences in the percentages of Tfh cells or Tregs in our study. Whilst this previous study used a week long time course, it appears that extension to 4 weeks still does not provide the necessary inflammatory environment needed for T cell activation.

Surprisingly, splenic CD4 and CD8 cells from ITP mice in fact appeared to have lower cytokine production than controls, although this was not significant. As discussed in more detail in the subsequent paragraph, this may be due to an influx of recent thymic emigrants (RTEs) into the spleen, generated by an increase in *de novo* production of T cells in the thymus. RTEs are immature, have diminished proliferative ability and produce less IL-2, IFN- γ , TNF- α , IL-4 and IL-17 when stimulated under non-polarising

or Th1 polarising conditions (372), therefore a higher contribution of RTEs to the CD4⁺/CD8⁺ phenotype in ITP may present as a higher frequency of splenocytes with reduced effector functions.

Increased numbers of RTEs in the ITP spleen was considered likely based upon the observation that there appeared to be a higher percentage of naïve CD4⁺ and CD8⁺ T cells at the expense of activated T cells, although this was not significant. Increased numbers of RTEs in ITP may be due to a general increase in BM haematopoiesis. Younger patients receiving HSC transplants are associated with better homing and engraftment capacity are also associated with faster immune reconstitution (373), whilst defective haematopoiesis (either due to intrinsic HSC changes or extrinsic changes in the BM microenvironment) is associated with defective lymphopoiesis (374).

Increased haematopoiesis may have also been reflected by a significant increase in the non-lymphocyte population in the ITP BM and spleen, whilst the proportion of T cells remained the same and the proportion of B cells decreased. As discussed in depth in Chapter 6, haematopoiesis occurred in the BM and spleen by 4 weeks, accompanied by substantial remodelling in the BM. This is likely reflected as a greater contribution to the non-lymphocyte population in ITP during flow cytometry analysis, however increased numbers of splenic macrophages may significantly contribute to the non-lymphocyte population as previously discussed. Again, it would have been informative to retain total cell counts and calculate the absolute number of lymphocytes. For example, as mild splenomegaly occurred during ITP progression, it is possible that the absolute splenic B cell number remained constant (rather than decreasing), whilst splenic T cell number increased (rather than remaining unaltered).

Together, the data indicates that the monocyte-macrophage system expands during ITP progression; monocyte expansion may replenish tissue resident macrophages, which are the main drivers of platelet clearance through FcγRIII mediated phagocytosis (Figure 5.14). However, despite sustained platelet clearance, macrophages (and other APCs) do not appear to be in the activated state necessary for upregulation of costimulatory molecules and therefore cannot drive T cell mediated autoimmunity. The contribution of autoreactive T cells to autoimmunity is considerable in ITP (201), however my data indicates that this was not captured in the presented model. Whilst active models of ITP exist, these mice have a severe bleeding phenotype not exhibited by ITP patients, which limits long term experiments (308). There is therefore an unmet need for an ITP mouse model that faithfully recapitulates the ITP setting, which would aid understanding of ITP progression.

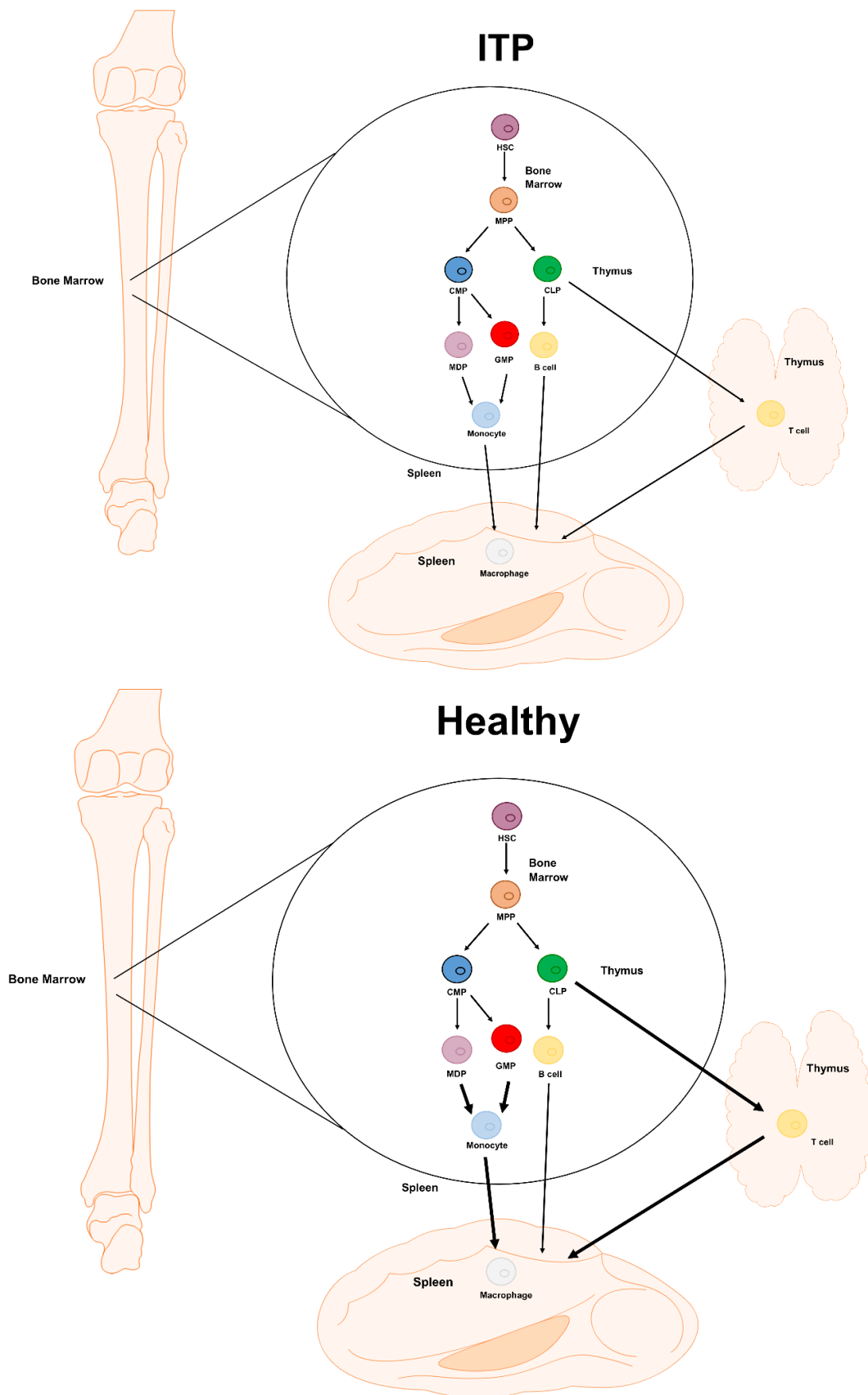


Figure 5.15. ITP is initiated and maintained by splenic macrophages and associated with an increase in naïve T cells . Opsonised platelets are phagocytosed by splenic macrophages. ITP progression is associated with expansion of circulating monocytes, which may infiltrate into the spleen and replenish the macrophage pool. ITP progression is also associated with an increased percentage of naïve T cells in the spleen, which may be driven by an increase in thymic output.

6 Haematopoiesis in immune thrombocytopenia

6.1 Introduction

During conditions of chronic haematopoietic stress, such as infection and inflammation, HSCs are activated to meet the increased demand in blood cell production (375, 376). Exit from quiescence has been previously associated with a loss in regenerative capacity and may eventually cause pancytopenia (109, 110, 377). During ITP, the requirement for HSC differentiation is twofold. Firstly, the increased platelet demand caused by autoimmune-mediated platelet destruction drives megakaryopoiesis (302-304, 378). Secondly, sustained immune system activation driving platelet destruction requires replenishment from progenitors (201, 375, 376). Despite this, there have been no reports of HSC exhaustion or pancytopenia in chronic ITP patients, suggesting that HSCs may receive additional support.

Recent evidence shows that the BM microenvironment provides supportive, rather than instructive input for HSC differentiation (379). Furthermore, the microenvironment is pliable, and can contribute to disease progression by driving the expression of proliferative/pro-inflammatory factors or by downregulating factors which traditionally support HSC function. Such changes may be induced by the presence of infection (96, 118), the development of malignancy (94, 380) or the administration of drugs (381). Whether the BM microenvironment actively remodels itself in response to various chemical or cellular insults to resolve and/or minimise hematopoietic stress remains unclear.

Using a mouse model of sustained ITP, I show that the increased demand on haematopoiesis is met by an increase in the number of functional HSCs, which appears to be achieved through an interactive and iterative relationship between differentiating HSCs and an adapting supportive BM microenvironment in an effort to maintain homeostasis.

6.2 Methods and materials

6.2.1.1 Cytokine analysis

Plasma was isolated from ITP or control mice via a cardiac puncture (2.5.1.2), whilst BM supernatant was obtained by flushing each femur with 500 μ L PBS and splenic supernatant was obtained by crushing the spleen in 1 mL PBS and filtering through a 70- μ m cell strainer, followed by centrifugation for 5 min at 300 g. Samples were analysed using the Proteome Profiler Mouse XL Cytokine Array Kit (ARY028; R&D systems), whilst the TPO and CXCL12 content was analysed using the Mouse Thrombopoietin and CXCL12/SDF-1 alpha Quantikine ELISA kits (MTP00 and MCX120 respectively,

R&D Systems) according to the manufacturer's instructions. Blots obtained from the Proteome Profiler Mouse XL Cytokine Array Kit were visualised on the Chemidoc MP (Bio-Rad) and saved as TIFF images. Images were imported into ImageJ software and the Integrated Density calculated per spot. The average measurement from each cytokine replicate was calculated and presented as the log₂ fold change of IgG and anti-CD41 treated mice. Upregulated proteins (log₂ fold change > 0.3) were subject to STRING analysis (<https://string-db.org/>) to form a protein-protein interaction network (PPI). Upregulated proteins were inputted with their associated log₂ fold change using the 'Proteins with Values/Ranks – Functional Enrichment Analysis' feature to visually identify the highest upregulated proteins within the PPI. Edges were formed if the interaction score was at least 0.4 (medium confidence), which was based on experimental, database and co-expression evidence. For analysis, proteins were clustered according to Gene Ontology terms within the biological process domain and the reactome pathway. To increase the meaningfulness of the data generated, large (> 500) gene sets were excluded.

6.2.2 Flow cytometry

6.2.2.1 Flow cytometry to analysis human haematopoietic progenitors

Cells were prepared for FACS analysis (2.6) and stained with the following antibodies in 100 µl FACS buffer for 20 min at 4 °C: CD34-APC, CD45RA-PerCP/Cy5.5, CD90-PE/CF594 and CD38-BB515. After staining, cells were washed three times in FACS buffer. After the final wash, cells were resuspended in FACS buffer and acquired on an LSR Fortessa (BD Biosciences) flow cytometer.

All cells were pre-gated on viable and single cells. Samples with < 75% viable cells were excluded. All data was analysed with FCS Express (De Novo) software.

6.2.2.2 Flow cytometry to analysis mouse haematopoietic progenitors

WT mice were administered anti-CD41 antibody/IgG1 for 4 weeks (4.2.1), then euthanised prior to BM and splenic harvest (2.5.2) and prepared for FACS analysis (2.6). All cell surface markers were stained with the following antibodies in 100 µl FACS buffer for 20 min at 4°C: mouse lineage antibody cocktail-PerCP/Cy5.5, CD48-PE/Cy7, CD117-BV421, CD150-BV605 and Sca-1-APC. For chimerism analysis the following panel was used in 100 µl of FACS buffer for 20 min at 4 °C: CD45.1-PE/Cy7 or PE and CD45.2-AF488. After staining, cells were washed three times in FACS buffer. After the final wash, cells were resuspended in FACS buffer and acquired on the Cytotflex LX or CytoFLEX S (Beckman Coulter).

All cells were pre-gated on viable and single cells. All data was analysed with FCS Express (De Novo) software.

6.2.3 Competitive transplantation

WT (CD45.2) donor mice were injected with anti-mouse CD41 antibody, whilst WT (CD45.1) donor mice were injected with IgG1 for 4 weeks (4.2.1). CD45.1 recipient mice were administered total body gamma radiation with two doses of 5.5 Gy, 24 h apart (lethal irradiation). Donor mice were euthanised and BM haematopoietic cells isolated (2.5.2) without red blood cell lysis. For primary transplants, donor BM was prepared by mixing CD45.1 and CD45.2 BM cells in a 3:1, 1:1, and 1:3 ratio and resuspended in sterile PBS. A total of 5×10^6 cells in a final volume of 200 μ L was injected into the tail vein of each of the recipient mice. For secondary transplants, 2×10^7 BM cells from primary transplant donors (pooled within each group) were further transplanted into CD45.1 recipient mice. All recipient mice were administered oral antibiotic Baytril (Bayer, Leverkusen, Germany) in drinking water for 14 days post-transplant as a prophylactic treatment against bacterial infection. Recipient mice were bled at 4, 8, 12, 16 and 20 weeks to monitor donor chimerism and relative mature cell production by flow cytometry.

6.2.4 Cell sorting and transplantation experiments

Lin^- donor cells were immunomagnetically enriched prior to cell sorting based upon the negative expression of lineage markers via the EasySep Mouse Hematopoietic Progenitor Cell Isolation Kit (19856, StemCell Technologies) according to the manufacturer's instructions. Following enrichment, cells were stained for progenitor markers followed by flow cytometry analysis (6.2.2.2).

For homing assays, approximately 15,000 $\text{Lin}^- \text{Sca1}^+ \text{c-Kit}^+$ (LSK) cells from naïve CD45.1 mice were administered in 100 μ L sterile PBS per recipient mouse via tail vein injection. Recipient mice were lethally irradiated 4 week anti-CD41 or IgG injected CD45.2 mice. 36 h later, BM was harvested and stained for donor cells followed by flow cytometry analysis (6.2.2.2).

For low dose HSC transplantation experiments, 100 LT-HSCs from either 4 week anti-CD41 or IgG injected CD45.2 mice were bulk sorted into 1 mL of PBS, and diluted so that each sub-lethally irradiated (one dose of 3.6 Gy) B6- W^{A1}/W^{A1} -CD45.1 mouse received either 10 or 3 LT-HSCs. Recipient B6- W^{A1}/W^{A1} -CD45.1 mice were bled 4, 8 or 11 weeks post transplantation and peripheral blood analysed to determine levels of chimerism (6.2.2.2). The experiment was terminated at 11 weeks due to COVID-19 restrictions, therefore it was not possible to confirm whether mice with < 1% chimerism

(trace chimerism) would progress to develop > 1% chimerism with time. Mice with trace chimerism are highlighted in the results.

For in vitro LT-HSC assays, 1 LT-HSC was sorted per well of a round bottom 96-well plate, with each well containing 50 µL of LT-HSC media as described in 6.2.5.

Cells were sorted using a four laser Beckman Coulter Astrios Eq sorter.

6.2.5 *In vitro* long term haematopoietic stem cell assays

LT-HSCs were sorted into and cultured in 50 µL StemSpan media (STEMCELL) supplemented with 10% fetal calf serum (Sigma-Aldrich), 300 ng/ml stem cell factor (STEMCELL) and 20 ng/ml IL-11 (STEMCELL). Every 24 h for 120 h, the number of cells in each well were manually counted and the cumulative proportion of clones having entered their first division (2 cells), second division (3-5 cells) or third division (> 6 cells) recorded. At 10 days, clones were estimated to be very small (< 50 cells), small (51-500 cells), medium (501-10,000 cells), or large (> 10,000 cells). Clone sizes were validated by analysing a constant volume of cell suspension (95% of suspension) by flow cytometry. Very small clones were pooled together due to low numbers of cells. Cells were then prepared for FACS analysis (2.6), followed by staining for the presence of lineage markers (mouse lineage antibody cocktail-PerCP/Cy5.5, 1:50 dilution) and progenitor markers (Sca-1-APC and CD117-BV421; both 1:400 dilution) in 100 µl FACS buffer for 20 min at 4 °C. After staining, cells were washed three times in FACS buffer. After the final wash, cells were resuspended in FACS buffer and acquired on the Cytotflex LX or CytoFLEX S (Beckman Coulter).

All cells were pre-gated on viable and single cells. All data was analysed with FCS Express (De Novo) software.

6.2.6 Immunostaining

Sections were blocked in 10% donkey serum/ 0.1% tween-20/PBS (PBST) for 1 h. Antibodies were used in 10% goat serum/PBS: primary antibodies were applied overnight at 4 °C whilst secondary antibodies were applied at room temperature in the dark. Primary antibodies were LepR (goat polyclonal, R&D systems; 1:100) and anti-laminin (rabbit polyclonal, Sigma, 1:200). All secondary antibodies were used at 1:400 dilution and were as follows: donkey anti-goat IgG-AF647 (ThermoFisher) and goat anti-rabbit IgG-AF488 (Molecular Probes). Samples were washed three times in PBST after each primary and secondary incubation. Sections were mounted with ProLong Gold with DAPI (ThermoFisher).

6.2.7 Imaging and image analysis

Images were acquired using a Zeiss 880 lsm confocal microscope with Zeiss Zen software at 40x objective (Plan-Apochromat 40x/1.4 Oil MIC M27) and 3x3 tilescan. Fluorochromes used were AF488 (laminin), AF647 (LepR) and DAPI. Images were acquired in lambda mode and spectrally unmixed to remove background autofluorescence. Non-linear adjustment (0.5 gamma) was applied to the DAPI channel only.

For relative quantification of LepR staining, spectrally unmixed LepR-AF647 images were saved as TIFF images and imported into ImageJ software and the Integrated Density calculated per image. Images with > 10% negative space (e.g. capturing the central vein, or edge of the BM) were excluded. Only images that were taken on the same day with the same imaging conditions were compared, therefore ensuring images had similar levels of background fluorescence.

For vessel analysis, image quantification was achieved using StrataQuest software (TissueGnostics GmbH). The confocal microscope images were imported and combined to create a grey virtual channel; median ('despeckle') and Gauss filters were applied, (kernel radius ('smoothing')=1: Gauss std=0.5). Bitwise NOT function was used to invert the image. Blood vessel 'seeds' were formed by combining inverted image from the laminin and DAPI mask (removing objects < 10 μm^2 function was used to discard data from intercellular spaces). Blood vessel seeds were selected from a scatter plot of area (μm^2) versus mean intensity of the combined grey virtual channel and a gate applied to identify the blood vessel lumens. Seeds were morphologically 'opened' to remove very small objects while maintaining the shape and size of blood vessels; Bwareopen function was used to remove connected objects that had fewer than 50 pixels. Tears in the tissue and any remaining small holes were visually verified by backgating on the image and excluded from the analysis. Manual correction was used to add or remove false positive or negative blood vessels visually identified.

6.2.8 Real-time polymerase chain reaction

RNA was isolated using the miRNeasy Mini Kit (QIAGEN) as described in 2.2.2 and transcribed using SuperScript IV First-Strand Synthesis System (ThermoFisher Scientific) according to the manufacturer's instructions. Following cDNA synthesis, duplex qPCR was performed using genes of interest (*Cxcl12*, Mm00445553_m1; *Kitl1*, Mm00442972_m1, or; *Angpt1* Mm00456503_m1) and housekeeping gene (*Hprt1*, Mm03024075_m1), TaqMan Fast Advanced MasterMix (ThermoFisher Scientific) and RNase-free water in the ratio 10:1:8; TaqMan Fast Advanced MasterMix, gene expression assay and RNase-free water. Each sample was prepared in triplicate. The

plates were run using the StepOne Plus Realtime PCR System (Applied Biosystems). Data was exported into Microsoft Excel and fold change was calculated using the delta-delta method where $\text{ratio} = 2^{-\Delta\Delta\text{CT}}$ (269).

6.3 Results

6.3.1 Immune thrombocytopenia progression drives haematopoietic stem cell and progenitor expansion

As discussed in Chapter 4, ITP patients have increased numbers of BM Mks (302-304), which is in agreement with the model presented. As inflammatory factors are known to drive emergency megakaryopoiesis independently of TPO (116), the plasma and BM supernatant were analysed. Biological processes involved in the inflammatory response and positive regulation of MAPK signalling (such as CCL21) were upregulated in both the plasma and the BM (Figure 6.1 and Figure 6.2). Upregulation of these biological processes were higher in the BM than the plasma which was of interest as inflammation and MAPK signalling have previously been shown to affect LT-HSC quiescence and function (116, 382). Additionally, some biological processes and reactome pathways also shown to affect LT-HSC quiescence and function such as IL-1 signalling and smooth muscle cell proliferation (such as VEGF, MMP2, WISP1 and IGFBP-3) were uniquely upregulated in the BM (Figure 6.1 and Figure 6.2) (112, 383-386).

To test whether sustained ITP affects BM haematopoietic progenitors, mice in the ITP group and controls were compared by flow cytometry (Figure 6.3). Whilst ITP had no effect on total BM cellularity (Figure 6.3C), ITP caused a 1.3-fold expansion in the percentage of BM-derived Lin⁻Sca1⁺c-Kit⁺ (LK cells, enriched for myeloid progenitors) and 1.7-fold expansion in LSK cells, which are enriched for HSCs (Figure 6.3Di and ii). Progenitor expansion in the spleen was also observed (Figure 6.4), with a 2 and 2.9-fold expansion in the LK and LSK populations, respectively, suggesting the presence of extramedullary hematopoiesis in ITP. The LSK population was subdivided further using SLAM markers (18), with the largest expansion in the LT-HSC fraction (2.8-fold in the BM and 9.7-fold in the spleen) (Figure 6.3v and Figure 6.4v, respectively). In addition, the LK population within the BM was subdivided further (Figure 6.5); showing an expansion in the common myeloid progenitor fraction, and possibly also an expansion in the common erythroid/Mk progenitor. In contrast, there were no differences in the common granulocyte/monocyte progenitor fraction of mice with ITP vs controls.

To confirm that ITP progression causes progenitor expansion, BM aspirate from 8 ITP patients was analysed by flow cytometry (Figure 6.6). An increase in progenitor frequency was observed, which was proportional to ITP duration in patients not undergoing treatment at the time of BM aspiration. Within CD34⁺CD38⁻ cells, there was

a 2.37 fold increase in CD34⁺CD38⁻CD90⁻CD45RA⁻ MPPs and a 3.31 fold increase in CD34⁺CD38⁻CD90⁺CD45RA⁻ HSCs from chronic ITP patients over newly diagnosed ITP patients, groups as defined by the 2019 ASH guideline on ITP (200). Patients undergoing treatment at the time of BM aspiration (steroids, IVIg or TPO-RA) did not follow this same trend, suggesting that intervention may correct progenitor expansion.

To determine the functional effect of ITP on LT-HSCs, single LT-HSCs from mice in the ITP group or controls were isolated and cultured in conditions which maintain LT-HSC activity (Figure 6.7) and analysed for changes in cell division, colony size and cell phenotype (387, 388). LT-HSCs from mice with ITP proliferated faster, with less time taken to complete first, second and third division (Figure 6.7B). This faster division formed larger colonies at day 10 of culture (Figure 6.7C), which were driven by an increase in LSK progenitors (Figure 6.7Di). However, despite the overall increase in number of cells per clone, ITP did not alter the proportion of differentiated and stem/progenitor cells within clones, suggesting that progenitor expansion was not accompanied by differentiation or self-renewal defects (Figure 6.7Dii-iii). The results indicate that sustained ITP induces the cycling of phenotypic LT-HSCs, causing an expansion of haematopoietic progenitors without compromising LT-HSC function.

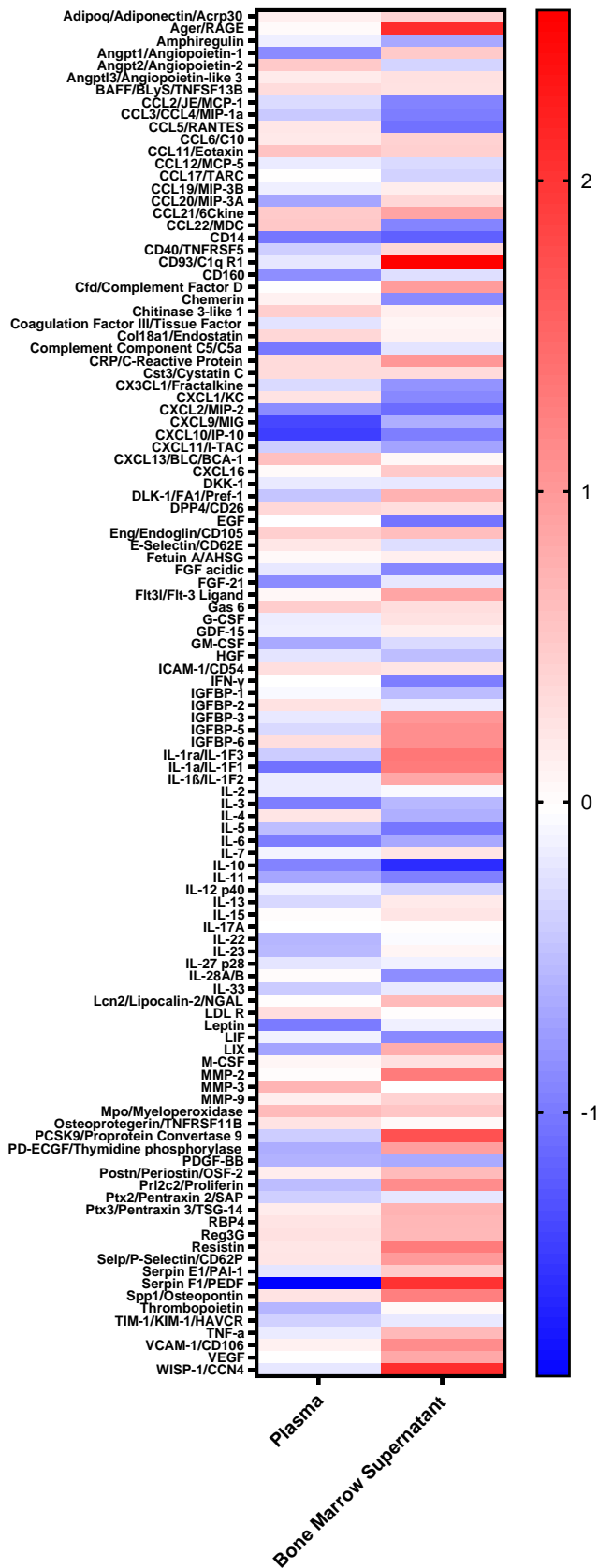


Figure 6.1. Cytokine signature in plasma and BM supernatant is altered in sustained ITP. Cytokine array data from the BM supernatant and plasma of IgG/anti-CD41 treated mice. Data is presented as log2 fold change of 4 week ITP relative to control. N = 1.

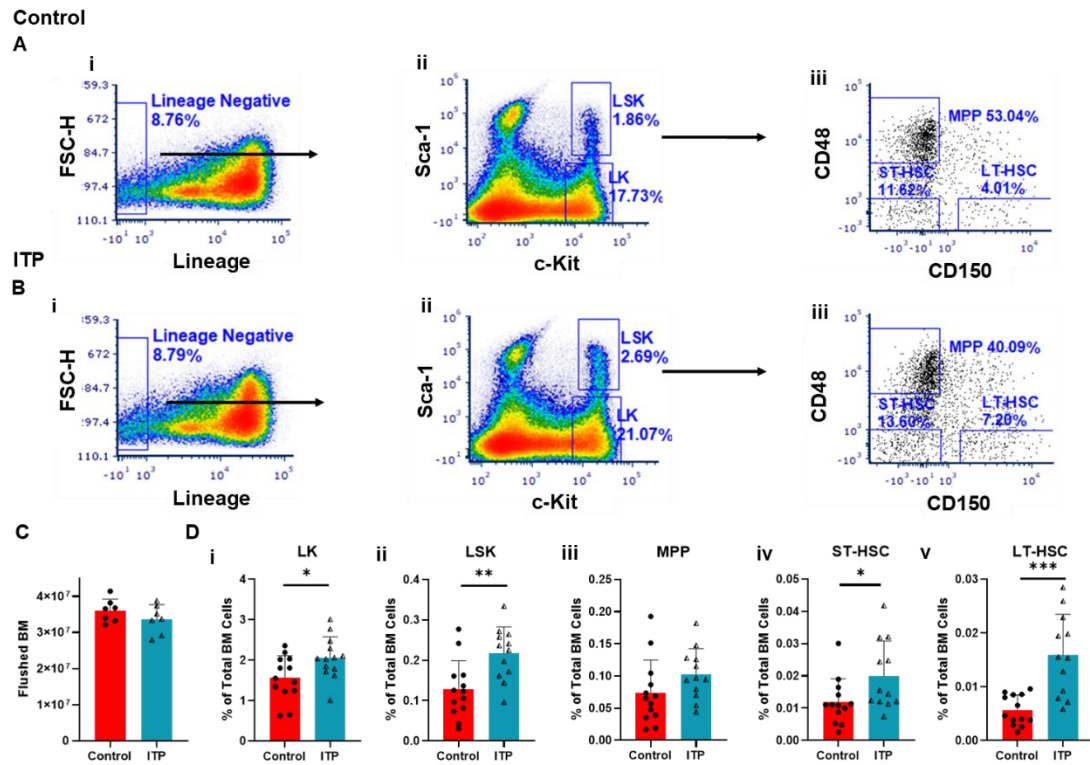


Figure 6.3. Sustained ITP drives BM primitive progenitor expansion. Representative flow cytometry gating strategy for haematopoietic progenitors in the BM of **A)** controls, **B)** mice with 4 week ITP. All cells are gated on live cells and singlets. **C)** Total cell counts from flushed BM (2x femur, tibia and humerus) $P = 0.46$ (Mann-Whitney test). $N = 7$, (2 independent experiments). **D)** Summary of flow cytometry analysis: **i)** Lin⁻c-Kit⁺ (LK); $*P = 0.034$, **ii)** Lin⁻Sca-1⁺c-Kit⁺ (LSK); $**P = 0.0055$, **iii)** LSK CD48⁺CD150⁻ (Multipotent Progenitors, MPP); $P = 0.068$, **iv)** LSK CD48⁻CD150⁻ (Short Term HSC, ST-HSC); $*P = 0.019$, **v)** LSK CD48⁻CD150⁺ (Long Term HSC, LT-HSC); $***P = 0.0005$. $N = 13$ (3 independent experiments), P values were calculated by Mann-Whitney tests.

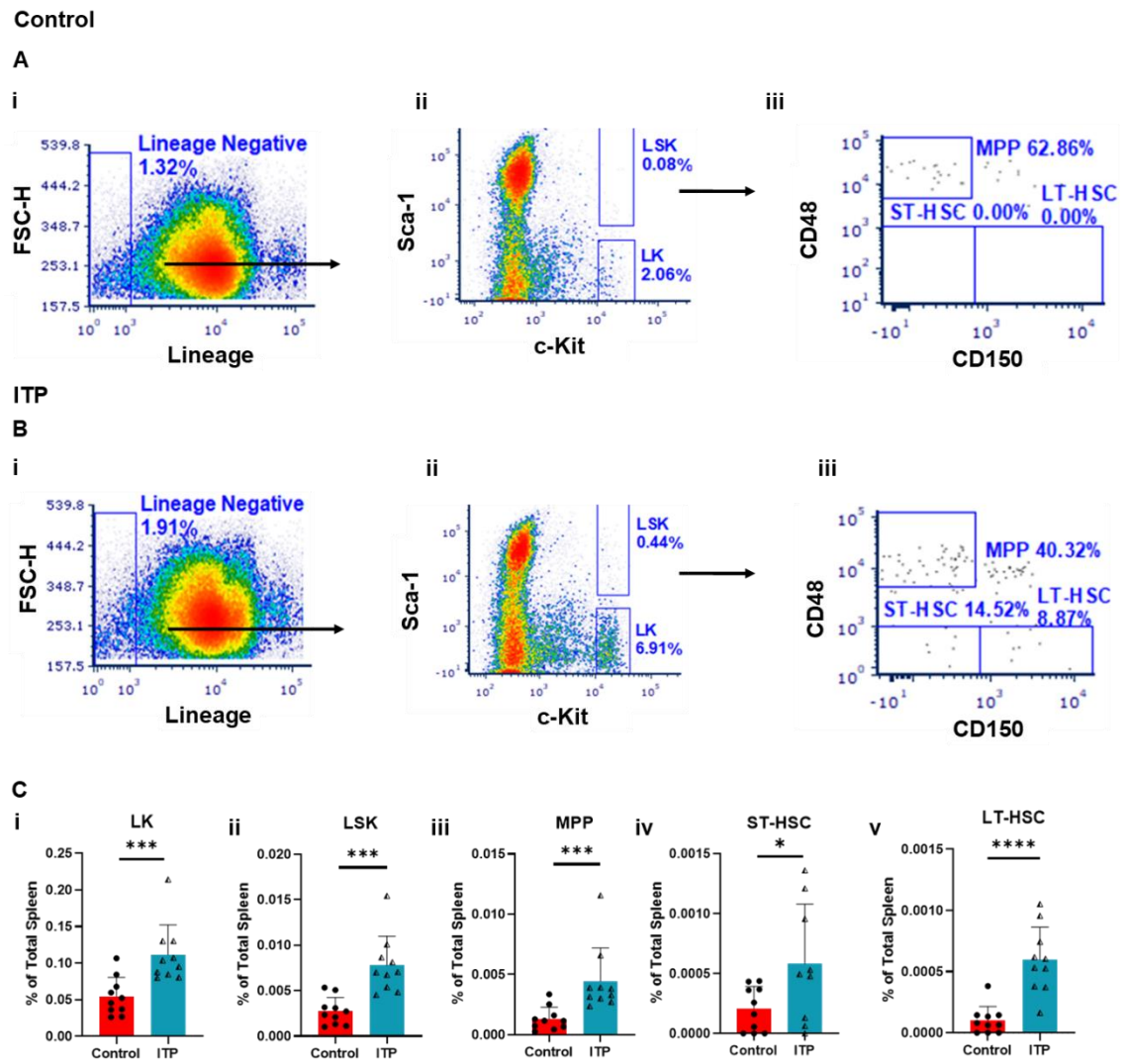


Figure 6.4. Sustained ITP drives extramedullary haematopoiesis. Representative flow cytometry gating strategy for haematopoietic progenitors in the spleen of **A)** controls, **B)** mice with 4 week ITP. All cells are gated on live cells and singlets. **C)** Summary of flow cytometry analysis: **i)** LK ($***P = 0.0007$), **ii)** LSK ($***P = 0.0001$), **iii)** MPP ($***P = 0.0003$), **iv)** ST-HSC ($*P = 0.045$), **v)** LT-HSC ($****P < 0.0001$). $N = 10$ mice per group, 2 independent experiments. P values were calculated by Mann-Whitney tests.

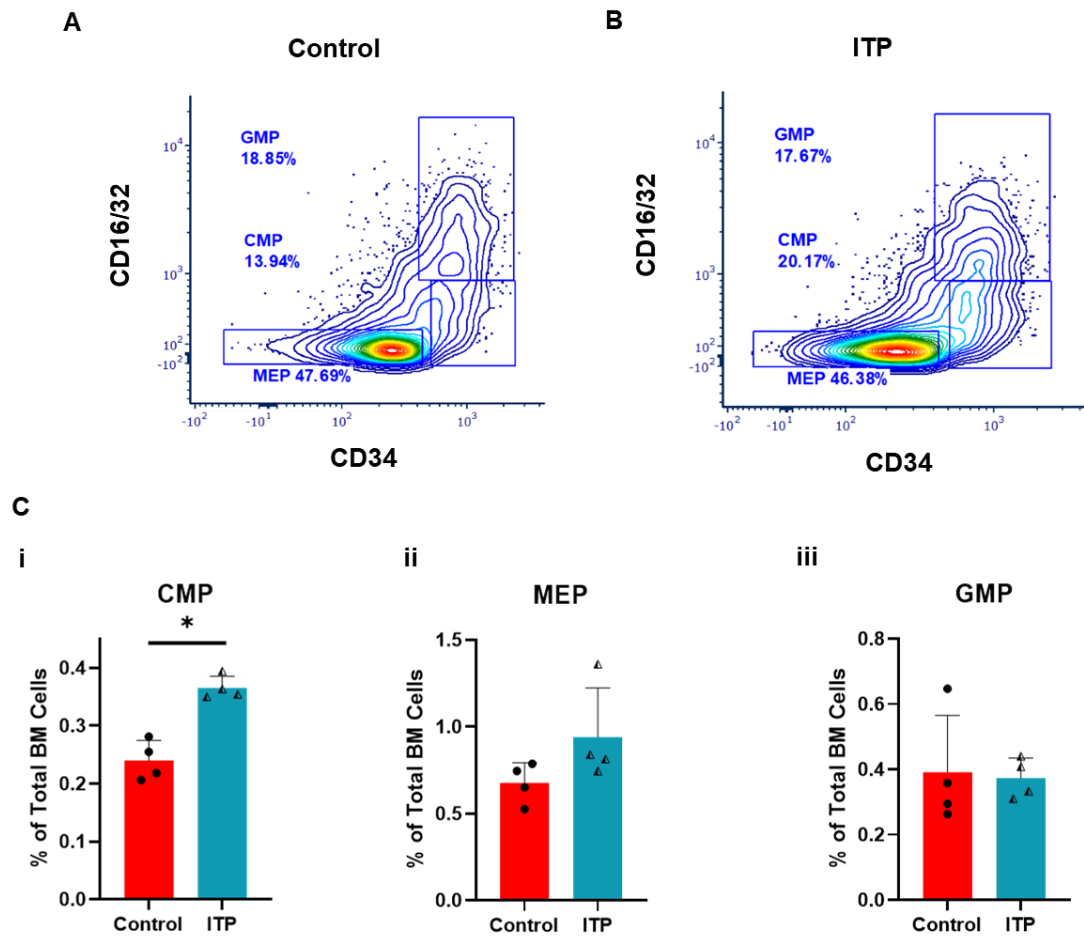
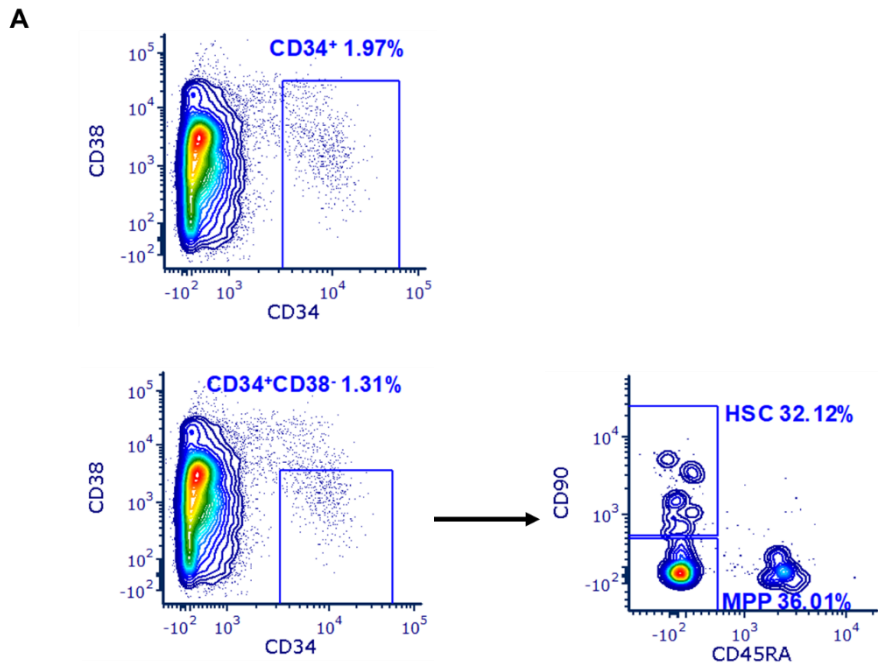


Figure 6.5. Sustained ITP drives BM committed progenitor expansion. Representative flow cytometry gating strategy showing example plots from **A)** controls, **B)** mice with 4 week ITP. All cells are gated on live cells, singlets and Lin⁻ cells. **C)** Summary of flow cytometry analysis: **i)** LK CD16/CD32^{low}CD34^{high} (common myeloid progenitor, CMP); * $P = 0.029$, **ii)** LK CD16/CD32^{low}CD34^{low} (common erythroid/Mk progenitor; MEP); $P = 0.11$, **iii)** LK CD16/CD32^{high}CD34^{high} (common granulocyte/monocyte progenitor; GMP); $P = 0.69$. $N = 4$ (1 independent experiment), P values were calculated by Mann-Whitney tests.



B

Disease Phase	Platelet Count (x10 ⁹ /L)	Treatment	CD34 ⁺ (%)	CD34 ⁺ CD38 ⁻ (%)	MPP (%)	HSC (%)
Newly diagnosed	62	No treatment	3.222	1.438	0.672	0.514
Newly diagnosed	12	No treatment	2.679	0.978	0.361	0.250
Newly diagnosed	23	No treatment	1.974	1.062	0.341	0.399
Chronic	10	No treatment	11.248	2.990	1.380	1.170
Chronic		No treatment	6.425	4.152	0.795	1.400
Newly diagnosed	1	Steroids+IVIg	1.925	0.897	0.569	0.006
Chronic	90	Steroids	1.347	0.581	0.107	0.376
Refractory	6	Eltrombopag	11.502	6.075	2.043	1.909

Figure 6.6. ITP progression is associated with progenitor expansion. A) Representative flow cytometry gating strategy for haematopoietic progenitors in BM aspirate samples from ITP patients. All cells are gated on live cells and singlets. **B)** Summary of flow cytometry analysis from 9 ITP patients (CD34⁺, CD34⁺CD38⁻, CD34⁺CD38⁻CD90⁺CD45RA⁻; HSC and CD34⁺CD38⁻CD90⁻CD45RA⁻; MPP). Newly diagnosed: ITP duration of < 3 months, Chronic ITP: ITP duration of > 12 months, Refractory ITP: ITP duration of > 12 months that is resistant to therapy. All aspirates had a viability of > 75%.

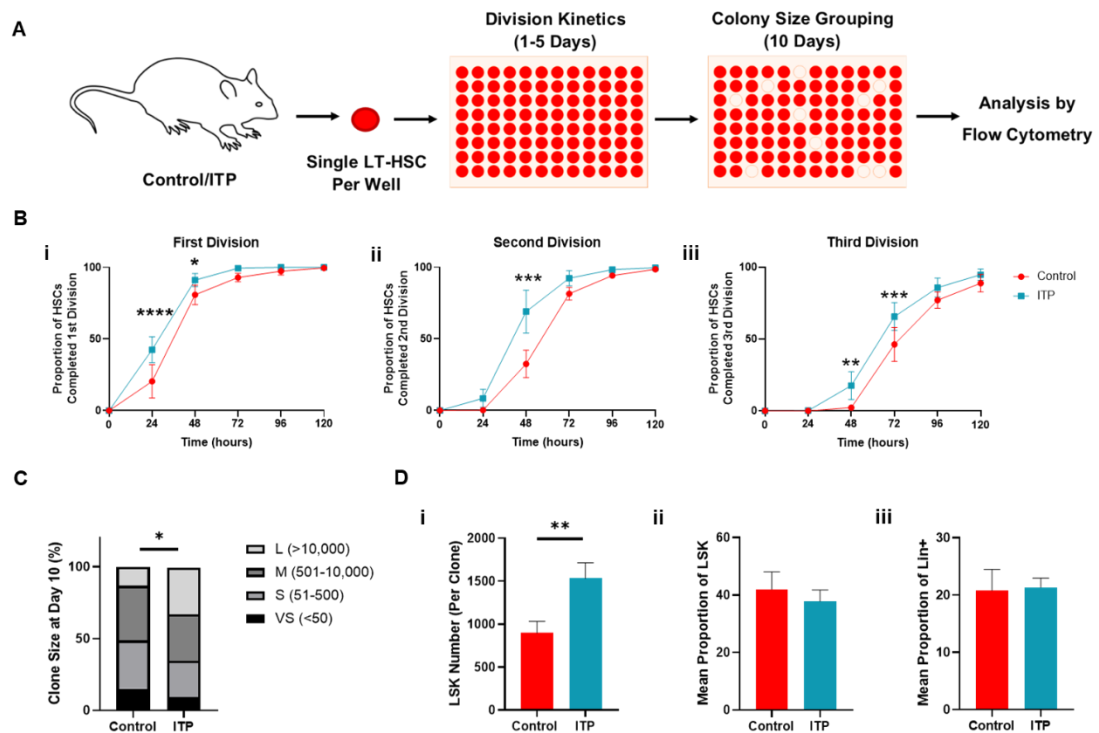


Figure 6.7. Sustained ITP drives progenitor proliferation. A) Experimental outline for B-D. **B)** Cumulative time taken for a single LT-HSC to complete first (i), second (ii), and third (iii) division. $N = 4-5$ (2 independent experiments), P values calculated by Two-way ANOVA with Sidak's multiple comparison test. **C)** Colony size after 10 days in culture ($*P = 0.020$). $N = 3-4$ (representative of 2 independent experiments). P values calculated by Two-way ANOVA. Colonies were categorised as very small (< 50), small (51-500), medium (501-10,000) or large (> 10,000). **D)** After 10 days in culture, colonies were analysed by flow cytometry for the expression of Lineage and LSK markers. LSK numbers (i, $P = 0.006$) and frequency (ii, $P = 0.92$). Frequency of Lin⁺ cells (iii, $P = 0.55$). P values were calculated by Mann-Whitney test. $n = 143$ and $n = 208$ clones from controls and mice with sustained ITP, respectively. $N = 3$ (representative of 2 independent experiments).

6.3.2 Sustained immune thrombocytopenia increases the number of functional haematopoietic stem cells

In order to assess the *in vivo* functional capacity of the expanded progenitor compartment in mice, competitive transplantation assays were performed using 5×10^6 whole BM cells from ITP and control donors in 3:1, 1:1 and 1:3 ratios (Figure 6.8A). This was followed by secondary transplantations after 20 weeks using 2×10^7 pooled whole BM cells from mice within each ratio group. In the 1:1 group (Figure 6.8C), the contribution of ITP donors to peripheral chimerism increased to $63 \pm 6\%$ (mean values \pm SD), accompanied by an expanded contribution to the BM LT-HSC phenotype at $85 \pm 10\%$. Secondary transplantation data similarly showed an increased contribution by donor cells derived from the ITP group to mature cell production. Together, these transplantation data demonstrate the existence of an expanded, self-renewing pool of functional LT-HSCs in the BM of mice with sustained ITP.

In order to test LT-HSC functional capacity more directly, we next transplanted limiting numbers of highly purified LT-HSCs isolated using the $\text{Lin}^- \text{Sca1}^+ \text{c-Kit}^+ \text{CD48}^- \text{CD150}^+$ phenotype. Either 3 or 10 LT-HSCs from the ITP or control groups were isolated and transplanted into sub-lethally irradiated B6- W^{fl}/W^{fl} -CD45.1 mice (Figure 6.9). Whereas 20% of mice receiving 3 LT-HSCs and 40% of mice receiving 10 LT-HSCs from the control group were positive, none of the mice receiving LT-HSCs from mice with ITP were repopulated, suggesting that the LT-HSC phenotype in the ITP group does not contain as high a frequency of functional LT-HSCs.

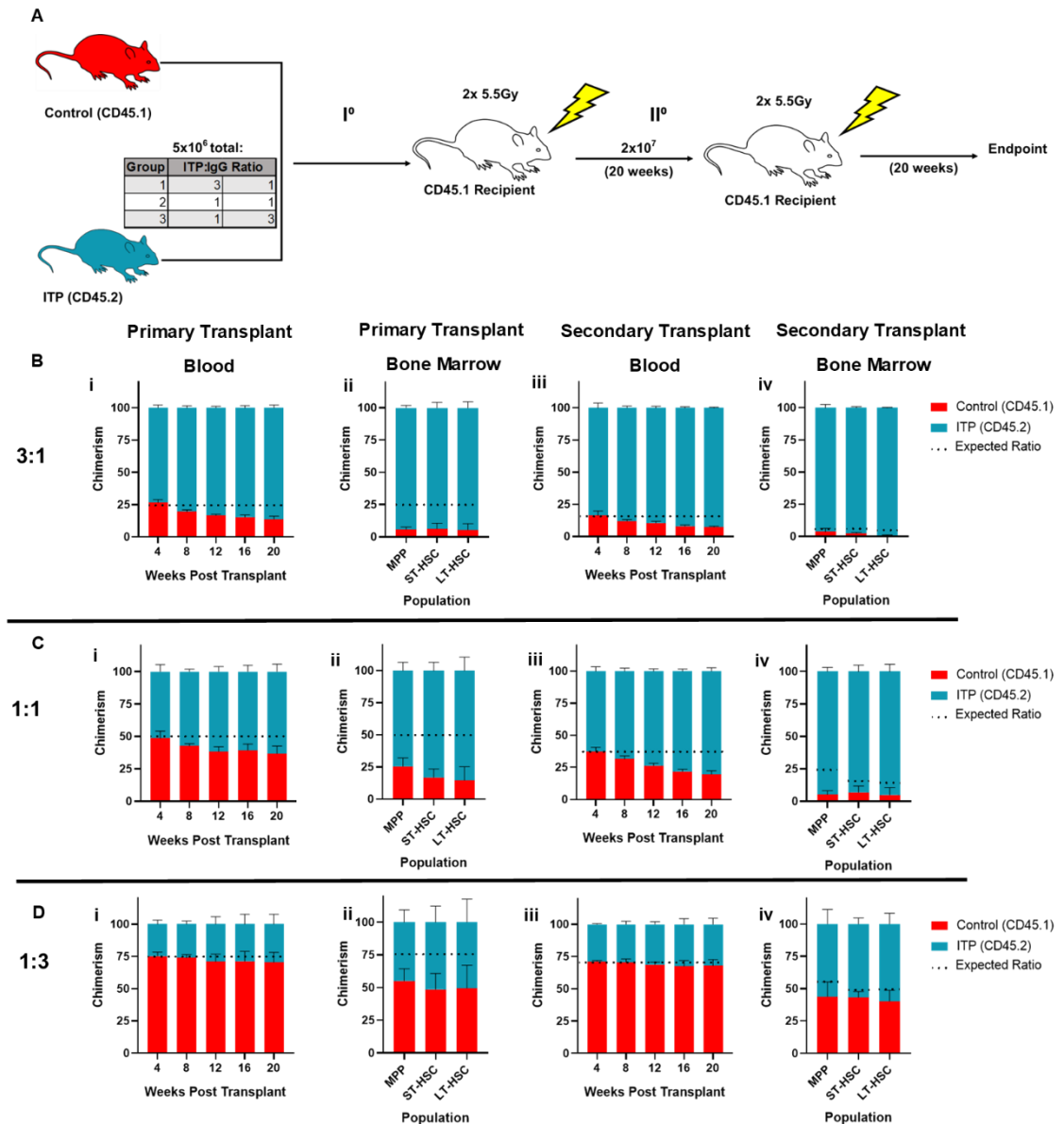
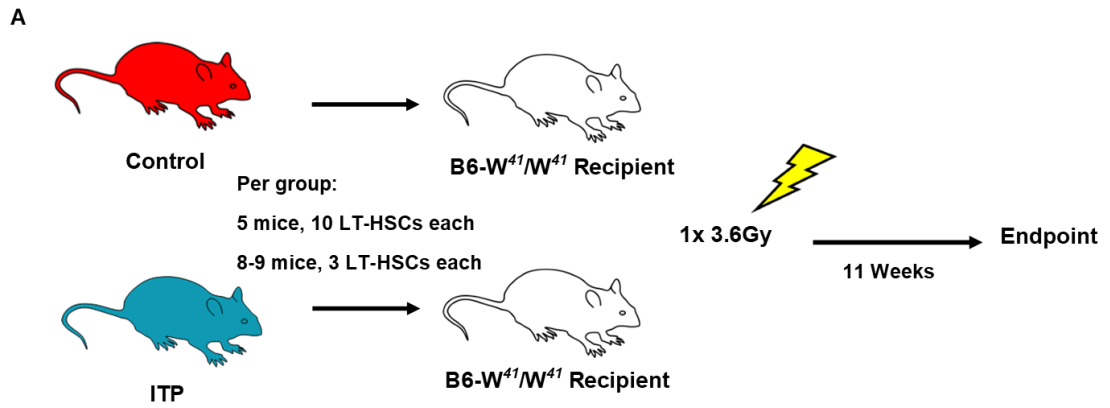


Figure 6.8. Sustained ITP increases the frequency of functional LT-HSCs *in vivo*. **A)** Experimental outline for B-D. **Bi, Ci and Di)** peripheral blood from primary recipients 4-20 weeks after transplantation. **Bii, Cii and Dii)** analysis of BM from primary recipients 20 weeks after transplantation. **Biii, Ciii and Diii)** analysis of peripheral blood from secondary recipients 4-20 weeks after transplantation. **Biv, Civ and Div)** analysis of BM from secondary recipients 20 weeks after transplantation. The dotted line shows the expected ratio if ITP had no effect on chimerism; for primary recipients this was calculated based upon the expected ratio of donor cells, for secondary recipients this was calculated based upon the end point of the primary recipients. N = 5 per recipient group.



B

HSC Dose	Positive	
	Control	ITP
3	2/9	0/8
10	2*/5	0/5

Figure 6.9. Fewer functional LT-HSCs exist in the phenotypic LT-HSC pool in ITP. A) Experimental outline for **B.** **B)** After 11 weeks, 2/9 recipients receiving 3 control LT-HSCs and 2/5 recipients receiving 10 LT-HSCs experienced chimerism, whilst 0 recipients receiving ITP LT-HSCs experienced chimerism, $P = 0.013$. P value was calculated by a Chi-squared test. A successful transplantation was defined as > 1% CD45.2 chimerism. After 11 weeks, 1 mouse transplanted with 10 control LT-HSCs showed > 1% CD45.2 chimerism, whilst 1 mouse showed trace amounts of chimerism (< 1%) as marked by an asterisk (*).

6.3.3 ITP progression drives physical and biochemical changes within the BM HSC microenvironment

LT-HSC function is maintained through cytokine-cytokine receptor interactions and direct cell-cell contact between the LT-HSC and components of the perivascular BM microenvironment, including ECs and LepR⁺ BMSCs (45, 60, 72). As sustained ITP causes expansion and functional changes in LT-HSCs, we next assessed whether this was accompanied by alterations in the BM microenvironment. Immunofluorescence microscopy identified significant changes in non-haematopoietic components of the HSC BM microenvironment, which were associated with ITP progression (Figure 6.10). Mice with 4 week ITP had a 2-fold increase in sum vessel area, which was attributed to an increase in average vessel area rather than any changes in vessel number. Effects were also observed at an earlier (2 week) time point, with a 1.5-fold increase in sum vessel area with no change in vessel number (Figure 6.11). Furthermore, at 4 weeks there was a significant LepR⁺ stromal cell expansion (1.5-fold increase) (Figure 6.10B), whilst there were no changes in stromal cell number at 2 weeks (Figure 6.10B).

To explore whether this remodelling of the BM microenvironment was reversible following recovery from thrombocytopenia, mice were allowed to recover for 4 weeks ('ITP Recovered' group) prior to BM analysis (Figure 6.10). During this period of recovery, the platelet count reverted back to baseline by day 18 after the final anti-CD41 antibody injection (Figure 6.12). Despite the amelioration of thrombocytopenia, the substantial structural differences observed in the BM vasculature persisted with a further 1.5-fold increase in sum vessel area relative to the initial ITP group. In these mice, a significant increase in vessel number was observed as opposed to a further increase in average vessel area (Figure 6.10C). Conversely, numbers of LepR⁺ perivascular stromal cells reverted back to control levels, suggesting that stromal cell expansion was transient (Figure 6.10B).

Since perivascular LepR⁺ stromal cells are a major source of factors influencing LT-HSC function, including key microenvironment factors CXCL12, SCF and Angiopoietin-1 (45, 72, 73, 88), and share the same microenvironment as LT-HSCs (69, 70, 72), I hypothesised that a transient increase in LepR⁺ stromal cells support LT-HSCs in response to sustained ITP. I measured the expression of *Cxcl12*, *Kitl* and *Angpt1* in the BM and found that *Cxcl12* expression transiently increased to 2-fold levels in the ITP group (Figure 6.13Ai), but there were no significant changes in *Kitl* or *Angpt1* (Figure 6.13Aii-iii). Additionally I measured *Cxcl12* expression in the spleen, but found that expression levels did not alter with ITP progression (Figure 6.13B).

There is considerable overlap between *Cxcl12*-DsRed and LepR BMSCs; 98.8% of LepR⁺ BMSCs are *Cxcl12*-DsRed BMSCs and 88.8% of *Cxcl12*-DsRed are LepR⁺ BMSCs (268). To confirm past studies, confocal microscopy was performed on the BM of *Cxcl12*^{DsRed/+} mice with sustained ITP and sections were stained with LepR antibody. As expected, there was strong co-localisation between perivascular LepR⁺ BMSCs and *Cxcl12*-DsRed BMSCs (Figure 6.14). When the BM microenvironment of *Cxcl12*^{DsRed/+} mice with 4 week ITP was compared to controls, it was found that the perivascular *Cxcl12* expression increased in mice with ITP (Figure 6.15). CXCL12 levels were increased 1.8-fold in the BM supernatant of mice with ITP, but not in circulation or spleen, confirming a BM specific elevation in CXCL12 (Figure 6.16). As CXCL12 has an essential role in progenitor homing to the BM (46, 47, 85, 90), I hypothesised that mice with ITP would show an increased potential for progenitor homing. Flow cytometry analysis of recipient BM revealed that naïve LSKs homed preferentially to the BM of irradiated mice with ITP relative to controls (5.5-fold increase; Figure 6.17B). Together, the data shows that the BM actively remodels in response to ITP progression to create a site preferential for haematopoiesis. Whilst the expansion in LepR⁺ BMSCs and associated CXCL12 expression was transient, vasculature changes persisted, the consequences of which are unknown.

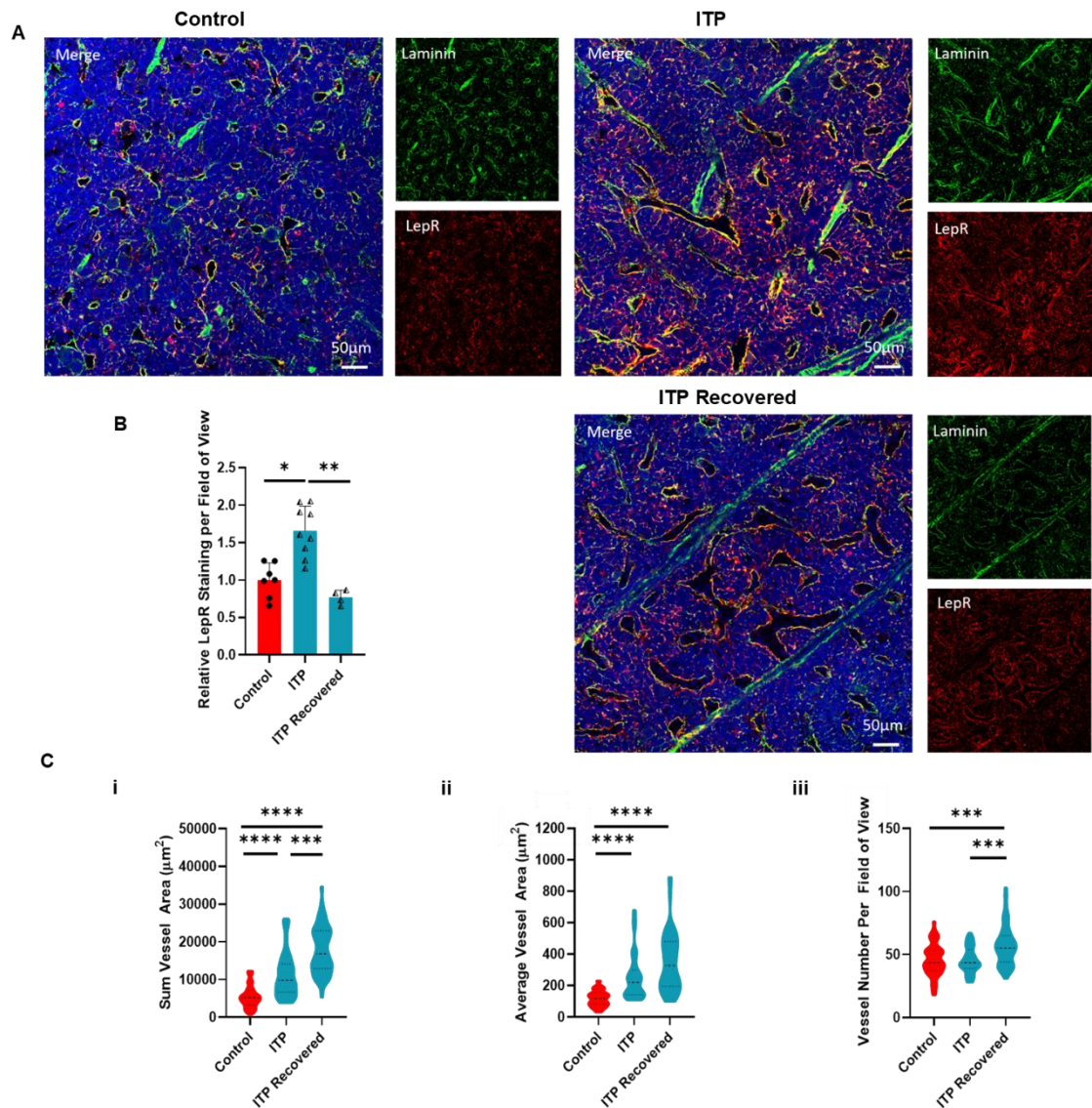


Figure 6.10. Sustained ITP remodels the BM niche. ITP progression was associated with blood vessel structural changes and reversible changes in stromal cell number. Mice were treated with IgG (control) or anti-CD41 (ITP) for 4 weeks. A further group of ITP mice were allowed to recover for a further 4 weeks after the last injection of anti-CD41, where platelet count returned to normal by day 18 ('ITP Recovered' group). All data shown from controls and mice with ITP are representative of 3 independent experiments, whilst the data from ITP Recovered mice is representative of 1 independent experiment. **A)** Representative confocal images of control, ITP and ITP Recovered diaphysis BM from WT femurs. **B)** Relative numbers of LepR⁺ stromal cells were inferred by comparing total LepR staining between groups. Staining was quantified by exporting the LepR channel images as TIFFs and quantifying total staining relative to controls using ImageJ software. Control vs ITP $*P = 0.018$, control vs ITP Recovered $P = 0.91$, ITP vs ITP Recovered $**P = 0.0021$. P values were calculated by a Kruskal-Wallis test with Dunn's multiple comparison test. $N = 4-9$. Values show mean values \pm SD, with an average of 10 images analysed per mouse. **C)** Vessel analysis showing: **i)** Sum vessel area (control vs ITP $****P < 0.0001$, control vs ITP Recovered $****P < 0.0001$, ITP vs ITP Recovered $***P = 0.0001$), **ii)** Average vessel area (control vs ITP $****P < 0.0001$, control vs ITP Recovered $****P < 0.0001$, ITP vs ITP Recovered $P = 0.066$), **iii)** Vessel number (control vs ITP $P > 0.99$, control vs ITP Recovered $***P = 0.0008$, ITP vs ITP Recovered $***P = 0.0007$). Vessel information was quantified using StrataQuest analysis software (TissueGnostics). P values were calculated by a Kruskal-Wallis test with Dunn's multiple comparison test, $n = 44-55$. Violin plots show median values and upper and lower quartiles, with an average of 10 images analysed per mouse.

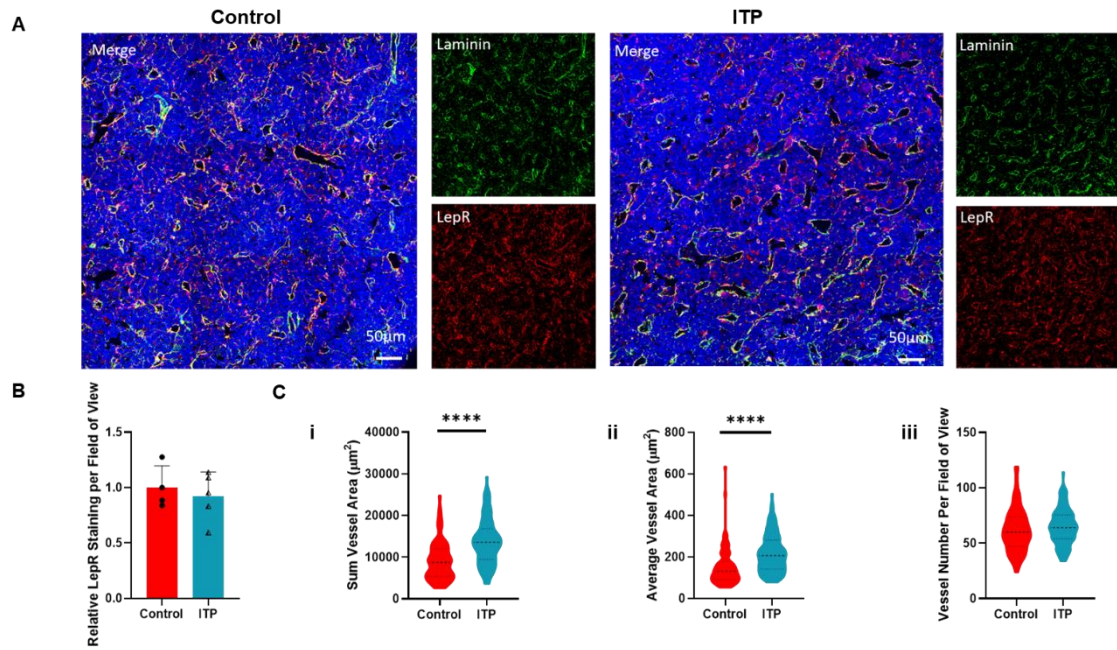


Figure 6.11. 2 Week ITP causes an increase in average vessel area but no changes in vessel number or LepR⁺ stromal cell number. **A)** Representative confocal images of diaphysis BM from the femurs of mice with 2 week ITP and controls. **B)** Relative numbers of LepR⁺ stromal cells were inferred by comparing total LepR staining between groups. Staining was quantified by exporting the LepR channel images as TIFFs and quantifying total staining relative to controls using ImageJ software. $P = 0.73$. P value was calculated by a Mann-Whitney test. $N = 4-5$. Values show mean values \pm SD, with an average of 10 images analysed per mouse. **C)** Vessel analysis showing: **i)** Sum vessel area ($****P < 0.0001$), **ii)** Average vessel area ($****P < 0.0001$), **iii)** Vessel number ($P = 0.144$). Vessel information was quantified using StrataQuest analysis software (TissueGnostics). P values were calculated by Mann-Whitney tests, $n = 75-113$. Violin plots show median values and upper and lower quartiles, with an average of 20 images analysed per mouse.

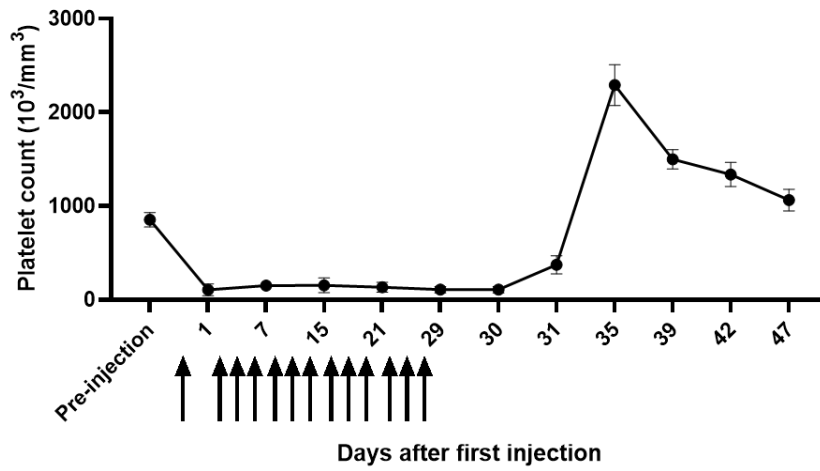


Figure 6.12. Platelet counts return to baseline after cessation of anti-CD41 administration in the sustained ITP model. Mice were administered anti-CD41 for 4 weeks as described previously. After the final injection on day 28, mice were regularly bled to monitor platelet recovery. By day 47 (18 days after the final injection), the platelet count had returned to baseline. Mice were sacrificed on day 56. N = 5.

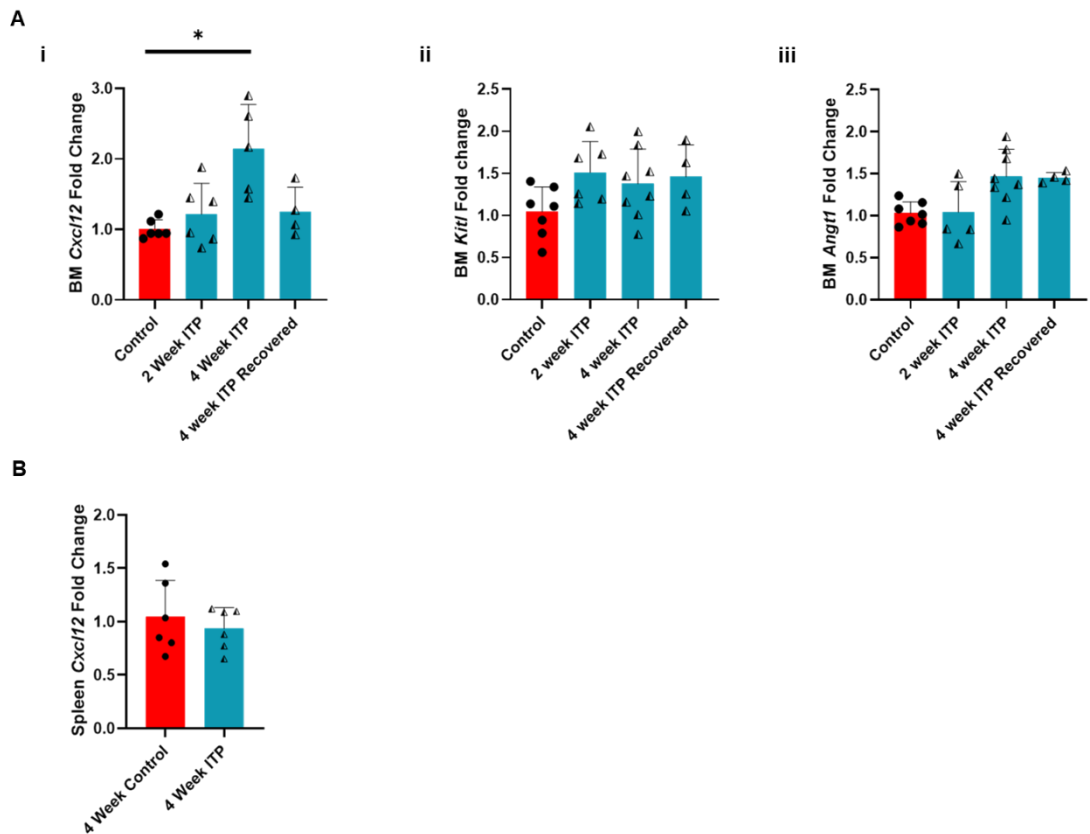


Figure 6.13. ITP progression increases BM *Cxcl12* expression. Cytokine expression of digested whole BM and spleen **Ai)** BM *Cxcl12* expression (control vs 2 week ITP $P > 0.99$, control vs 4 week ITP $*P = 0.021$, control vs 4 week ITP Recovered $P > 0.99$, 2 week ITP vs 4 week ITP $P = 0.14$, 4 week ITP vs 4 week ITP Recovered $P = 0.43$). **Aii)** BM *Kitl* expression (control vs 2 week ITP $P = 0.17$, control vs 4 week ITP $P = 0.68$, control vs 4 week ITP Recovered $P = 0.61$, 2 week ITP vs 4 week ITP $P > 0.99$, 4 week ITP vs 4 week ITP Recovered $P > 0.99$). **Aiii)** BM *Anpt1* expression (control vs 2 week ITP $P > 0.99$, control vs 4 week ITP $P = 0.090$, control vs 4 week ITP Recovered $P = 0.10$, 2 week ITP vs 4 week ITP $P = 0.19$, 4 week ITP vs 4 week ITP Recovered $P > 0.99$). $N = 4-8$. 1-3 independent experiments, P values calculated by Kruskal-Wallis tests with Dunn's multiple comparison test. **B)** Spleen *Cxcl12* expression ($P = 0.82$). $N = 6$ (2 independent experiments). P values were calculated by Mann-Whitney tests.

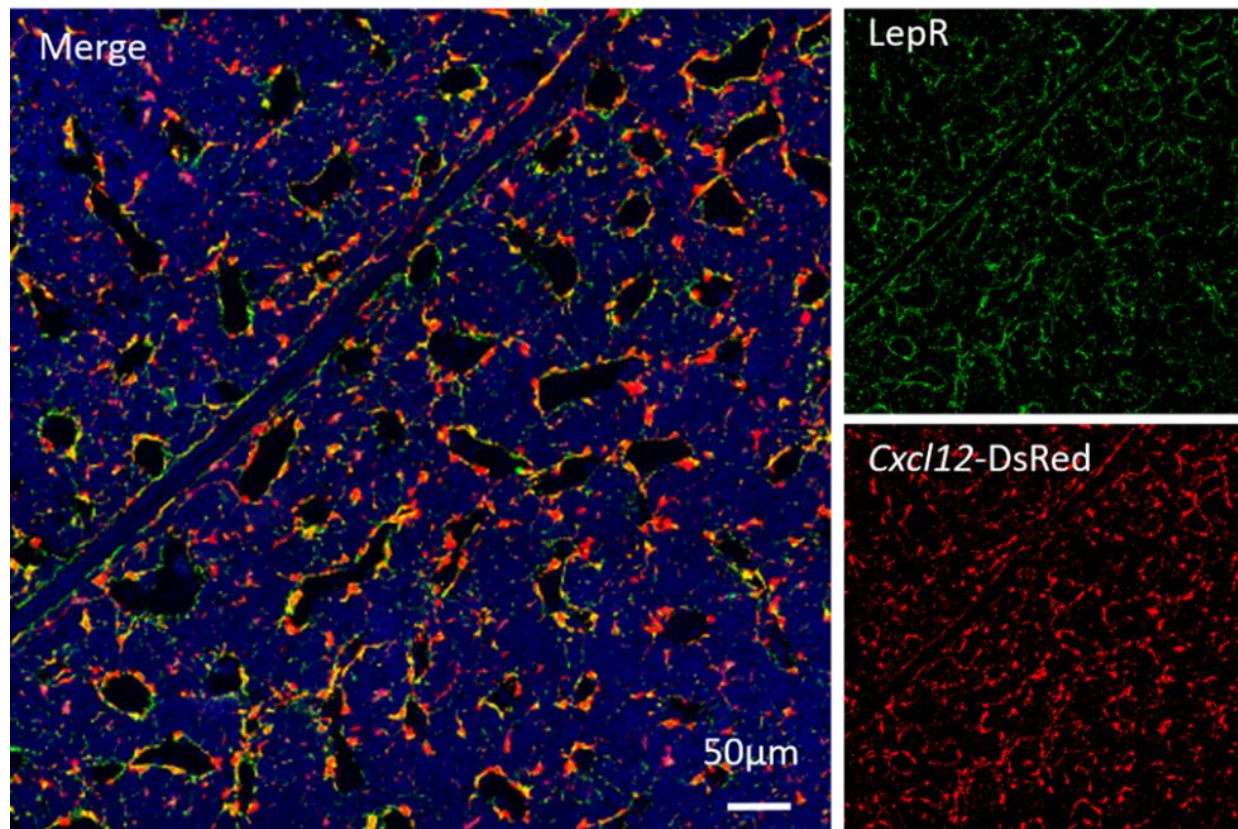


Figure 6.14. Strong co-localisation between perivascular LepR⁺ stromal cells and Cxcl12 expression. Representative confocal image of BM from *Cxcl12^{Dsred/+}* mice with 4 week ITP stained for LepR⁺ BMSCs.

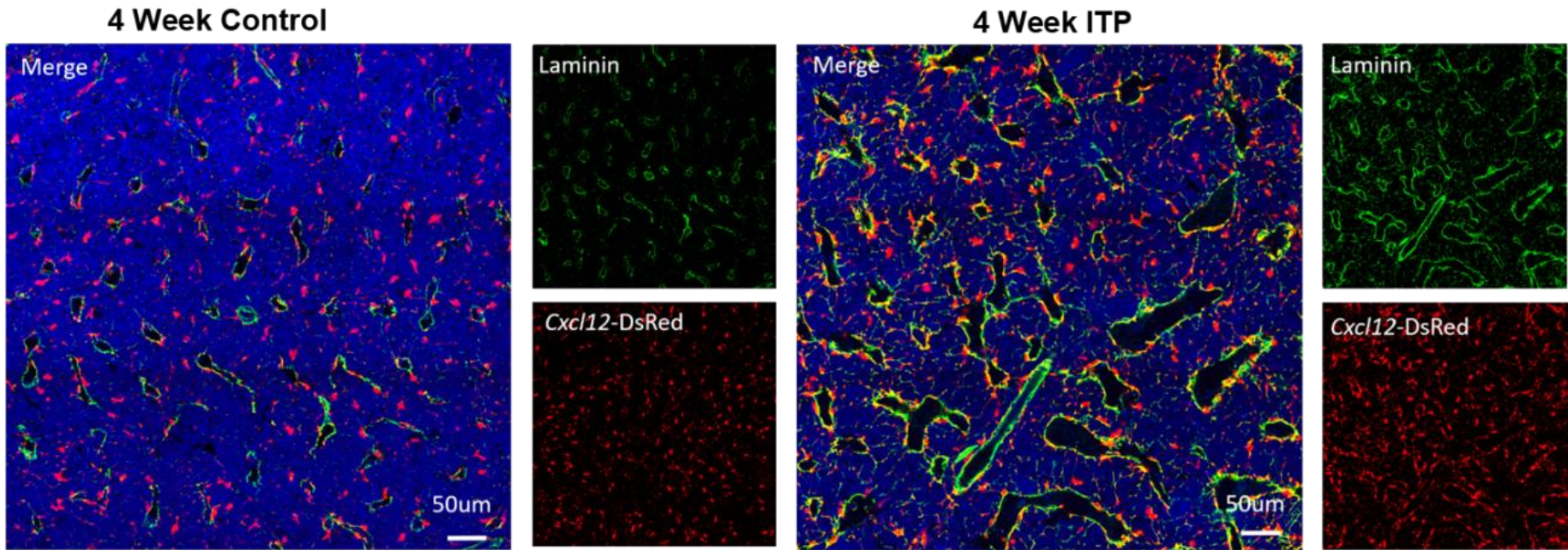


Figure 6.15. Expansion of *Cxcl12* expressing perivascular cells in ITP. Representative confocal images of BM from *Cxcl12*^{Dsred/+} mice with sustained ITP vs controls.

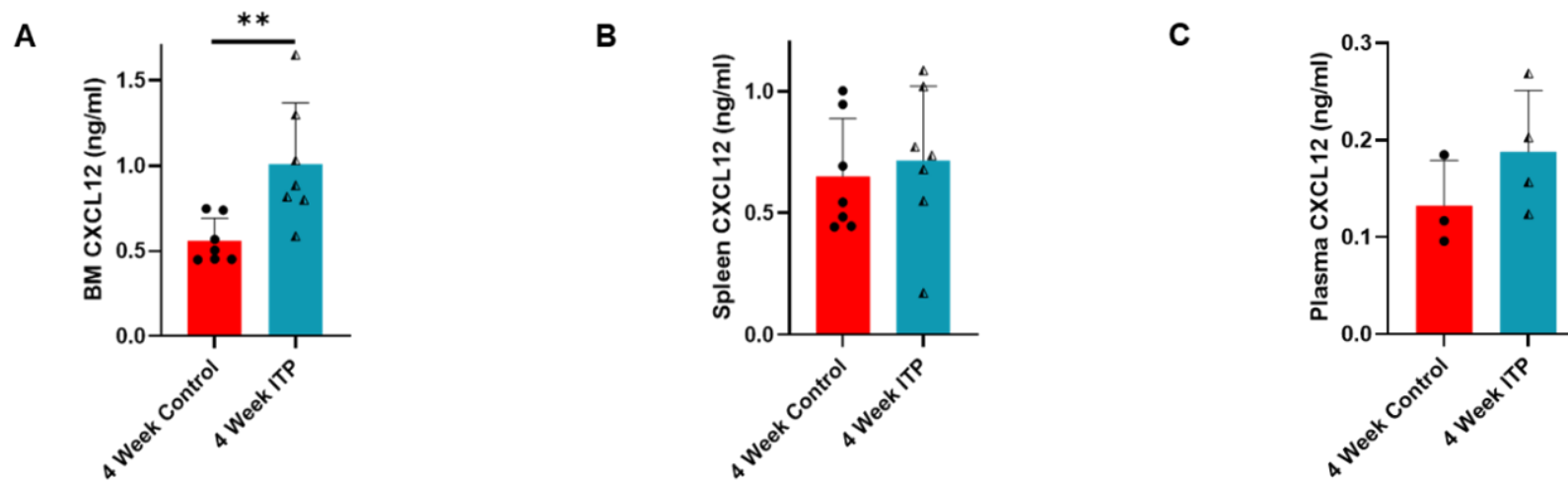


Figure 6.16. ITP progression increases BM CXCL12 expression. CXCL12 ELISA using: **A)** BM supernatant (** $P = 0.0023$, $N = 7$), **B)** spleen homogenate ($P = 0.38$, $N = 7$), **C)** and plasma ($P = 0.23$, $N = 3-4$). 2 independent experiments, P values were calculated by Mann-Whitney tests.

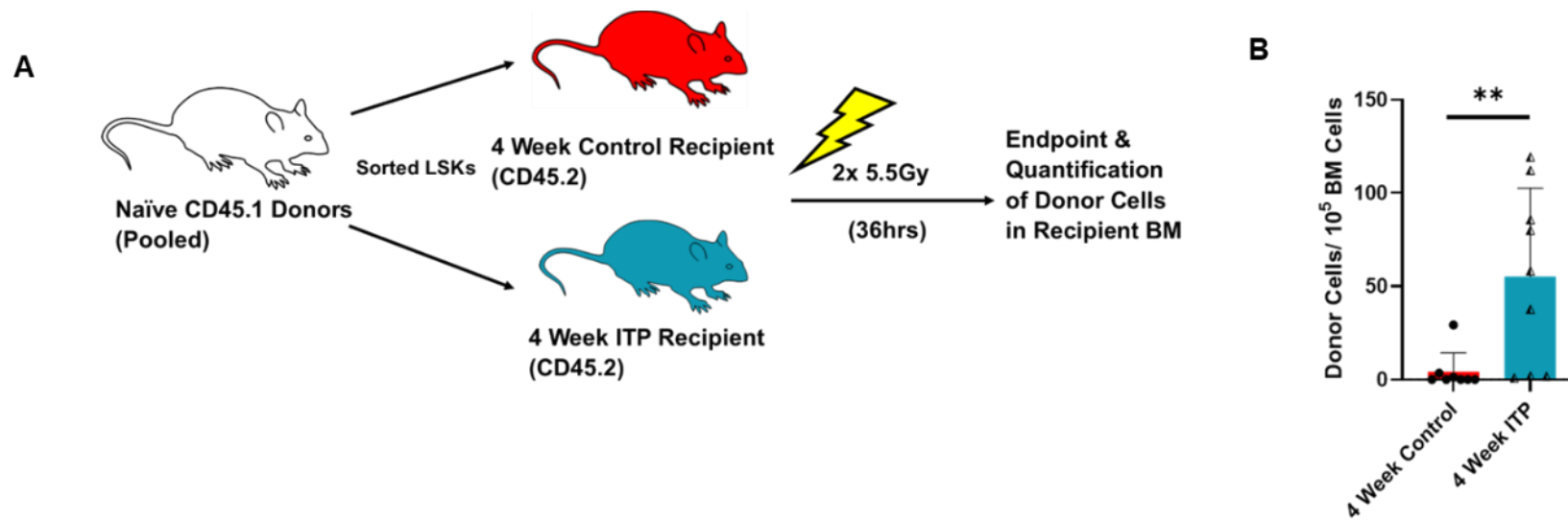


Figure 6.17. ITP progression is associated with increased BM homing. **A)** Experimental outline for **B).** **B)** Homing of naïve progenitors to the BM of mice with 4 week ITP vs controls ($P = 0.004$, $N = 8-9$). 2 independent experiments, P value was calculated by a Mann-Whitney Test.

6.4 Discussion

Whilst the mechanisms behind the development and maintenance of thrombocytopenia have been the subject of intensive research, the wider long-term effects of ITP progression are unclear. Here, I identify a significant expansion in phenotypic haematopoietic progenitors in both the murine model of sustained ITP and in human patients with chronic ITP, accompanied by a remodelling of the BM microenvironment in mice with sustained ITP. Functional assays demonstrated an increased proliferation and self-renewal potential of LT-HSCs from mice with ITP, but also indicated a shift in LT-HSC frequency within the LT-HSC phenotype. Assessment of the BM microenvironment identified alterations in key mediators of LT-HSC function, including an increase in total blood vessel area and a specific increase in LepR⁺ BMSCs. Together, these changes in LT-HSC activation and BM remodelling combine to counteract the stress of sustained ITP to ensure homeostasis within the haematopoietic system.

Cytokine analysis of BM and plasma samples from mice with sustained ITP identified that proteins involved in the inflammatory response were upregulated, which has been previously shown to drive megakaryopoiesis (116). As the cytokine signature in the ITP BM appeared to be more divergent from controls than the periphery, and that several upregulated biological processes and pathways have been previously shown to affect LT-HSC function (112, 382, 383), I asked if sustained ITP may affect haematopoiesis more broadly.

The expansion in stem and progenitor cell numbers in ITP in combination with the increase in proliferation observed in single LT-HSC *in vitro* assays suggests that LT-HSCs might be activated in response to ITP. Competitive transplantation assays revealed that ITP drives an expansion of LT-HSCs with durable self-renewal, suggesting that this activation did not compromise LT-HSC activity. However, caution is needed when interpreting the relative numbers and activation status of LT-HSCs in diseased states. Whereas whole BM competitive transplants allow LT-HSC activity to be assessed in an unbiased fashion and indicate that numbers of functional LT-HSC are increased, experiments assume that the expression of cell surface markers are not altered as a result of the experimental conditions. Indeed, it has been reported that during immune stimulation, BM cells have increased expression of Sca1 and CD150, causing non-HSC populations to appear in gates expected to be enriched in LT-HSC populations (389). This can lead to dilution of experimental LT-HSCs vs control LT-HSCs when performing downstream experiments. The low dose LT-HSC transplantation

experiments suggest that this may also occur in sustained ITP, where sub-lethally irradiated mice receiving LT-HSCs from ITP CD45.2 mice failed to repopulate compared to control CD45.2 mice. Together these data indicate that LT-HSCs might reside outside the traditional phenotype and that the LT-HSC phenotype is contaminated with a larger proportion of non-HSCs in an ITP setting.

It has been shown recently that progenitors activate and proliferate in response to acute antibody mediated thrombocytopenia (117). However, when ITP is extended to two weeks, LT-HSC functionality was impaired during serial transplants. This discrepancy with our results is potentially due to differences in experimental setup. Ramasz et al (117) performed a primary competitive transplant using 300 LT-HSCs from mice with sustained ITP and 5×10^5 BM competitor cells from controls. After 16 weeks, they transplanted 300 ITP LT-HSCs from primary recipients into secondary recipients alongside 5×10^5 fresh BM competitor cells. The decreased contribution to peripheral blood reconstitution after each round of competitive transplant can be explained by our observation that the traditional LT-HSC phenotype is contaminated with a larger proportion of non-HSCs in ITP. However, when analysing the LT-HSC pool as a whole (e.g. using unbiased whole BM transplants), LT-HSC functionality is increased and preserves haematopoiesis long-term.

The ability of LT-HSCs to maintain functionality in conditions of haematological stress is essential for the preservation of haematopoiesis long term. When LT-HSCs are unable to meet the increased demand such as in chronic infection (96, 118) or the development of malignancy (94, 380), LT-HSCs exit quiescence and pancytopenia may arise. The increase in the functional LT-HSC pool in ITP therefore presents an intriguing dichotomy and we studied the HSC BM microenvironment to determine whether beneficial changes in cell extrinsic factors may occur. ITP progression was associated with vasodilation and angiogenesis as well as LepR⁺ BMSC expansion. The BMSCs maintained their classically defined perivascular location and therefore close/adjacent proximity to LT-HSCs (45, 88, 268) and their expansion was associated with an increase in CXCL12, which has a crucial role in maintaining LT-HSC function, including retention in the BM (45-47), repopulating activity (48) and quiescence (49, 85). Furthermore, this increase in CXCL12 was BM specific and was expected to be primarily derived from LepR⁺ BMSCs (45, 268), which I confirmed by confocal microscopy. Intriguingly, LepR⁺ BMSC number reverted back to levels seen in control mice after recovery from ITP, suggesting that thrombocytopenia may indirectly feedback to increase LT-HSC support during ITP progression.

The BM is the primary and preferential site for steady state haematopoiesis in healthy adults, which is maintained by complex and multifactorial interactions from many different niche components (2). Extramedullary haematopoiesis during infection or malignancy is often associated with loss of BM CXCL12 signalling (94-98). Our observation that ITP progression coincides with a transient increase in BM CXCL12 expression and associated increase in LT-HSC BM homing may be an important mechanism to maintain LT-HSC functionality in conditions of elevated differentiation pressure, which is essential for maintenance of homeostasis long-term. As BM sinusoids are the preferred sites of progenitor homing due to low blood flow velocities and low wall shear rates (390), it is possible that the increase in average vessel area in ITP would further reduce blood flow velocity and aid progenitor homing. Additionally, a transient increase in BM CXCL12 expression may further act to increase thrombopoiesis in ITP (335). As discussed, it has been shown that progenitors activate and proliferate in response to acute antibody mediated thrombocytopenia, driven by the relocalisation of SCF from the cytoplasm to the cell membrane of Mks (117). Interestingly, this was not accompanied by an increase in total BM *Kitl* expression, suggesting that the proliferative effect on progenitors was post-transcriptionally regulated. In addition to its proliferative effects, SCF is essential for LT-HSC function (60, 72). We have not assessed membrane bound SCF expression in our model of sustained ITP, which may present a further mechanism acting to preserve LT-HSC functionality during sustained ITP.

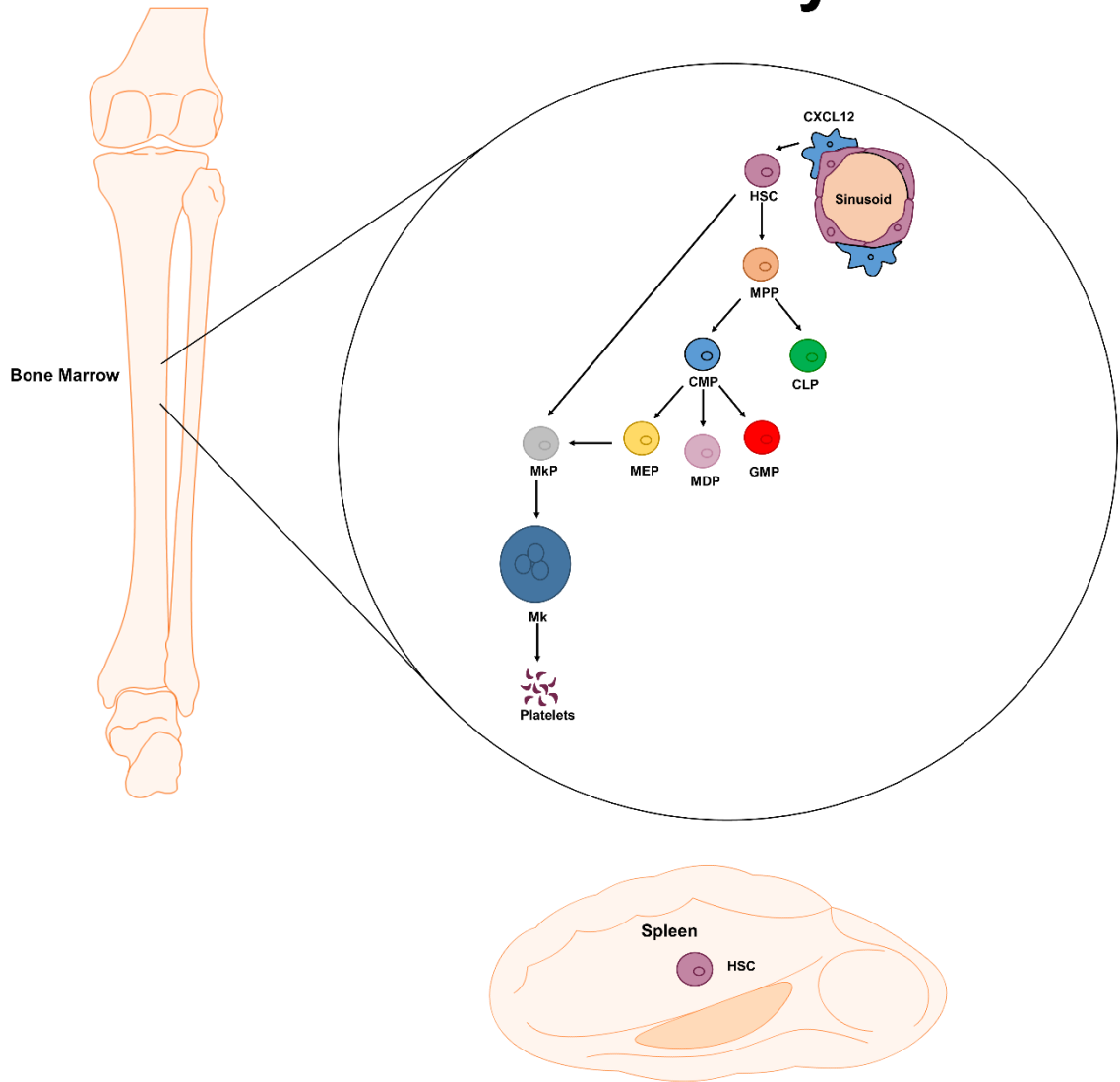
Progenitor expansion was also observed in BM aspirates from ITP patients which was proportional to ITP duration, suggesting that BM changes similar to those observed in the mouse model may exist in ITP patients. Interestingly, this trend was only observed in ITP patients not undergoing therapy at the time of collection, indicating that steroidal treatment may limit the emergency haematopoiesis observed in mice. This excludes the refractory patient (who was taking eltrombopag at the time of collection, which is an MPL agonist known to drive progenitor expansion (391, 392)). Whilst steroidal treatment may be an effective mechanism to limit platelet destruction, it may also have unintended consequence of disrupting emergency haematopoiesis in some patients, which our data suggests may be a compensatory mechanism to increase platelet counts. Further research is needed in this area, as disruption of emergency haematopoiesis may explain why some patients are refractory to steroids (200, 205, 393).

My research therefore points to a holistic transformation of the BM microenvironment to create a nurturing environment maximising megakaryopoiesis whilst minimising LT-HSC exhaustion (Figure 6.18). As BM examination is not routinely performed for chronic ITP

patients (200), it is possible therefore that significant changes in BM architecture go undetected which require further investigation.

A

Healthy



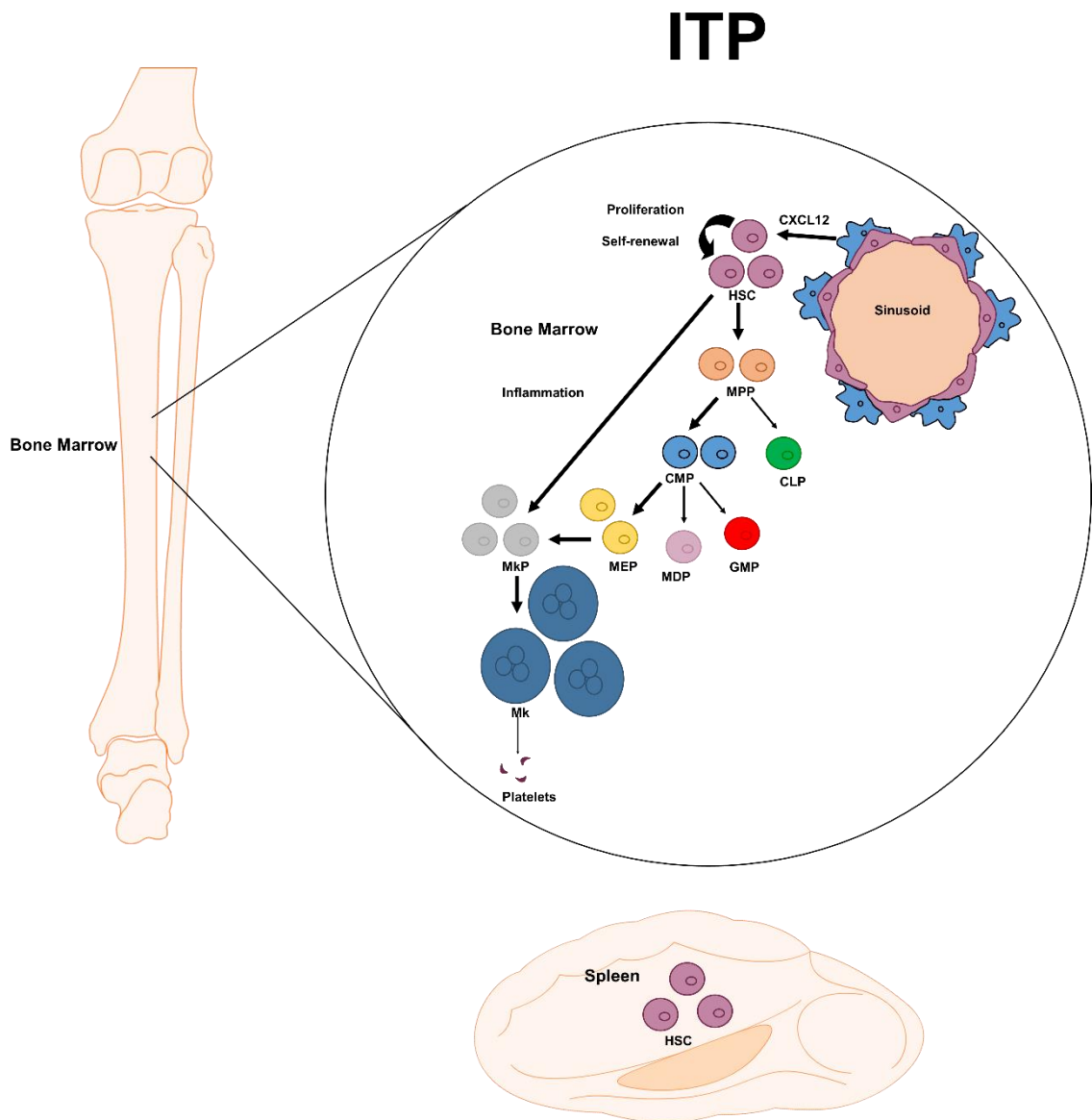
B

Figure 6.18. Sustained ITP causes expansion of HSCs in the BM and spleen. A) Healthy haematopoiesis. **B)** Haematopoiesis in ITP. ITP progression is associated with BM progenitor expansion, and local inflammation which may drive emergency megakaryopoiesis. The HSC pool is maintained through remodelling of the BM niche, such as increased CXCL12 production which is associated with a transient expansion in LepR⁺ BMSCs. Extramedullary haematopoiesis in the spleen also contributes to an increased HSC pool, the role of which is unclear.

7 General discussion

The initial aim of this thesis was to characterise the sources and roles of TPO in HSC self-renewal, whilst subsequent aims were to characterise the immune and haematopoietic system using a murine model of sustained ITP.

Using murine BM as a model, I concluded that an antibody previously used to show that Mks are major sources of TPO in the murine BM is non-specific (163). This was also indicated by the observation that Mks do not transcribe *Thpo*, a finding shared by Decker and colleagues (147). In contrast, LepR⁺ and *Cxcl12*-DsRed^{high} BMSCs express *Thpo* at 0.29 and 0.25 fold WT liver levels respectively, which was remarkably similar to the 0.30 fold level shown to be expressed by LepR⁺ BMSCs (147). Recent evidence at the single cell level indicates that LepR⁺/*Cxcl12*-DsRed^{high} BMSCs are heterogeneous (81), which agrees with my finding using human BMSCs of overlapping phenotype suggesting that not all LepR⁺/*Cxcl12*-DsRed^{high} BMSCs express *Thpo*. Although *Thpo* is transcribed in the murine BM, it is not translated under steady state or stress conditions, and TPO utilised in the BM is produced distally in the liver (147). My own study indicated that haematopoietic stress driven by acute thrombocytopenia does not influence *Thpo* expression by LepR⁺ or *Cxcl12*-DsRed^{high} BMSCs in mice, although this may occur in humans during chronic ITP or other conditions of haematopoietic stress such as aplastic anaemia or irradiation (148, 149, 160).

To study the effects of sustained ITP on the immune and haematopoietic system, I developed a model of sustained ITP in mice by administering anti-CD41 antibody through intraperitoneal injections every 48 h for up to 4 weeks. Similarly to the model developed by Katsman and colleagues (299), maintenance of thrombocytopenia required dose escalation over time. However unlike WT mice, *Rag2*^{-/-} mice did not require an escalating dose to maintain severe ITP, which is suggestive of the development of antibodies against the injected rat anti-CD41 rather than compensatory thrombopoiesis (299). Mice with sustained ITP displayed characteristics of ITP: isolated thrombocytopenia associated with an increase in MPV (205, 312), mild splenomegaly (205, 309), normal levels of circulating TPO and normal or increased megakaryopoiesis (153, 302-304). In addition, some mice showed signs of spontaneous bleeding at post-mortem which is consistent with the development of bleeding events in ITP patients (201) and reports of spontaneous bleeding in a similar passive transfer ITP mouse model (294). Confirming previous reports, I demonstrated that the injected anti-CD41 antibody binds to BM BKs (294) and platelet recovery

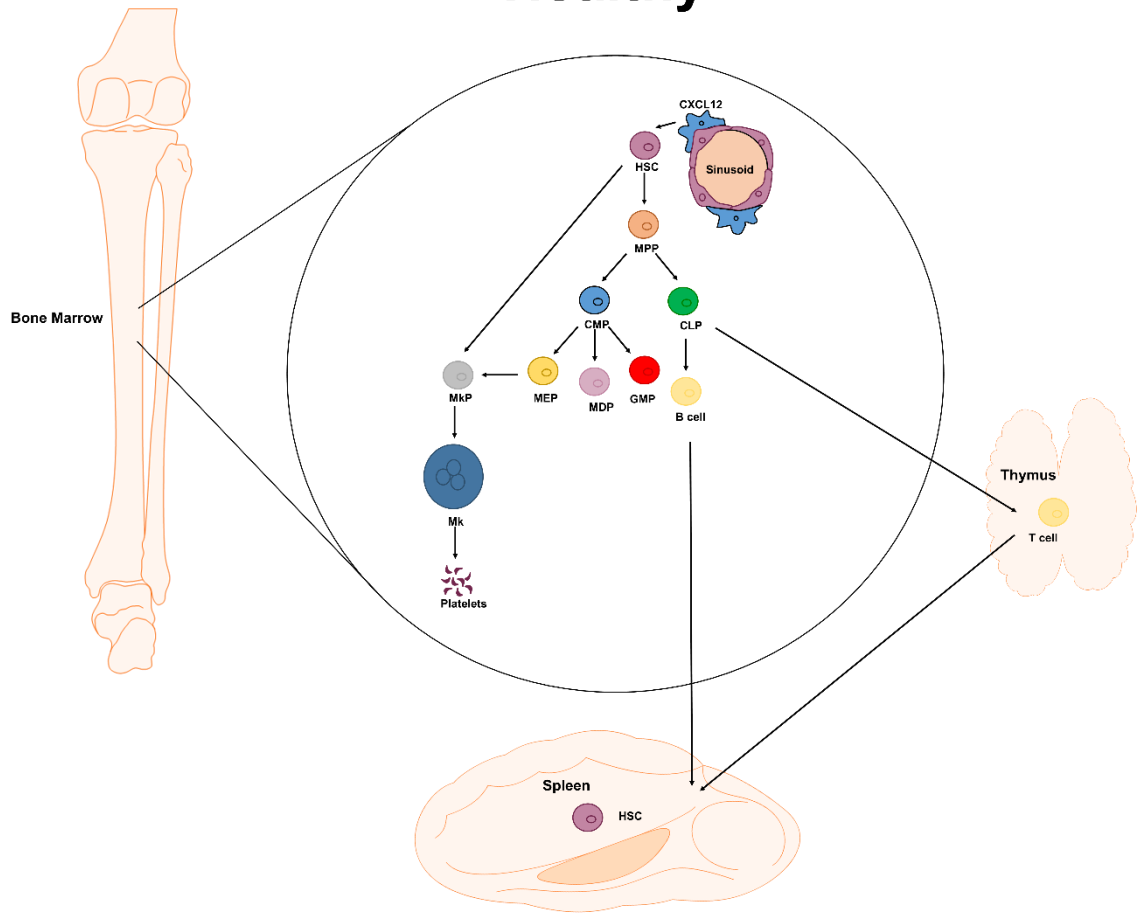
experiments suggested that sustained anti-CD41 treatment compromised thrombopoiesis (327, 328). Interestingly, confocal microscopy suggested that in addition to MKs, injected anti-CD41 binds to smaller nucleated cells (possibly progenitors) which may suppress megakaryopoiesis (218, 325, 326).

I used the model of sustained ITP to characterise the immune and haematopoietic system during ITP progression. Mice with sustained ITP were associated with monocyte and naïve T cell expansion, however analysed cells did not appear to be activated which was suggestive of a general increase in haematopoiesis rather than a coordinated immune response. In support of this, phenotypic BM LT-HSCs and committed progenitors were significantly expanded in ITP (Figure 7.1), whilst functional assays demonstrated an increased proliferation and self-renewal potential of LT-HSCs. This coincided with considerable BM remodelling and a transient increase in stromal derived CXCL12, which may combine to create a nurturing environment maximising megakaryopoiesis whilst minimising LT-HSC exhaustion. A preliminary experiment using ITP BM aspirates revealed that ITP patients similarly have HSC expansion associated with ITP progression, and importantly, treatment (such as steroidal treatment) may disrupt emergency haematopoiesis and therefore limit compensatory platelet production.

In agreement with a previous study (371), my results indicate that the passive transfer model of ITP does not mimic the human T cell response in ITP and therefore active models are better suited to study cell-mediated autoimmunity in ITP (308, 394). However, my results also indicate that sustained ITP may have a significant influence on haematopoiesis and the BM niche which requires further investigation. Additionally, my results adds further support to the emerging idea that the local BM response to thrombocytopenia may be driven independently of TPO, such as through local inflammation (116, 292, 298) or through distinct receptor kinases (117).

A

Healthy



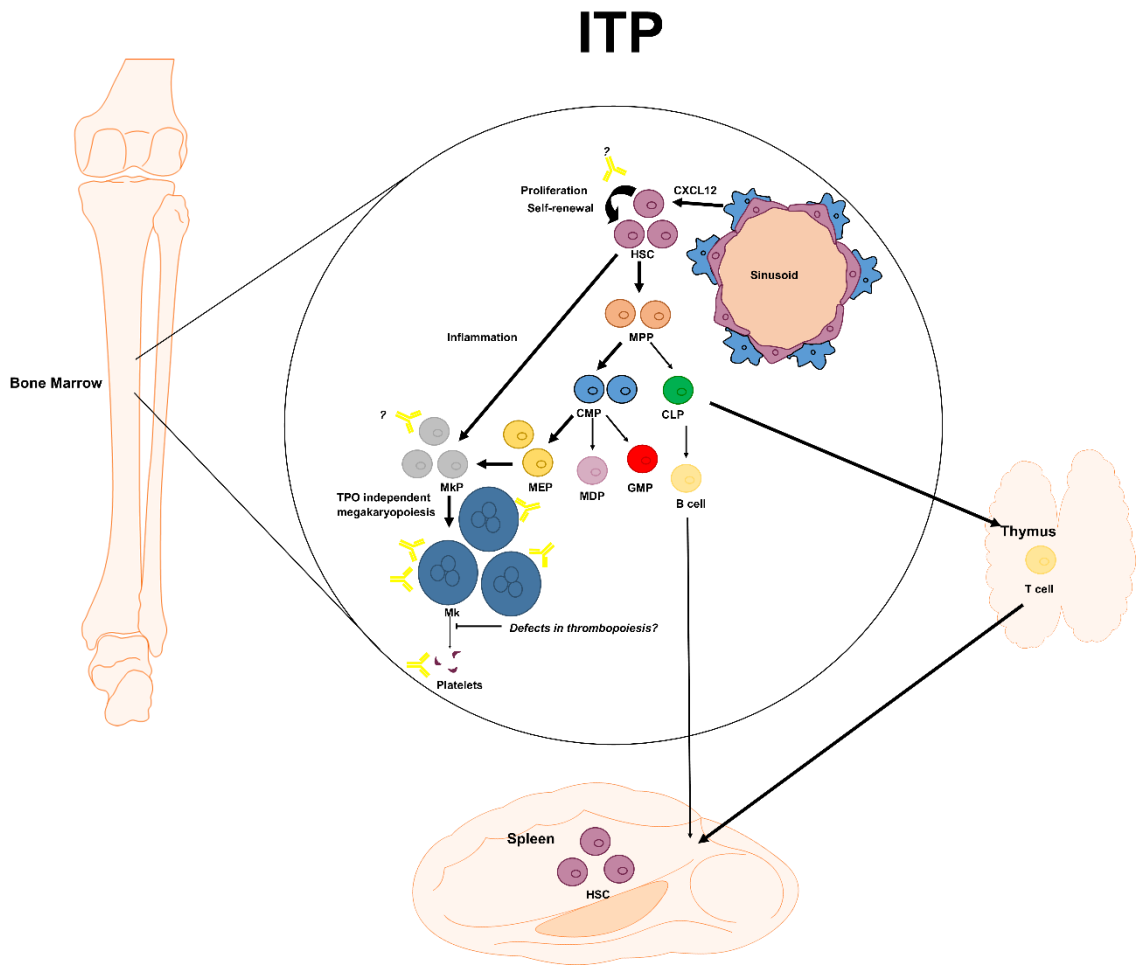
B

Figure 7.1. A summary of data using the murine model of sustained ITP. ITP is initiated and maintained by splenic macrophages which remove opsonised platelets from the circulation. ITP progression is associated with BM progenitor expansion, and local inflammation which may drive emergency megakaryopoiesis and T cell replenishment. The HSC pool is maintained through remodelling of the BM niche, such as increased CXCL12 production which is associated with a transient expansion in LepR⁺ BMSCs. Extramedullary haematopoiesis in the spleen also contributes to an increased HSC pool, the role of which is unclear.

7.1 The sustained model of immune thrombocytopenia

ITP is a complex, acquired autoimmune disease characterised by both the destruction of functionally normal platelets and reduced platelet production. Despite decades of research, the exact cause of ITP is still unknown. Both the loss of tolerance and exposure of platelet surface antigens are likely required for the development of ITP (201), which are not reflected in current models of ITP (395). Each model is able to recapitulate some but not all aspects of ITP progression, necessitating the need to carefully choose the appropriate model to best answer the experimental question.

Passive transfer models are the most widely used, involving the transfer of anti-platelet antiserum or platelet specific monoclonal antibodies into recipients, causing thrombocytopenia via antibody mediated platelet destruction. The passive model allows a degree of fine-tuning with respect to the severity or duration of the induced ITP depending on the frequency, quantity and type of antibody administered (395). Repeated administration maintains ITP, however can be significantly more laborious and costly depending on the desired duration. An alternative approach is via the continuous peritoneal infusion of antibody via an osmotic pump (396, 397), however platelet recovery can occur due to compensatory thrombopoiesis (299). In the model of sustained ITP reported in this thesis, compensatory thrombopoiesis was not observed, most likely as a higher starting anti-CD41 (MWReg30) dose was used. As such, while the ability to fine tune ITP could be seen as an advantage of the model, it is also its inherent disadvantage; the lack of a standardised approach with regard to frequency, quantity and type of antibody administration has led to conflicting results between different groups. For example, whilst MWReg30 injection into mice causes acute thrombocytopenia universally amongst research groups, this has been accompanied by different effects ranging from mild petechiae (294) to severe effects such as hypothermia and acute lung injury (398) or intestinal and subcutaneous haemorrhages with markedly decreased haematocrits (399), depending on the frequency and quantity of dose. In contrast, the mice used in this model of sustained ITP presented in this thesis had thrombocytopenia accompanied by mild subcutaneous bleeding in a minority of mice with no changes in haematocrits. Additionally, the model captures other clinical features of ITP progression including progressive megakaryopoiesis despite normal TPO levels and mild splenomegaly. Mice tolerated sustained anti-CD41 injections well, allowing its sustained application for prolonged periods of time and the subsequent study of ITP progression.

The active model of ITP involves the transfer of splenocytes from immunised mice against platelet CD61 or CD41 into SCID mice (developed in 2010 and 2019

respectively), resulting in severe and non-recoverable thrombocytopenia with bleeding diathesis in the intestines, lungs, subcutaneous tissues and brain (308, 394). Mice receiving CD61 reactive splenocytes had a more severe bleeding phenotype than mice receiving CD41 reactive splenocytes (80% bleeding mortality within 21 days in the former which prevented long term experiments) (308, 394). As CD61 can be expressed on ECs during proinflammatory conditions (400), it was thought that some off target effects on activated ECs may contribute to the severe bleeding mortality seldom seen in ITP patients (308). As such, the model using CD61 reactive splenocytes is inappropriate for long term studies such as those performed in this thesis. In isolation, the CD41 reactive model could be considered too severe to accurately represent ITP progression as 100% of mice exhibited severe bleeding events, with 33.3% exhibiting intracranial haemorrhage (ICH), far higher than that exhibited in ITP patients (non-ICH severe bleeding are recorded in 9.6% of adults with ITP, whilst ICH events are recorded in 1.4% of ITP patients) (394, 401, 402). However, experiments described in this thesis (which are independent of T cell autoimmunity) may be strengthened using this CD41 reactive model as CD8⁺ mediated effects on platelet destruction and platelet production are considerable in ITP (201).

7.2 Future research

The observations that HSCs and the BM niche respond to ITP progression by driving haematopoiesis are clinically important, however they are correlative and based on associations rather than mechanistic understanding. HSC expansion in response to inflammation and thrombocytopenia has been described previously (116, 117), however the suggestion that the BM niche remodels itself to resolve and/or minimise haematopoietic stress is a novel phenomenon and further research is needed to elucidate the molecular mechanisms behind these changes. An emerging hypothesis is that normal ageing of the haematopoietic system and chronic inflammation (coined 'Inflamm-Aging') may be mechanistically linked is based upon the observation that myeloid skewing and a proinflammatory BM microenvironment is a common hallmark of both states (135). Cytokines involved in the inflammatory response were highly upregulated in the BM of mice with sustained ITP, whilst the overall microenvironmental change in ITP (vasodilation of sinusoids and expansion of vascular niches) resembles the changes described during premature and physiological mouse aging, where a similar expansion of megakaryocytic cells and HSCs occurs (130). In that study of premature and physiological mouse aging, HSC expansion was associated with myeloid lineage bias and was driven by an age associated imbalance in $\beta 2/\beta 3$ signalling (130).

CBC analysis during ITP progression did not suggest reactive myelopoiesis during the course of the experiments as mature granulocytes were not expanded at the expense of lymphoid cells, whilst flow cytometry analysis of committed progenitors indicated that differentiation was skewed towards Mk and erythroid differentiation, rather than granulocyte differentiation. Furthermore, key drivers of reactive myelopoiesis such as BM IL-6, IL-6 and RANTES are decreased, rather than increased in the BM of mice with ITP (128, 130). However, this contrasts with the results of the pilot experiment described in Chapter 5, where analysis of the peripheral blood and BM by flow cytometry suggested that monocyte populations were expanded in ITP. Further experiments are needed to resolve this contradictory data, additionally using a 4 week time point as monocyte expansion may occur at earlier, at 2 weeks during an acute phase response, but not 4 weeks. Additionally, further experiments are needed to confirm that the expanded LT-HSCs in ITP remain balanced long term, rather than displaying lineage skewing with time. In this regard, experiments using the vWF reporter mouse that labels platelet/myeloid biased LT-HSCs would be particularly informative (30, 31). Platelet biased LT-HSCs reside at the apex of the haematopoietic stem cell hierarchy and are primed for short and long-term reconstitution of platelets, however they can also have a long term myeloid lineage bias and have potential for multipotency (30). An expansion in vWF⁺ platelet primed LT-HSCs indicate preferential (or exclusive) expansion of platelet biased HSCs in the short term, but in the long term may contain platelet/myeloid biased HSCs as well as platelet biased HSCs (30). Such long term myeloid skewing could increase susceptibility to infections and propagate immune dysregulation over time, both of which are associated with ITP (201, 403). In this instance, modulation of the BM microenvironment (such as through a β 3 RA) may be a viable therapeutic option (130).

Second-line therapies for ITP patients who are corticosteroid dependent or unresponsive to treatment include TPO-RAs such as eltrombopag or romiplostim to increase platelet production, however these are expensive therapies which require ongoing use (200, 404-407). Clinical use of rTPO has been discontinued due to the formation of antibodies to the molecule (408), however stimulating the endogenous production of TPO may have therapeutic potential. As discussed in Chapter 3, TPO is transcribed, but not translated by LepR⁺/Cxc12-DsRed^{high} BMSCs. Further research is needed to determine the mechanism behind this translational repression and whether the repression can be overcome by pharmaceutical intervention.

7.3 Concluding remarks

Over 40 years have passed since Schofield first hypothesised that HSCs were dependent upon the BM niche for maintenance of their stem like state. Since then, a plethora of experimental evidence has confirmed this to be the case, and key niche cells have been identified. However, the function and composition of niche cells exhibit plasticity during disease progression and the normal ageing process which causes disruption of normal haematopoiesis, leading to lineage skewing or one or more cytopenias. The BM niche can respond during haematopoietic stress to expand one or more progenitor subsets in an effort to maintain homeostasis, however this is usually coupled with functional exhaustion over time (116, 117). The research presented in this thesis using a murine model of sustained ITP is the first experimental evidence suggesting that the BM niche can adapt during disease progression to both expand HSC number and to maintain HSC functionality during haematopoietic stress. Further research is needed to explore the exact mechanism behind these, as well as whether this is observed in ITP patients as modulation of the BM niche could hold therapeutic promise.

8 Abbreviations

5-FU	5-fluorouracil
AF	Alexa Fluor
AMR	Ashwell-Morell receptor
ANOVA	Analysis of variance
APC	Antigen presenting cell
APC	Allophycocyanin
AR	Adrenergic
ASH	American Society of Hematology
BHK	Baby hamster kidney fibroblasts
BM	Bone marrow
BMSC	Bone marrow stromal cell
BV	Brilliant violet
CBC	Complete blood count
CD	Cluster of differentiation
cDNA	Complementary DNA
CFU-S	Spleen colony-forming cells
CLP	Common lymphoid progenitor
CMP	Common myeloid progenitor
CXCL12	C-X-C motif chemokine ligand 12
CXCR4	C-X-C-chemokine receptor 4
Cy	Cyanine
DAPI	4',6-diamidino-2-phenylindole
DC	Dendritic cell
DMEM	Dulbecco's Modified Eagle Medium
DNA	Deoxyribonucleic acid
EC	Endothelial cell
EDTA	Ethylenediaminetetraacetic acid
EMH	Extramedullary haematopoiesis
EPCR	Endothelial protein C receptor
EPO	Erythropoietin
FACS	Fluorescence-activated cell sorting
FBS	Fetal Bovine Serum
FcyR	Fcy-receptor
FITC	Fluorescein
G-CSF	Granulocyte colony-stimulating factor
gDNA	Genomic DNA
GFP	Green fluorescence protein
GMP	Common granulocyte/monocyte progenitor
GP	Platelet glycoprotein
H&E	Haematoxylin and eosin
HSC	Haematopoietic stem cell
HSPC	Haematopoietic stem and progenitor cell
hTERT	Human telomerase reverse transcriptase
ICH	Intracranial haemorrhage
IFN	Interferon
IGFBP-3	Insulin-like growth factor-binding protein 3
IgG	Immunoglobulin G
IL	Interleukin
ITP	Immune thrombocytopenia
IVIG	Intravenous immunoglobulin
LepR	Leptin receptor
Lin	Lineage
LSK	Lineage ⁻ Sca-1 ⁺ c-kit ⁺
LSM	Laser scanning microscope

LT-HSC	Long term haematopoietic stem cell
MACS	Magnetic-activated cell sorting
MAPK	Mitogen-activated protein kinase
MEP	Common erythroid/megakaryocyte progenitor
MkP	Megakaryocyte progenitor
MMP2	Matrix metalloproteinase-2
MPL	Myeloproliferative leukemia virus
MPP	Multipotent progenitor cell
mRNA	Messenger RNA
neo^r	neomycin-resistance gene
NC3R	National Centre for the Replacement Refinement and Reduction of Animals in Research
NK	Natural killer
NOD	Non-obese diabetic
NSG	NOD. <i>scid</i> . <i>Il2Ryc^{null}</i>
OCT	Optimal cutting temperature
PBS	Phosphate-buffered saline
PBS-T	Tween-20/PBS
PD-1	Programmed cell death protein 1
PE	Phycoerythrin
PFA	Paraformaldehyde
qPCR	Real-time polymerase chain reaction
RNA	Ribonucleic acid
RANTES	Regulated on activation, normal T cell expressed and secreted
RTE	Recent thymic emigrants
Sca-1	Stem cell antigen-1
SCF	Stem cell factor
SCID	Severe combined immunodeficiency
ST-HSC	Short term haematopoietic stem cell
STRING	Search Tool for the Retrieval of Interacting Genes/Proteins
TAE	Agarose/tris-acetate-EDTA
T_{CM}	Central memory T cell
TCR	T cell receptor
T_{EM}	Effector memory T cell
Tfh	T follicular helper cell
Th	T helper cell
TLR	Toll-like receptors
TNFα	Tumour necrosis factor α
TPO	Thrombopoietin
TPO-RA	Thrombopoietin receptor agonist
Treg	Regulatory T cell
VEGF	Vascular endothelial growth factor
vWF	von Willebrand factor
WISP1	Wnt1-inducible signaling pathway protein-1

9 References

1. Goodman JW, Smith LH. Erythrocyte life span in normal mice and in radiation bone marrow chimeras. *Am J Physiol.* 1961;200:764-70.
2. Crane GM, Jeffery E, Morrison SJ. Adult haematopoietic stem cell niches. *Nat Rev Immunol.* 2017;17(9):573-90.
3. Oguro H, Ding L, Morrison SJ. SLAM Family Markers Resolve Functionally Distinct Subpopulations of Hematopoietic Stem Cells and Multipotent Progenitors. *Cell Stem Cell.* 2013;13(1):102-16.
4. Pietras EM, Reynaud D, Kang YA, Carlin D, Calero-Nieto FJ, Leavitt AD, et al. Functionally Distinct Subsets of Lineage-Biased Multipotent Progenitors Control Blood Production in Normal and Regenerative Conditions (vol 17, pg 35, 2015). *Cell Stem Cell.* 2015;17(2):246-.
5. Pinho S, Frenette PS. Haematopoietic stem cell activity and interactions with the niche. *Nat Rev Mol Cell Bio.* 2019;20(5):303-20.
6. Till JE, McCulloch EA. A Direct Measurement of the Radiation Sensitivity of Normal Mouse Bone Marrow Cells. *Radiat Res.* 1961;175(2):145-9.
7. Becker AJ, McCulloch EA, Till JE. CYTOLOGICAL DEMONSTRATION OF THE CLONAL NATURE OF SPLEEN COLONIES DERIVED FROM TRANSPLANTED MOUSE MARROW CELLS *Nature.* 1963;197(11):452-4.
8. Siminovitch L, McCulloch EA, Till JE. Distribution of Colony-Forming Cells among Spleen Colonies. *J Cell Compar Physl.* 1963;62(3):327-&.
9. Hodgson GS, Bradley TR. Properties of haematopoietic stem cells surviving 5-fluorouracil treatment: evidence for a pre-CFU-S cell? *Nature.* 1979;281(5730):381-2.
10. Down JD, Vanos R, Ploemacher RE. Radiation Sensitivity and Repair of Long-Term Repopulating Bone-Marrow Stem-Cells. *Exp Hematol.* 1991;19(6):474-.
11. Challen GA, Boles N, Lin KK, Goodell MA. Mouse hematopoietic stem cell identification and analysis. *Cytometry A.* 2009;75(1):14-24.
12. Morrison SJ, Weissman IL. The Long-Term Repopulating Subset of Hematopoietic Stem-Cells Is Deterministic and Isolatable by Phenotype. *Immunity.* 1994;1(8):661-73.
13. Osawa M, Hanada K, Hamada H, Nakauchi H. Long-term lymphohematopoietic reconstitution by a single CD34-low/negative hematopoietic stem cell. *Science.* 1996;273(5272):242-5.
14. Goodell MA, Brose K, Paradis G, Conner AS, Mulligan RC. Isolation and functional properties of murine hematopoietic stem cells that are replicating in vivo. *J Exp Med.* 1996;183(4):1797-806.
15. Trevisan M, Yan XQ, Iscove NN. Cycle initiation and colony formation in culture by murine marrow cells with long-term reconstituting potential in vivo. *Blood.* 1996;88(11):4149-58.
16. Uchida N, Dykstra B, Lyons KJ, F.Y. L, Eaves CJ. Different in vivo repopulating activities of purified hematopoietic stem cells before and after being stimulated to divide in vitro with the same kinetics. *Exp Hematol.* 2003;31(12):1338-47.
17. Matsuzaki Y, Kinjo K, Mulligan RC, Okano H. Unexpectedly efficient homing capacity of purified murine hematopoietic stem cells. *Immunity.* 2004;20(1):87-93.
18. Kiel MJ, Yilmaz ÖH, Iwashita T, Yilmaz OH, Terhorst C, Morrison SJ. SLAM Family Receptors Distinguish Hematopoietic Stem and Progenitor Cells and Reveal Endothelial Niches for Stem Cells. *Cell.* 2005;121(7):1109-21.
19. Balazs AB, Fabian AJ, Esmen CT, Mulligan RC. Endothelial protein C receptor (CD201) explicitly identifies hematopoietic stem cells in murine bone marrow. *Blood.* 2006;107(6):2317-21.

20. Kent DG, Copley MR, Benz C, Wohrer S, Dykstra BJ, Ma E, et al. Prospective isolation and molecular characterization of hematopoietic stem cells with durable self-renewal potential. *Blood*. 2009;113(25):6342-50.
21. Seita J, Weissman IL. Hematopoietic stem cell: self-renewal versus differentiation. *Wires Syst Biol Med*. 2010;2(6):640-53.
22. Ho MS, Medcalf RL, Livesey SA, Traianedes K. The dynamics of adult haematopoiesis in the bone and bone marrow environment. *Br J Haematol*. 2015;170(4):472-86.
23. Dykstra B, Kent D, Bowie M, McCaffrey L, Hamilton M, Lyons K, et al. Long-term propagation of distinct hematopoietic differentiation programs in vivo. *Cell Stem Cell*. 2007;1(2):218-29.
24. Muller-Sieburg CE, Cho RH, Karlsson L, Huang JF, Sieburg HB. Myeloid-biased hematopoietic stem cells have extensive self-renewal capacity but generate diminished lymphoid progeny with impaired IL-7 responsiveness. *Blood*. 2004;103(11):4111-8.
25. Perie L, Duffy KR, Kok L, de Boer RJ, Schumacher TN. The Branching Point in Erythro-Myeloid Differentiation. *Cell*. 2015;163(7):1655-62.
26. Paul F, Arkin Y, Giladi A, Jaitin DA, Kenigsberg E, Keren-Shaul H, et al. Transcriptional Heterogeneity and Lineage Commitment in Myeloid Progenitors. *Cell*. 2016;164(1-2):325.
27. Velten L, Haas SF, Raffel S, Blaszkiewicz S, Islam S, Hennig BP, et al. Human haematopoietic stem cell lineage commitment is a continuous process. *Nat Cell Biol*. 2017;19(4):271-+.
28. Olsson A, Venkatasubramanian M, Chaudhri VK, Aronow BJ, Salomonis N, Singh H, et al. Single-cell analysis of mixed-lineage states leading to a binary cell fate choice. *Nature*. 2016;537(7622):698-+.
29. Notta F, Zandi S, Takayama N, Dobson S, Gan OI, Wilson G, et al. Distinct routes of lineage development reshape the human blood hierarchy across ontogeny. *Science*. 2016;351(6269):aab2116.
30. Sanjuan-Pla A, Macaulay IC, Jensen CT, Woll PS, Luis TC, Mead A, et al. Platelet-biased stem cells reside at the apex of the haematopoietic stem-cell hierarchy. *Nature*. 2013;502(7470):232-+.
31. Carrelha J, Meng Y, Kettle LM, Luis TC, Norfo R, Alcolea V, et al. Hierarchically related lineage-restricted fates of multipotent haematopoietic stem cells. *Nature*. 2018;554(7690):106-11.
32. Rodriguez-Fraticelli AE, Wolock SL, Weinreb CS, Panero R, Patel SH, Jankovic M, et al. Clonal analysis of lineage fate in native haematopoiesis. *Nature*. 2018;553(7687):212-6.
33. Miyake T, Kung CK, Goldwasser E. Purification of human erythropoietin. *J Biol Chem*. 1977;252(15):5558-64.
34. Pluznik DH, Sachs L. The induction of clones of normal mast cells by a substance from conditioned medium. *Exp Cell Res*. 1966;43(3):553-63.
35. Zeigler FC, de Sauvage F, Widmer HR, Keller GA, Donahue C, Schreiber RD, et al. In vitro megakaryocytopoietic and thrombopoietic activity of c-mpl ligand (TPO) on purified murine hematopoietic stem cells. *Blood*. 1994;84(12):4045-52.
36. Kaushansky K, Broudy VC, Lin N, Jorgensen MJ, McCarty J, Fox N, et al. Thrombopoietin, the Mpl Ligand, Is Essential for Full Megakaryocyte Development. *P Natl Acad Sci USA*. 1995;92(8):3234-8.
37. Metcalf D. Hematopoietic cytokines. *Blood*. 2008;111(2):485-91.
38. Socolovsky M, Dusanter-Fourt I, Lodish HF. The prolactin receptor and severely truncated erythropoietin receptors support differentiation of erythroid progenitors. *J Biol Chem*. 1997;272(22):14009-12.
39. Stoffel R, Ziegler S, Ghilardi N, Ledermann B, de Sauvage FJ, Skoda RC. Permissive role of thrombopoietin and granulocyte colony-stimulating factor receptors in hematopoietic cell fate decisions in vivo. *Proc Natl Acad Sci U S A*. 1999;96(2):698-702.

40. Evans CA, Pierce A, Winter SA, Spooncer E, Heyworth CM, Whetton AD. Activation of granulocyte-macrophage colony-stimulating factor and interleukin-3 receptor subunits in a multipotential hematopoietic progenitor cell line leads to differential effects on development. *Blood*. 1999;94(5):1504-14.
41. Tsapogas P, Swee LK, Nusser A, Nuber N, Kreuzaler M, Capoferri G, et al. In vivo evidence for an instructive role of fms-like tyrosine kinase-3 (FLT3) ligand in hematopoietic development. *Haematologica*. 2014;99(4):638-46.
42. Wilkinson AC, Ishida R, Kikuchi M, Sudo K, Morita M, Crisostomo RV, et al. Long-term ex vivo haematopoietic-stem-cell expansion allows nonconditioned transplantation. *Nature*. 2019;571(7766).
43. Cui L, Moraga I, Lerbs T, Van Neste C, Wilmes S, Tsutsumi N, et al. Tuning MPL signaling to influence hematopoietic stem cell differentiation and inhibit essential thrombocythemia progenitors. *Proc Natl Acad Sci U S A*. 2021;118(2).
44. Zsebo KM, Wypych J, McNiece IK, Lu HS, Smith KA, Karkare SB, et al. Identification, purification, and biological characterization of hematopoietic stem cell factor from buffalo rat liver--conditioned medium. *Cell*. 1990;63(1):195-201.
45. Ding L, Morrison SJ. Haematopoietic stem cells and early lymphoid progenitors occupy distinct bone marrow niches. *Nature*. 2013;495(7440):231-5.
46. Peled A, Petit I, Kollet O, Magid M, Ponomaryov T, Byk T, et al. Dependence of human stem cell engraftment and repopulation of NOD/SCID mice on CXCR4. *Science*. 1999;283(5403):845-8.
47. Bonig H, Priestley GV, Nilsson LM, Jiang Y, Papayannopoulou T. PTX-sensitive signals in bone marrow homing of fetal and adult hematopoietic progenitor cells. *Blood*. 2004;104(8):2299-306.
48. Tzeng YS, Li H, Kang YJ, Chen W, Cheng W, Lai DM. Loss of Cxcl12/Sdf-1 in adult mice decreases the quiescent state of hematopoietic stem/progenitor cells and alters the pattern of hematopoietic regeneration after myelosuppression. *Blood*. 2011;117(2):429-39.
49. Nie Y, Han Y-C, Zou Y-R. CXCR4 is required for the quiescence of primitive hematopoietic cells. *J Exp Med*. 2008;205(4):777-83.
50. Williams DE, Eisenman J, Baird A, Rauch C, Van Ness K, March CJ, et al. Identification of a ligand for the c-kit proto-oncogene. *Cell*. 1990;63(1):167-74.
51. Flanagan JG, Leder P. The kit ligand: a cell surface molecule altered in steel mutant fibroblasts. *Cell*. 1990;63(1):185-94.
52. Zsebo KM, Williams DA, Geissler EN, Broudy VC, Martin FH, Atkins HL, et al. Stem cell factor is encoded at the Sl locus of the mouse and is the ligand for the c-kit tyrosine kinase receptor. *Cell*. 1990;63(1):213-24.
53. Anderson DM, Lyman SD, Baird A, Wignall JM, Eisenman J, Rauch C, et al. Molecular-Cloning of Mast-Cell Growth-Factor, a Hematopoietin That Is Active in Both Membrane-Bound and Soluble Forms. *Cell*. 1990;63(1):235-43.
54. Kuter DJ, Beeler DL, Rosenberg RD. The Purification of Megapoietin - a Physiological Regulator of Megakaryocyte Growth and Platelet Production. *P Natl Acad Sci USA*. 1994;91(23):11104-8.
55. Lok S, Kaushansky K, Holly RD, Kuijper JL, Loftonday CE, Oort PJ, et al. Cloning and Expression of Murine Thrombopoietin Cdna and Stimulation of Platelet Production in-Vivo. *Nature*. 1994;369(6481):565-8.
56. Kaushansky K, Lok S, Holly RD, Broudy VC, Lin N, Bailey MC, et al. Promotion of Megakaryocyte Progenitor Expansion and Differentiation by the C-Mpl Ligand Thrombopoietin. *Nature*. 1994;369(6481):568-71.
57. de Sauvage FJ, Hass PE, Spencer SD, Malloy BE, Gurney AL, Spencer SA, et al. Stimulation of Megakaryocytopoiesis and Thrombopoiesis by the C-Mpl Ligand. *Nature*. 1994;369(6481):533-8.
58. Bartley TD, Bogenberger J, Hunt P, Li YS, Lu HS, Martin F, et al. Identification and Cloning of a Megakaryocyte Growth and Development Factor That Is a Ligand for the Cytokine Receptor Mpl. *Cell*. 1994;77(7):1117-24.

59. Zou YR, Kottmann AH, Kuroda M, Taniuchi I, Littman DR. Function of the chemokine receptor CXCR4 in haematopoiesis and in cerebellar development. *Nature*. 1998;393(6685):595-9.
60. Barker JE. Sl/Slid hematopoietic progenitors are deficient in situ. *Exp Hematol*. 1994;22(2):174-7.
61. Dexter TM, Allen TD, Lajtha LG. Conditions controlling the proliferation of haemopoietic stem cells in vitro. *J Cell Physiol*. 1977;91(3):335-44.
62. Lord BI, Testa NG, Hendry JH. The relative spatial distributions of CFUs and CFUc in the normal mouse femur. *Blood*. 1975;46(1):65-72.
63. Schofield R. The relationship between the spleen colony-forming cell and the haemopoietic stem cell. *Blood Cells*. 1978;1-2(4):7-25.
64. Calvi LM, Adams GB, Weibrecht KW, Weber JM, Olson DP, Knight MC, et al. Osteoblastic cells regulate the haematopoietic stem cell niche. *Nature*. 2003;425(6960):841-6.
65. Zhang J, Niu C, Ye L, Huang H, He X, Tong WG, et al. Identification of the haematopoietic stem cell niche and control of the niche size. *Nature*. 2003;425(6960):836-41.
66. Kiel MJ, Radice GL, Morrison SJ. Lack of evidence that hematopoietic stem cells depend on N-cadherin-mediated adhesion to osteoblasts for their maintenance. *Cell Stem Cell*. 2007;1(2):204-17.
67. Nombela-Arrieta C, Pivarnik G, Winkel B, Canty KJ, Harley B, Mahoney JE, et al. Quantitative imaging of haematopoietic stem and progenitor cell localization and hypoxic status in the bone marrow microenvironment. *Nat Cell Biol*. 2013;15(5):533-43.
68. Chen JY, Miyanishi M, Wang SK, Yamazaki S, Sinha R, Kao KS, et al. Hoxb5 marks long-term haematopoietic stem cells and reveals a homogenous perivascular niche. *Nature*. 2016;530(7589):223-7.
69. Acar M, Kocherlakota KS, Murphy MM, Peyer JG, Oguro H, Inra CN, et al. Deep imaging of bone marrow shows non-dividing stem cells are mainly perisinusoidal. *Nature*. 2015;526(7571):126-30.
70. Kokkaliaris K, Kunz L, Cabezas-Wallscheid N, Christodoulou C, Renders S, Camargo F, et al. Adult blood stem cell localization reflects the abundance of reported bone marrow niche cell types and their combinations *Blood*. 2020;136(20):2296-307.
71. Kiel MJ, Morrison SJ. Uncertainty in the niches that maintain haematopoietic stem cells. *Nat Rev Immunol*. 2008;8(4):290-301.
72. Ding L, Saunders TL, Enikolopov G, Morrison SJ. Endothelial and perivascular cells maintain haematopoietic stem cells. *Nature*. 2012;481(7382):457-U65.
73. Baryawno N, Przybylski D, Kowalczyk MS, Kfoury Y, Severe N, Gustafsson K, et al. A Cellular Taxonomy of the Bone Marrow Stroma in Homeostasis and Leukemia. *Cell*. 2019;177(7):1915-32 e16.
74. Lo Celso C, Fleming HE, Wu JWW, Zhao CX, Miake-Lye S, Fujisaki J, et al. Live-animal tracking of individual haematopoietic stem/progenitor cells in their niche. *Nature*. 2009;457(7225):92-U6.
75. Hooper AT, Butler JM, Nolan DJ, Kranz A, Iida K, Kobayashi M, et al. Engraftment and Reconstitution of Hematopoiesis Is Dependent on VEGFR2-Mediated Regeneration of Sinusoidal Endothelial Cells. *Cell Stem Cell*. 2009;4(3):263-74.
76. Morrison SJ, Scadden DT. The bone marrow niche for haematopoietic stem cells. *Nature*. 2014;505(7483):327-34.
77. Zhu J, Garrett R, Jung Y, Zhang Y, Kirn N, Wang J, et al. Osteoblasts support B-lymphocyte commitment and differentiation from hematopoietic stem cells. *Blood*. 2007;109(9):3706-12.
78. Baryawno N, Severe N, Scadden DT. Hematopoiesis: Reconciling Historic Controversies about the Niche. *Cell Stem Cell*. 2017;20(5):590-2.
79. Kunisaki Y, Bruns I, Scheiermann C, Ahmed J, Pinho S, Zhang D, et al. Arteriolar niches maintain haematopoietic stem cell quiescence. *Nature*. 2013;502(7473):637-43.

80. Xu CL, Gao X, Wei QZ, Nakahara F, Zimmerman SE, Mar J, et al. Stem cell factor is selectively secreted by arterial endothelial cells in bone marrow. *Nature Communications*. 2018;9.
81. Baccin C, Al-Sabah J, Velten L, Helbling PM, Grunschlager F, Hernandez-Malmierca P, et al. Combined single-cell and spatial transcriptomics reveal the molecular, cellular and spatial bone marrow niche organization. *Nat Cell Biol*. 2020;22(1):38-+.
82. Sugiyama T, Kohara H, Noda M, Nagasawa T. Maintenance of the hematopoietic stem cell pool by CXCL12-CXCR4 chemokine signaling in bone marrow stromal cell niches. *Immunity*. 2006;25(6):977-88.
83. Peled A, Kollet O, Ponomaryov T, Petit I, Franitza S, Grabovsky V, et al. The chemokine SDF-1 activates the integrins LFA-1, VLA-4, and VLA-5 on immature human CD34(+) cells: role in transendothelial/stromal migration and engraftment of NOD/SCID mice. *Blood*. 2000;95(11):3289-96.
84. Barker JE. Early transplantation to a normal microenvironment prevents the development of Steel hematopoietic stem cell defects. *Exp Hematol*. 1997;25(6):542-7.
85. Greenbaum A, Hsu YMS, Day RB, Schuettpelez LG, Christopher MJ, Borgerding JN, et al. CXCL12 in early mesenchymal progenitors is required for haematopoietic stem-cell maintenance. *Nature*. 2013;495(7440):227-30.
86. Tikhonova AN, Dolgalev I, Hu H, Sivaraj KK, Hoxha E, Cuesta-Dominguez A, et al. The bone marrow microenvironment at single-cell resolution. *Nature*. 2019;569(7755):222-+.
87. Haas S. Hematopoietic Stem Cells in Health and Disease—Insights from Single-Cell Multi-omic Approaches. *Current Stem Cell Reports*. 2020;6(3):67-76.
88. Asada N, Kunisaki Y, Pierce H, Wang Z, Fernandez NF, Birbrair A, et al. Differential cytokine contributions of perivascular haematopoietic stem cell niches. *Nat Cell Biol*. 2017;19(3):214-23.
89. Mendez-Ferrer S, Michurina TV, Ferraro F, Mazloom AR, Macarthur BD, Lira SA, et al. Mesenchymal and haematopoietic stem cells form a unique bone marrow niche. *Nature*. 2010;466(7308):829-34.
90. Mendez-Ferrer S, Lucas D, Battista M, Frenette PS. Haematopoietic stem cell release is regulated by circadian oscillations. *Nature*. 2008;452(7186):442-7.
91. O'Malley DP. Benign extramedullary myeloid proliferations. *Modern Pathol*. 2007;20(4):405-15.
92. Morita Y, Iseki A, Okamura S, Suzuki S, Nakauchi H, Ema H. Functional characterization of hematopoietic stem cells in the spleen. *Exp Hematol*. 2011;39(3):351-9 e3.
93. Inra CN, Zhou BO, Acar M, Murphy MM, Richardson J, Zhao ZY, et al. A perisinusoidal niche for extramedullary haematopoiesis in the spleen. *Nature*. 2015;527(7579):466-+.
94. Schepers K, Pietras E, Reynaud D, Flach J, Binnewies M, Garg T, et al. Myeloproliferative neoplasia remodels the endosteal bone marrow niche into a self-reinforcing leukemic niche. *Cell Stem Cell*. 2013;13(3):285-99.
95. Decker M, Martinez-Morentin L, Wang G, Lee Y, Liu Q, Leslie J, et al. Leptin-receptor-expressing bone marrow stromal cells are myofibroblasts in primary myelofibrosis. *Nat Cell Biol*. 2017;19(6):677-88.
96. Preham O, Pinho FA, Pinto AI, Rani GF, Brown N, Hitchcock IS, et al. CD4+ T Cells Alter the Stromal Microenvironment and Repress Medullary Erythropoiesis in Murine Visceral Leishmaniasis. *Front Immunol*. 2018;9(2958).
97. Johns JL, Borjesson DL. Downregulation of CXCL12 signaling and altered hematopoietic stem and progenitor cell trafficking in a murine model of acute *Anaplasma phagocytophilum* infection. *Innate Immun*. 2012;18(3):418-28.
98. Wang X, Cho SY, Hu CS, Chen D, Roboz J, Hoffman R. C-X-C motif chemokine 12 influences the development of extramedullary hematopoiesis in the spleens of myelofibrosis patients. *Exp Hematol*. 2015;43(2):100-9 e1.

99. Foudi A, Hochedlinger K, Van Buren D, Schindler JW, Jaenisch R, Carey V, et al. Analysis of histone 2B-GFP retention reveals slowly cycling hematopoietic stem cells. *Nature Biotechnology*. 2009;27(1):84-90.
100. Rossi DJ, Bryder D, Seita J, Nussenzweig A, Hoeijmakers J, Weissman IL. Deficiencies in DNA damage repair limit the function of haematopoietic stem cells with age. *Nature*. 2007;447(7145):725-9.
101. Orford KW, Scadden DT. Deconstructing stem cell self-renewal: genetic insights into cell-cycle regulation. *Nat Rev Genet*. 2008;9(2):115-28.
102. Warr MR, Binnewies M, Flach J, Reynaud D, Garg T, Malhotra R, et al. FOXO3A directs a protective autophagy program in haematopoietic stem cells. *Nature*. 2013;494(7437):323-7.
103. Ho TT, Warr MR, Adelman ER, Lansinger OM, Flach J, Verovskaya EV, et al. Autophagy maintains the metabolism and function of young and old stem cells. *Nature*. 2017;543(7644):205-+.
104. Simsek T, Kocabas F, Zheng JK, DeBerardinis RJ, Mahmoud AI, Olson EN, et al. The Distinct Metabolic Profile of Hematopoietic Stem Cells Reflects Their Location in a Hypoxic Niche. *Cell Stem Cell*. 2010;7(3):380-90.
105. Signer RAJ, Magee JA, Salic A, Morrison SJ. Haematopoietic stem cells require a highly regulated protein synthesis rate. *Nature*. 2014;509(7498):49-+.
106. van Galen P, Kreso A, Mbong N, Kent DG, Fitzmaurice T, Chambers JE, et al. The unfolded protein response governs integrity of the haematopoietic stem-cell pool during stress. *Nature*. 2014;510(7504):268-+.
107. Takizawa H, Manz MG. In vivo divisional tracking of hematopoietic stem cells. *Ann Ny Acad Sci*. 2012;1266:40-6.
108. Takizawa H, Fritsch K, Kovtonyuk LV, Saito Y, Yakkala C, Jacobs K, et al. Pathogen-Induced TLR4-TRIF Innate Immune Signaling in Hematopoietic Stem Cells Promotes Proliferation but Reduces Competitive Fitness. *Cell Stem Cell*. 2017;21(2):225-40 e5.
109. Essers MA, Offner S, Blanco-Bose WE, Waibler Z, Kalinke U, Duchosal MA, et al. IFNalpha activates dormant haematopoietic stem cells in vivo. *Nature*. 2009;458(7240):904-8.
110. Baldrige MT, King KY, Boles NC, Weksberg DC, Goodell MA. Quiescent haematopoietic stem cells are activated by IFN-gamma in response to chronic infection. *Nature*. 2010;465(7299):793-7.
111. Pietras EM, Lakshminarasimhan R, Techner JM, Fong S, Flach J, Binnewies M, et al. Re-entry into quiescence protects hematopoietic stem cells from the killing effect of chronic exposure to type I interferons. *J Exp Med*. 2014;211(2):245-62.
112. Pietras EM, Mirantes-Barbeito C, Fong S, Loeffler D, Kovtonyuk LV, Zhang S, et al. Chronic interleukin-1 exposure drives haematopoietic stem cells towards precocious myeloid differentiation at the expense of self-renewal. *Nat Cell Biol*. 2016;18(6):607-18.
113. Morrison SJ, Wright DE, Weissman IL. Cyclophosphamide/granulocyte colony-stimulating factor induces hematopoietic stem cells to proliferate prior to mobilization. *Proc Natl Acad Sci U S A*. 1997;94(5):1908-13.
114. Zhao JL, Ma C, O'Connell RM, Mehta A, DiLoreto R, Heath JR, et al. Conversion of Danger Signals into Cytokine Signals by Hematopoietic Stem and Progenitor Cells for Regulation of Stress-Induced Hematopoiesis. *Cell Stem Cell*. 2014;14(4):445-59.
115. Herval A, Binnewies M, Leong S, Calero-Nieto FJ, Zhang SY, Kang YA, et al. Myeloid progenitor cluster formation drives emergency and leukaemic myelopoiesis. *Nature*. 2017;544(7648):53-8.
116. Haas S, Hansson J, Klimmeck D, Loeffler D, Velten L, Uckelmann H, et al. Inflammation-Induced Emergency Megakaryopoiesis Driven by Hematopoietic Stem Cell-like Megakaryocyte Progenitors. *Cell Stem Cell*. 2015;17(4):422-34.

117. Ramasz B, Kruger A, Reinhardt J, Sinha A, Gerlach M, Gerbault A, et al. Hematopoietic stem cell response to acute thrombocytopenia requires signaling through distinct receptor tyrosine kinases. *Blood*. 2019;134(12):1046-58.
118. Matatall KA, Jeong M, Chen S, Sun D, Chen F, Mo Q, et al. Chronic Infection Depletes Hematopoietic Stem Cells through Stress-Induced Terminal Differentiation. *Cell reports*. 2016;17(10):2584-95.
119. Papadaki HA, Gibson FM, Psyllaki M, Gordon-Smith EC, Marsh JCW, Eliopoulos GD. Assessment of bone marrow stem cell reserve and function and stromal cell function in patients with severe congenital neutropenia. *European Journal of Haematology*. 2001;67(4):245-51.
120. Papadaki HA, Kritikos HD, Gemetzi C, Koutala H, Marsh JCW, Boumpas DT, et al. Bone marrow progenitor cell reserve and function and stromal cell function are defective in rheumatoid arthritis: evidence for a tumor necrosis factor alpha-mediated effect. *Blood*. 2002;99(5):1610-9.
121. deHaan G, Nijhof W, VanZant G. Mouse strain-dependent changes in frequency and proliferation of hematopoietic stem cells during aging: Correlation between lifespan and cycling activity. *Blood*. 1997;89(5):1543-50.
122. Morrison SJ, Wandycz AM, Akashi K, Globerson A, Weissman IL. The aging of hematopoietic stem cells. *Nat Med*. 1996;2(9):1011-6.
123. Dykstra B, Olthof S, Schreuder J, Ritsema M, de Haan G. Clonal analysis reveals multiple functional defects of aged murine hematopoietic stem cells. *J Exp Med*. 2011;208(13):2691-703.
124. Rossi DJ, Bryder D, Zahn JM, Ahlenius H, Sonu R, Wagers AJ, et al. Cell intrinsic alterations underlie hematopoietic stem cell aging. *P Natl Acad Sci USA*. 2005;102(26):9194-9.
125. Beerman I, Bhattacharya D, Zandi S, Sigvardsson M, Weissman IL, Bryder D, et al. Functionally distinct hematopoietic stem cells modulate hematopoietic lineage potential during aging by a mechanism of clonal expansion. *P Natl Acad Sci USA*. 2010;107(12):5465-70.
126. Liang Y, Van Zant G, Szilvassy SJ. Effects of aging on the homing and engraftment of murine hematopoietic stem and progenitor cells. *Blood*. 2005;106(4):1479-87.
127. Yamamoto R, Wilkinson AC, Ooehara J, Lan X, Lai CY, Nakauchi Y, et al. Large-Scale Clonal Analysis Resolves Aging of the Mouse Hematopoietic Stem Cell Compartment. *Cell Stem Cell*. 2018;22(4):600-+.
128. Ergen AV, Boles NC, Goodell MA. Rantes/Ccl5 influences hematopoietic stem cell subtypes and causes myeloid skewing. *Blood*. 2012;119(11):2500-9.
129. Poulos MG, Ramalingam P, Gutkin MC, Llanos P, Gilleran K, Rabbany SY, et al. Endothelial transplantation rejuvenates aged hematopoietic stem cell function. *J Clin Invest*. 2017;127(11):4163-78.
130. Ho YH, Del Toro R, Rivera-Torres J, Rak J, Korn C, Garcia-Garcia A, et al. Remodeling of Bone Marrow Hematopoietic Stem Cell Niches Promotes Myeloid Cell Expansion during Premature or Physiological Aging. *Cell Stem Cell*. 2019;25(3):407-18 e6.
131. Maryanovich M, Zahalka AH, Pierce H, Pinho S, Nakahara F, Asada N, et al. Adrenergic nerve degeneration in bone marrow drives aging of the hematopoietic stem cell niche. *Nat Med*. 2018;24(6):782-91.
132. Singh L, Brennan TA, Russell E, Kim JH, Chen Q, Brad Johnson F, et al. Aging alters bone-fat reciprocity by shifting in vivo mesenchymal precursor cell fate towards an adipogenic lineage. *Bone*. 2016;85:29-36.
133. Liu H, Xia X, Li B. Mesenchymal stem cell aging: Mechanisms and influences on skeletal and non-skeletal tissues. *Exp Biol Med (Maywood)*. 2015;240(8):1099-106.
134. Naveiras O, Nardi V, Wenzel PL, Hauschka PV, Fahey F, Daley GQ. Bone-marrow adipocytes as negative regulators of the haematopoietic microenvironment. *Nature*. 2009;460(7252):259-U124.

135. Kovtonyuk LV, Fritsch K, Feng XM, Manz MG, Takizawa H. Inflamm-Aging of Hematopoiesis, Hematopoietic Stem Cells, and the Bone Marrow Microenvironment. *Frontiers in Immunology*. 2016;7.
136. Baylis D, Bartlett DB, Patel HP, Roberts HC. Understanding how we age: insights into inflammaging. *Longevity & Healthspan*. 2013;2(1):8.
137. Zambetti NA, Ping Z, Chen S, Kenswil KJG, Mylona MA, Sanders MA, et al. Mesenchymal Inflammation Drives Genotoxic Stress in Hematopoietic Stem Cells and Predicts Disease Evolution in Human Pre-leukemia. *Cell Stem Cell*. 2016;19(5):613-27.
138. Schneider RK, Schenone M, Ferreira MV, Kramann R, Joyce CE, Hartigan C, et al. Rps14 haploinsufficiency causes a block in erythroid differentiation mediated by S100A8 and S100A9. *Nat Med*. 2016;22(3):288-97.
139. Schneider RK, Mullally A, Dugourd A, Peisker F, Hoogenboezem R, Van Strien PMH, et al. Gli1(+) Mesenchymal Stromal Cells Are a Key Driver of Bone Marrow Fibrosis and an Important Cellular Therapeutic Target. *Cell Stem Cell*. 2017;20(6):785-800 e8.
140. Ballmaier M, Schulze H, Strauss G, Cherkaoui K, Wittner N, Lynen S, et al. Thrombopoietin in patients with congenital thrombocytopenia and absent radii: Elevated serum levels, normal receptor expression, but defective reactivity to thrombopoietin. *Blood*. 1997;90(2):612-9.
141. Ballmaier M, Germeshausen M, Schulze H, Cherkaoui K, Lang S, Gaudig A, et al. c-mpl mutations are the cause of congenital amegakaryocytic thrombocytopenia. *Blood*. 2001;97(1):139-46.
142. Qian H, Buza-Vidas N, Hyland CD, Jensen CT, Antonchuk J, Mansson R, et al. Critical role of thrombopoietin in maintaining adult quiescent hematopoietic stem cells. *Cell Stem Cell*. 2007;1(6):671-84.
143. Kelemen E, Cserhati I, Tanos B. Demonstration and some properties of human thrombopoietin in thrombocythaemic sera. *Acta Haematol*. 1958;20(6):350-5.
144. Ng AP, Kauppi M, Metcalf D, Hyland CD, Josefsson EC, Lebois M, et al. Mpl expression on megakaryocytes and platelets is dispensable for thrombopoiesis but essential to prevent myeloproliferation. *Proceedings of the National Academy of Sciences*. 2014;111(16):5884-9.
145. Deutsch VR, Tomer A. Megakaryocyte development and platelet production. *Br J Haematol*. 2006;134(5):453-66.
146. Xavier-Ferruccio J, Krause DS. Concise Review: Bipotent Megakaryocytic-Erythroid Progenitors: Concepts and Controversies. *Stem Cells*. 2018;36(8):1138-45.
147. Decker M, Leslie J, Liu Q, Ding L. Hepatic thrombopoietin is required for bone marrow hematopoietic stem cell maintenance. *Science*. 2018;360(6384):106-10.
148. Sungaran R, Markovic B, Chong BH. Localization and regulation of thrombopoietin mRNA expression in human kidney, liver, bone marrow, and spleen using in situ hybridization. *Blood*. 1997;89(1):101-7.
149. McCarty JM, Sprugel KH, Fox NE, Sabath DE, Kaushansky K. Murine thrombopoietin mRNA levels are modulated by platelet count. *Blood*. 1995;86(10):3668-75.
150. Guerriero A, Worford L, Sheehan K, Guo G, Holland HK, Hornkohl AC, et al. Thrombopoietin (TPO) is synthesized by bone marrow stromal cells. *Blood*. 1997;90(9):3444-45.
151. Fielder PJ, Gurney AL, Stefanich E, Marian M, Moore MW, Carver Moore K, et al. Regulation of thrombopoietin levels by c-mpl - Mediated binding to platelets. *Blood*. 1996;87(6):2154-61.
152. Kuter D, Rosenberg R. The reciprocal relationship of thrombopoietin (c-Mpl ligand) to changes in the platelet mass during busulfan-induced thrombocytopenia in the rabbit. *Blood*. 1995;85(10):2720-30.
153. Hou M, Andersson PO, Stockelberg D, Mellqvist UH, Ridell B, Wadenvik H. Plasma thrombopoietin levels in thrombocytopenic states: implication for a regulatory role of bone marrow megakaryocytes. *Br J Haematol*. 1998;101(3):420-4.

154. Grozovsky R, Begonja AJ, Liu K, Visner G, Hartwig JH, Falai H, et al. The Ashwell-Morell receptor regulates hepatic thrombopoietin production via JAK2-STAT3 signaling. *Nat Med.* 2015;21(1):47-54.
155. Eulenfeld R, Dittrich A, Khouri C, Muller PJ, Mutze B, Wolf A, et al. Interleukin-6 signalling: More than Jaks and STATs. *Eur J Cell Biol.* 2012;91(6-7):486-95.
156. Wolber EM, Jelkmann W. Interleukin-6 increases thrombopoietin production in human hepatoma cells HepG2 and Hep3B. *J Interf Cytok Res.* 2000;20(5):499-506.
157. Kaser A, Brandacher G, Steurer W, Kaser S, Offner FA, Zoller H, et al. Interleukin-6 stimulates thrombopoiesis through thrombopoietin: role in inflammatory thrombocytosis. *Blood.* 2001;98(9):2720-5.
158. Wolber EM, Fandrey J, Frackowski U, Jelkmann W. Hepatic thrombopoietin mRNA is increased in acute inflammation. *Thrombosis and Haemostasis.* 2001;86(6):1421-4.
159. Nagahisa H, Nagata Y, Ohnuki T, Osada M, Nagasawa T, Abe T, et al. Bone marrow stromal cells produce thrombopoietin and stimulate megakaryocyte growth and maturation but suppress proplatelet formation. *Blood.* 1996;87(4):1309-16.
160. McIntosh B, Kaushansky K. Transcriptional regulation of bone marrow thrombopoietin by platelet proteins. *Exp Hematol.* 2008;36(7):799-806.
161. Yoshihara H, Arai F, Hosokawa K, Hagiwara T, Takubo K, Nakamura Y, et al. Thrombopoietin/MPL signaling regulates hematopoietic stem cell quiescence and interaction with the osteoblastic niche. *Cell Stem Cell.* 2007;1(6):685-97.
162. Yin T, Li L. The stem cell niches in bone. *J Clin Invest.* 2006;116(5):1195-201.
163. Nakamura-Ishizu A, Takubo K, Fujioka M, Suda T. Megakaryocytes are essential for HSC quiescence through the production of thrombopoietin. *Biochem Bioph Res Co.* 2014;454(2):353-7.
164. Nakamura-Ishizu A, Takubo K, Kobayashi H, Suzuki-Inoue K, Suda T. CLEC-2 in megakaryocytes is critical for maintenance of hematopoietic stem cells in the bone marrow. *J Exp Med.* 2015;212(12):2133-46.
165. McIntosh BJ, Fox NE, Kaushansky K. Factors Affecting Thrombopoietin Production from Bone Marrow Stromal Cells. *Blood.* 2004;104:1280-.
166. Sungaran R, Chisholm OT, Markovic B, Khachigian LM, Tanaka Y, Chong BH. The role of platelet alpha-granular proteins in the regulation of thrombopoietin messenger RNA expression in human bone marrow stromal cells. *Blood.* 2000;95(10):3094-101.
167. Gasteiger G, D'Ossualdo A, Schubert DA, Weber A, Bruscia EM, Hartl D. Cellular Innate Immunity: An Old Game with New Players. *J Innate Immun.* 2017;9(2):111-25.
168. Geissmann F, Jung S, Littman DR. Blood monocytes consist of two principal subsets with distinct migratory properties. *Immunity.* 2003;19(1):71-82.
169. Italiani P, Boraschi D. From Monocytes to M1/M2 Macrophages: Phenotypical vs. Functional Differentiation. *Front Immunol.* 2014;5:514.
170. Jakubzick C, Gautier EL, Gibbings SL, Sojka DK, Schlitzer A, Johnson TE, et al. Minimal differentiation of classical monocytes as they survey steady-state tissues and transport antigen to lymph nodes. *Immunity.* 2013;39(3):599-610.
171. Yona S, Kim KW, Wolf Y, Mildner A, Varol D, Breker M, et al. Fate mapping reveals origins and dynamics of monocytes and tissue macrophages under homeostasis. *Immunity.* 2013;38(1):79-91.
172. Auffray C, Fogg D, Garfa M, Elain G, Join-Lambert O, Kayal S, et al. Monitoring of blood vessels and tissues by a population of monocytes with patrolling behavior. *Science.* 2007;317(5838):666-70.
173. Carlin LM, Stamatides EG, Auffray C, Hanna RN, Glover L, Vizcay-Barrena G, et al. Nr4a1-dependent Ly6C(low) monocytes monitor endothelial cells and orchestrate their disposal. *Cell.* 2013;153(2):362-75.
174. Stuart LM, Ezekowitz RA. Phagocytosis: elegant complexity. *Immunity.* 2005;22(5):539-50.

175. Watanabe S, Alexander M, Misharin AV, Budinger GRS. The role of macrophages in the resolution of inflammation. *J Clin Invest*. 2019;129(7):2619-28.
176. Varol C, Mildner A, Jung S. Macrophages: development and tissue specialization. *Annu Rev Immunol*. 2015;33:643-75.
177. Liu K, Nussenzweig MC. Origin and development of dendritic cells. *Immunol Rev*. 2010;234(1):45-54.
178. Naik SH, Metcalf D, van Nieuwenhuijze A, Wicks I, Wu L, O'Keeffe M, et al. Intrasplenic steady-state dendritic cell precursors that are distinct from monocytes. *Nat Immunol*. 2006;7(6):663-71.
179. Liu K, Victora GD, Schwickert TA, Guermonprez P, Meredith MM, Yao K, et al. In vivo analysis of dendritic cell development and homeostasis. *Science*. 2009;17(5925):392-7.
180. Kumar BV, Connors TJ, Farber DL. Human T Cell Development, Localization, and Function throughout Life. *Immunity*. 2018;48(2):202-13.
181. Nikolich-Zugich J, Slifka MK, Messaoudi I. The many important facets of T-cell repertoire diversity. *Nat Rev Immunol*. 2004;4(2):123-32.
182. Pennock ND, White JT, Cross EW, Cheney EE, Tamburini BA, Kedl RM. T cell responses: naive to memory and everything in between. *Adv Physiol Educ*. 2013;37(4):273-83.
183. Zhu JF, Paul WE. CD4 T cells: fates, functions, and faults. *Blood*. 2008;112(5):1557-69.
184. Aavani P, Allen LJS. The role of CD4 T cells in immune system activation and viral reproduction in a simple model for HIV infection. *Appl Math Model*. 2019;75:210-22.
185. Zhang N, Bevan MJ. CD8(+) T Cells: Foot Soldiers of the Immune System. *Immunity*. 2011;35(2):161-8.
186. Golubovskaya V, Wu LJ. Different Subsets of T Cells, Memory, Effector Functions, and CAR-T Immunotherapy. *Cancers*. 2016;8(3).
187. Kuniyasu Y, Takahashi T, Itoh M, Shimizu J, Toda G, Sakaguchi S. Naturally anergic and suppressive CD25(+)CD4(+) T cells as a functionally and phenotypically distinct immunoregulatory T cell subpopulation. *International Immunology*. 2000;12(8):1145-55.
188. Hori S, Nomura T, Sakaguchi S. Control of regulatory T cell development by the transcription factor Foxp3. *Science*. 2003;299(5609):1057-61.
189. Romano M, Fanelli G, Albany CJ, Giganti G, Lombardi G. Past, Present, and Future of Regulatory T Cell Therapy in Transplantation and Autoimmunity. *Frontiers in Immunology*. 2019;10.
190. Fontenot JD, Gavin MA, Rudensky AY. Foxp3 programs the development and function of CD4(+)CD25(+) regulatory T cells. *Nature Immunology*. 2003;4(4):330-6.
191. Grant FM, Yang J, Nasrallah R, Clarke J, Sadiyah F, Whiteside SK, et al. BACH2 drives quiescence and maintenance of resting Treg cells to promote homeostasis and cancer immunosuppression. *J Exp Med*. 2020;217(9).
192. Breitfeld D, Ohl L, Kremmer E, Ellwart J, Sallusto F, Lipp M, et al. Follicular B helper T cells express CXC chemokine receptor 5, localize to B cell follicles, and support immunoglobulin production. *J Exp Med*. 2000;192(11):1545-51.
193. Shi JW, Hou SY, Fang Q, Liu X, Liu XL, Qi H. PD-1 Controls Follicular T Helper Cell Positioning and Function. *Immunity*. 2018;49(2):264-+.
194. Buchholz VR, Schumacher TNM, Busch DH. T Cell Fate at the Single-Cell Level. *Annual Review of Immunology*, Vol 34. 2016;34:65-92.
195. Schwartz RH. T cell anergy. *Annu Rev Immunol*. 2003;21:305-34.
196. Hathcock KS, Laszlo G, Pucillo C, Linsley P, Hodes RJ. Comparative analysis of B7-1 and B7-2 costimulatory ligands: expression and function. *J Exp Med*. 1994;180(2):631-40.
197. Inaba K, Witmer-Pack M, Inaba M, Hathcock KS, Sakuta H, Azuma M, et al. The tissue distribution of the B7-2 costimulator in mice: abundant expression on dendritic cells in situ and during maturation in vitro. *J Exp Med*. 1994;180(5):1849-60.

198. Maxwell JR, Weinberg A, Prell RA, Vella AT. Danger and OX40 receptor signaling synergize to enhance memory T cell survival by inhibiting peripheral deletion. *J Immunol.* 2000;164(1):107-12.
199. Ron Y, De Baetselier P, Gordon J, Feldman M, Segal S. Defective induction of antigen-reactive proliferating T cells in B cell-deprived mice. *Eur J Immunol.* 1981;11(12):964-8.
200. Neunert C, Terrell DR, Arnold DM, Buchanan G, Cines DB, Cooper N, et al. American Society of Hematology 2019 guidelines for immune thrombocytopenia. *Blood Adv.* 2019;3(23):3829-66.
201. Swinkels M, Rijkers M, Voorberg J, Vidarsson G, Leebeek FWG, Jansen AJG. Emerging Concepts in Immune Thrombocytopenia. *Front Immunol.* 2018;9:880.
202. Neunert C, Noroozi N, Norman G, Buchanan GR, Goy J, Nazi I, et al. Severe bleeding events in adults and children with primary immune thrombocytopenia: a systematic review. *J Thromb Haemost.* 2015;13(3):457-64.
203. Neunert CE, Buchanan G, Blanchette V, Barnard D, Young N, Curtis C, et al. Relationships among bleeding severity, health-related quality of life, and platelet count in children with immune thrombocytopenic purpura. *Pediatr blood cancer.* 2009;53(4):652-4.
204. Page LK, Psaila B, Provan D, Hamilton JM, Jenkins JM, Elish AS, et al. The immune thrombocytopenic purpura (ITP) bleeding score: assessment of bleeding in patients with ITP. *Brit J Haematol.* 2007;138(2):245-8.
205. Provan D, Stasi R, Newland AC, Blanchette VS, Bolton-Maggs P, Bussel JB, et al. International consensus report on the investigation and management of primary immune thrombocytopenia. *Blood.* 2010;115(2):168-86.
206. Schoonen WM, Kucera G, Coalson J, Li L, Rutstein M, Mowat F, et al. Epidemiology of immune thrombocytopenic purpura in the General Practice Research Database. *Br J Haematol.* 2009;145(2):235-44.
207. Segal JB, Powe NR. Prevalence of immune thrombocytopenia: analyses of administrative data. *J Thromb Haemost.* 2006;4(11):2377-83.
208. Terrell DR, Beebe LA, Vesely SK, Neas BR, Segal JB, George JN. The incidence of immune thrombocytopenic purpura in children and adults: A critical review of published reports. *Am J Hematol.* 2010;85(3):174-80.
209. Moulis G, Sailler L, Lapeyre-Mestre M. Severe bleeding events in adults and children with primary immune thrombocytopenia: a systematic review: comment. *J Thromb Haemost.* 2015;13(8):1521-2.
210. Cines DB, Bussel JB, Liebman HA, Luning Prak ET. The ITP syndrome: pathogenic and clinical diversity. *Blood.* 2009;113(26):6511-21.
211. Cines DB, Liebman H, Stasi R. Pathobiology of secondary immune thrombocytopenia. *Semin Hematol.* 2009;46(1 Suppl 2):S2-14.
212. Van Belle TL, Coppieters KT, Von Herrath MG. Type 1 Diabetes: Etiology, Immunology, and Therapeutic Strategies. *Physiol Rev.* 2011;91(1):79-118.
213. Harrington WJ, Minnich V, Hollingsworth JW, Moore CV. Demonstration of a thrombocytopenic factor in the blood of patients with thrombocytopenic purpura. *J Lab Clin Med.* 1951;38(1):1-10.
214. van Leeuwen EF, van der Ven JT, Engelfriet CP, von dem Borne AE. Specificity of autoantibodies in autoimmune thrombocytopenia. *Blood.* 1982;59(1):23-6.
215. McMillan R, Tani P, Millard F, Berchtold P, Renshaw L, Woods VL, Jr. Platelet-associated and plasma anti-glycoprotein autoantibodies in chronic ITP. *Blood.* 1987;70(4):1040-5.
216. Kiyomizu K, Kashiwagi H, Nakazawa T, Tadokoro S, Honda S, Kanakura Y, et al. Recognition of highly restricted regions in the beta-propeller domain of alphaIIb by platelet-associated anti-alphaIIbbeta3 autoantibodies in primary immune thrombocytopenia. *Blood.* 2012;120(7):1499-509.

217. Kiefel V, Santoso S, Kaufmann E, Mueller-Eckhardt C. Autoantibodies against platelet glycoprotein Ib/IX: a frequent finding in autoimmune thrombocytopenic purpura. *Br J Haematol.* 1991;79(2):256-62.
218. Chang M, Nakagawa PA, Williams SA, Schwartz MR, Imfeld KL, Buzby JS, et al. Immune thrombocytopenic purpura (ITP) plasma and purified ITP monoclonal autoantibodies inhibit megakaryocytopoiesis in vitro. *Blood.* 2003;102(3):887-95.
219. Zhao C, Li X, Zhang F, Wang L, Peng J, Hou M. Increased cytotoxic T-lymphocyte-mediated cytotoxicity predominant in patients with idiopathic thrombocytopenic purpura without platelet autoantibodies. *Haematologica.* 2008;93(9):1428-30.
220. Audia S, Samson M, Mahevas M, Ferrand C, Trad M, Ciudad M, et al. Preferential splenic CD8(+) T-cell activation in rituximab-nonresponder patients with immune thrombocytopenia. *Blood.* 2013;122(14):2477-86.
221. Olsson B, Andersson PO, Jernas M, Jacobsson S, Carlsson B, Carlsson LM, et al. T-cell-mediated cytotoxicity toward platelets in chronic idiopathic thrombocytopenic purpura. *Nat Med.* 2003;9(9):1123-4.
222. Zhang F, Chu X, Wang L, Zhu Y, Li L, Ma D, et al. Cell-mediated lysis of autologous platelets in chronic idiopathic thrombocytopenic purpura. *Eur J Haematol.* 2006;76(5):427-31.
223. Li S, Wang L, Zhao C, Li L, Peng J, Hou M. CD8+ T cells suppress autologous megakaryocyte apoptosis in idiopathic thrombocytopenic purpura. *Br J Haematol.* 2007;139(4):605-11.
224. Qiu J, Liu X, Li X, Zhang X, Han P, Zhou H, et al. CD8(+) T cells induce platelet clearance in the liver via platelet desialylation in immune thrombocytopenia. *Sci Rep.* 2016;6:27445.
225. Najean Y, Rain JD, Billotey C. The site of destruction of autologous 111In-labelled platelets and the efficiency of splenectomy in children and adults with idiopathic thrombocytopenic purpura: a study of 578 patients with 268 splenectomies. *Br J Haematol.* 1997;97(3):547-50.
226. Sandler SG. The spleen and splenectomy in immune (idiopathic) thrombocytopenic purpura. *Semin Hematol.* 2000;37(1 Suppl 1):10-2.
227. Kojouri K, Vesely SK, Terrell DR, George JN. Splenectomy for adult patients with idiopathic thrombocytopenic purpura: a systematic review to assess long-term platelet count responses, prediction of response, and surgical complications. *Blood.* 2004;104(9):2623-34.
228. Kuwana M, Okazaki Y, Ikeda Y. Splenic macrophages maintain the anti-platelet autoimmune response via uptake of opsonized platelets in patients with immune thrombocytopenic purpura. *J Thromb Haemost.* 2009;7(2):322-9.
229. Wang T, Zhao H, Ren H, Guo J, Xu M, Yang R, et al. Type 1 and type 2 T-cell profiles in idiopathic thrombocytopenic purpura. *Haematologica.* 2005;90(7):914-23.
230. Zhang J, Ma D, Zhu X, Qu X, Ji C, Hou M. Elevated profile of Th17, Th1 and Tc1 cells in patients with immune thrombocytopenic purpura. *Haematologica.* 2009;94(9):1326-9.
231. Panitsas F, Theodoropoulou M, Kouraklis A, Karakantza M, Theodorou G, Zoumbos N, et al. Adult chronic idiopathic thrombocytopenic purpura (ITP) is the manifestation of a type-1 polarized immune response. *Blood.* 2004;103(7):2645-7.
232. Stasi R, Del Poeta G, Stipa E, Evangelista ML, Trawinska MM, Cooper N, et al. Response to B-cell depleting therapy with rituximab reverts the abnormalities of T-cell subsets in patients with idiopathic thrombocytopenic purpura. *Blood.* 2007;110(8):2924-30.
233. Panitsas FP, Mouzaki A. Effect of splenectomy on type-1/type-2 cytokine gene expression in a patient with adult idiopathic thrombocytopenic purpura (ITP). *BMC Blood Disord.* 2004;4(1):4.
234. Audia S, Rossato M, Santegoets K, Spijkers S, Wichers C, Bekker C, et al. Splenic TFH expansion participates in B-cell differentiation and antiplatelet-antibody production during immune thrombocytopenia. *Blood.* 2014;124(18):2858-66.

235. Sakakura M, Wada H, Tawara I, Nobori T, Sugiyama T, Sagawa N, et al. Reduced Cd4+ Cd25+ T cells in patients with idiopathic thrombocytopenic purpura. *Thromb Res.* 2007;120(2):187-93.
236. Sojka DK, Huang YH, Fowell DJ. Mechanisms of regulatory T-cell suppression - a diverse arsenal for a moving target. *Immunology.* 2008;124(1):13-22.
237. Gotot J, Gottschalk C, Leopold S, Knolle PA, Yagita H, Kurts C, et al. Regulatory T cells use programmed death 1 ligands to directly suppress autoreactive B cells in vivo. *P Natl Acad Sci USA.* 2012;109(26):10468-73.
238. Stasi R, Cooper N, Del Poeta G, Stipa E, Laura Evangelista M, Abruzzese E, et al. Analysis of regulatory T-cell changes in patients with idiopathic thrombocytopenic purpura receiving B cell-depleting therapy with rituximab. *Blood.* 2008;112(4):1147-50.
239. Li Z, Mou W, Lu G, Cao J, He X, Pan X, et al. Low-dose rituximab combined with short-term glucocorticoids up-regulates Treg cell levels in patients with immune thrombocytopenia. *Int J Hematol.* 2011;93(1):91-8.
240. Provan D, Newland A. Fifty years of idiopathic thrombocytopenic purpura (ITP): management of refractory itp in adults. *Br J Haematol.* 2002;118(4):933-44.
241. Vianelli N, Galli M, de Vivo A, Intermesoli T, Giannini B, Mazzucconi MG, et al. Efficacy and safety of splenectomy in immune thrombocytopenic purpura: long-term results of 402 cases. *Haematologica.* 2005;90(1):72-7.
242. Tao L, Zeng Q, Li J, Xu M, Wang J, Pan Y, et al. Platelet desialylation correlates with efficacy of first-line therapies for immune thrombocytopenia. *J Hematol Oncol.* 2017;10(1):46.
243. Li J, van der Wal DE, Zhu G, Xu M, Yougbare I, Ma L, et al. Desialylation is a mechanism of Fc-independent platelet clearance and a therapeutic target in immune thrombocytopenia. *Nat Commun.* 2015;6:7737.
244. Li J, Callum JL, Lin YL, Zhou Y, Zhu GH, Ni HY. Severe platelet desialylation in a patient with glycoprotein Ib/IX antibody-mediated immune thrombocytopenia and fatal pulmonary hemorrhage. *Haematologica.* 2014;99(4):E61-E3.
245. Quach ME, Dragovich MA, Chen W, Syed AK, Cao W, Liang X, et al. Fc-independent immune thrombocytopenia via mechanomolecular signaling in platelets. *Blood.* 2018;131(7):787-96.
246. Ballem PJ, Segal GM, Stratton JR, Gernsheimer T, Adamson JW, Slichter SJ. Mechanisms of thrombocytopenia in chronic autoimmune thrombocytopenic purpura. Evidence of both impaired platelet production and increased platelet clearance. *J Clin Invest.* 1987;80(1):33-40.
247. Louwes H, Zeinali Lathori OA, Vellenga E, de Wolf JT. Platelet kinetic studies in patients with idiopathic thrombocytopenic purpura. *Am J Med.* 1999;106(4):430-4.
248. Vainchenker W, Deschamps JF, Bastin JM, Guichard J, Titeux M, Breton-Gorius J, et al. Two monoclonal antiplatelet antibodies as markers of human megakaryocyte maturation: immunofluorescent staining and platelet peroxidase detection in megakaryocyte colonies and in in vivo cells from normal and leukemic patients. *Blood.* 1982;59(3):514-21.
249. Arnold DM, Nazi I, Toltl LJ, Ross C, Ivetic N, Smith JW, et al. Antibody binding to megakaryocytes in vivo in patients with immune thrombocytopenia. *Eur J Haematol.* 2015;95(6):532-7.
250. Al-Samkari H, Kuter DJ. Optimal use of thrombopoietin receptor agonists in immune thrombocytopenia. *Ther Adv Hematol.* 2019;10:1-13.
251. James S, Fox J, Afsari F, Lee J, Clough S, Knight C, et al. Multiparameter Analysis of Human Bone Marrow Stromal Cells Identifies Distinct Immunomodulatory and Differentiation-Competent Subtypes. *Stem Cell Reports.* 2015;4(6):1004-15.
252. Nagasawa T, Hirota S, Tachibana K, Takakura N, Nishikawa S, Kitamura Y, et al. Defects of B-cell lymphopoiesis and bone-marrow myelopoiesis in mice lacking the CXC chemokine PBSF/SDF-1. *Nature.* 1996;382(6592):635-8.
253. deSauvage FJ, CarverMoore K, Luoh SM, Ryan A, Dowd M, Eaton DL, et al. Physiological regulation of early and late stages of megakaryocytopoiesis by thrombopoietin. *J Exp Med.* 1996;183(2):651-6.

254. Takai T, Li M, Sylvestre D, Clynes R, Ravetch JV. FcR gamma chain deletion results in pleiotropic effector cell defects. *Cell*. 1994;76(3):519-29.
255. Shinkai Y, Rathbun G, Lam KP, Oltz EM, Stewart V, Mendelsohn M, et al. RAG-2-deficient mice lack mature lymphocytes owing to inability to initiate V(D)J rearrangement. *Cell*. 1992;68(5):855-67.
256. Nicolini FE, Cashman JD, Hogge DE, Humphries RK, Eaves CJ. NOD/SCID mice engineered to express human IL-3, GM-CSF and Steel factor constitutively mobilize engrafted human progenitors and compromise human stem cell regeneration. *Leukemia*. 2004;18(2):341-7.
257. Shultz LD, Schweitzer PA, Christianson SW, Gott B, Schweitzer IB, Tennent B, et al. Multiple defects in innate and adaptive immunologic function in NOD/LtSz-scid mice. *J Immunol*. 1995;154(1):180-91.
258. Bosma GC, Custer RP, Bosma MJ. A severe combined immunodeficiency mutation in the mouse. *Nature*. 1983;301(5900):527-30.
259. Yoshino H, Ueda T, Kawahata M, Kobayashi K, Ebihara Y, Manabe A, et al. Natural killer cell depletion by anti-asialo GM1 antiserum treatment enhances human hematopoietic stem cell engraftment in NOD/Shi-scid mice. *Bone Marrow Transplant*. 2000;26(11):1211-6.
260. Ohbo K, Suda T, Hashiyama M, Mantani A, Ikebe M, Miyakawa K, et al. Modulation of hematopoiesis in mice with a truncated mutant of the interleukin-2 receptor gamma chain. *Blood*. 1996;87(3):956-67.
261. Billerbeck E, Barry WT, Mu K, Dorner M, Rice CM, Ploss A. Development of human CD4(+)FoxP3(+) regulatory T cells in human stem cell factor-, granulocyte-macrophage colony-stimulating factor-, and interleukin-3-expressing NOD-SCID IL2R gamma(null) humanized mice. *Blood*. 2011;117(11):3076-86.
262. Nocka K, Tan JC, Chiu E, Chu TY, Ray P, Traktman P, et al. Molecular bases of dominant negative and loss of function mutations at the murine c-kit/white spotting locus: W37, Wv, W41 and W. *EMBO J*. 1990;9(6):1805-13.
263. Fleishman RA. Engraftment of W/c-kit mutant mice is determined by stem cell competition, not by increased marrow 'space'. *Exp Hematol*. 1996;24(2):209-13.
264. Waskow C, Madan V, Bartels S, Costa C, Blasig R, Rodewald HR. Hematopoietic stem cell transplantation without irradiation. *Nat Methods*. 2009;2009(4):267-9.
265. Harrison DE, Astle CM. Lymphoid and erythroid repopulation in B6 W-anemic mice: a new unirradiated recipient. *Exp Hematol*. 1991;19(5):374-7.
266. Jacobi PM, Kanaji S, Jakab D, Gehrand AL, Johnsen JM, Haberichter SL. von Willebrand factor propeptide to antigen ratio identifies platelet activation and reduced von Willebrand factor survival phenotype in mice. *J Thromb Haemost*. 2018;16(3):546-54.
267. Chan CKF, Gulati GS, Sinha R, Tompkins JV, Lopez M, Carter AC, et al. Identification of the Human Skeletal Stem Cell. *Cell*. 2018;175(1):43-56 e21.
268. Zhou BO, Yue R, Murphy MM, Peyer JG, Morrison SJ. Leptin-receptor-expressing mesenchymal stromal cells represent the main source of bone formed by adult bone marrow. *Cell Stem Cell*. 2014;15(2):154-68.
269. Livak KJ, Schmittgen TD. Analysis of relative gene expression data using real-time quantitative PCR and the 2(-Delta Delta C) method. *Methods*. 2001;25(4):402-8.
270. Schmitt A, Guichard J, Masse JM, Debili N, Cramer EM. Of mice and men: comparison of the ultrastructure of megakaryocytes and platelets. *Exp Hematol*. 2001;29(11):1295-302.
271. Leven RM. Isolation of Primary Megakaryocytes and Studies of Proplatelet Formation. In: Gibbins JM, Mahaut-Smith MP, editors. *Platelets and Megakaryocytes: Volume 1: Functional Assays*. Totowa, NJ: Humana Press; 2004. p. 281-91.
272. Tolhurst G, Carter RN, Miller N, Mahaut-Smith MP. Purification of native bone marrow megakaryocytes for studies of gene expression. *Methods Mol Biol*. 2012;788:259-73.

273. Ostad SN, Babaei S, Bayat AA, Mahmoudian J. Photobleaching Comparison of R-Phycoerythrin-Streptavidin and Streptavidin-Alexa Fluor 568 in a Breast Cancer Cell Line. *Monoclon Antib Immunodiagn Immunother*. 2019;38(1):25-9.
274. Heazlewood SY, Williams B, Storan MJ, Nilsson SK. The prospective isolation of viable, high ploidy megakaryocytes from adult murine bone marrow by fluorescence activated cell sorting. *Methods Mol Biol*. 2013;1035:121-33.
275. Madisen L, Zwingman TA, Sunkin SM, Oh SW, Zariwala HA, Gu H, et al. A robust and high-throughput Cre reporting and characterization system for the whole mouse brain. *Nat Neurosci*. 2010;13(1):133-40.
276. Longley DB, Harkin DP, Johnston PG. 5-fluorouracil: mechanisms of action and clinical strategies. *Nat Rev Cancer*. 2003;3(5):330-8.
277. Ghilardi N, Wiestner A, Skoda RC. Thrombopoietin production is inhibited by a translational mechanism. *Blood*. 1998;92(11):4023-30.
278. Kozak M. The scanning model for translation: an update. *J Cell Biol*. 1989;108(2):229-41.
279. Eliasson P, Jönsson JI. The hematopoietic stem cell niche: low in oxygen but a nice place to be. *J Cell Physiol*. 2010;222(1):17-22.
280. Daoud R, Mies G, Smialowska A, Olah L, Hossmann KA, Stamm S. Ischemia induces a translocation of the splicing factor tra2-beta 1 and changes alternative splicing patterns in the brain. *J Neurosci*. 2002;22(14):5889-99.
281. Bashour F, Teran JC, Mullen KD. Prevalence of peripheral blood cytopenias (hypersplenism) in patients with nonalcoholic chronic liver disease. *Am J Gastroenterol*. 2000;95(10):2936-9.
282. Sacchetti B, Funari A, Michienzi S, Di Cesare S, Piersanti S, Saggio I, et al. Self-renewing osteoprogenitors in bone marrow sinusoids can organize a hematopoietic microenvironment. *Cell*. 2007;131(2):324-36.
283. Seiki Y, Sasaki Y, Hosokawa K, Saito C, Sugimori N, Yamazaki H, et al. Increased plasma thrombopoietin levels in patients with myelodysplastic syndrome: a reliable marker for a benign subset of bone marrow failure. *Haematologica*. 2013;98(6):901-7.
284. Horikawa Y, Matsumura I, Hashimoto K, Shiraga M, Kosugi S, Tadokoro S, et al. Markedly reduced expression of platelet c-mpl receptor in essential thrombocythemia. *Blood*. 1997;90(10):4031-8.
285. Harrison CN, Gale R, Pezella F, Mire-Sluis S, MacHin S, Linch DC. Platelet c-mpl expression is dysregulated in patients with essential thrombocythaemia but this is not of diagnostic value. *Br J Haematol*. 1999;107(1):137-47.
286. He R, Reid DM, Jones CE, Shulman NR. Spectrum of Ig classes, specificities, and titers of serum antiglycoproteins in chronic idiopathic thrombocytopenic purpura. *Blood*. 1994;83(4):1024-32.
287. Al-Samkari H, Rosovsky RP, Karp Leaf RS, Smith DB, Goodarzi K, Fogerty AE, et al. A modern reassessment of glycoprotein-specific direct platelet autoantibody testing in immune thrombocytopenia. *Blood Adv*. 2020;4(1):9-18.
288. Porcelijn L, Huiskes E, Oldert G, Schipperus M, Zwaginga JJ, de Haas M. Detection of platelet autoantibodies to identify immune thrombocytopenia: state of the art. *Br J Haematol*. 2018;182(3):423-6.
289. Catani L, Fagioli ME, Tazzari PI, Ricci F, Curti A, Rovito M, et al. Dendritic cells of immune thrombocytopenic purpura (ITP) show increased capacity to present apoptotic platelets to T lymphocytes. *Exp Hematol*. 2006;34(7):879-87.
290. Kuwana M, Okazaki Y, Kaburaki J, Kawakami Y, Ikeda Y. Spleen is a primary site for activation of platelet-reactive T and B cells in patients with immune thrombocytopenic purpura. *J Immunol*. 2002;168(7):3675-82.
291. Corash L, Levin J. The relationship between megakaryocyte ploidy and platelet volume in normal and thrombocytopenic C3H mice. *Exp Hematol*. 1990;18(9):985-9.
292. Cox LH, Downs T, Dagg K, Henthorn J, Burstein SA. Interleukin-6 mRNA and protein increase in vivo following induction of acute thrombocytopenia in mice. *Blood*. 1991;77(2):286.

293. Rolovic Z, Baldini M, Dameshek W. Megakaryocytopoiesis in experimentally induced immune thrombocytopenia. *Blood*. 1970;35(2):173-88.
294. Xiao J, Zhang C, Zhang Y, Zhang X, Zhao J, Liang J, et al. Transplantation of adipose-derived mesenchymal stem cells into a murine model of passive chronic immune thrombocytopenia. *Transfusion*. 2012;52(12):2551-8.
295. Zhang A, Fu J, Ning B, Li D, Sun N, Wei W, et al. Tolerogenic dendritic cells generated with IL-10/TGFbeta1 relieve immune thrombocytopenia in mice. *Thromb Res*. 2013;132(1):63-8.
296. Siragam V, Crow AR, Brinc D, Song S, Freedman J, Lazarus AH. Intravenous immunoglobulin ameliorates ITP via activating Fc gamma receptors on dendritic cells. *Nat Med*. 2006;12(6):688-92.
297. Morodomi Y, Kanaji S, Won E, Ruggeri ZM, Kanaji T. Mechanisms of anti-GPIIb/IIIa antibody-induced thrombocytopenia in mice. *Blood*. 2020;135(25):2292-301.
298. Kanaji T, Vo MN, Kanaji S, Zarpellon A, Shapiro R, Morodomi Y, et al. Tyrosyl-tRNA synthetase stimulates thrombopoietin-independent hematopoiesis accelerating recovery from thrombocytopenia. *Proc Natl Acad Sci U S A*. 2018;115(35):E8228-E35.
299. Katsman Y, Foo AH, Leontyev D, Branch DR. Improved mouse models for the study of treatment modalities for immune-mediated platelet destruction. *Transfusion*. 2010;50(6):1285-94.
300. Buttarello M, Mezzapelle G, Freguglia F, Plebani M. Reticulated platelets and immature platelet fraction: Clinical applications and method limitations. *Int J Lab Hematol*. 2020;42(4):363-70.
301. Maia MD, Lopes EP, Ferraz AA, Barros FM, Domingues AL, Ferraz EM. Evaluation of splenomegaly in the hepatosplenic form of mansonic schistosomiasis. *Acta Trop*. 2007;101(3):183-6.
302. Jubelirer SJ, Harpold R. The role of the bone marrow examination in the diagnosis of immune thrombocytopenic purpura: case series and literature review. *Clin Appl Thromb Hemost*. 2002;8(1):73-6.
303. Pisciotta AV, Stefanini M, Dameshek W. Studies on platelets. X. Morphologic characteristics of megakaryocytes by phase contrast microscopy in normals and in patients with idiopathic thrombocytopenic purpura. *Blood*. 1953;8(8):703-23.
304. Dameshek W, Miller EB. The megakaryocytes in idiopathic thrombocytopenic purpura, a form of hypersplenism. *Blood*. 1946;1:27-50.
305. Sim X, Jarocho D, Hayes V, Hanby HA, Marks MS, Camire RM, et al. Identifying and enriching platelet-producing human stem cell-derived megakaryocytes using factor V uptake. *Blood*. 2017;130(2):192-204.
306. Gertz JM, Meuser M, Bouchard BA. Simultaneous flow cytometric analysis of megakaryocyte polyploidy and a labile intracellular protein using zinc-based fixation. *Cytometry A*. 2017;91(7):713-20.
307. Hunt P, Zsebo KM, Hokom MM, Hornkohl A, Birkett NC, del Castillo JC, et al. Evidence that stem cell factor is involved in the rebound thrombocytosis that follows 5-fluorouracil treatment. *Blood*. 1992;80(4):904-11.
308. Chow L, Rukhsana A, Speck E, Kim M, Cridland N, Webster M, et al. A murine model of severe immune thrombocytopenia is induced by antibody- and CD8+ T cell-mediated responses that are differentially sensitive to therapy. *Blood*. 2010;115:1247-53.
309. Geyer JT, Bussel JB. The spleen in immune thrombocytopenia. *HemaSphere*. 2018;2(2):169-72.
310. Ingram M, Coopersmith A. Reticulated platelets following acute blood loss. *Br J Haematol*. 1969;17(3):225-9.
311. Dale GL, Friese P, Hynes LA, Burstein SA. Demonstration that thiazole-orange-positive platelets in the dog are less than 24 hours old. *Blood*. 1995;85(7):1822-5.
312. Kaito K, Otsubo H, Usui N, Yoshida M, Tanno J, Kurihara E, et al. Platelet size deviation width, platelet large cell ratio, and mean platelet volume have sufficient

- sensitivity and specificity in the diagnosis of immune thrombocytopenia. *Br J Haematol*. 2005;128(5):698-702.
313. Ali RA, Wuescher LM, Worth RG. Platelets: essential components of the immune system. *Curr Trends Immunol*. 2015;16:65-78.
314. Song S, Crow AR, Freedman J, Lazarus AH. Monoclonal IgG can ameliorate immune thrombocytopenia in a murine model of ITP: an alternative to IVIG. *Blood*. 2003;101(9):3708.
315. Crow AR, Song S, Semple JW, Freedman J, Lazarus AH. IVIG induces dose-dependent amelioration of ITP in rodent models. *Blood*. 2003;101(4):1658-9; author reply 9.
316. Olsson M, Bruhns P, Frazier WA, Ravetch JV, Oldenborg PA. Platelet homeostasis is regulated by platelet expression of CD47 under normal conditions and in passive immune thrombocytopenia. *Blood*. 2005;9(3577-3582).
317. Prisolovsky A, Marathe B, Hosni A, Bolen AL, Nimmerjahn F, Jackson CW, et al. Rapid platelet turnover in WASP(-) mice correlates with increased ex vivo phagocytosis of opsonized WASP(-) platelets. *Exp Hematol*. 2008;36(5):609-23.
318. Hang LM, Izui S, Dixon FJ. (NZW x BXSB)F1 hybrid. A model of acute lupus and coronary vascular disease with myocardial infarction. *J Exp Med*. 1981;154(1):216-21.
319. Bonilla FA, Oettgen HC. Adaptive immunity. *J Allergy Clin Immunol*. 2010;125(2 Suppl 2):S33-40.
320. Pozo AL, Godfrey EM, Bowles KM. Splenomegaly: investigation, diagnosis and management. *Blood Rev*. 2009;23(3):105-11.
321. Yang JC, Rickman LS, Bosser SK. The clinical diagnosis of splenomegaly. *West J Med*. 1991;155(1):47-52.
322. Loftus WK, Metreweli C. Ultrasound assessment of mild splenomegaly: spleen/kidney ratio. *Pediatr Radiol*. 1998;28(2):98-100.
323. Moeller T, Reif E. Normal findings in CT and MRI. 1 ed: Thieme; 2000. 256 p.
324. Linguraru MG, Sandberg JK, Jones EC, Summers RM. Assessing splenomegaly: automated volumetric analysis of the spleen. *Acad Radiol*. 2013;20(6):675-84.
325. Yang L, Wang L, Zhao CH, Zhu XJ, Hou Y, Jun P, et al. Contributions of TRAIL-mediated megakaryocyte apoptosis to impaired megakaryocyte and platelet production in immune thrombocytopenia. *Blood*. 2010;116(20):4307-16.
326. McMillan R, Wang L, Tomer A, Nichol J, Pistillo J. Suppression of in vitro megakaryocyte production by antiplatelet autoantibodies from adult patients with chronic ITP. *Blood*. 2004;103(4):1364-9.
327. Takahashi R, Sekine N, Nakatake T. Influence of monoclonal antiplatelet glycoprotein antibodies on in vitro human megakaryocyte colony formation and proplatelet formation. *Blood*. 1999;93(6):1951-8.
328. Yang J, Zhang Q, Li P, Dong T, Wu MX. Low-level light treatment ameliorates immune thrombocytopenia. *Sci Rep*. 2016;6:38238.
329. Urbensky JR, Moore JE, Arnold DM, Smith JW, Kelton JG, Nazy I. The sensitivity and specificity of platelet autoantibody testing in immune thrombocytopenia: a systematic review and meta-analysis of a diagnostic test. *Journal of Thrombosis and Haemostasis*. 2019;17(5):787-94.
330. Hu ZB, Slayton WB, Rimsza LM, Bailey M, Sallmon H, Sola-Visner MC. Differences between Newborn and Adult Mice in Their Response to Immune Thrombocytopenia. *Neonatology*. 2010;98(1):100-8.
331. Bhasin TS, Sharma S, Manjari M, Mannan R, Kansal V, Chandey M, et al. Changes in megakaryocytes in cases of thrombocytopenia: bone marrow aspiration and biopsy analysis. *J Clin Diagn Res*. 2013;7(3):473-9.
332. Deka L, Gupta S, Gupta R, Pant L, Kaur CJ, Singh S. Morphometric evaluation of megakaryocytes in bone marrow aspirates of immune-mediated thrombocytopenic purpura. *Platelets*. 2013;24(2):113-7.

333. Kuter DJ, Gernsheimer TB. Thrombopoietin and Platelet Production in Chronic Immune Thrombocytopenia. *Hematol Oncol Clin N*. 2009;23(6):1193-+.
334. Hacein-Bey-Abina S, Estienne M, Bessoles S, Echchakir H, Pederzoli-Ribeil M, Chiron A, et al. Erythropoietin is a major regulator of thrombopoiesis in thrombopoietin-dependent and -independent contexts. *Exp Hematol*. 2020.
335. Avecilla ST, Hattori K, Heissig B, Tejada R, Liao F, Shido K, et al. Chemokine-mediated interaction of hematopoietic progenitors with the bone marrow vascular niche is required for thrombopoiesis. *Nat Med*. 2004;10(1):64-71.
336. MacVittie TJ, Farese AM, Patchen ML, Myers LA. Therapeutic efficacy of recombinant interleukin-6 (IL-6) alone and combined with recombinant human IL-3 in a nonhuman primate model of high-dose, sublethal radiation-induced marrow aplasia. *Blood*. 1994;84(8):2515-22.
337. Schumacher A, Denecke B, Braunschweig T, Stahlschmidt J, Ziegler S, Brandenburg L-O, et al. Angptl4 is upregulated under inflammatory conditions in the bone marrow of mice, expands myeloid progenitors, and accelerates reconstitution of platelets after myelosuppressive therapy. *J Hematol Oncol*. 2015;8(1):64.
338. Tsuji-Takayama K, Harashima A, Tahata H, Izumi N, Nishida Y, Namba M, et al. IFN-gamma in combination with IL-3 accelerates platelet recovery in mice with 5-fluorouracil-induced marrow aplasia. *J Interferon Cytokine Res*. 1996;16(6):447-51.
339. Tsuji-Takayama K, Tahata H, Harashima A, Nishida Y, Izumi N, Fukuda S, et al. Interferon-gamma enhances megakaryocyte colony-stimulating activity in murine bone marrow cells. *J Interferon Cytokine Res*. 1996;16(9):701-8.
340. Li J, Kuter D. The end is just the beginning: megakaryocyte apoptosis and platelet release. *International Journal of Hematology*. 2001;74(4):365-74.
341. Kunz D, Hoffkes HG, Kunz WS, Gressner AM. Standardized flow cytometric method for the accurate determination of platelet counts in patients with severe thrombocytopenia. *Cytometry*. 2000;42(5):284-9.
342. Thon JN, Italiano JE. Platelet formation. *Semin Hematol*. 2010;47(3):220-6.
343. Gekas C, Graf T. CD41 expression marks myeloid-biased adult hematopoietic stem cells and increases with age. *Blood*. 2013;121(22):4463-72.
344. Yamamoto R, Morita Y, Ooehara J, Hamanaka S, Onodera M, Rudolph KL, et al. Clonal analysis unveils self-renewing lineage-restricted progenitors generated directly from hematopoietic stem cells. *Cell*. 2013;154(5):1112-26.
345. Bernitz JM, Kim HS, MacArthur B, Sieburg H, Moore K. Hematopoietic Stem Cells Count and Remember Self-Renewal Divisions. *Cell*. 2016;167(5):1296-309 e10.
346. Psaila B, Mead AJ. Single-cell approaches reveal novel cellular pathways for megakaryocyte and erythroid differentiation. *Blood*. 2019;133(13):1427-35.
347. Sayed AA, Malik A, Khoder A, Adams G, Cooper N. Active Immune Thrombocytopenia (ITP) Disease Is Characterised By a Reduced Treg:CD8 Effector T Cell Ratio Which Is Modulated By Thrombopoietin-Receptor Agonists (TPO-RA). *Blood*. 2018;132.
348. Zhong H, Bao W, Li X, Miller A, Seery C, Haq N, et al. CD16+ monocytes control T-cell subset development in immune thrombocytopenia. *Blood*. 2012;120(16):3326-35.
349. Yang Y, Zhang X, Zhang D, Li H, Ma L, Xuan M, et al. Abnormal Distribution and Function of Monocyte Subsets in Patients With Primary Immune Thrombocytopenia. *Clin Appl Thromb Hemost*. 2017;23(7):786-92.
350. Serreze DV, Gaedeke JW, Leiter EH. Hematopoietic Stem-Cell Defects Underlying Abnormal Macrophage Development and Maturation in Nod Lt Mice - Defective Regulation of Cytokine Receptors and Protein-Kinase-C. *P Natl Acad Sci USA*. 1993;90(20):9625-9.
351. Serreze DV, Gaskins HR, Leiter EH. Defects in the Differentiation and Function of Antigen Presenting Cells in Nod/Lt Mice. *J Immunol*. 1993;150(6):2534-43.
352. Ra C, Jouvin MH, Blank U, Kinet JP. A macrophage Fc gamma receptor and the mast cell receptor for IgE share an identical subunit. *Nature*. 1989;341(6244):752-4.

353. Ravetch JV, Kinetic JP. Fc Receptors. *Annual Review of Immunology*. 1991;9(1):457-92.
354. Bruhns P. Properties of mouse and human IgG receptors and their contribution to disease models. *Blood*. 2012;119(24):5640-9.
355. Joslin J, Gilligan J, Anderson P, Garcia C, Sharif O, Hampton J, et al. A Fully Automated High-Throughput Flow Cytometry Screening System Enabling Phenotypic Drug Discovery. *SLAS Discov*. 2018;23(7):697-707.
356. Swanepoel AC, Stander A, Pretorius E. Flow cytometric comparison of platelets from a whole blood and finger-prick sample: impact of 24 hours storage. *Hematology*. 2013;18(2):106-14.
357. Sintnicolaas K, de Vries W, van der Linden R, Gratama JW, Bolhuis RL. Simultaneous flow cytometric detection of antibodies against platelets, granulocytes and lymphocytes. *J Immunol Methods*. 1991;142(2):215-22.
358. Gregoire C, Chasson L, Luci C, Tomasello E, Geissmann F, Vivier E, et al. The trafficking of natural killer cells. *Immunol Rev*. 2007;220:169-82.
359. Becker S, Warren MK, Haskill S. Colony-Stimulating Factor-Induced Monocyte Survival and Differentiation into Macrophages in Serum-Free Cultures. *J Immunol*. 1987;139(11):3703-9.
360. Langmuir PB, Bridgett MM, Bothwell AL, Crispe IN. Bone marrow abnormalities in the non-obese diabetic mouse. *Int Immunol*. 1993;5(2):169-77.
361. Pai RK, Askew D, Boom WH, Harding CV. Regulation of class II MHC expression in APCs: Roles of types I, III, and IV class II transactivator. *J Immunol*. 2002;169(3):1326-33.
362. Roche PA, Furuta K. The ins and outs of MHC class II-mediated antigen processing and presentation. *Nat Rev Immunol*. 2015;15(4):203-16.
363. Mosmann TR, Coffman RL. Th1-Cell and Th2-Cell - Different Patterns of Lymphokine Secretion Lead to Different Functional-Properties. *Annual Review of Immunology*. 1989;7:145-73.
364. Buxade M, Encabo HH, Riera-Borrull M, Quintana-Gallardo L, Lopez-Cotarelo P, Tellechea M, et al. Macrophage-specific MHCII expression is regulated by a remote Ciita enhancer controlled by NFAT5. *J Exp Med*. 2018;215(11):2901-18.
365. De Riva A, Varley MC, Bluck LJ, Cooke A, Deery MJ, Busch R. Accelerated turnover of MHC class II molecules in NOD mice is developmentally and environmentally regulated in vivo and dispensable for autoimmunity. *Immunology*. 2013;140:49-.
366. Martinic MM, Rulicke T, Althage A, Odermatt B, Hochli M, Lamarre A, et al. Efficient T cell repertoire selection in tetraparental chimeric mice independent of thymic epithelial MHC. *Proc Natl Acad Sci U S A*. 2003;100(4):1861-6.
367. Yi W, Seth NP, Martillotti T, Wucherpfennig KW, Sant'Angelo DB, Denzin LK. Targeted regulation of self-peptide presentation prevents type I diabetes in mice without disrupting general immunocompetence. *J Clin Invest*. 2010;120(4):1324-36.
368. Zhao YL, Tian PX, Han F, Zheng J, Xia XX, Xue WJ, et al. Comparison of the characteristics of macrophages derived from murine spleen, peritoneal cavity, and bone marrow. *J Zhejiang Univ-Sc B*. 2017;18(12):1055-63.
369. Duque GA, Descoteaux A. Macrophage cytokines: involvement in immunity and infectious diseases. *Frontiers in Immunology*. 2014;5:1-12.
370. Francke A, Herold J, Weinert S, Strasser RH, Braun-Dullaeus RC. Generation of Mature Murine Monocytes from Heterogeneous Bone Marrow and Description of Their Properties. *Journal of Histochemistry & Cytochemistry*. 2011;59(9):813-25.
371. Zhang G, Zhang P, Liu H, Liu X, Xie S, Wang X, et al. Assessment of Th17/Treg cells and Th cytokines in an improved immune thrombocytopenia mouse model. *Hematology*. 2017;22(8):493-500.
372. Cunningham CA, Helm EY, Fink PJ. Reinterpreting recent thymic emigrant function: defective or adaptive? *Curr Opin Immunol*. 2018;51:1-6.
373. Gonzalez-Vicent M, Molina B, Deltoro N, Sevilla J, Vicario JL, Castillo A, et al. Donor age matters in T-cell depleted haploidentical hematopoietic stem cell

- transplantation in pediatric patients: Faster immune reconstitution using younger donors. *Leukemia Res.* 2017;57:60-4.
374. Velardi E, Tsai JJ, van den Brink MRM. T cell regeneration after immunological injury. *Nat Rev Immunol.* 2020.
375. Takizawa H, Manz MG. Impact of inflammation on early hematopoiesis and the microenvironment. *Int J Hematol.* 2017;106(1):27-33.
376. Zhang CC. Hematopoietic stem cells: interplay with immunity. *Am J Blood Res.* 2012;2(4):219-27.
377. Pinto AI, Brown N, Preham O, Doehl JSP, Ashwin H, Kaye PM. TNF signalling drives expansion of bone marrow CD4+ T cells responsible for HSC exhaustion in experimental visceral leishmaniasis. *PLoS Pathog.* 2017;13(7):e1006465.
378. Kuter DJ. The physiology of platelet production. *Stem Cells.* 1996;14 Suppl 1:88-101.
379. Yu VWC, Yusuf RZ, Oki T, Wu J, Saez B, Wang X, et al. Epigenetic Memory Underlies Cell-Autonomous Heterogeneous Behavior of Hematopoietic Stem Cells. *Cell.* 2016;167(5):1310-22 e17.
380. Schmidt T, Kharabi Masouleh B, Loges S, Cauwenberghs S, Fraisl P, Maes C, et al. Loss or inhibition of stromal-derived PIGF prolongs survival of mice with imatinib-resistant Bcr-Abl1(+) leukemia. *Cancer Cell.* 2011;19(6):740-53.
381. Ghanima W, Geyer JT, Lee CS, Boiocchi L, Imahiyerobo AA, Orazi A, et al. Bone marrow fibrosis in 66 patients with immune thrombocytopenia treated with thrombopoietin-receptor agonists: a single-center, long-term follow-up. *Haematologica.* 2014;99(5):937-44.
382. Ramalingam P, Poulos MG, Lazzari E, Gutkin MC, Lopez D, Kloss CC, et al. Chronic activation of endothelial MAPK disrupts hematopoiesis via NFkB dependent inflammatory stress reversible by SCGF. *Nat Commun.* 2020;11(1):666.
383. Kobayashi H, Butler JM, O'Donnell R, Kobayashi M, Ding BS, Bonner B, et al. Angiocrine factors from Akt-activated endothelial cells balance self-renewal and differentiation of haematopoietic stem cells. *Nat Cell Biol.* 2010;12(11):1046-56.
384. Gerber HP, Malik AK, Solar GP, Sherman D, Liang XH, Meng G, et al. VEGF regulates haematopoietic stem cell survival by an internal autocrine loop mechanism. *Nature.* 2002;417(6892):954-8.
385. Famili F, Brugman MH, Taskesen E, Naber BEA, Fodde R, Staal FJT. High Levels of Canonical Wnt Signaling Lead to Loss of Stemness and Increased Differentiation in Hematopoietic Stem Cells. *Stem Cell Reports.* 2016;6(5):652-9.
386. Liu LQ, Sposato M, Liu HY, Vaudrain T, Shi MJ, Rider K, et al. Functional cloning of IGFBP-3 from human microvascular endothelial cells reveals its novel role in promoting proliferation of primitive CD34+CD38- hematopoietic cells in vitro. *Oncol Res.* 2003;13(6-10):359-71.
387. Kent DG, Dykstra BJ, Cheyne J, Ma E, Eaves CJ. Steel factor coordinately regulates the molecular signature and biologic function of hematopoietic stem cells. *Blood.* 2008;112(3):560-7.
388. Shepherd MS, Li J, Wilson NK, Oedekoven CA, Li J, Belmonte M, et al. Single-cell approaches identify the molecular network driving malignant hematopoietic stem cell self-renewal. *Blood.* 2018;132(8):791-803.
389. Bujanover N, Goldstein O, Greenshpan Y, Turgeman H, Klainberger A, Scharff Y, et al. Identification of immune-activated hematopoietic stem cells. *Leukemia.* 2018;32(9):2016-20.
390. Bixel MG, Kusumbe AP, Ramasamy SK, Sivaraj KK, Butz S, Vestweber D, et al. Flow Dynamics and HSPC Homing in Bone Marrow Microvessels. *Cell Rep.* 2017;18(7):1804-16.
391. Sun H, Tsai Y, Nowak I, Liesveld J, Chen Y. Eltrombopag, a thrombopoietin receptor agonist, enhances human umbilical cord blood hematopoietic stem/primitive progenitor cell expansion and promotes multi-lineage hematopoiesis. *Stem Cell Res.* 2012;9(2):77-86.

392. Kao YR, Chen J, Narayanagari SR, Todorova TI, Aivalioti MM, Ferreira M, et al. Thrombopoietin receptor-independent stimulation of hematopoietic stem cells by eltrombopag. *Sci Transl Med*. 2018;10(458).
393. Provan D, Arnold DM, Bussel JB, Chong BH, Cooper N, Gernsheimer T, et al. Updated international consensus report on the investigation and management of primary immune thrombocytopenia. *Blood Adv*. 2019;3(22):3780-817.
394. Li X, Wang SW, Feng Q, Hou Y, Lu N, Ma CH, et al. Novel Murine Model of Immune Thrombocytopenia through Immunized CD41 Knockout Mice. *Thrombosis and Haemostasis*. 2019;119(3):377-83.
395. Neschadim A, Branch DR. Mouse models of autoimmune diseases: immune thrombocytopenia. *Curr Pharm Des*. 2015;21(18):2487-97.
396. Deng R, Balthasar JP. Comparison of the effects of antibody-coated liposomes, IVIG, and anti-RBC immunotherapy in a murine model of passive chronic immune thrombocytopenia. *Blood*. 2007;109(6):2470-6.
397. Teeling JL, Jansen-Hendriks T, Kuijpers TW, de Haas M, van de Winkel JG, Hack CE, et al. Therapeutic efficacy of intravenous immunoglobulin preparations depends on the immunoglobulin G dimers: studies in experimental immune thrombocytopenia. *Blood*. 2001;98(4):1095-9.
398. Nieswandt B, Echtenacher B, Wachs FP, Schroder J, Gessner JE, Schmidt RE, et al. Acute systemic reaction and lung alterations induced by an antiplatelet integrin gpIIb IIIa antibody in mice. *Blood*. 1999;94(2):684-93.
399. Nieswandt B, Bergmeier W, Rackebrandt K, Gessner JE, Zirngibl H. Identification of critical antigen-specific mechanisms in the development of immune thrombocytopenic purpura in mice. *Blood*. 2000;96(7):2520-7.
400. Byzova TV, Rabbani R, D'Souza SE, Plow EF. Role of integrin alpha(v)beta3 in vascular biology. *Thromb Haemost*. 1998;80(5):726-34.
401. Neunert C, Arnold DM. Severe bleeding events in adults and children with primary immune thrombocytopenia: a systematic review: reply. *J Thromb Haemost*. 2015;13(8):1522-3.
402. Khellaf M, Michel M, Schaeffer A, Bierling P, Godeau B. Assessment of a therapeutic strategy for adults with severe autoimmune thrombocytopenic purpura based on a bleeding score rather than platelet count. *Haematologica*. 2005;90(6):829-32.
403. Qu MM, Liu Q, Zhao HG, Peng J, Ni HY, Hou M, et al. Low platelet count as risk factor for infections in patients with primary immune thrombocytopenia: a retrospective evaluation. *Ann Hematol*. 2018;97(9):1701-6.
404. Allen R, Bryden P, Grotzinger KM, Stapelkamp C, Woods B. Cost-Effectiveness of Eltrombopag versus Romiplostim for the Treatment of Chronic Immune Thrombocytopenia in England and Wales. *Value Health*. 2016;19(5):614-22.
405. Tremblay G, Dolph M, Roy AN, Said Q, Forsythe A. The Cost-effectiveness of Eltrombopag for the Treatment of Immune Thrombocytopenia in the United States. *Clin Ther*. 2020;42(5):860-+.
406. Tremblay G, Dolph M, Bhor M, Said Q, Elliott B, Briggs A. Cost-consequence model comparing eltrombopag versus romiplostim for adult patients with chronic immune thrombocytopenia. *Clinicoeconomic Outc*. 2018;10:705-13.
407. Ghanima W, Cooper N, Rodeghiero F, Godeau B, Bussel JB. Thrombopoietin receptor agonists: ten years later. *Haematologica*. 2019;104(6):1112-23.
408. Kuter DJ. Thrombopoietin and Thrombopoietin Mimetics in the Treatment of Thrombocytopenia. *Annual Review of Medicine*. 2009;60:193-206.